STUDIES OF STELLAR POPULATIONS: STAR CLUSTERS IN M31, THE GALAXY AND THE MAGELLANIC CLOUDS

Thesis by
Douglas Mark Rabin

In Partial Fulfillment of the Requirements
for the Degree of
Doctor of Philosophy

California Institute of Technology
Pasadena, California

1981
(Submitted September 23, 1980)

To Ruth

ACKNOWLEDGMENTS

I thank Leonard Searle for suggesting the study of integrated spectra, for making available valuable observing time in which to acquire them, and for many subsequent discussions. Judy Cohen was of great help in the latter stages of this work, reading drafts and allowing me the use of unpublished data. In his own way, Wal Sargent provided a certain moral - not to mention financial - support. Jim Gunn deserves mention just for managing to remain nearly himself; but he also designed the SIT vidicon that I used to take much of the data.

I would need a separate chapter in order to acknowledge properly the help given by many people. Still, hoping that it is preferable to the alternative ("It is not possible to thank. . ."), I list below those whom a faulty memory can recall. Space permits only the names, but each represents a personal contribution for which I am grateful.

At Caltech:

Tom Ake
Earle Emery
Richard Green
Lilo Hauck
John Hoessel
Helen Holloway
Edith Huang
Margaret Katz
Steve Kent
Helen Knudsen
Ron Moore
Bill Sebok
Richard Wade
Barbara Zimmerman
Hal Zirin

At Palomar:

Larry Blakée
Juan Carrasco
Skip Staples
Gary Tuton
Chip Williams
Dorothy Williams

At Cerro Tololo:

Bruce Atwood
Pat Osmer
Juan Rios
François Schweitzer

And Elsewhere:

R. B. Ciardullo (University of California, Los Angeles)
S. C. B. Gascoigne (Australian National University)
J. P. Huchra (Smithsonian Astrophysical Observatory)
R. P. Kraft (University of California, Santa Cruz)
R. L. Kurucz (Smithsonian Astrophysical Observatory)
Mother (Watsonville, California)
S. A. Shectman (Mount Wilson and Las Campanas Observatories)
A. V. Sweigart (Goddard Space Flight Center)
R. F. Wing (Ohio State University)
B. and B. Yandell & Assoc. (Altadena, California)

ABSTRACT

This study focusses on medium resolution spectra of the integrated light of star clusters in our own Galaxy and in three nearby systems: M 31 and the two Magellanic Clouds. Since only integrated properties will normally be observable for clusters in more distant galaxies, or for the galaxies themselves, it is important to develop quantitative techniques which relate features of the integrated light to physical characteristics such as age and chemical composition. Here, digital SIT spectra are analyzed both internally, as multivariate data sets, and externally, by comparison with evolutionary models of star clusters and with detailed observations of nearby clusters.

For 22 clusters in M31, direct comparison of the equivalent widths of various metallic features in the wavelength region λλ3800–5300 shows that they determine a one-dimensional sequence in cluster metallicity. However, a robust principal components analysis reveals that the Balmer lines (Hδ, Hγ, Hβ) behave distinctively, both in the Galaxy and in M31. For galactic globular clusters, the independence of the hydrogen lines shows up as a poor correlation between the strength of the Balmer lines in the integrated spectrum and the observed distribution of stars along the horizontal branch. Synthesis models are used to evaluate possible explanations, none wholly satisfactory. Compared with spectra of standard stars, the M 31 spectra provide a clue which may bear on the problem in both galaxies: all the Balmer lines are contaminated by metallic features, and this is advanced as the cause of the enhanced Hβ strength in strong lined M31 clusters. In some cases the enhancement is seen directly.

It is speculatively suggested that the M 31 clusters exhibit in integrated light a mild form of the "hyperstrong line" phenomenon ascribed to some stars and to the nuclei of some elliptical galaxies.

Balmer lines are also central to the interpretation of the spectra of 17 "red" clusters in the Magellanic Clouds, but now as a manifestation of stars at the turnoff in the HR diagram and hence as direct indicators of age. In these spectra, the strength of the Ca II K line is well correlated with the strength of the G band, but the relation between K and $<H>$, the median Balmer line strength, scatters widely. The K–$<H>$ diagram is interpreted with the guidance of a (metallicity) sequence of galactic globular clusters and an age sequence of model clusters. It is shown that the K–$<H>$ diagram maintains sensitivity to turnoffs which are impracticable to reach by conventional methods, and thus that this technique resolves some outstanding questions of relative age, and to some extent metallicity, raised by previous analyses of color-magnitude diagrams.

It is found that the strength of the spectrum break at Ca K correlates poorly with the strength of metallic features but correlates well with a break in the slope of the spectrum near the G band. The cause of this additional degree of freedom is not known.

Finally, I trace the steps in modifying theoretical isochrones and in combining them with empirical and theoretical stellar data to produce integrated colors, integrated spectra, and theoretical color-magnitude diagrams. The model colors are compared with observations. Also, apart from the details of stellar evolution, it is shown that strict limits on the allowed colors of composite models may be derived solely from properties of the stellar synthesis library.

A brief analysis of the color-magnitude diagrams provides no support for an age-abundance correlation among globular clusters. However, the models strongly exclude ages less than 1.3×10^{10} y and thus conflict with ages implied by standard Friedman models having $H_0 \approx 100\,\mathrm{km\,s^{-1}\,Mpc^{-1}}$ (particularly if the universe is dense, $\Omega \gtrsim 0.2$).

TABLE OF CONTENTS

INTRODUCTORY NOTE

The first two chapters are self-contained, substantially in the form of journal articles. As such, there is some redundancy, particularly with regard to references to the synthesis models in the third chapter. There the models are described in more detail than would normally characterize published work.

Chapter 1

COMPARATIVE SPECTROSCOPY OF OLD STAR CLUSTERS IN M31 AND THE GALAXY

I. INTRODUCTION

Star clusters in M31 have been the object of lively interest since Hubble (1932) catalogued and discussed some 140 of them. From their compact, symmetrical forms and from approximate color indices, he provisionally identified them with the globular clusters in our galaxy, although, because of the compressed distance scale then in use, the M31 clusters were apparently less luminous than galactic globulars by 1–2 magnitudes. It is interesting that Hubble regarded the comparison with "known" globular clusters in the Magellanic Clouds as perhaps more telling (the relative distances being more securely known), since it now seems likely that few of the clusters in the Clouds are like galactic globulars in more than surface appearance (Chapter 2).

Photoelectric PV colors for 71 clusters by Kron and Mayall (1960) and photographic $B-V$ colors for 121 clusters by Kinman (1963) confirmed that their range in color was similar to that occupied by galactic globulars, although some blue clusters were evident and uncertainty over reddening precluded strong conclusions about the redder group.

By the time the availability of image tubes enabled the first major spectroscopic investigation of M31 clusters (van den Bergh 1969), a much more refined picture of galactic globular clusters and their origin had developed, so a sharper comparison could be made. Galactic globulars were viewed as ancient systems which had all formed during the brief collapse of the galaxy envisioned by Eggen, Lynden-Bell and Sandage (1962). Supernovae had enriched the gas as it collapsed, accounting for the observed correlation of metallicity with distance from the galactic plane (or from the galactic center). van den Bergh found individual strong-lined clusters well into the halo of M31 and argued from his group of 37 spectra that line strength and position were not well correlated. He suggested that this indicated that considerable enrich-

ment of the gas in M31 had occurred before its collapse. From the spectra and from the photometric parameter Q, known to be well correlated with Morgan's (1959) metallicity classification for galactic globulars (van den Bergh 1967), van den Bergh further argued that the mean metallicity of the clusters in M31 was higher than the mean for galactic globulars.

Some of van den Bergh's conclusions have been challenged or modified by subsequent work. For example, Hanes (1977) replaced Q with Racine's more accurately reddening-free parameter R (Racine 1973) and concluded that the distribution over R in M31 and in the galaxy could not be statistically distinguished. On the other hand, Searle (1978) used a sample of over 100 clusters, purified of young objects and background galaxies, to show that the distributions over abundance in the Galaxy and in M31 have similar shapes, but that the mean in M31 is indeed displaced to higher metallicity. He also compared the trend of metallicity with distance from the nucleus with an extensive survey in the Galaxy using the same instrumentation (Searle and Zinn 1978) and found that gradients could be identified in both systems, but only over a rather small range in galactocentric distance.

There is clearly room for many future investigations to clarify the properties of the cluster system in M31. However, from recent work a point may be gleaned which reinforces our retrospective view of Hubble's conclusions: just as the globulars in the Magellanic Clouds are in some respects less "known" than they were to Hubble, so is our knowledge of galactic globulars perhaps less a stable referent than has been supposed. Attempts to match observed color–magnitude diagrams with theoretical models have indicated the possibility that the metal rich clusters M71 and 47 Tuc are several billion years younger than the metal poor clusters M15 and M92 (Hartwick and Vanden Berg 1973; Demarque and McClure 1977). Carney (1980) has suggested, again on the basis of theoretical isochrones, that there is a general correlation of metallicity with age (however, see the discussion in Chapter 3). On quite different

grounds, Searle and Zinn (1978) have argued that the clusters of the outer halo have a greater range in age and metallicity than clusters nearer the nucleus. Even in the fundamental matter of cluster abundances, despite increasingly refined rankings by metallicity (Kukarkin 1975; Searle and Zinn 1978; Zinn 1980a), recent work on 47 Tuc (Pilachowski, Wallerstein and Leep 1980) and on M 71 (Cohen 1980) has suggested that the absolute scale may require substantial revision. Furthermore, the notion of a single metallicity is itself inadequate to account for the most detailed observations of individual clusters (reviewed by Kraft 1979).

This burgeoning mass of data has yet to be integrated into a coherent picture of the cluster system comparable to the "classical" collapse scenario (which is by no means wholly refuted).

The present investigation will stress a direct quantitative comparison of a sample of high quality spectra of clusters in M 31 with a similar sample in the Galaxy. The aim will be to explore in detail the similarities and differences in their patterns of line strengths. Our greater knowledge of galactic globulars can be put to good use in exploring hypotheses about the underlying stellar populations, but, in view of the complications mentioned above, it is prudent to admit the the possibility that the spectra may as much reveal the limitations of that knowledge as establish the stellar content of clusters in M 31.

II. DATA

a) Observations

An SIT digital spectrograph (Kent 1979) was used at the Cassegrain focus of the Palomar 5 meter telecope to obtain spectra of the integrated light of 19 clusters in M 31, the inner bulge of M 31, and 13 galactic globular clusters. 512 pixels along the dispersion covered the spectral range $\lambda\lambda 3700-5300$, giving 3.2 Å pixel^{-1}. A 1'' slit was used initially, but, because of the nearly critical sampling defined by the

spectrograph-detector combination, the use of a 2" slit was later found to entail a negligible loss of resolution. The unsmoothed resolution is about 5 Å (FWHM). Table 1 summarizes the observations.

The galactic globulars were observed by scanning in declination over a range chosen at the telescope from the appearance of the cluster on the television field viewer. The aim was to include as many bright giants as possible without introducing excessive field contamination or prolonging exposures unduly. The adopted range for each cluster, given in Table 1, was always greater than the cluster's core diameter, usually by a comfortable factor (2.7 on average). Since the reduction procedure also integrates at each wavelength along the 1' slit, the resulting spectra are a fair sample of the integrated light.[1] There was no need to throw the images out of focus. With the scanning procedure, exposures for the impressive galactic globulars were often longer than for the bright clusters in M31. Many well studied clusters of low concentration, the most readily accessible to color–magnitude work, were simply too faint. As a guide to future observations with similar detectors, exposure times (for a 2" slit) are listed in Table 1.

For M31 clusters, sky subtraction could be carried out on a single frame with bands along the slit flanking the cluster spectrum; for clusters projected against the inner bulge, neither the level nor the gradient of the background light could be neglected. M31 clusters were all observed near the zenith. Except for a few galactic globulars with high surface brightness, all observations were made in the dark of the moon. Outside of emission lines, the sky signal for the galactic globulars was usually inconsequential.

---

1. Consider M71 as an example; with a ratio between scan range and core diameter of 1.5, it is one of the least favorable cases. From the plates in Arp and Hartwick (1971), it may be roughly estimated that the scanned area includes about 30 giants brighter than the level of the horizontal branch and about 300 stars above the base of the giant branch. Such a ratio is consistent with measured globular cluster luminosity functions (*e.g.*, Hartwick 1970).

Clusters were typically exposed to about 2/3 of the full digital range (which is set at a level below that of physical saturation of the target). Averaged over wavelength, this corresponds to roughly 500 photons pixel^{-1}. Since 20 or more pixels along the slit were available for galactic globulars and often two frames were added for each object, the net signal was well over 10^4 photons at most wavelengths. However, as discussed below, photon statistics is not the limiting influence in the reproducibility of equivalent widths determined from these spectra. For M 31 clusters, the net signal was typically $2-4 \times 10^4$ photons at each wavelength.

b) Reduction Procedure

In outline the reduction procedure for each night was standard: subtraction of the SIT erase level, correction for pixel-to-pixel response variation by application of a "flat" field, correction for *S*-distortion of the spectrum, wavelength calibration using a helium arc and reduction to fluxes using observations through an 8" aperture of at least two spectrophotometric standards calibrated on the system of Oke and Schild (1970). A few special considerations apply to the present data.

First, and most important, the data were corrected for apparent zero-level shifts of up to 5% of full scale. Since the projected slit is shorter than the silicon target, about ten pixels beyond each end of the slit are exposed only to scattered light. This reference level, monitored for each frame, seemed to vary at random (though with some time coherence) and could not be well correlated with the length of exposure, the temperature of the instrument or the level of the target in its exposed portion. The pure erase level was sampled several times throughout the night and showed stability generally to better than 1/2% of full scale.

The effect of this secular instability varies with the circumstances. For observations of stars or of clusters in M 31, the practice of subtracting sky bands placed symmetrically about the object spectrum compensates approximately for level shifts and

for linear trends; the effect may never be noticed. For full-frame observations of large clusters or of galaxies with sky subtraction from separate frames, the violet region of the spectrum may be seriously affected, particularly where Ca H and K or the CN bands dip below the already moderate signal to small residual intensities.

The following procedure was adopted to correct for level shifts. For each of the 512 columns along the dispersion, the signal (positive or negative, after erase subtraction) in 5 pixels on either side of the exposed portion was averaged to produce two tie points for the correction. Again for each column separately, linear interpolation was used to generate corrections for intermediate (exposed) pixels. Although this interpolation is given no physical justification, limited evidence from long dark frames indicates that the shift at least behaves smoothly and monotonically across the target. Separate determinations are made for the object frames and the sky frames before they are combined. The practical justification for the procedure is simply that, where repeated observations are available, it yields consistent results for the appearance of the spectrum and for derived equivalent widths, whereas the uncorrected spectra are sometimes inconsistent.

The M 31 spectra are subject to a different problem which limits their potential accuracy. It is seen by direct calculation that for frames with a mean net signal $\gtrsim 500$ photons pixel^{-1}, the pixels in the flattened field vary more than expected from photon statistics alone. For example, one line along the dispersion may clearly show Hδ with 15% central depth while the adjacent line barely indicates the presence of an absorption. Examination of the frames on a large-format scan converter shows that this phenomenon is manifest as a generally enhanced graininess and is not the result of blemishes or ion spots. In consequence, the variance at a given point in the spectrum involves a factor n^{-1}, where n is the number of pixels at that wavelength, and this factor is dominant when photon noise subsides. It is more for this reason than because of the greater total signal that the spectra of the extended galactic objects

are smoother and more reproducible than the spectra of the M31 clusters.

Some of this effect may be due to flattening. The low-level Moiré pattern covering the target (< 5–10% of full scale) varies slightly with the pointing of the telescope and has not been calibrated out (Simkin 1979). Beam pulling during target readout (Schechter and Gunn 1979) depends on the exposure level and its gradient, the latter being poorly matched between stellar sources and the cool incandescent source used for flat fields. For whatever reasons, flattening on average increases pixel-to-pixel variance by roughly 5%. Nevertheless, flattening has generally been applied to the present data because it removes a local feature associated with the grating response. In critical cases, equivalent widths have been determined both from the unflattened and the flattened data, the choice depending on target region.

The need for the precautions and corrections described above may perhaps be judged by the objective: to discriminate among weak-lined absorption spectra in which, for example, the mean equivalent width and central depth of Hγ are 1.7 Å and 12%.

It may be last noted that, although continuum fluxes are used only locally in determining equivalent widths, a full spectrophotometric reduction has been maintained throughout. Although the observations were made through a slit (except for standards), the effects of differential refraction are small for the compact M31 clusters observed near the zenith and are completely negated by the scanning procedure adopted for galactic globulars. Repeated observations suggest about 10% photometric accuracy.

c) Line Indices

It was decided at the outset to measure every available feature of significant strength, reserving to analysis the questions of predictive power, redundancy and reproducibility. The features are defined in Table 2. Of course, at Cassegrain

dispersion the continuum is never available, so a choice had to be made between two approaches to the measurement of feature strength. One may define one or two sidebands associated with each feature and use some ratio of the feature and sideband fluxes to specify a feature index (e.g., O'Connell 1973; Pritchet and van den Bergh 1977). For fixed passbands this has the advantage of circumventing the determination of a pseudocontinuum, but from Figure 1 it is clear that at the present resolution the corresponding disadvantage of contaminating features in the sidebands is a serious one. Various methods for generating a pseudocontinuum were tried: running averages, taut splines tied to selected peak points, broad Fourier smoothing of the total spectrum, *etc.* Of these, the last was most faithful to the overall shape, but the necessary shift to a "continuum" level could not be convincingly prescribed. No method was judged satisfactory.

A purely local procedure was adopted. Nominal limiting wavelengths were selected for each feature. Since redshift (up to 500 km s^{-1} in M 31) could not be neglected in view of the steep-sided line profiles, the data were rebinned logarithmically, detrended and tapered with a 5% cosine window on each end, and shifted to rest wavelength in the Fourier domain. Once there, it was easy to apply a small amount of smoothing in the guise of a Gaussian velocity dispersion, a form chosen with a view to eventual comparison wth galactic nuclei; σ = 120 km s^{-1} achieved the desired pixel-to-pixel smoothing without blurring to invisibility the weak metallic features in M 15. Back in the data domain, the continuum trend was restored for maximum fidelity to the observed spectrum. The two reference wavelengths for each feature were then connected by a straight line to define the local pseudocontinuum. Since the sample of clusters encompasses a broad range of line strength, each feature in each object was examined to determine whether the reference wavelengths satisfactorily delimited the line. Adjustments of up to 8 Å, but typically 2–3 Å, were applied in about one third of the cases. The resulting pseudoequivalent widths were determined by

numerical integration and will be referred to subsequently as equivalent widths (EWs) without qualification. Figure 1 shows a fairly strong lined spectrum with the adopted continuum segments. Table 3 lists the equivalent widths.

III. RESULTS

a) Comparison with van den Bergh's L

By comparing cluster spectra with a series of main sequence MK standards, van den Bergh (1969) estimated four distinct spectral types for each cluster based on four metallic features. He defined the line-strength index L as

$$L = 1/4\,[\,\mathrm{Sp(Ca\,II\,H{+}K)} + \mathrm{Sp}(\lambda 4227) + \mathrm{Sp(G\ band)} + \mathrm{Sp}(\lambda 4325)\,]$$

where numerical values 0, 10 and 20 were assigned to types F0V, G0V and K0V. A comparison of the L-values with the EWs of this study is interesting not only in terms of calibrating L for van den Berghs's larger total sample, but also because it allows a point of contact between the present purely local, numerically defined procedure and the classical photographic technique which relies on a complex visual impresssion of several hundred angstroms of spectrum. In analogy to L, define $\mathscr{L}$ by

$$\mathscr{L} = 1/4\,[\mathrm{EW(Ca\,II\,K)}] + \mathrm{EW}(\lambda 4227) + 1/3\,[\mathrm{EW(G\ band])} + \mathrm{EW}(\lambda 4325)$$

where the numerical coefficients make the widths roughly comparable while allowing for the greater relative accuracy of K and the G band (Ca H has been omitted because of the blend with Hε). Three points may be noted from the comparison between L and $\mathscr{L}$ shown in Figure 2. First, the correlation may be taken to be nearly unity when errors in both coordinates are considered. Second, the galactic globulars and M31 clusters intermingle over the full range of line strength. Third, the relation flattens off at large L, indicating either that the visual classification procedure loses sensitivity when the lines become strong or that it subjectively incorporates subtle aspects

of the spectra other than the nominal classification features.

van den Bergh's data indicated that the relationship between L and its component spectral types differed systematically between M31 and the Galaxy. The analogous relations for $\mathscr{L}$ and its constituent quantitative features (Figure 3) show no convincing separation. This favors the possibility, raised by van den Bergh, that the comparatively narrow photographic spectra of the M31 clusters introduced small systematic biases into the classification.

The comparison between L and $\mathscr{L}$ affirms the utility of van den Bergh's classification and furthermore suggests that metallic features define a one-dimensional sequence of clusters which is common to the Galaxy and M31. This hypothesis will explored more sensitively by focussing on the internal structure of the set of equivalent widths.

b) Metallic Line Indices

Two preliminary remarks will apply generally to the discussion of line indices. First, features will often be denoted by the name of a principal atomic or molecular contributor, particularly when the assignment is conventional. This should not be allowed to obscure the fact that all the features are blends; for the weaker features, even the principal contributor may not be securely known over the full range of line strength. Second, the "error" flags shown in the plots represent an attempt to assess the spread in repeated measurements, but, because the error for a given line in a given object is a complex amalgam of effects due to photon statistics, properties of the SIT (§I*b*), the width and depth of the feature, and even the overall level of line blanketing, no general prescription is satisfactory. A constant fractional error in the EWs is usually closer to the truth than a constant absolute error, but weak lines do have a larger fractional error. The flags given apply roughly to the middle range of each plot. When information from repeated measurements was inconclusive (as it

fairly often was, due to fortuitous concordance or to an outlier), a lower limit set by photon statistics proved to be a useful guide.

A general tendency was found for noisier spectra to be biased toward greater line strength. This is not surprising in view of the procedure for continuum placement, which anchors to local (albeit somewhat smoothed) maxima. This effect must be weighed in addition to selection effects when comparing the range of line strengths in M31 clusters with the range in galactic globulars.

We begin with a comparison of two lines of the same element, Ca I λ4227 and Ca II K. Figure 4*a* shows that the correlation is absolute to within the estimated errors and that it can be perceived for EWs as small as 0.5 Å. This conclusion is repeated by Figure 4*b* for the G band (CH + Fe) and the λ4325 feature (Fe + detached *Q* band of CH). Figure 4*c* extends the comparison to two features with distinct contributing elements, Ca K and the G band. The correlation is no less tight than in Figure 4*ab*. Furthermore, there is no perceptible separation between the relations for M31 clusters and for galactic globulars. The twin features of high correlation and lack of separation are reinforced (Figures 4*de*) by plotting Ca K against the magnesium triplet ($Mg\,b_{4+2+1}$ + Mg H) and against the violet CN bands (CN + Fe + H).

The notion of a common one-dimensional sequence in metals may be further examined by comparing single major features with a composite metals index. The index *M* is defined as the sum of all EWs except violet CN, Ca H+K, the G band, the Mg triplet and Balmer lines. Beyond the increased reliability to be expected from a sum of quantities with independent errors, *M* has the advantage of reflecting in an average sense the line blanketing over the whole spectral range considered. Although the separate behavior of the constituent indices is lost, their relatively low precision already precludes definite conclusions about individual differences; furthermore, Fe I is probably the principal absorber in most of the features.

Figure 5*abc* shows that the relationship between *M* and CaK, the G band or the Mg triplet has no more scatter than is typical of single major features against each other, and that once again the M31 clusters and galactic globular clusters intermingle. This supports the hypothesis that to a first approximation the two cluster families define a single sequence in overall metallicity.[2]

Apart from any estimates of error, an appreciation of the degree of scatter in Figures 4 and 5 is important in judging the significance of the behavior of the hydrogen lines, next considered.

c) Balmer Lines

In Figure 6*abc*, the composite index *H*, defined as the sum of the equivalent widths of Hδ, Hγ and Hβ, is plotted against CaK, Mgb and the composite metals index *M*. There is only a slight negative correlation between *H* and metallic line strength, and at all strengths the scatter is larger than the scatter in the relation between any two metallic features. *The Balmer lines reflect a characteristic of the underlying stellar population which is substantially independent of overall metallicity.* It may be emphasized that this conclusion is valid for the clusters in M31 and the clusters in the Galaxy considered as separate samples, as well as to the aggregate.

There is moreover in Figure 6 a suggestion of a separation between M31 clusters and galactic globulars, although, as with the metallic features, the full areas occupied by the two groups are essentially coextensive. Figure 7*ab* establishes unequivocally a separation in the relations between Hβ alone and CaK or Mgb. The galactic globulars show a weak but definite negative correlation with metallicity. The weak lined M31 clusters mingle with metal poor globulars, but at higher metallicities H does not weaken in M31 clusters. Based on the overlap at low metallicity, it might be supposed that M31 clusters depart from the galactic trend because the hydrogen line is

---

2. "Metallicity" here refers only to the strength of metallic features in the integrated spectrum.

blended with metallic lines which become increasingly serious contaminants as overall metallicity rises; some evidence in favor of this view will be discussed later. Alternatively, one may infer that the true strength of Hβ is nearly independent of metallicity in M 31, and thus that the physical cause of the negative correlation in the Galaxy is absent in M 31. Regardless of the explanation, *the behavior of Hβ represents a new degree of freedom which distinguishes the two families of star clusters.* This is so even if metallic contamination is at fault: the blending would still have to affect the integrated spectrum differently in the two galaxies, implying thereby at least a subtle structure within the overall metallicity sequence defined by major features.

Of the three Balmer lines, Hβ is the least affected by blanketing and can be measured most reproducibly. Unfortunately, external problems limit the reliability of individual measurements of Hγ and Hδ. Hg λ4358 lies just to the red of Hγ and sometimes prevents good continuum placement. Subtraction of this line is usually excellent in the M 31 clusters, but a higher average air mass (and thus a stronger line) combines with differential beam bending between the separate sky and object frames to give a poorer result for galactic globulars. Hδ, on the other hand, suffers more in the M 31 clusters because of its location in the fainter part of the spectrum, which usually has less signal and covers less of the target than does the same wavelength range in a galactic globular. Figure 7*c* shows Hδ against Ca K. Weak trends could be lost in the scatter, as could evidence for the separation between M 31 and the Galaxy. However, failure to find these refinements should not obscure the fact that the scatter confirms the role of the hydrogen line strength as an independent parameter in both galaxies. Comparison may be made to Figure 4*a* where Ca I λ4227, even weaker than Hδ and also in the blue, heavily blanketed region, is shown to be well correlated with Ca K.

d) Analysis of Principal Components

We undertake a principal components analysis (PCA) not to "confirm" the foregoing analysis based on selected pairs of variables (the PCA in fact preceded it), but rather to allow a more distant and unified view of this large and complex data set (for earlier applications see, *e.g.*, Deeming 1964 or Faber 1973). It may be helpful to recall that each PC is simply a linear combination of the original variables (equivalent widths) and that any two PCs are uncorrelated. If the original variables are visualized as orthogonal axes against which objects are "plotted", the principal components transformation represents a rotation in this hyperspace. The scatter (variance) of the data along the first principal axis is larger than the scatter along any other direction; among directions orthogonal to the first PC, the second PC has maximal variance – and so on. Here, attention will be focussed on the potential of PCA to reveal structure within the original set of variables.

Experience with several multivariate techniques has suggested that two main pitfalls are failure to account for the systematic influence of observational errors and overreliance on formal tests of significance. The present treatment responds to the first problem by incorporating estimates of error directly into the preliminary scaling of variables and by weighting individual observations; to the second by emphasizing graphical displays which do not allow outliers to distort the basic structure. Some of the techniques are briefly described in the Appendix.

Figure 8 shows the variances along the principal components arranged in decreasing order of importance. The degree to which the first PC dominates the others is striking; this can happen only if the variables have a high degree of linear correlation and are relatively error free. Again: a single sequence dominates the combined data for M 31 and the Galaxy. The next step is to decide how many of the remaining components are worthy of close inspection. In line with our general approach, a graphical

technique is preferred. The "scree" test illustrated in Figure 8 indicates that at most four components could indicate structure sufficiently removed from noise as to have even the potential of interpretation (Catell 1978 discusses extensive trials of this test on real and artificial data).

Figure 9 displays the correlation of the original variables with the first two principal components. *All* of the variables but three group into a single cluster. The three exceptions are labelled: Hδ, Hγ, Hβ. There may be lower level structure in the elongated main cloud, but its cohesiveness demands caution in interpreting individual variables such as CN and $\lambda\lambda$4127-4139 which, from their factor correlations judged separately, would appear to behave quite differently. The same cohesiveness emphasizes the isolation of the Balmer lines. Still, it is suggestive that Hβ lies about half way between the main cloud and Hδ–Hγ; this may reflect the metallic contamination previously suggested in connection with the Hβ–Ca K relation.

Figure 10 shows in another way how well the principal metallic features follow general line strength. Had this plot of the G band against the first PC been intermixed with the plots shown earlier of one feature against another, there would have been no reason to select it as unusual (although it would have been among the smoother of the relations).

On the other hand, the next few PCs do not so easily yield to interpretation. The correlations of the original variables with PCs 2 and 3 (Figure 11) show no obvious structure. The Balmer lines mingle with the other features, and none of the correlations is strikingly large. For example, Figure 12 reveals no structure in the relation between Hβ and the second PC. Yet, if one selects the variable having the highest (absolute) correlation with a given PC, this variable is a Balmer line for seven of the first eleven PCs. In the context of factor analysis (Mulaik 1972), such a distribution over components suggests that a further rotation to "simple structure" in the sub-

space orthogonal to the first PC could concentrate the Balmer lines into one or two components. This approach is not further explored here; however, it is well to appreciate that the distribution of objects in the plane of the first two principal components can mislead as much as inform when the second PC cannot be clearly associated with a small group of variables.

IV. AN [Fe/H] SCALE FOR THE M31 CLUSTERS

The first principal component, PC1, is the natural choice to represent overall metallic line strength in the integrated spectrum. If values of [Fe/H] from Zinn (1980a) for the 13 galactic globulars in the present sample are plotted (dependent variable) against PC1 (independent variable), one finds through unweighted least squares the linear fit

$$[\mathrm{Fe/H}]_{\mathrm{Zinn}} = -0.06\,(\mathrm{PC1}) - 1.06 \qquad (1)$$

with a product moment correlation $r = 0.98$ and a standard deviation from the fit $\sigma_{[\mathrm{Fe/H}]} = 0.15$. Since the sample principal components are subject to stochastic variation, and the calibrating values of [Fe/H] are subject to errors of estimation, neither variable fulfills the requirements of an independent variable in ordinary regression analysis – the relationship is *structural* (Kendall and Stuart 1973). It would be possible to estimate the ratio λ of the error variance of [Fe/H] to that of PC1, both assumed constant, and thereby to obtain a unique maximum likelihood linear relationship. This is unnecessary here. If [Fe/H] instead of PC1 is considered to be independent, the least squares solution is still given by (1), to within the formal 1σ errors of the fit. Since Kendall and Stuart (1973) show that the two regression lines (with each variable in turn taken as independent) *bracket* the structural line in the case of known λ, (1) may still be taken as the best estimate when errors in both coordinates are allowed.

There is considerable uncertainty over the metallicity which should be assigned to metal rich clusters such as M71 or 47Tuc (Cohen 1980; Pilachowski, Canterna and Wallerstein 1980). In Chapter 3, where the problem is considered more fully, it is found that synthesis models favor $[Fe/H] \approx -0.9$ for M71 or 47Tuc (Dickens, Bell and Gustafsson 1979), compared to -0.40, adopted for M71 by Zinn (1980a), and -1.27, recommended for M71 by Cohen (1980). If Zinn's values for the four most metal rich clusters in the present sample (N6441, M71, M69 and N6356) are arbitrarily decreased by 0.5 dex, the following linear relation results:

$$[Fe/H]_{Mod} = -0.04\,(PC1) - 1.29 \qquad (2)$$

with $r = 0.97$ and $\sigma_{[Fe/H]} = 0.12$. As with (1), (2) may be considered to estimate the structural relationship.

Table 4 gives derived values of [Fe/H] for the M31 clusters and the galactic globulars on both the Zinn scale and the "modified" scale. One or the other should prove serviceable for interpolation when the uncertainty over calibration at the metal rich end is resolved.[3] Naturally, neither relation applies to objects unlike globular clusters – for example, the M31 nucleus or the cluster in the WLM galaxy (Ables and Ables 1977).

Relations similar to (1) or (2) could be derived for an individual index, such as EW(Ca K) (a primary ingredient in Zinn's Q_{39}). However, the calibration in Table 4 aims to associate individual *clusters* with values of [Fe/H]. An index calibration would be dangerous, since the pseudoequivalent widths used in this work are not comparable to those derived by different methods.

---

3. Zinn (1980b) has recently recalibrated Q_{39}, his metallicity ranking variable, to return Cohen's (1980) value of [Fe/H] for M71. Values on his new scale are labelled $[Fe/H]_{II}$. The graph of $[Fe/H]_{II}$ against PC1 is sensibly curved. A curvilinear fit to this scale is not attempted here, but, given the sketchy calibration, the effect of adopting $[Fe/H]_{II}$ may be adequately estimated by decreasing $[Fe/H]_{Mod}$ (Table 4) by 0.3 dex for $[Fe/H]_{Mod} \gtrsim -1.4$.

V. DISCUSSION OF BALMER LINES IN INTEGRATED SPECTRA

We have seen that the strengths of metallic lines in globular clusters reveal a dominant one-dimensional sequence with which the strength of the hydrogen lines is largely uncorrelated. Since the horizontal branch is traditionally the prime suspect in "second parameter" cases, it will be useful (and sobering) first to examine the correlation between hydrogen line strength and horizontal branch type for galactic globulars. Then, using synthesis models as a guide, we shall examine two complementary effects of a horizontal branch on the integrated spectrum: weakening of metallic lines and strengthening of hydrogen lines. The first effect, dilution, will bear on the relationship of the dominant metallic line strength sequence to a true metallicity sequence. The second effect will be shown to be sizable, leading to a problem in understanding the poor correlation between the strength of the Balmer lines and the horizontal branch. Variations in several properties (luminosity function, age, helium abundance, number of horizontal branch stars) will be investigated, but no one effect provides a clear explanation. Another factor, contamination by metallic lines, will be discussed in connection with the suggestion that its behavior differs between M31 and the Galaxy.

a) The Integrated Spectrum, the CMD and the "Second Parameter"

M13 and N7006 are often cited as extremes of the variation of the second paramater in color–magnitude diagrams (CMDs), with M3 occupying the middle ground (Sandage and Wildey 1967). It is therefore of interest to compare the present spectroscopic data for these three clusters with their photometric properties and estimates of their metallicity. This is done in Table 5, where the integrated *UBV* colors and reddening are from Harris and Racine (1979) and $V-K$ (adjusted to the adopted reddening) is from Aaronson *et al.* (1978). Columns 5–7 give reddening-insensitive integrated colors on the Gunn system (Thuan and Gunn 1976) obtained by

Zinn (1980a) along with his index Q_{39}, which measures line blanketing near the K line. Columns 8–11 list three parameters characterizing the giant branch in the CMD and a fourth parameter quantifying the distribution of stars along the horizontal branch; definitions and values are taken from the compendium by Philip, Cullen and White (1976). Three estimates of the metals-to-hydrogen ratio (expressed logarithmically relative to the Sun) are given in columns 12–14. The method of Searle and Zinn (1978) is based on individual giant stars; Zinn's (1980a) estimate is based on Q_{39}, a measurement in integrated light; Kukarkin's (1975) procedure attempts to combine many indicators. The second part of Table 5 gives equivalent widths abstracted from Table 3 along with the composite metals index M (§ IIIb) and the coordinate along the first principal component.

With a wide variety of photometric and spectroscopic data, Table 5 bolsters the notion that the three clusters have very similar overall metallicities and indeed challenge the best available ranking techniques. On the other hand, the horizontal branch ranges from fairly red to very blue. What integrated properties reflect this degree of freedom? Of the photometric quantities, only the ultraviolet color hints at M13's blue horizontal branch. In a much broader sample, however, Zinn (1980a) remarks on the poor correlation of horizontal branch type with position within the scatter of his reddening-insensitive color-color relation. Given a common metallicity for M3 and M13 (particularly in view of nearly coincident giant branches), the equivalent widths in the blue region, consistently smaller for M13, do indicate a greater dilution of metallic features by light from blue stars. However – the main point of this section – it is striking that *the hydrogen lines themselves completely fail to indicate horizontal branch type.* In fact, on the basis of a composite index of spectral similarity, M13 and N7006 are among the most closely matched pairs of clusters in the whole sample. The high degree of similarity may be judged directly from the spectra in Figure 13.

We thus seem to face a somewhat discomforting situation: (1) abundance analyses show that clusters with nearly the same [Fe/H] may have very different horizontal branches; (2) Zinn's photometric data exhibit scatter in the dominant one-dimensional sequence which cannot be attributed to reddening or to observational error; (3) the present spectroscopic data single out the behavior behavior of the Balmer lines, which should be sensitive to the horizontal branch contribution; and yet, we are hard pressed to connect the second and third properties with the clearest examples of the first statement, the original "anomaly".

In the following sections this problem will be explored in more detail, since it implies a potentially serious deficiency in our ability to infer an underlying stellar population from integrated properties. However, it may first be established that the problem is not confined to the three clusters used as examples. Figure 14 shows the relationships of Hδ, Hγ, and Hβ to the Dickens (1972) horizontal branch type. The type ranges from 1 for very blue horizontal branches (M 13) to 7 for horizontal branches confined to the red side of the RR Lyrae gap (M 69, M 71, N 6356). Hδ shows no correlation with Dickens type. The weak correlation seen in Hβ may in part reflect metallic contamination, since, at least at the extremes of metallicity, composition and horizontal branch type are well correlated.

b) Effect of the Horizontal Branch: Balmer Lines and Dilution

The synthesis models used here will be completely described in Chapter 3. Briefly, they are based on the theoretical isochrones of Ciardullo and Demarque (1977), on model stellar atmospheres (Kurucz 1979; Bell and Gustafsson, 1978), and on empirical stellar data. In view of the importance of the Balmer lines, two complementary approaches to their calculation were adopted. In the first, SIT spectra of MK standard stars and stars with abundance analyses, all obtained with instrumentation nearly identical to that used to acquire the integrated spectra, are combined according to

the isochrones to yield synthetic spectra over the range λλ3750-4450 with 7 Å (FWHM) resolution. This approach realistically incorporates the effects of line blanketing and instrumental resolution. However, along the horizontal branch, particularly near the RR Lyrae gap, both temperature and gravity are changing rapidly in the very regime where the Balmer lines are most sensitive; this is best handled by a grid of theoretical line profiles (from Kurucz 1979). The resulting synthetic profiles are convolved with an approximation to the instrumental profile. Equivalent widths and central depths are then reckoned from a pseudocontinuum tied to the same nominal wavelengths as were established for the cluster spectra (Table 2).

Three standard distributions along the horizontal branch (HB) were derived from CMDs for 47 Tucanae, M3 and M92; RR Lyrae variables were of course included. As a reference approximation, the ratio of the number of stars on the horizontal branch to the number of stars on the giant branch above the horizontal branch (excluding asymptotic branch stars) was set at $R_{hbgb} = 1.6$ (Renzini 1977). In order to avoid confusion with the corresponding clusters, the horizontal branches modeled after 47 Tuc, M3 and M92 will be denoted RHB, BRHB, and BHB.

A selection of model results is given in Table 6 for the composition (Y, Z) = (0.3, 0.001). A power law form for the initial mass function has been assumed with index $s = 2.35$ (horizontal branch and asymptotic branch excepted). [$s = 2.35$ corresponds to $x = 1.35$ in Tinsley's notation.] The table emphasizes ratios of EWs since these are less sensitive to details of the synthesis procedure.

The horizontal branch markedly influences EW(Hδ), raising it by 60% as the type changes from red to blue. The two methods of Balmer line synthesis agree completely in this prediction. Enrichment is still substantial at Hβ, over 40%, but drops to 25% at Hα. Dilution by a BHB reduces the equivalent width of the K line by 30% from its value with an RHB; the effect is 20% at the G band.

Two remarks apply generally to the model results for the horizontal branch. First, the change from an intermediate HB to an extreme blue HB does not greatly affect most observational quantities. Equivalent widths typically change by less than 20%, broad band colors by less then 0.1 mag. Thus, such differences in HB structure are easily lost in comparing a given pair of objects and may even be difficult to establish systematically, in view of competing effects. Second, it is particularly interesting that $U-B$ is useless as a diagnostic of horizontal branch type, failing even to distinguish RHB from BHB. This lack of sensitivity is due to the double-valued nature of $U-B$ wth temperature and to the large bolometric corrections for blue stars.[4] Of course, far ultraviolet photometry can regain discrimination at the expense of sensitivity to small numbers of UV-bright stars (Welch and Code 1980; van Albada, de Boer and Dickens 1979). Also, the effect in $U-B$ is larger if a BHB is grafted onto a metal rich torso ($Z=0.01$); but no examples are seen in the Galaxy. It may be noted that the contribution of the horizontal branch to the total light in the U and B pass bands is *not* small: 24%, 23% and 17% in U for BHB, BRHB and RHB, and almost the same percentages for B. An RHB contributes almost as much light in U as does a BHB.

We may now confront more quantitatively the difficulty mentioned in the last section. Even allowing for the fact that the horizontal branch of N7006 is not as red as that of 47 Tuc, we expect Hδ–Hγ–Hβ to be 30–40% stronger than they are in N7006. The data in Table 5 deny this for each line. Figure 15 illustrates another aspect of the expected horizontal branch contribution. As the distribution changes from red to blue, K weakens, H+Hε strengthens, and the ratio of their central depths reverses. The CN–Fe–H blend strengthens dramatically. None of these tendencies is seen in the actual spectra. It seems necessary to conclude either that the horizontal branch is less important to the integrated spectrum than CMDs might lead one to suppose, or that the horizontal branch contribution is partially masked by other effects.

---

4. This result incidentally tends to discredit what appeared to be the only photometric indicator of M13's BHB.

c) Effects of Age, Luminosity Function, He Abundance, and the Number of HB Stars

Age. Table 6 gives equivalent widths and colors for ages 7–16 Gy; an RHB was assumed in order to allow the turnoff better to shine through. In brief, all effects are small over the range 10–16 Gy. Even a small uncertainty in the the relative metallicity of two clusters would obscure a difference in age. Only for ages $\lesssim$ 7 Gy (or, more generally, for turnoffs hotter than $\sim$ 7000 K) does Hδ begin to strengthen appreciably (the steepness of this effect with age will serve in Chapter 2 to establish the relative youth of some "intermediate age" clusters in the Magellanic Clouds). Thus, the variation in age required to decorrelate equivalent widths and horizontal branch type is so large that it cannot be considered seriously without strong independent evidence. Figure 14 also implies that the variation would necessarily have a systematic component in that clusters of high metallicity would be younger on average.

Despite its slight variation with age, the contribution of the main sequence to the blue light is large: about 50% in *U*, 45% in *B*. Of this, 70-80% is due to the first 2 mag below turnoff.

Luminosity function. Figure 16 shows that the variations in the pre-horizontal-branch luminosity function engendered by variations in the initial mass function from $s = 0$ through $s = 2.35$ to $s = 3.5$ have only a minor impact on the integrated spectrum over the range $\lambda\lambda$3750-4450.

Helium abundance. We here consider effects other than a possible direct influence on the horizontal branch. A change in He abundance from 0.3 to 0.2 shifts the giant branch by less than 15 K, an inconsequential amount. The main sequence become about 150 K cooler. Since only the turnoff region contributes importantly to the spectral range of the present data, the effect of such a shift is much like a change in age. However, even a change from 10 Gy to 13 Gy moves the turnoff by more than 250 K, and we have seen this to be undetectable in integrated light.

Number of horizontal branch stars. Table 7 shows that the effect of reducing R_{hbgb} from 1.6 to 0.9 is surprisingly modest: for a BHB, EW(Hδ) decreases by 15%; for an RHB, the increased contribution from the turnoff actually causes a slight increase in EW(Hδ). The change in $B-V$ is larger than typical photometric errors, but $U-B$ is again wholly insensitive.

The degree to which a variation in R_{hbgb} might be invoked as a cause of scatter in relationships involving HB type is both an observational and a theoretical problem. On the observational side, Iben *et al.* (1969) advocate $R_{hbgb} \approx 0.8-1.0$. Renzini (1977) instead finds $R_{hbgb} \approx 1.5-1.8$ from plate material extending to fainter magnitudes. That these two estimates should be quite different in magnitude but similar in range is perhaps not so surprising when the theoretical orientation is considered. Helium abundance, Y, is the only theoretical parameter known to affect strongly the relative lifetimes of stars on the giant branch and the horizontal branch, and a (nearly) universal Y is favored for reasons of economy and big-bang nucleosynthesis. For the purpose of interpreting integrated spectra, it is sufficient to note that if Y is taken to be a constant and if no other factor determines R_{hbgb}, then R_{hbgb} may usually be ignored – the *type* of horizontal branch is more important that moderate variations in its numerical weight. If R_{hbgb} is allowed to vary by (say) 50%, the most observable consequence (outside the far UV) might be increased scatter in a color-color plot (*e.g.*, Zinn 1980) due to changes in the blue-green continuum.

d) Summary and Observational Prospects

The synthesis models have suggested several sources for the variation of the Balmer lines, but none is dominant or able by itself to decorrelate Balmer line strength and horizontal branch type. Nevertheless, it would be premature to abandon either the observational indication of independence in the hydrogen lines or the synthesis models as a guide to the influence of different regions of the HR diagram.

Observational errors are clearly a significant source of scatter in Figure 14. It is important to remember that the range of the model results arising from variation of its parameters within reasonable limits *should* be smaller than the apparent range in the data. However, the unmistakable correlation between metallic lines as weak as and weaker than the Balmer lines (§IIIc) argues against error as the sole cause of the apparent independence. The principal components analysis emphasizes this point: if error is to blame, it must be error distinctive both in magnitude and in *kind*, so that of all the variables, only the Balmer lines separate from the main "cloud".

The observations necessary to place this argument on firm ground are straightforward. Since there are representative clusters of high central surface brightness for Dickens types 1–4, a fair fraction of the observing time must be devoted to types 5–7 in order to avoid systematic errors due to spectra of uneven quality. At least the region Hδ–Hα should be covered in order to exploit the gradient in the effect of the horizontal branch. Somewhat higher resolution ($\approx$ 1.5 Å FWHM) could help to expose metallic blends and might allow the Balmer line profiles to supply information beyond that contained in EWs. More important than specific parameters, however, is the observational experience (§IIb) that the potential of vidicon detectors to measure 10% variations in weak absorption features probably cannot be realized with "one good exposure," whatever its apparent statistical weight.

A final point will lead us into a specific examination of the M31 clusters. Of the factors considered in c) above, only relative youth could explain the fact that the hydrogen lines in M71 and in N6356 appear to be as strong as those in M13 and M15; the observed horizontal branches in the former clusters are too red to raise the Balmer line strength. Since the observed turnoff in M71 is also too red (whatever its age), one is forced to conclude that a factor not yet considered is at work in the metal rich globular clusters. It is interesting in this connection that van den Bergh (1969) uses two clusters from Morgan class VIII (the most strong lined) to illustrate

the statement, "there is some indication that the intensity of the hydrogen lines may differ between galactic globular clusters of similar metallicity."

VI. DISCUSSION OF THE M 31 CLUSTERS

The unique feature of the M 31 clusters in the present sample is the apparent strength of Hβ, particularly at the metal rich end. Comparing six M 31 clusters with a sample of galactic globulars, Faber, Gaskell and Burstein (1979) find that, given comparable strengths in the Mgb–MgH feature, Hβ in the M 31 clusters is about 30% stronger than it is in the galactic globulars. They attribute the excess to a larger contribution from A-type stars. The present data do not favor this interpretation. Hδ and Hγ should reflect the presence of A-type stars even more strongly than does Hβ, yet they are not significantly enhanced in M 31. However, as discussed in § IIc, these lines are more difficult to measure with respect both to absolute value and to consistency between M 31 and the Galaxy. Table 6 indicates that at Z = 0.001, the addition of horizontal branch stars in number sufficient to raise EW(Hβ) by 30% would also make $B-V$ bluer by about 0.07 mag, leaving $U-B$ unchanged; the effect is somewhat larger at Z = 0.01. If such an effect is present in M 31 over the full range of metallicity, accurate colors and individual reddenings such as those reported by Searle (1980) may allow the question to be addresed from a photometric viewpoint.

We have seen that the hydrogen lines in metal rich galactic globulars are not as weak as might have been supposed from their cool giant branches and red horizontal branches. There is at least suggestive evidence from Figure 14 and from van den Bergh (1969) that real variation also occurs within the metal rich group. It is worth inquiring whether this phenomenon could be related to the apparent Hβ excess in M 31. At least two possibilities can be suggested. First, there could be a degree of freedom in the equivalent widths of hydrogen lines arising from stars on the giant branch. Unfortunately, because of the influence of an extended atmosphere and

mass loss in cool giants, available theoretical models are an inadequate guide.[5] The effect of the giant branch would of course be greatest for clusters with cool turnoffs and red or stub horizontal branches, and this is consistent with the present data for the galactic globulars (and for M 31 if at least the most metal rich clusters have a red HB).

However, a second possibility is perhaps more plausible and is certainly easier to investigate. It will be shown below that for late-type stars of solar composition, observed with typical Cassegrain resolution, Hβ is seriously blended with metallic lines. Such blending could, to a lesser extent, increase the apparent equivalent width of hydrogen lines in metal rich globulars. An additional degree of freedom in this contamination, beyond overall metallicity, could account for the Hβ enhancement in M 31.

a) The Blended Nature of Hβ for Late-type Stars

The spectra in Figures 17–18 were obtained with the 1.5 meter telescope at Palomar. Both the spectrograph and the detector were essentially identical to those used on the 5 meter telescope to obtain the integrated spectra. Except for BS 7576, classified K3 III SMR by Spinrad and Taylor (1969), the stars are MK "dagger" standards from Morgan and Keenan (1973) (subsequently, King's notation, "HSL" for "hyperstrong-lined", will be preferred to "SMR"). Each final spectrum is a sum of many frames, on each of which the spectrum was greatly broadened. Each apparent feature is a real absorption.

The encroachment of a metallic feature in the red wing of Hβ is evident in Figure 17 as the spectral type proceeds from G0 III to K3 III. A solar atlas indicts multiplet

---

5. This may be verified by comparing, for example, the model profiles in Carbon and Gingerich (1969) with the Arcturus atlas (Griffin 1968); and for this reason, empirical profiles from echelle spectra of globular cluster stars, kindly made available by J. Cohen, were used to supplement Kurucz's models in the construction of the synthetic "theoretical" profiles of § V*b*.

318 of FeI as the main offender. In the case of Hδ, blending appears to infect the whole line profile. Figure 18 illustrates the "eaten-away" appearance of Hδ in BS 7576 and emphasizes that a blending feature has the potential to reduce the total equivalent width reckoned from a local pseudocontinuum, not just increase it as in the case of Hβ. In contrast, light from A-stars must strengthen all the hydrogen lines.

b) Evidence for Metallic Contamination of Balmer Lines in M 31 Clusters

Searle and Boksenberg have graciously made available a small set of high quality spectra of M 31 clusters which allows a better evaluation of the Balmer line problem than is possible with the SIT spectra. Their data were taken with the University College London Image Photon Counting System (Boksenberg and Burgess 1973) at the Cassegrain focus of the 5 meter telescope.

In Figures 19–20 the clusters have been arranged in order of increasing metallic line strength, culminating in a spectrum of the nucleus/inner bulge of M 31. The contamination of the red wing of Hβ grows with overall line strength until, at the nucleus, the effects of high metallicity and velocity dispersion combine to reform a beautiful "Hβ" profile. Similarly, Figure 20 recapitulates the erosion of Hδ shown in Figure 18.

Unfortunately, no spectra of galactic globular clusters were taken with this instrument, so future observations must test definitively the hypothesis that the excess Hβ strength in M 31 clusters is due to enhanced contamination (at given "overall metallicity"). However, these spectra leave no doubt that contamination becomes significant at metallicities well below solar. There is every reason to believe that the hydrogen lines in metal rich globular clusters such as M 71 are also affected.

c) Is the Hβ Excess a Hyperstrong Line Phenomenon?

It has been noted by many authors (*e.g.*, Spinrad and Taylor 1969; Faber 1972; O'Connell 1976) that population models of the nucleus/bulge of M 31 work better when they are allowed to draw from the synthesis library stars which have been by

some criterion deemed HSL for their nominal spectral types. Debate has raged over the possibilities that HSL stars have iron-to-hydrogen ratios significantly greater than the solar value, that some elements are selectively enriched, or that the enhanced line strengths are caused mainly by a difference in atmospheric structure; and the possibilities are not exclusive. There is similar uncertainty over whether the bulge of M31 should be assigned an overall metallicity around twice solar (Faber 1977) or whether the abundance of the iron peak elements is nearly solar (Faber 1977; Pritchet and Campbell 1980), thereby requiring other processes to enhance some metallic features (Peterson 1976).

If small but systematic differences in the pattern of line blanketing are the source of the separation between M31 clusters and galactic globulars, with the degree of freedom beyond overall metallity this implies, it is tempting at least to speculate on further connections with the HSL phenomenon.

Na D and Na I λ8190 have figured prominently in the discussion of supermetallicity, selective overabundances and dwarf-enrichment in the nucleus/bulge of M31 (Spinrad and Taylor 1971; Faber and French 1980; Pritchet and Campbell 1980). Figure 21 shows the integrated spectra of M69, K1/MII and K280/B282 in the immediate vicinity of Na D. From the composite iron index (§III*b*) and from the overall appearance of the blue spectra, M69 has stronger lines than K1 and somewhat weaker lines than K280. But Figure 21 indicates that Na D is as strong in K1 as it is in M69 and is markedly stronger in K280. This is only a tantalizing fragment, but it encourages further observations.

d) Concluding Note

Since considerable discussion has been expended on the possible sources of the Hβ excess in M31, it is appropriate to balance the scales by recalling how well a single sequence embraces the colors (Frogel, Persson and Cohen 1980; Searle 1980) and the

line strengths of old star clusters, both in M31 and in the Galaxy. Increasingly detailed observations of individual stars in galactic globulars still suggest only mild variations in the relative pattern of abundances *between* clusters (Kraft 1979). If selectively enhanced blanketing accounts for the Hβ excess in M31, it is nevertheless a perturbation which is usually able to masquerade as a small change in overall line strength, so that a short trip up or down the dominant sequence suffices to "renormalize" the errant cluster. The possibility of this secondary behavior can be noticed only when metallic lines blend with a hydrogen line which itself, from the evidence of the horizontal branch in galactic globular clusters, has a measure of independence from the larger scheme.

APPENDIX

USING ESTIMATES OF ERROR IN PRINCIPAL COMPONENTS ANALYSIS

I. INTRODUCTION

The large truth in stellar spectra is that temperature affects everything, usually more than anything else. It recalls the experience of Charles Spearman, a pioneer of multivariate techniques, who found in test of academic ability a "general intelligence factor" which always combined with specific skills to determine a student's scores in various subjects. For astronomy, temperature is that general factor. A change in an underlying physical parameter, such as metallicity, will often be recognized mainly as a temperature effect, such as a cooling of the giant branch.

So, if we seek structure beyond an overall sequence, we must accept that it will be relatively small. Errors in the data that hardly affect the primary sequence may seriously distort lesser dimensions. In § II I discuss the general problem of errors in the context of principal components analysis and outline a technique for eliminating the systematic effects of errors when they can be estimated (technical details are relegated to § III).

II. A UNIFIED APPROACH TO ERRORS AND SCALES

Even in spectra over a small wavelength range, features of widely varying strength will be found, the strongest not necessarily the most sensitive to the physical parameters of interest. Furthermore, we may wish to incorporate measurements different in kind, such as photometric colors, counts of RR Lyrae variables, or even nominal variables such as "horizontal branch type". For principal components analysis (PCA), this poses the much-discussed problem of scale.

A simple, determinate, universal and dangerous prescription is to scale all variables to have unit variance. This is the usual procedure in the social sciences and has

been followed in astronomical applications by Deeming (1964) and by Faber (1973). However, astronomers are fortunate in usually having one thing social scientists almost always lack: quantitative estimates of error in each variable, often separately for each object. I suggest that these estimates should be incorporated into the analysis *ab initio* rather than entering only in *a posteriori* tests of "significance".

Let us scale each variable by the standard deviation estimated to arise from errors alone,

$$x_j \rightarrow x_j/s_j$$

A geometric viewpoint will suggest an interpretation beyond mere scaling. Let the true (error-free) data be arrayed in the many dimensional space of variables roughly as a hyperellipsoid; the variables are highly correlated, so the principal axis is much larger than the others and points somewhere between the coordinate axes. For the moment, suppose the errors to be uncorrelated, so that the axes of their ellipsoid coincide with the coordinate axes. Already we see that the errors have a *directional* character which bears no relation to the directions intrinsic to the data. If some variables have errors much smaller than their total variance (usually the case for data worth analyzing), the long axis of the data is easy to find, even in the presence of competing error directions. However, if we analyze further, we must probe cross sections of the ellipsoid. It is these smaller dimensions which must be compared to the largest estimated error, since we have no way of knowing how the cross sectional plane will be oriented relative to the error ellipsoid. The second principal component (PC) of the errorful data may lie at a large angle to the true component. Scores along the errorful component have suboptimal variance and contain substantial contributions from the third true PC.

A preliminary scaling to unit *error* variance has the salutary effect of "spherizing" the error ellipsoid so that it can define no competing direction. The first PC will be

little affected. Subsequent components may or may not be significant, but the systematic distortion caused by errors has been purged to the extent that their relative sizes have been justly estimated.

By analogy, it is now clear how we should proceed in the case of correlated errors. We first find the principal components of the *error* covariance, thereby aligning the coordinate system with the principal axes of the error ellipsoid. Now we may spherize the errors by differential contraction or expansion along the new axes and still be free to effect a further rotation to the principal axes of the rescaled data.

It may also be noted that scaling by the error variance has introduced for each variable an intrinsic unit, so that changing the original measurement unit has no effect. Less obviously, scale invariance can be extended to the case of correlated errors (§III). This is of practical concern with photometric data, which are usually reported as colors, often with the same reference filter occuring in every color (in "reddening-free" colors, two or even three variables may be common to each). Forming colors is of clear advantage in reducing systematic errors but also ensures that the random errors are correlated. Other effects, such as reddening uncertain in amount or character, may produce correlated errors which we cannot prevent but can estimate.

For these *weighted principal components* (Mulaik 1972), a rough estimate of significance is immediate: since the error ellipsoid has been transformed into the unit sphere, the variance attributable to error along a line in any direction is unity, and this is the benchmark eigenvalue (more "precise" tests are dubiously founded – and have usually been applied incorrectly). However, significance is not the real issue. If the error-free data are largely confined to a low dimensional subspace of the full multivariate space, we wish primarily to ensure that the first few principal components span this and not another subspace. The significance of the configuration

can then be evaluated on extrinsic grounds. This viewpoint is strengthened by the consideration that ratios of error variances may often be estimated more securely than the values separately (reddening is a case in point), whereas *a posteriori* tests require such values.

III. FORMAL DEVELOPMENT

We make no attempt to motivate or explicate PCA in general; an introduction may be found in most texts on multivariate analysis.

a) Basic Equations

Write the basic equations of PCA as

$$\mathbf{X} = \mathbf{M} + \mathbf{E} = \mathbf{Y}\mathbf{F}' + \mathbf{E} \tag{1}$$

$$\mathbf{F}\mathbf{F}' = \mathbf{I} \tag{2}$$

$$\mathbf{C} = \mathbf{X}'\mathbf{X}/n = \mathbf{C}^* + \mathbf{U} \tag{3}$$

$$\mathbf{M}'\mathbf{E}/n = 0 \tag{4}$$

where $\mathbf{X}$, the $n \times m$ matrix of data, is composed of an error-free part $\mathbf{M}$ and a matrix of errors $\mathbf{E}$. $\mathbf{F}$ is the $m \times m$ collection of m orthonormal column eigenvectors. $\mathbf{Y}$ is the $m \times m$ collection of column components or latent variables. The observed covariance matrix $\mathbf{C}$ may also be decomposed into an error-free part $\mathbf{C}^*$ and a part $\mathbf{U} = \mathbf{E}'\mathbf{E}/n$ attributable to errors, using (4) which states that the errors are uncorrelated with the true values. $\mathbf{U}$ need not be diagonal.

We seek a transformation $\mathbf{Z} = \mathbf{X}\mathbf{K}$ which transforms $\mathbf{U}$ into $\mathbf{I}$, the unit matrix, and under that condition maximizes the variance of $\mathbf{Z}$:

$$\mathbf{Z}'\mathbf{Z}/n = \mathbf{K}'\mathbf{C}\mathbf{K} \quad .$$

Introduce the auxiliary function F representing the variance along the first transfor-

mation vector $\mathbf{k}_1$, with a Lagrange multiplier λ to enforce the sphericity condition:

$$F = \mathbf{k}_1' \mathbf{C} \mathbf{k}_1 - \lambda (\mathbf{k}_1' \mathbf{U} \mathbf{k}_1 - 1) \quad . \tag{5}$$

Differentiating,

$$\partial \mathbf{F} / \partial \mathbf{k}_1' = \mathbf{C} \mathbf{k}_1 - \lambda \mathbf{U} \mathbf{k}_1 = 0 \quad , \tag{6}$$

we arrive at

$$(\mathbf{C} - \lambda \mathbf{U}) \mathbf{k}_1 = 0 \quad . \tag{7}$$

For the full system of transformation vectors, this is the generalized eigenvalue problem

$$\mathbf{C} \mathbf{K} = \mathbf{U} \mathbf{K} \Lambda \quad , \tag{8}$$

which may be described as finding the eigenstructure of **C** *in the metric of the errors*, **U**. Assuming that **U** is nonsingular, (8) may also be written as

$$(\mathbf{U}^{-1} \mathbf{C}) \mathbf{K} = \mathbf{K} \Lambda \quad .$$

The eigenvectors and eigenvalues will be real, but since $\mathbf{U}^{-1}\mathbf{C}$ need not be symmetric (although $\mathbf{U}^{-1}$ and **C** are), the eigenvectors need *not* be orthogonal.

The formal structure of this problem is similar to that of Rao's canonical factor analysis, with the crucial difference that **U** is here given externally, not estimated from the communalities of the variables during the process of factor extraction.

b) Scale Invariance

Rescale **X** by the diagonal matrix **S**,

$$\mathbf{X}_s = \mathbf{X} \mathbf{S} \quad . \tag{9}$$

Then

$$\mathbf{F}_s = \mathbf{k}_1' \mathbf{S} \mathbf{C} \mathbf{S} \mathbf{k}_1 - \lambda (\mathbf{k}_1' \mathbf{S} \mathbf{U} \mathbf{S} \mathbf{k}_1 - 1) \quad . \tag{10}$$

Let

$$\mathbf{k}_{1s} = \mathbf{S}\mathbf{k}_1 \quad , \tag{11}$$

so that

$$\mathbf{F}_s = \mathbf{k}_{1s}'\mathbf{C}\mathbf{k}_{1s} - \lambda(\mathbf{k}_{1s}'\mathbf{U}\mathbf{k}_{1s} - 1) \quad . \tag{12}$$

Comparing with (5) above, we see that the rescaled problem yields the same eigenvalues and merely rescaled eigenvectors.

c) Interpretation as a Composite Principal Components Transformation

Consider the system $\mathbf{Q}$ of eigenvectors of U, the error covariance:

$$\mathbf{U}\mathbf{Q} = \mathbf{Q}\Lambda \quad . \tag{13}$$

We may define the square roots

$$\mathbf{U}^{\frac{1}{2}} = \mathbf{Q}'\Xi^{\frac{1}{2}}\mathbf{Q} \tag{14}$$

$$\mathbf{U}^{-\frac{1}{2}} = \mathbf{Q}'\Xi^{-\frac{1}{2}}\mathbf{Q} \quad ,$$

which are easily formed since Ξ is diagonal and which have the implied properties

$$\mathbf{U}^{\frac{1}{2}}\mathbf{U}^{-\frac{1}{2}} = \mathbf{U}^{-1} \tag{15}$$

$$\mathbf{U}^{-\frac{1}{2}}\mathbf{U}^{\frac{1}{2}} = \mathbf{U}^{-1} \quad .$$

$\mathbf{U}^{\frac{1}{2}}$ is symmetric.

In (7), substitute the auxiliary vector

$$\mathbf{v}_1 = \mathbf{U}^{\frac{1}{2}}\mathbf{k}_1 \quad , \tag{16}$$

yielding

$$\mathbf{C}\mathbf{U}^{-\frac{1}{2}}\mathbf{v}_1 = \lambda\mathbf{U}^{\frac{1}{2}}\mathbf{v}_1$$

or

$$[\,\mathbf{U}^{-\frac{1}{2}}\mathbf{C}\mathbf{U}^{\frac{1}{2}}\,]\mathbf{v}_1 = \lambda\mathbf{v}_1 \quad . \tag{17}$$

This may be illuminated by calculating, for

$$\tilde{\mathbf{X}} = \mathbf{X}\mathbf{U}^{-\frac{1}{2}} \quad , \tag{18}$$

the quantity

$$\tilde{\mathbf{X}}'\tilde{\mathbf{X}} = \mathbf{U}^{-\frac{1}{2}}(\mathbf{X}'\mathbf{X}/n)\mathbf{U}^{-\frac{1}{2}}$$

$$= \mathbf{U}^{-\frac{1}{2}}\mathbf{C}^*\mathbf{U}^{-\frac{1}{2}} + \mathbf{U}^{-\frac{1}{2}}\mathbf{U}\mathbf{U}^{-\frac{1}{2}}$$

$$= \mathbf{U}^{-\frac{1}{2}}\mathbf{C}^*\mathbf{U}^{-\frac{1}{2}} + \mathbf{I} \quad . \tag{19}$$

U represents a rotation to the principal components of the error ellipsoid. $\mathbf{U}^{-\frac{1}{2}}$ effects in addition a scaling so that the errors are spherized. $U^{-\frac{1}{2}}\mathbf{C}\mathbf{U}^{-\frac{1}{2}}$ results when **C** is subjected to the same transformation, and since the errors define no direction, we are free to maximize by rotation the transformed covariance without disturbing the error sphere. This is (17) above. Notice that $\mathbf{U}^{-\frac{1}{2}}\mathbf{C}\mathbf{U}^{-\frac{1}{2}}$ is symmetric, so that $\mathbf{V}\mathbf{V}' = \mathbf{I}$. However, the overall transformation

$$\mathbf{Y} = \mathbf{X}\mathbf{U}^{-\frac{1}{2}}\mathbf{V}$$

is *not* a rotation; because of the scaling, the latent variables form an oblique system when viewed in the space of the original variables.

TABLE 1

OBSERVATIONS

Cluster	Other Name	L	Exposure (s)	n
M31				
K 1	MII	10	250	6
3			1000	1
29	V2		2000	2
33	V4	1	850	3
38	V5		1000	2
58	V55	11	1000	3
76	V12	8	500	5
78	V42	14	1000	2
104	V227		2000	2
130	V32		1800	2
144	V39		500	1
148	V62	5:	500	6
170	V56		1200	4
189			1000	1
204			750	1
213	V64	8	500	2
217	V100	13:	1000	2
229	V95		400	2
244	V116	12	500	2
258			1000	1
272	V101	9	1000	1
280	V282	15	800	7
302	V196	4	600	2
305	V125		1200	2
351	V140	8	1000	1
bulge			100	10

Cluster	Other Name	Class	Exposure (s)	Scan Range (")	n
Galaxy					
5272	M3	II	600	220	2
5904	M5	II	700	145	2
6205	M13	III	750	225	2
6341	M92	I	400	195	2
6356		VI	900	55	3
6441			400	40	2
6522		IV	500	70	2
6637	M69	VII	500	95	2
6712		V	1500	110	2
6838	M71	VI	2500	145	3
7006		II	1500	50	5
7078	M15	I	500	90	2
7089	M2	II	750	150	1

TABLE 2

MEASURED ABSORPTION FEATURES

No.	λ_-	λ_+	Feature
1	3805	3895	CN, FeI
2	3915	3951	CaII K
3	3951	3990	CaII H, Hε
4	4026	4040	
5	4072	4091	
6	4091	4113	Hδ , FeI
7	4127	4139	
8	4139	4164	
9	4164	4190	
10	4190	4211	
11	4220	4234	CaI
12	4267	4280	
13	4280	4320	G band
14	4320	4330	
15	4330	4349	Hγ
16	4378	4397	FeI
17	4452	4477	
18	4507	4545	
19	4613	4697	weak blends
20	4697	4797	weak blends
21	4850	4879	Hβ
22	4898	4932	
23	4950	4977	
24	5035	5060	
25	5060	5092	
26	5092	5121	
27	5121	5162	
28	5162	5202	MgI b_{1+2+4} , MgH
39	5202	5220	
30	5220	5245	
31	5245	5283	

TABLE 3

EQUIVALENT WIDTHS (Å)

Cluster	FEATURE															
	1	2	3	4	5	6	7	8	9	10	11	12	13	14	15	16
M31																
K 1	23.3	9.8	9.0	0.6	1.1	2.6	0.5	0.8	0.8	0.7	0.8	0.8	5.4	0.7	1.4	0.9
3	28.3	16.2	12.4	2.7	4.0	2.3	1.1	2.2	4.2	2.1	3.9	1.8	11.5	2.0	1.0	2.0
29	32.4	13.7	9.0	0.4	1.2	1.8	0.2	1.4	1.2	1.1	1.0	0.6	6.0	1.2	1.6	1.0
33	16.2	5.5	5.6	0.4	0.9	3.2	0.3	0.5	-0.1	0.2	0.3	0.1	2.2	0.4	2.1	0.3
38	19.4	4.2	9.6	0.2	0.0	10.4	0.7	0.1	0.0	0.3	0.7	0.6	1.2	0.0	6.9	0.4
58	50.5	13.5	10.6	0.2	1.7	2.8	0.6	1.7	0.7	2.8	1.7	2.2	7.3	1.4	2.0	1.6
76	13.7	8.8	7.9	0.4	0.4	3.0	0.6	1.3	0.6	0.8	0.9	0.6	4.4	0.5	1.5	0.4
78	18.8	11.1	8.5	0.5	0.7	3.3	0.4	0.8	0.7	0.7	0.8	0.8	6.1	0.7	1.6	0.9
104	33.0	14.7	12.1	1.4	0.3	2.2	0.6	1.6	1.7	2.2	...	0.5	6.7	1.0	2.3	1.2
130	25.7	11.2	10.5	0.9	0.2	3.2	1.1	2.5	2.4	1.0	1.4	1.6	8.1	1.5	1.4	1.9
144	50.1	18.1	10.5	0.1	0.4	1.0	0.8	3.0	3.9	1.3	3.4	1.1	7.7	1.3	2.4	1.2
148	11.4	6.6	7.5	1.0	1.2	2.9	0.8	1.0	0.8	0.7	0.6	0.7	2.3	0.3	1.9	0.4
170	32.6	12.7	10.5	1.3	2.3	2.5	0.4	2.0	2.9	1.2	1.4	1.2	7.6	1.3	2.2	1.2
189	27.6	10.4	6.9	0.9	0.0	2.5	0.2	1.7	2.4	1.4	1.3	0.8	5.0	1.2	2.3	1.0
204	39.0	14.1	11.6	3.1	0.7	2.7	1.9	1.8	2.4	2.0	...	2.3	8.1	1.9	1.5	2.1
213	22.4	12.3	10.0	0.6	0.8	1.4	0.3	1.4	0.2	1.0	0.9	1.1	5.3	0.8	2.0	1.6
217	34.2	13.2	9.4	0.5	0.6	1.9	0.3	2.1	1.6	1.3	1.1	1.2	7.5	1.3	1.5	1.6
229	19.5	6.7	8.0	0.7	2.2	2.4	0.5	1.0	1.2	1.0	0.6	1.0	5.4	0.3	1.9	0.8
258	21.6	11.6	11.3	1.0	0.4	2.1	0.4	1.3	1.7	0.3	0.9	0.8	4.7	...	2.8	1.9
272	21.5	10.4	9.1	1.0	0.7	3.4	1.3	1.7	2.0	0.7	0.9	0.8	5.0	0.8	1.3	0.7
280	28.5	12.1	8.2	1.4	0.6	2.5	0.7	1.0	1.2	1.2	1.3	1.0	6.3	1.1	1.7	1.2
305	22.8	12.6	9.2	1.2	1.3	1.6	0.9	0.9	0.8	0.9	1.3	0.9	6.8	1.0	1.9	0.9
Bulge 1	33.1	11.6	8.7	0.9	0.4	1.8	0.5	1.5	1.5	0.7	1.4	1.2	6.1	0.7	0.9	1.6
Bulge 2	28.8	11.3	8.1	0.9	0.5	1.6	0.5	1.3	1.2	0.7	1.3	1.1	6.7	0.9	0.8	1.6

NOTE.----Bulge 1 is a slit sample through the M31 nucleus and inner bulge to a radius of about 4".
Bulge 2 includes light between 8" and 45" radius.

TABLE 3 - Continued

EQUIVALENT WIDTHS (Å)

Cluster	FEATURE														
	17	18	19	20	21	22	23	24	25	26	27	28	29	30	31
M31															
K 1	1.8	1.4	1.7	2.1	3.3	0.9	0.5	1.1	1.3	1.0	1.8	3.5	0.5	0.8	2.1
3	2.9	2.7	4.3	4.6	2.2	2.9	0.7	2.5	2.1	2.0	5.1	6.8	1.2	1.1	6.7
29	2.2	2.5	1.7	3.2	2.0	1.4	1.1	0.8	1.1	1.6	3.0	3.8	0.7	0.8	3.4
33	0.7	0.7	1.6	2.3	2.2	0.6	0.2	0.6	0.7	0.4	1.1	2.2	0.3	0.7	1.3
38	0.7	1.1	4.0	5.3	8.9	1.2	1.5	1.3	0.1	-0.1	-0.3	0.9	1.1	1.3	1.0
58	2.1	1.8	3.2	5.9	3.5	4.1	1.0	2.0	0.8	0.8	2.4	5.1	0.4	1.4	4.7
76	1.4	2.0	1.9	1.7	2.5	0.8	0.4	1.2	1.5	0.8	1.2	2.2	0.3	1.2	2.5
78	1.1	2.2	1.6	2.0	2.2	1.2	0.3	1.0	0.9	1.1	1.7	3.7	0.6	1.4	1.8
104	2.1	2.2	2.3	2.0	2.9	1.5	1.0	0.4	2.0	1.3	2.8	3.8	1.1	0.5	2.0
130	2.5	2.9	3.0	5.1	2.6	1.8	2.1	1.5	2.0	1.6	2.8	5.4	0.8	1.0	5.2
144	1.8	5.5	4.5	8.3	2.8	2.5	1.5	0.6	2.5	1.9	1.9	3.4	0.6	1.3	4.4
148	0.6	1.0	2.0	3.7	2.5	0.4	1.4	0.3	1.0	0.8	1.3	1.8	0.7	1.1	0.8
170	2.2	3.3	4.7	6.6	3.1	2.1	3.6	0.5	2.1	2.2	4.2	6.5	1.9	1.6	5.9
189	2.3	1.7	4.1	4.2	1.7	0.5	1.6	0.5	1.5	1.8	2.1	3.8	0.9	1.5	-0.1
204	3.2	3.7	5.6	8.1	3.5	2.7	1.8	2.4	2.3	2.4	3.9	7.9	1.7	1.4	3.8
213	1.3	1.0	3.3	6.7	2.2	1.0	0.7	0.4	1.1	1.1	2.4	3.5	0.8	1.2	3.0
217	1.7	2.2	5.0	2.7	3.2	1.7	0.2	1.9	1.9	1.9	3.9	7.3	1.5	1.0	2.8
229	1.2	1.0	2.9	2.2	2.3	1.2	0.9	1.6	1.1	0.9	1.4	2.6	1.0	1.1	3.3
258	2.0	3.2	1.7	4.3	2.8	1.2	-0.1	1.6	1.4	1.3	1.8	3.5	0.3	0.7	1.6
272	0.3	2.2	1.8	2.5	2.5	0.5	0.9	0.5	1.6	1.4	2.1	2.5	0.6	-0.1	0.9
280	2.0	1.7	3.1	2.5	2.1	1.6	0.7	1.7	1.7	1.6	3.2	5.4	0.8	1.0	3.8
305	2.3	1.7	2.0	3.3	2.5	1.6	0.6	1.2	1.9	1.5	2.5	4.6	0.8	1.0	3.4
Bulge 1	2.3	2.0	3.2	3.0	2.1	1.3	0.7	1.2	1.6	0.9	1.3	5.7	1.1	0.8	3.8
Bulge 2	2.2	1.8	2.5	2.9	1.9	1.2	0.7	1.1	1.5	0.8	1.1	5.5	0.9	0.7	3.0

TABLE 3 - Continued

EQUIVALENT WIDTHS (Å)

Cluster	FEATURE															
	1	2	3	4	5	6	7	8	9	10	11	12	13	14	15	16
Galaxy																
5272	12.7	7.6	7.6	0.3	0.6	2.4	0.4	0.5	0.6	0.4	0.4	0.5	3.5	0.3	1.6	0.3
5904	11.9	6.2	8.0	0.3	0.3	3.1	0.4	0.5	1.1	0.6	0.5	0.4	3.3	0.2	2.0	0.3
6205	11.9	5.7	6.7	0.3	0.4	2.6	0.3	0.8	0.3	0.5	0.4	0.2	2.3	0.1	1.8	0.3
6341	10.7	4.0	5.0	0.2	0.0	3.0	0.4	0.4	0.2	0.3	0.4	0.2	2.1	0.2	1.8	0.4
6356	27.0	12.7	8.7	0.6	1.1	2.9	0.5	1.5	1.7	1.1	1.3	0.8	6.9	1.1	1.6	1.1
6441	23.6	11.8	10.8	0.7	1.0	3.5	0.6	1.1	1.4	0.7	1.2	0.8	5.9	0.9	1.7	0.9
6522	14.4	8.4	10.9	0.4	1.1	3.2	0.5	1.3	0.9	0.4	1.0	0.8	3.8	0.4	1.5	0.6
6637	20.9	13.5	9.6	0.1	0.7	2.2	0.4	1.1	1.1	1.0	1.4	1.0	7.0	0.8	1.2	0.7
6712	14.4	9.0	9.6	0.8	0.9	2.5	0.6	1.2	0.9	0.8	0.8	0.3	6.1	0.6	1.4	0.6
6838	27.8	10.3	7.9	1.2	2.7	3.0	0.8	1.3	1.6	1.3	1.1	1.4	7.3	1.5	1.7	0.4
7006	13.9	5.8	7.0	0.3	0.4	2.8	0.2	0.5	0.6	0.9	0.4	0.5	2.9	0.2	2.0	0.3
7078	8.4	2.9	6.1	0.2	0.2	2.5	0.1	0.5	0.4	0.1	0.2	0.0	0.9	0.1	1.9	0.2
7089	13.5	6.0	7.1	0.3	0.5	2.9	0.5	0.6	0.7	0.2	0.5	0.4	3.8	0.3	1.8	0.2

TABLE 3 - Continued

EQUIVALENT WIDTHS (Å)

Cluster	FEATURE														
	17	18	19	20	21	22	23	24	25	26	27	28	29	30	31
Galaxy															
5272	0.7	0.7	1.2	1.6	1.9	0.7	0.6	0.8	0.7	0.8	1.1	1.6	0.2	0.7	1.6
5904	0.6	0.8	0.8	1.9	2.7	0.6	0.3	0.6	0.5	0.6	1.5	2.1	0.2	0.4	1.1
6205	0.7	1.0	0.8	1.5	2.4	0.3	0.3	0.6	0.7	0.5	0.7	1.3	0.3	0.3	0.4
6341	0.5	0.3	0.8	0.7	2.4	0.2	0.4	0.8	0.7	0.3	0.6	1.1	0.0	0.5	0.7
6356	1.6	1.7	1.8	2.2	2.2	1.3	0.7	1.2	1.3	1.0	2.5	4.5	0.8	0.9	2.3
6441	1.4	1.6	2.0	2.3	1.7	0.9	0.7	0.9	1.3	0.7	1.8	4.0	0.7	0.6	2.1
6522	1.0	1.0	1.1	2.5	1.9	0.7	0.3	0.8	0.9	0.8	1.4	3.0	0.8	0.4	1.5
6637	1.7	2.2	2.7	3.3	1.9	1.1	1.3	1.3	1.5	0.4	1.8	4.2	0.9	0.9	...
6712	1.0	0.8	1.6	1.8	1.9	0.8	0.3	1.0	1.8	0.8	1.7	2.8	0.4	1.1	1.5
6838	1.1	2.2	4.6	4.1	1.5	1.8	0.4	0.9	1.5	0.7	2.2	4.0	0.6	1.0	2.7
7006	0.5	0.8	0.9	1.4	2.4	0.6	0.6	0.7	0.8	0.7	1.0	1.4	0.2	0.8	1.3
7078	0.1	0.2	0.6	0.7	2.1	0.1	0.3	0.4	0.4	0.7	0.4	1.3	0.2	0.3	0.7
7089	0.5	0.6	0.7	1.2	2.5	0.5	0.4	0.7	1.1	0.7	1.4	1.8	0.4	0.5	0.9

TABLE 4

VALUES OF [Fe/H] FOR CLUSTERS IN M31 AND IN THE GALAXY

Cluster	[Fe/H]		Cluster	[Fe/H]	
	Zinn Scale	Modified Scale		Zinn Scale	Modified Scale
K 1	-0.88	-1.17	N 5272	-1.57	-1.63
29	-0.40	-0.85	5904	-1.65	-1.68
33	-1.85	-1.82	6205	-1.89	-1.84
76	-1.21	-1.39	6341	-2.11	-1.99
78	-0.71	-1.06	6356	-0.35	-0.82
104	-0.27	-0.76	6441	-0.62	-0.99
130	0.00	-0.58	6522	-1.26	-1.43
148	-1.63	-1.67	6637	-0.32	-0.79
170	0.46	-0.27	6712	-0.99	-1.24
189	-0.69	-1.04	6838	-0.47	-0.90
204	0.78	-0.06	7006	-1.76	-1.76
213	-0.67	-1.03	7078	-2.34	-2.14
217	0.09	-0.52	7089	-1.65	-1.68
229	-1.17	-1.37			
258	-0.67	-1.03			
272	-0.95	-1.22			
280	-0.38	-0.84			
305	-0.35	-0.82			

TABLE 5

MEASURED PROPERTIES OF M3, M13 AND NGC 7006

Cluster	Integrated Photometry							CMD				[Fe/H]		
	1	2	3	4	5	6	7	8	9	10	11	12	13	14
	$(U-B)_o$	$(B-V)_o$	$(V-K)_o$	E(B-V)	Q(ugr)	Q(vgr)	Q_{39}	$(B-V)_{o,g}$	$S_{0.6}$	ΔV	B/B+R	SZ	Z	K
5272	0.09	0.68	2.05	0.01	0.13	0.06	0.07	0.82	4.49	2.70	0.56	-1.7	-1.7	-1.4
6205	0.01	0.67	2.35	0.02	0.08	0.05	0.06	0.80	4.75	2.61	0.97	-1.6	-1.7	-1.5
7006	0.10	0.65	2.16	0.09[a]	0.13	0.07	0.10	0.70	4.27	2.65	0.25	-1.5	-1.5	-1.5

	Integrated Spectrum Equivalent Width (Å)								
Cluster	CN	K	H+Hε	G band	Hδ	Hγ	Hβ	M	PC1
5272	12.7	7.6	7.6	3.5	2.1	1.6	1.9	6.0	8.5
6205	11.9	5.7	6.7	2.3	2.6	1.8	2.4	5.4	13.8
7006	13.9	5.8	8.0	2.9	2.8	2.0	2.4	5.8	11.7

[a] Harris and Racine (1979): 0.13; Zinn (1980a): 0.05.

TABLE 6

EQUIVALENT WIDTHS AND UBVK COLORS FROM SYNTHESIS MODELS

$Y = 0.3 \quad Z = 10^{-3} \quad s = 2.35$

Effect of Horizontal Branch (at 13 Gy)

Feature /Color	Horizontal Branch Type			
	Red		Red/Blue	Blue
Hδ	1	1.33	1.61	
	2.81	3.73		4.53
K	1	0.84	0.69	
	9.99	8.37		6.90
G band	1	0.88	0.78	
	4.59	4.04		3.57
U-B	0.13	0.12		0.11
B-V	0.76	0.69		0.65
V-K	2.26	2.20		2.21

Effect of Age (with Red HB)

Feature /Color	Age (Gy)			
	7	10	13	16
Hδ	1.33	1.13	1.05	1
	3.57	3.04	2.81	2.68
K	0.88	0.97	0.98	1
	8.95	9.82	9.99	10.16
G band	0.84	0.88	0.97	1
	3.99	4.19	4.59	4.74
U-B	0.09	0.10	0.13	0.19
B-V	0.66	0.72	0.76	0.82
V-K	2.11	2.23	2.26	2.45

Balmer Line Ratios
from Theoretical Profiles (at 13 Gy)

Feature /Color	Horizontal Branch Type		
	Red	Red/Blue	Blue
Hδ	1	1.39	1.60
Hβ	1	1.29	1.44
Hα	1	1.18	1.24

NOTE.—in first two sections, second line gives equivalent widths (Å); first line is normalized to ratios.

TABLE 7

EFFECT OF REDUCING THE NUMBER OF HORIZONTAL BRANCH STARS

Age = 13 Gy Y = 0.3 Z = 0.001 s = 2.35

HB Type	Ratio $EW(R_{0.9})$ / $EW(R_{1.6})$		Difference $Color(R_{0.9})$ - $Color(R_{1.6})$		
	Hδ	Ca K	Δ(U-B)	Δ(B-V)	Δ(V-K)
Red	0.95	1.00	0.002	0.007	0.027
Red/Blue	0.94	1.05	0.006	0.033	0.049
Blue	0.89	1.12	0.007	0.046	0.050

REFERENCES

Aaronson, M., Cohen, J. G., Mould, J., and Malkan, M. 1978, *Ap. J.*, 223, 824.

Ables, H. D., and Ables, P. G. 1977, *Ap. J. Suppl.*, **34**, 245.

Arp, H. C., and Hartwick, F. D. A. 1971, *Ap. J.*, **167**, 499.

Bell, R. A., and Gustafsson, B. 1978, *Astr. Ap. Suppl.*, **34**, 229.

Boksenberg, A., and Burgess, D. E. 1973, in *Astronomical Observations with Television Type Sensors*, ed. J. W. Glaspey and G. A. H. Walker (Vancouver: Univ. Brit. Col.).

Carbon, D. F., and Gingerich, O. 1969, in *Theory and Observations of Normal Stellar Photospheres*, ed. O. Gingerich (Cambridge: M.I.T. Press), p.377.

Carney, B. W. 1980, *Ap. J. Suppl.*, **42**, 481.

Catell, R. B. 1978, *The Scientific Uses of Factor Analysis* (New York: Plenum).

Ciardullo, R. B., and Demarque, P. 1977, *Trans. Yale Univ. Obs.*, **33, 34, 35.**

Cohen, J. G. 1979, *Ap. J.*, **228**, 405.

-----. 1980, *Ap. J.*, in press.

Deeming, T. J. 1964, *M. N. R. A. S.*, **157**, 281.

Demarque, P., and McClure, R. D. 1977, *Ap. J.*, **213**, 716.

-----. 1977, in *The Evolution of Galaxies and Stellar Populations*, ed. B. M. Tinsley and R. B. Larson (New Haven: Yale Univ. Obs.), p. 199.

Dickens, R. J. 1972, *M. N. R. A. S.*, **157**, 281.

Dickens, R. J., Bell, R. A., and Gustafsson, B. 1979, *Ap. J.*, **232**, 428.

Eggen, O. J., Lynden-Bell, D., and Sandage, A. R. 1962, *Ap. J.*, **136**, 748.

Faber, S. M. 1972, *Astr. Ap.*, **20**, 361.

-----. 1973, *Ap. J.*, **179**, 731.

-----. 1977, in *The Evolution of Galaxies and Stellar Populations*, ed. B. M. Tinsley and R. B. Larson (New Haven: Yale Univ. Obs.), p. 157.

Faber, S. M., and French, H. B. 1980, *Ap. J.*, **235**, 405.

Faber, S. M., Gaskell, C. M., and Burstein, D. 1979, *Bull. A.A.S.*, **11**, 431.

Frogel, J. A., Persson, S. E., and Cohen, J. G. 1980, preprint.

Griffin, R. F. 1968, *A Photometric Atlas of the Spectrum of Arcturus* (Cambridge: Cambridge Philosophical Society).

Hanes, D. A. 1977, *M. N. R. A. S.*, **179**, 331.

Harris, W. E., and Racine, R. 1979, *Ann. Rev. Astr. Ap.*, **17**, 241.

Hartwick, F. D. A. 1970, *Ap. J.*, **161**, 845.

Hartwick, F. D. A., and Vanden Berg, D. A. 1973, *Ap. J.*, **185**, 887.

Hubble, E. 1932, *Ap. J.*, **76**, 44.

Iben, I., Jr., Rood, R. T., Strom, K. H., and Strom, S. E. 1969, *Nature*, **224**, 1006.

Kendall, M. G., and Stuart, A. 1973, *The Advanced Theory of Statistics* (Vol. 2), third edition (London: Griffin), p. 391 *et seq.*

Kent, S. M. 1979, *Pub. A. S. P.*, **91**, 394.

Kinman, T. D. 1963, *Ap. J.*, **137**, 213.

Kraft, R. P. 1979, *Ann. Rev. Astr. Ap.*, **17**, 309.

Kron, G. E., and Mayall, N. U. 1960, *A. J.*, **65**, 581.

Kukarkin, B. V. 1975, *Globular Star Clusters* (Washington: NASA Technical Translation).

Kurucz, R. L. 1979, *Ap. J. Suppl.*, **40**, 1.

Morgan, W. W. 1959, *A. J.*, **64**, 432.

Morgan, W. W., and Keenan, P. C. 1973, *Ann. Rev. Astr. Ap.*, **11**, 29.

Mulaik, S. A. 1972, *The Foundations of Factor Analysis* (New York: McGraw-Hill).

O'Connell, R. W. 1973, Ph.D. thesis, California Institute of Technology.

-----. 1976, *Ap. J.*, **206**, 370.

Oke, J. B., and Schild, R. E. 1970, *Ap. J.*, **161**, 1015.

Peterson, R. C. 1976, *Ap. J. (Letters)*, **210**, L123.

Philip, A. G. D., Cullen, M. F., and White, R. E. 1976, *Dudley Obs. Report*, No. 11.

Pilachowski, C. A., Wallerstein, G., and Leep, E. M. 1980, *Ap. J.*, **236**, 508.

Pritchet, C. 1977, *Ap. J. Suppl.*, **35**, 397.

Pritchet, C., and Campbell, B. 1980, preprint.

Pritchet, C., and van den Bergh, S. 1977, *Ap. J. Suppl.*, **34**, 101.

Racine, R. 1973, *A. J.*, **78**, 180.

Renzini, A. 1977, in *Advanced Stages of Stellar Evolution*, ed. P. Bouvier (Geneva: Geneva Obs.), p. 213.

Sandage, A. R., and Wildey, R. 1967, *Ap. J.*, **150**, 469.

Sargent, W. L. W., Kowal, C. T., Hartwick, F. D. A., and van den Bergh, S. 1977, *A. J.*, **82**, 947.

Schechter, P. L., and Gunn, J. E. 1979, *Ap. J.*, **229**, 472.

Searle, L. 1978, invited presentation at NATO Advanced Study Institute on Globular Clusters, Cambridge, England.

Searle, L., and Zinn, R. 1978, *Ap. J.*, **225**, 357.

Searle, L. 1980, in preparation.

Simkin, S. M. 1979, *Ap. J.*, **234**, 56.

Spinrad, H., and Schweizer, F. 1972, *Ap. J.*, **171**, 403.

Spinrad, H., and Taylor, B. J. 1969, *Ap. J.*, **157**, 1279.

-----. 1971, *Ap. J. Suppl.*, **22**, 445.

Thuan, T. X., and Gunn, J. E. 1976, *Pub. A. S. P.*, **88**, 543.

van Albada, T. S., de Boer, K. S., and Dickens, R. J. 1979, *Astr. Ap. (Letters)*, **75**, L11.

van den Bergh, S. 1967, *A. J.*, **72**, 70.

-----. 1969, *Ap. J. Suppl.*, **19**, 145.

Vetesnik, M. 1962, *B.A.C.*, **13**, 180.

Welch, G. A., and Code, A. D. 1980, preprint.

Zinn, R. 1980a, *Ap. J. Suppl.*, **42**, 19.

-----. 1980b, *Ap. J.*, **241**, in press.

FIGURE CAPTIONS

Figure 1. The integrated spectrum of the M 31 cluster K213 = V64, with adopted pseudocontinuum segments shown. van den Bergh's line strength classification is $L = 8$. The original spectrum has been detrended and smoothed to a "velocity dispersion" of $\sigma = 100$ km s^{-1}. Noteworthy features are: (1) the difficulty of defining, particularly blueward of the G band, any smooth pseudocontinuum for which the resulting equivalent widths would not depend *as much on the adopted curve as on the absorption features themselves;* for K280 or K130, the difficulty is still worse. (2) the absence of feature "sidebands" which are both local to the target feature and consistently weak with respect to it. (3) the dip in and the extension of the red wing of "Hβ", and the eroded red wing of "Hδ"; the possible significance of these features is discussed in § V.

Figure 2. A comparison of van den Bergh's photographic classification index L with the quantitative parameter $\mathcal{L}$ (from the present data). L and $\mathcal{L}$ are based on the same features. L correlates very well with $\mathcal{L}$ for most of the range but appears to lose sensitivity at the greatest line strengths. The short and the long error bars give van den Bergh's estimates of the internal errors of L for the Galaxy and for M 31.

Figure 3. The correlations between L and quantitative measurements of its constituent features show no evidence for the systematic separation of M 31 clusters and galactic globular clusters which was seen in van den Bergh's original data. As in Figure 2: *filled circles*, M 31 clusters; *open circles*, galactic globular clusters. The λ4325 feature of CH and Fe is unusual in showing almost dichotomous behavior with overall line strength; this is probably associated with its position between Hγ and the G band.

Figure 4. Correlations between the equivalent widths of different metallic features. Here and in subsequent figures: *filled circles*, M 31 clusters; *open circles*, galactic globular clusters; *open circle with central dot*, nucleus and inner bulge of

M 31, to about 4" radius; *annulus*, M 31 bulge between 8" and 45" radius; *circled cross*, a composite "cluster" comprising M 15, N 7006, N 6522 and N 6441 in equal measure (note the range of metallicity); *triangle*, bright star cluster in the WLM galaxy (Ables and Ables 1977). (*a*) and (*b*) show pairs of related features of Ca and CH. The flat behavior of λ4325, seen in Figure 3*b* for weak lined objects, is again evident. (*c*)–(*e*) plot the K line against the G band, Mg b (triplet) and the violet CN (+Fe+H) feature; the correlations are not discernibly weaker than those in (*a*) and (*b*). There is no separation between M 31 clusters and galactic globular clusters.

Figure 5. The major features (*a*) CaK, (*b*) the G band and (*c*) Mg b are plotted against *M*, a composite index of metallic line strength defined in the text (*Symbols*: see Figure 4). Each feature follows overall line strength, with no evidence for an independent component beyond the expected errors. Again there is no separation between the two familes of clusters.

Figure 6. *H*, the sum of the equivalent widths of Hδ, Hγ and Hβ, is plotted against (*a*) CaK, (*b*) Mg b, and (*c*) the metals index *M*. There is a slight negative correlation in each case, but the scatter is much larger than the scatter in the comparable relations of Figure 5. This is particularly striking in (*c*), where two composite indices are compared, each having large equivalent width.

Figure 7. The galactic globular clusters show a definite negative correlation between Hβ and (*a*) CaK or (*b*) Mg b (although, again, with more scatter than is seen in the correlation between any two metallic lines). In the M 31 clusters, Hβ weakens little, if at all, with increasing metallic line strength; thus, for metal rich clusters, Hβ is on average considerably stronger in M 31. This behavior is the first definite point of separation between the families of old star clusters in M 31 and in the Galaxy. (*c*) The scatter of Hδ against CaK.

Figure 8. The *solid line* connects the variances of the error-weighted EWs as pro-

jected along each of the first 20 principal components (directions) in turn. The strong dominance of the first PC shows that the integrated spectra are drawn from a predominantly one-dimensional distribution. Moreover, behavior which differs systematically between clusters in M31 and clusters in the Galaxy must be distinctly weaker than the overall sequence. The *crosses* repeat the variances on a scale expanded fivefold. Two *line segments* delimit the "scree" at the base of the mountain of variation (Catell 1978) and suggest that at most four components could reflect significant structure.

Figure 9. Each point in this diagram represents one of the original variables (EWs); some of the major features are labelled. The coordinates of a point are the correlations of that variable with the first two principal components. A single, compact cluster comprises all of the variables except three: Hδ, Hγ and Hβ. The Balmer lines depend on the overall sequence less than any other feature in the integrated spectrum.

Figure 10. The strength of the G band is tightly correlated with the first principal component. Since PC1 and the metals index M are both linear combinations of the original variables, comparison may be made to Figure 5*b*. PC1 is even better than M as a tracer of the dominant sequence. (Because of scaling transformations, the strength of the G band in this figure is not equivalent width.)

Figure 11. The structure of the plot is the same as in Figure 10, but the axes now represent PC2 and PC3. The variables form a single, amorphous cluster (the outlier is a feature in the blue which is too weak to have independent significance).

Figure 12. The strength of Hβ does not correlate with PC2. Thus, the second principal component would not point to the feature that is most independent of the dominant sequence. However, the Balmer lines *are* significant determinants of the higher PCs (see text).

Figure 13. M13, M3 and N7006: three clusters of nearly the same metallicity which typify the degree of freedom associated with the horizontal branch (extremely blue for M13, red for N7006). The integrated spectra have been detrended and smoothed to σ = 100 km s^{-1}. It is instructive to compare M13 and NGC 7006 in terms of Hδ, the ratio CaK/(CaH+Hε), and the higher members of the Balmer series. The relationship of these spectra to known horizontal branch properties is discussed further in the text.

Figure 14. The equivalent width of Hδ is uncorrelated with Dickens's horizontal branch type (1 for the bluest HBs, 7 for the reddest). Hβ shows only a weak negative correlation.

Figure 15. Synthetic sprectra illustrating the reversal in the ratio CaK/(CaH+Hε) as the horizontal branch changes from red to blue (with other parts of the color-magnitude array held constant). The hydrogen component of the violet CN–Fe–H blend strengthens markedly.

Figure 16. Synthetic spectra showing the small differences arising from a change in the initial mass function of the evolutionary models from $s = 0$ through $s = 2.35$ (the Salpeter value) to $s = 3.5$.

Figure 17. SIT spectra of MK standards and the HSL star BS7576 showing the blended nature of Hβ for late spectral types. The magnesium triplet is seen at the right.

Figure 18. For the same stars as in Figure 17, SIT spectra show the progressive erosion of the red wing of Hδ and its increasingly glaciated profile as metallic lines become significant.

Figure 19. The vicinity of Hβ from IPCS spectra of five clusters in M31 and of the M31 bulge. As overall line strength increases from top to bottom, the red wing of Hβ suffers increasingly from contamination by iron lines. At slightly lower resolution, the

"Hβ" feature in K213 would appear to be a smooth, unexceptional profile. Since these profiles are excerpted from flux plots having slightly different scales, features should be compared in form, not in scale.

Figure 20. IPCS spectra of clusters in M31 showing the erosion of the red wing of Hδ as overall metallicity increases. The threshold for this effect appears to be at higher metallicity than that for Hβ.

Figure 21. A manifestation of hyperstrong line (HSL) characteristics in integrated light? The Mgb triplet is considerably weaker in the M31 cluster K1/MII than it is in the galactic globular cluster M69, but Na D is as strong in K1 as it is in M69. K280/V282 is stronger-lined overall than M69, but the contrast is greatest at NaD.

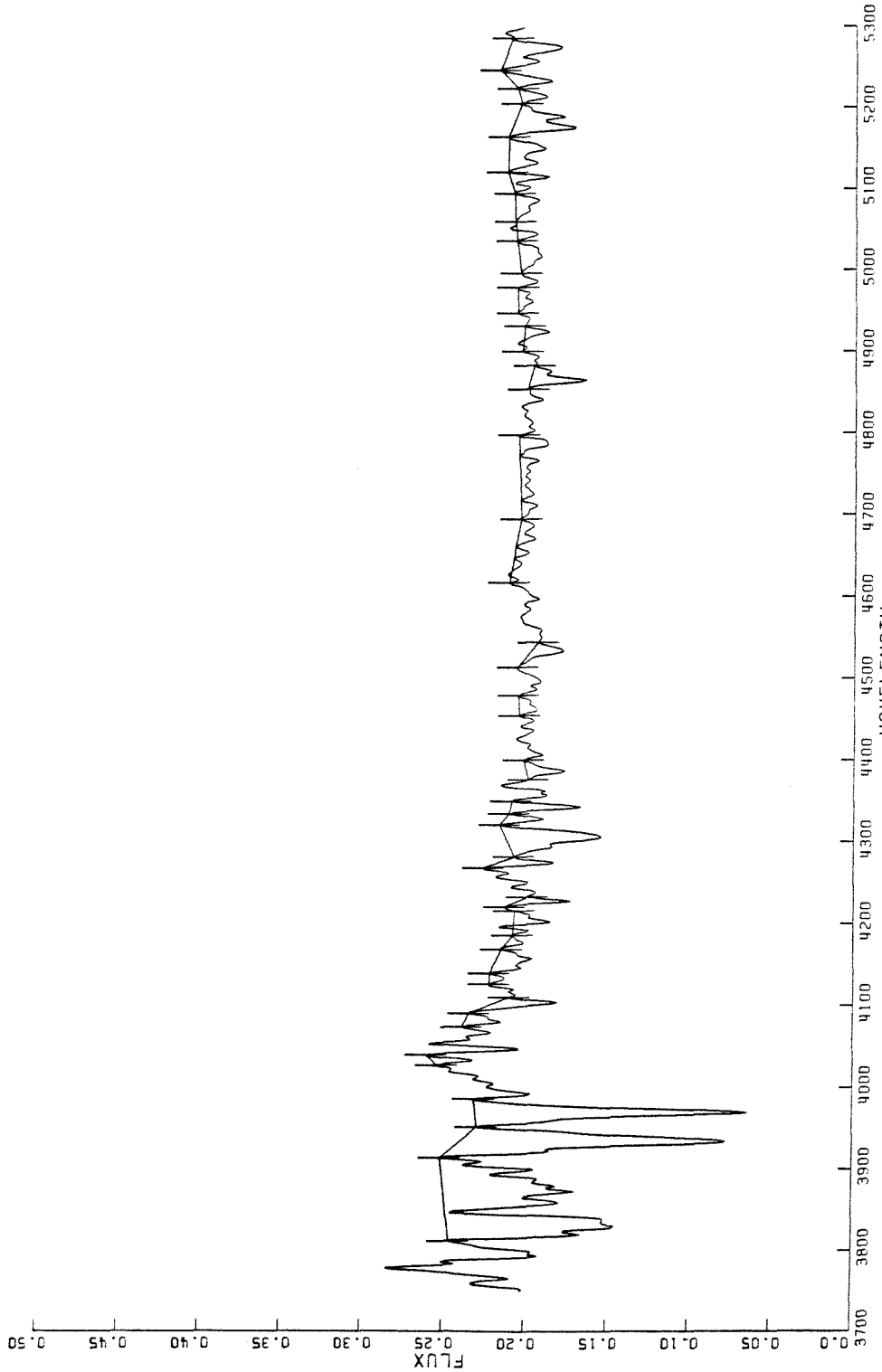
FLUX
0.0
0.05
0.10
0.15
0.20
0.25
0.30
0.35
0.40
0.45
0.50
WAVELENGTH
3700
3800
3900
4000
4100
4200
4300
4400
4500
4600
4700
4800
4900
5000
5100
5200
5300

Figure 1

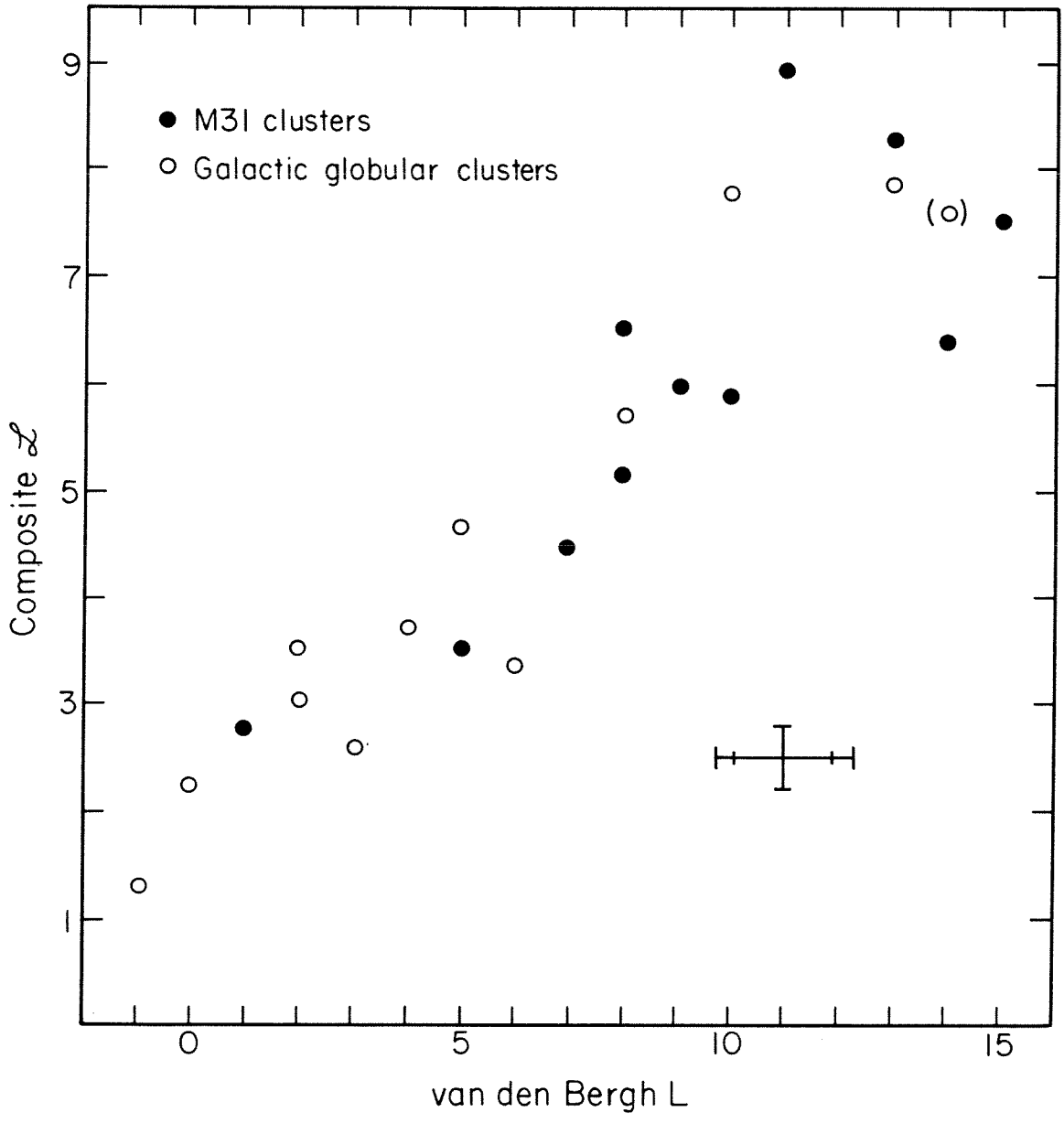
M31 clusters
Galactic globular clusters
(o)
Composite ℒ
van den Bergh L
9
7
5
3
1
0
5
10
15

Figure 2

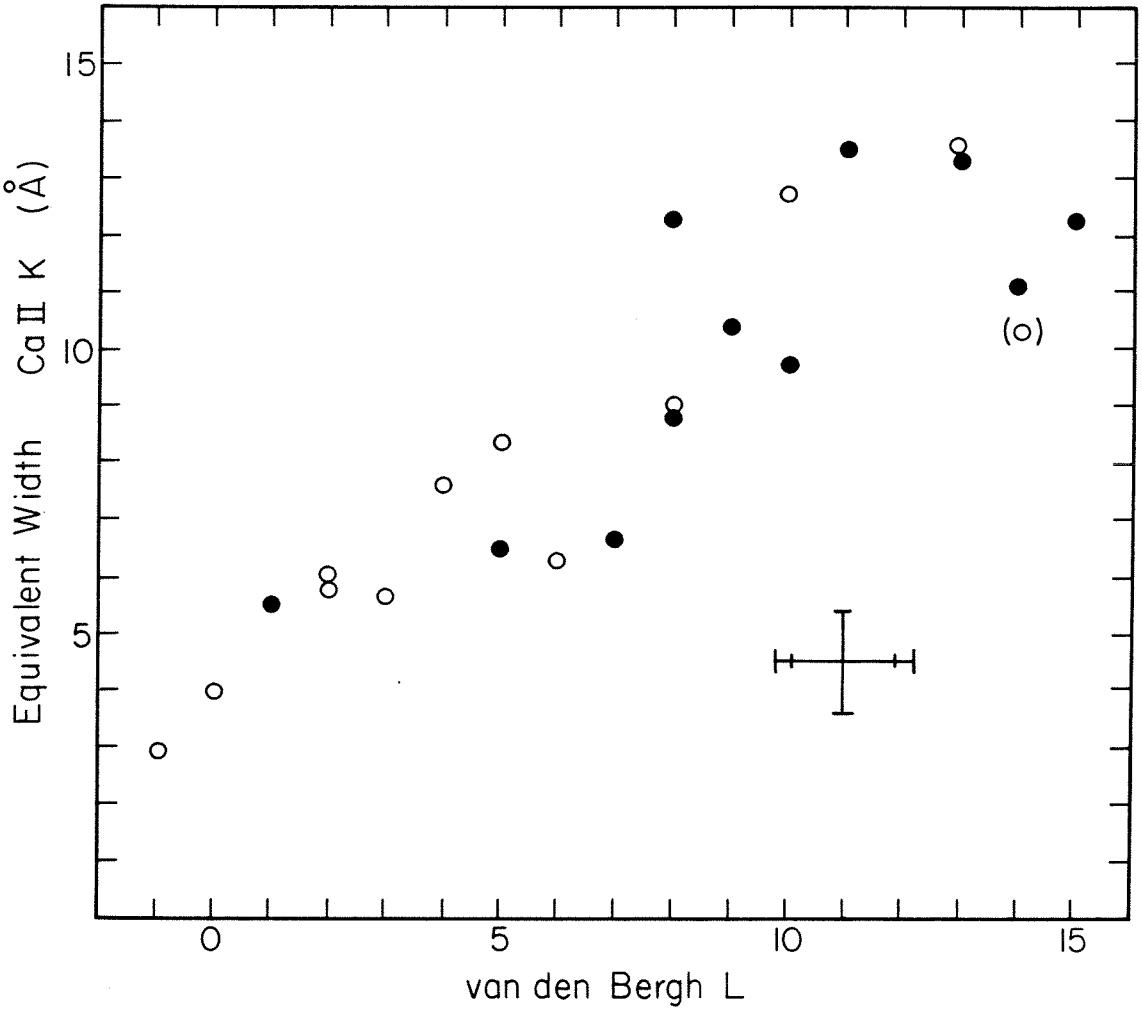

Figure 3a

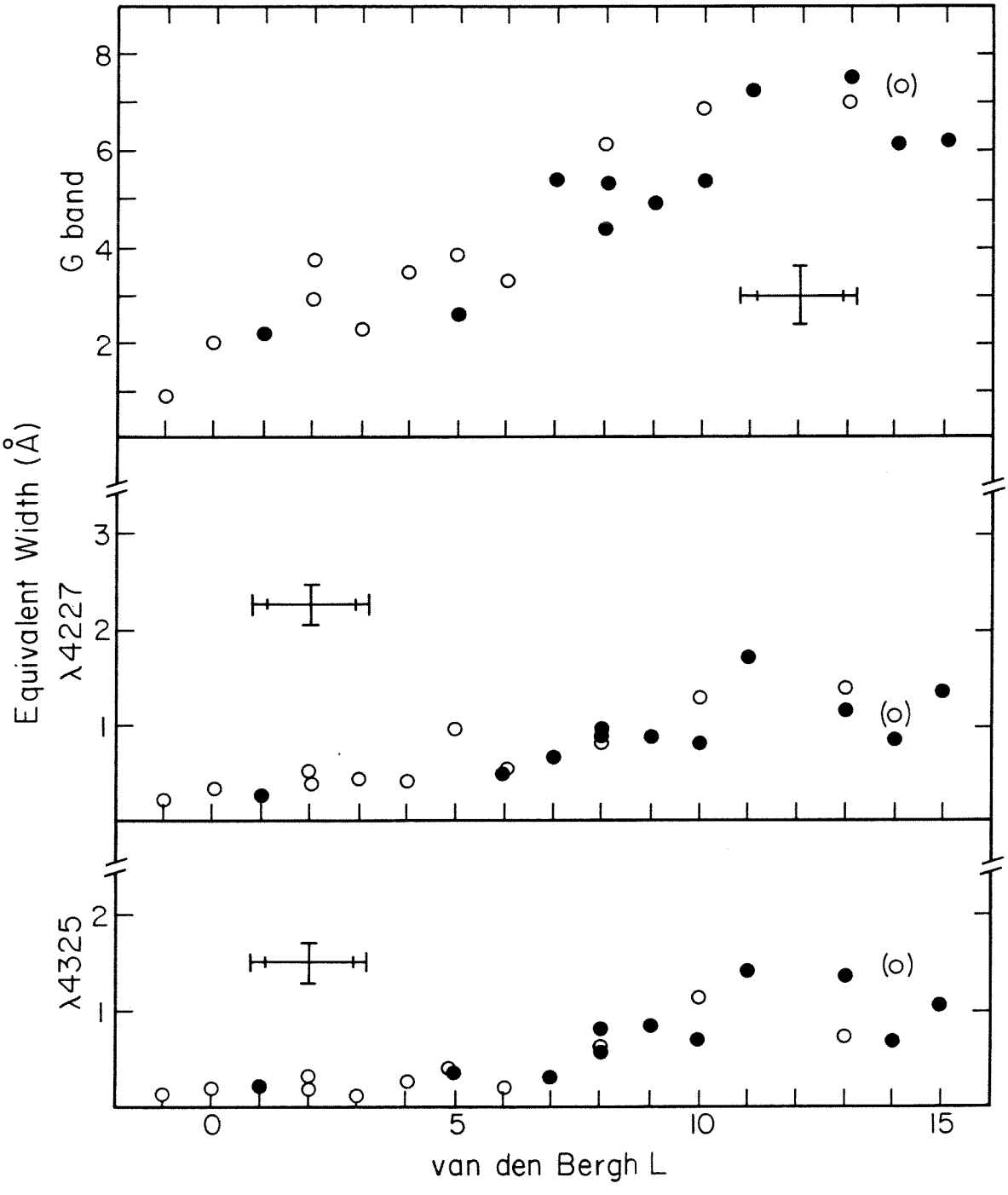
Equivalent Width (Å)
G band
λ4227
λ4325
(o)
van den Bergh L
0
5
10
15

Figure 3b

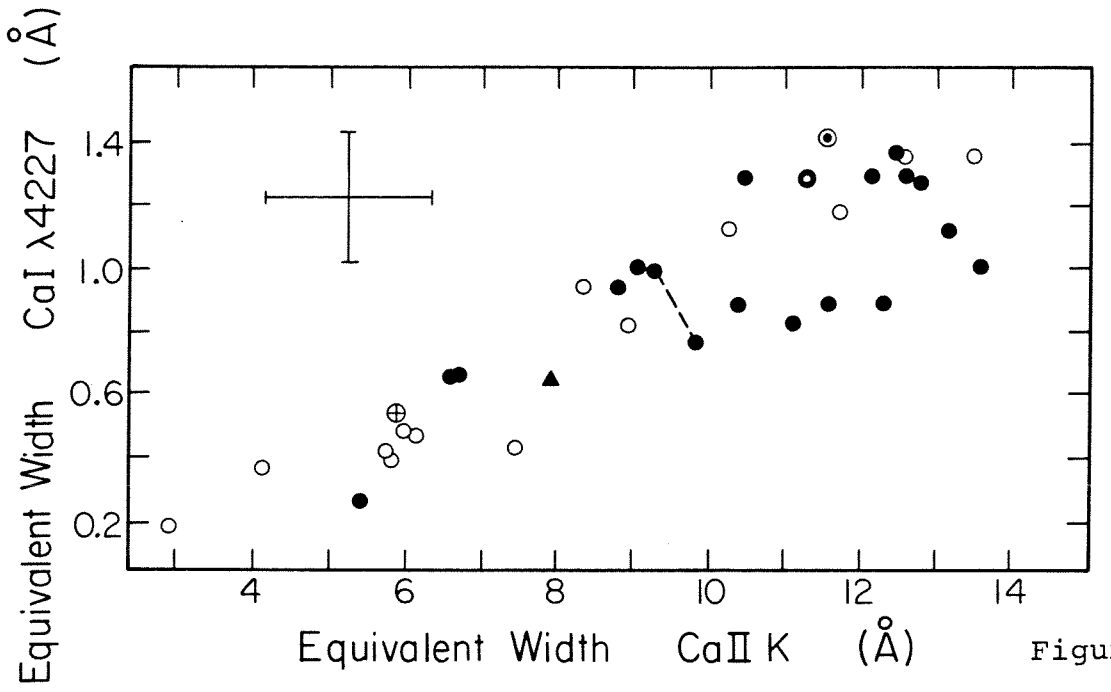

Figure 4a

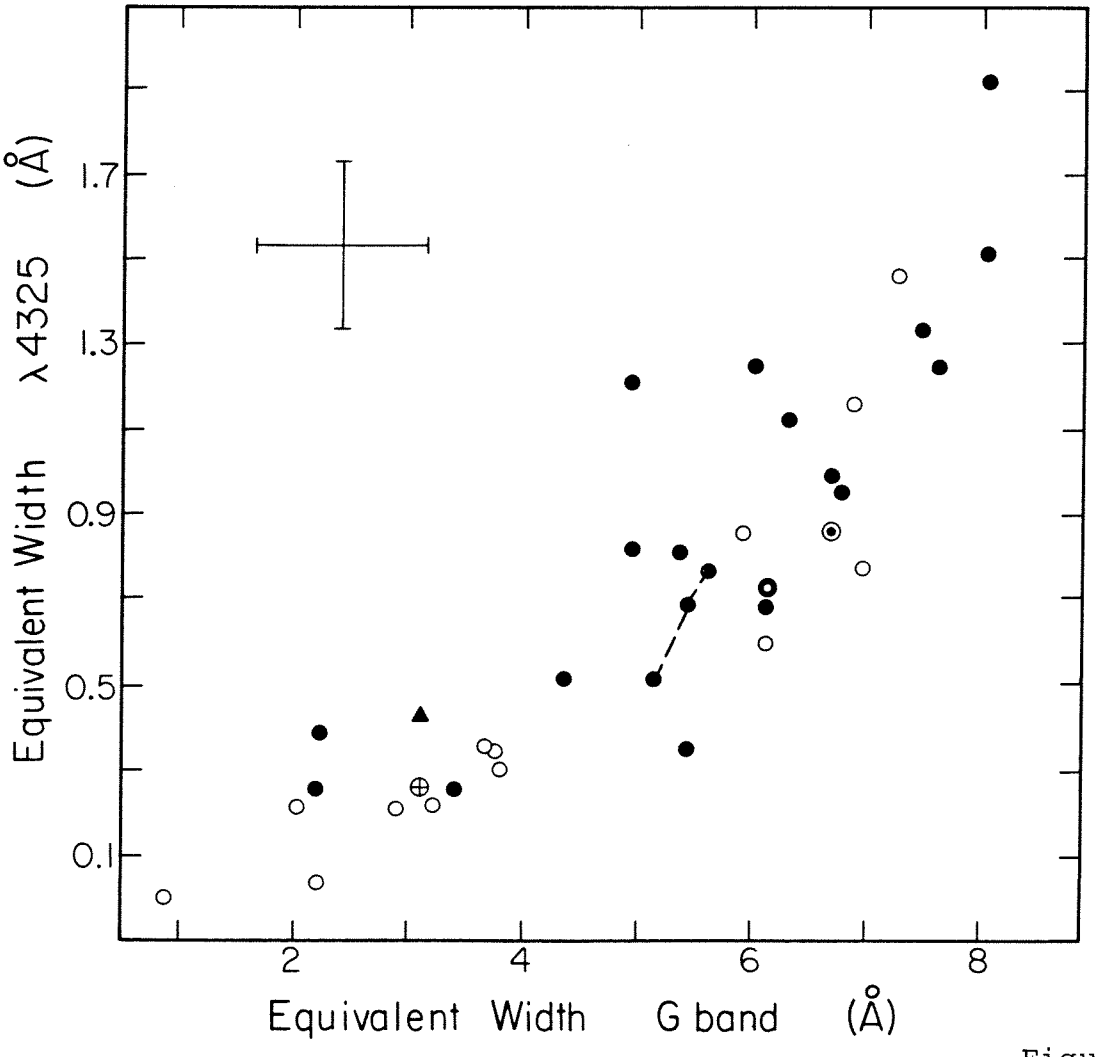

Figure 4b

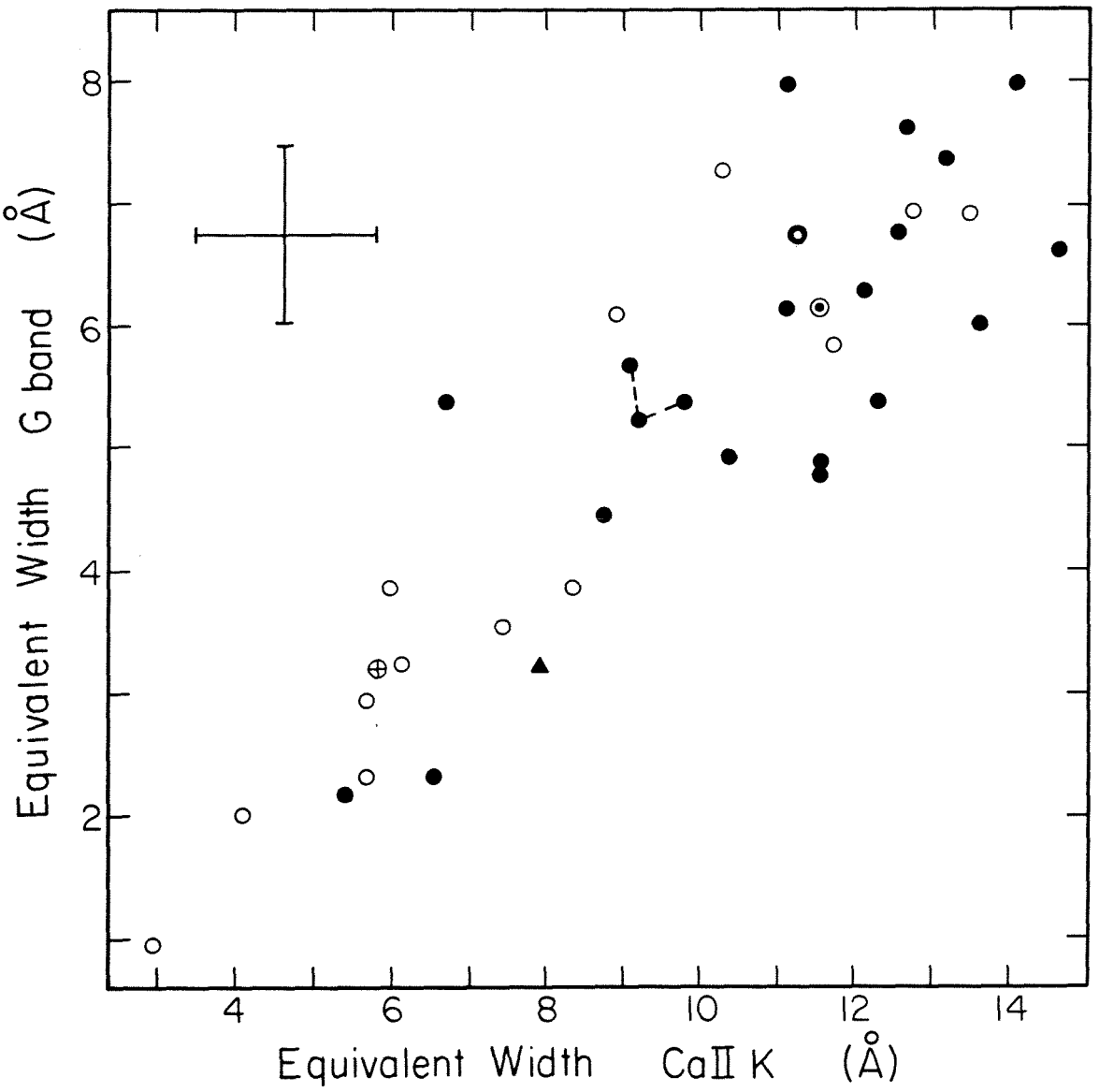
Equivalent Width G band (Å)
Equivalent Width CaII K (Å)
2
4
6
8
4
6
8
10
12
14

Figure 4c

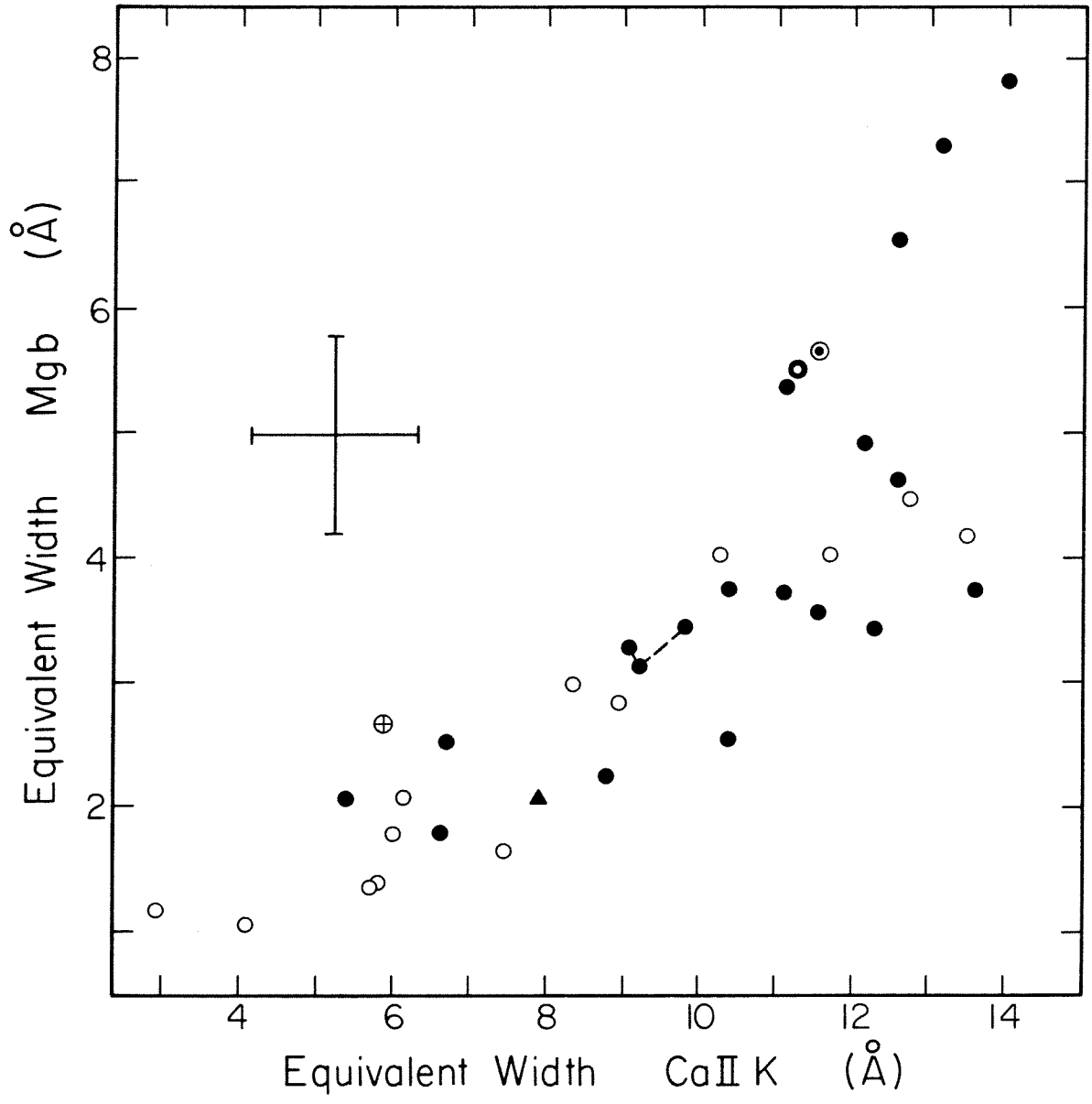
Equivalent Width Mgb (Å)
Equivalent Width CaII K (Å)
2
4
6
8
4
6
8
10
12
14

Figure 4d

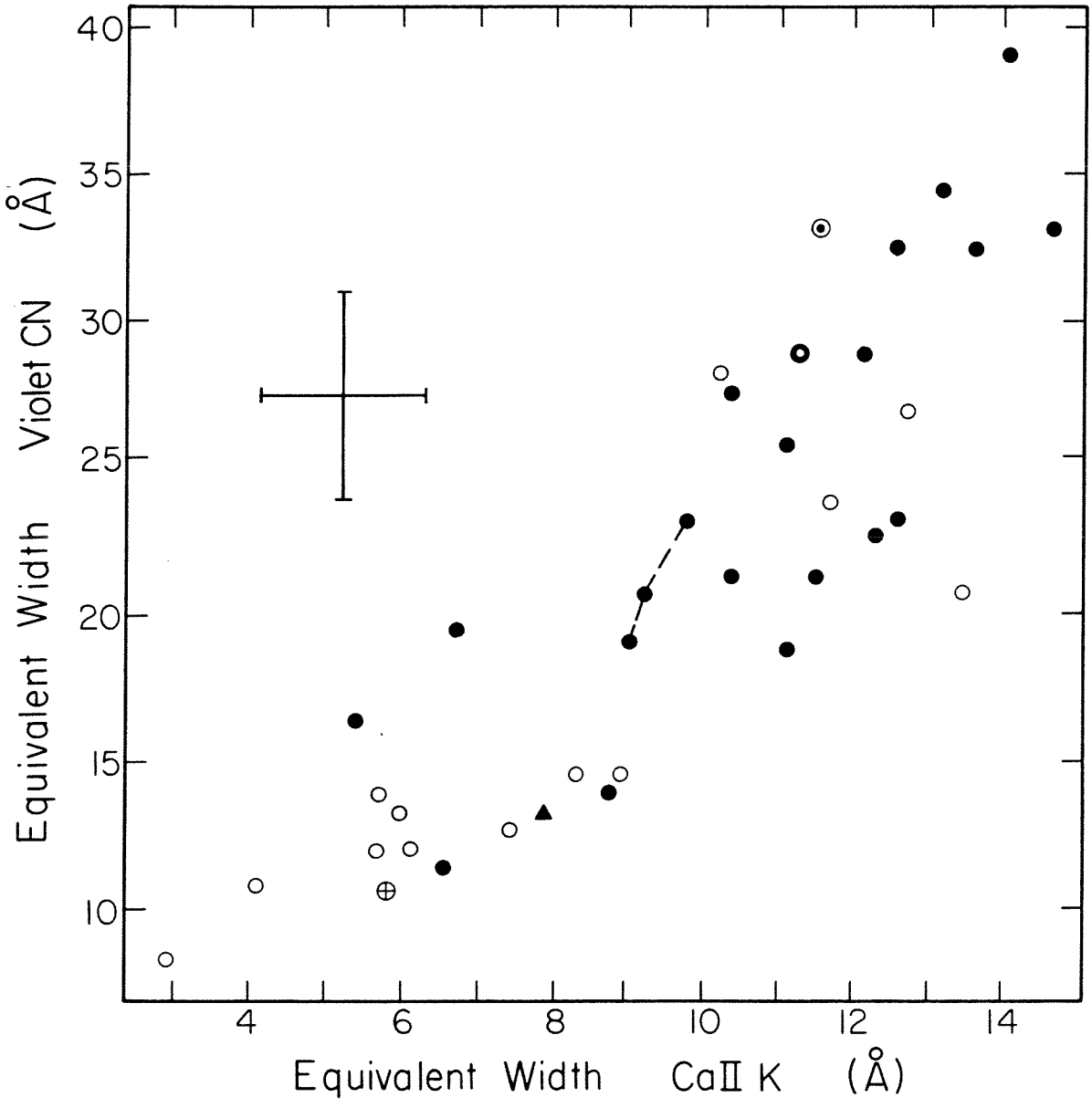
Equivalent Width Violet CN (Å)
40
35
30
25
20
15
10
4
6
8
10
12
14
Equivalent Width CaII K (Å)

Figure 4e

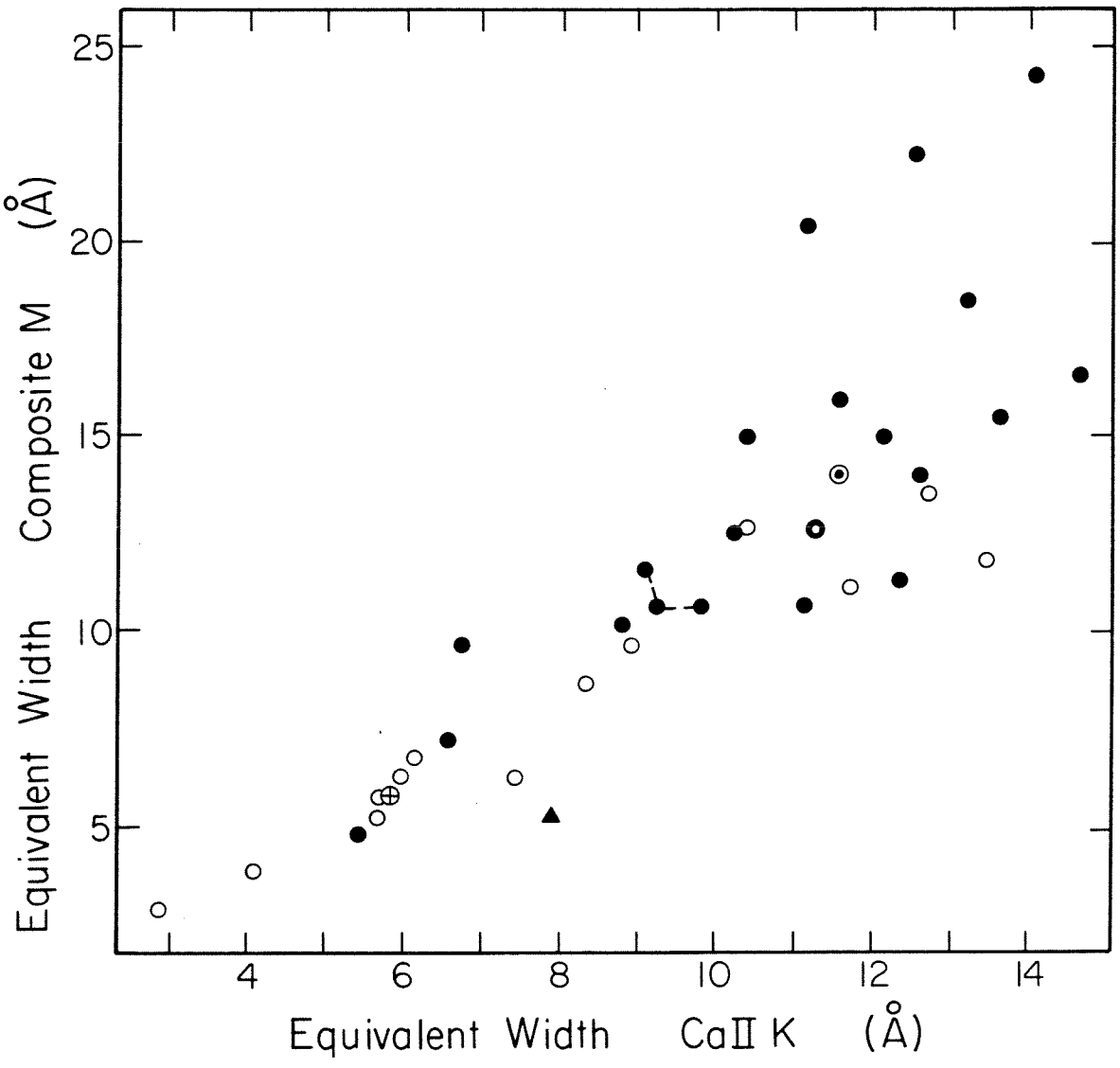
Equivalent Width Composite M (Å)
25
20
15
10
5
4
6
8
10
12
14
Equivalent Width CaII K (Å)

Figure 5a

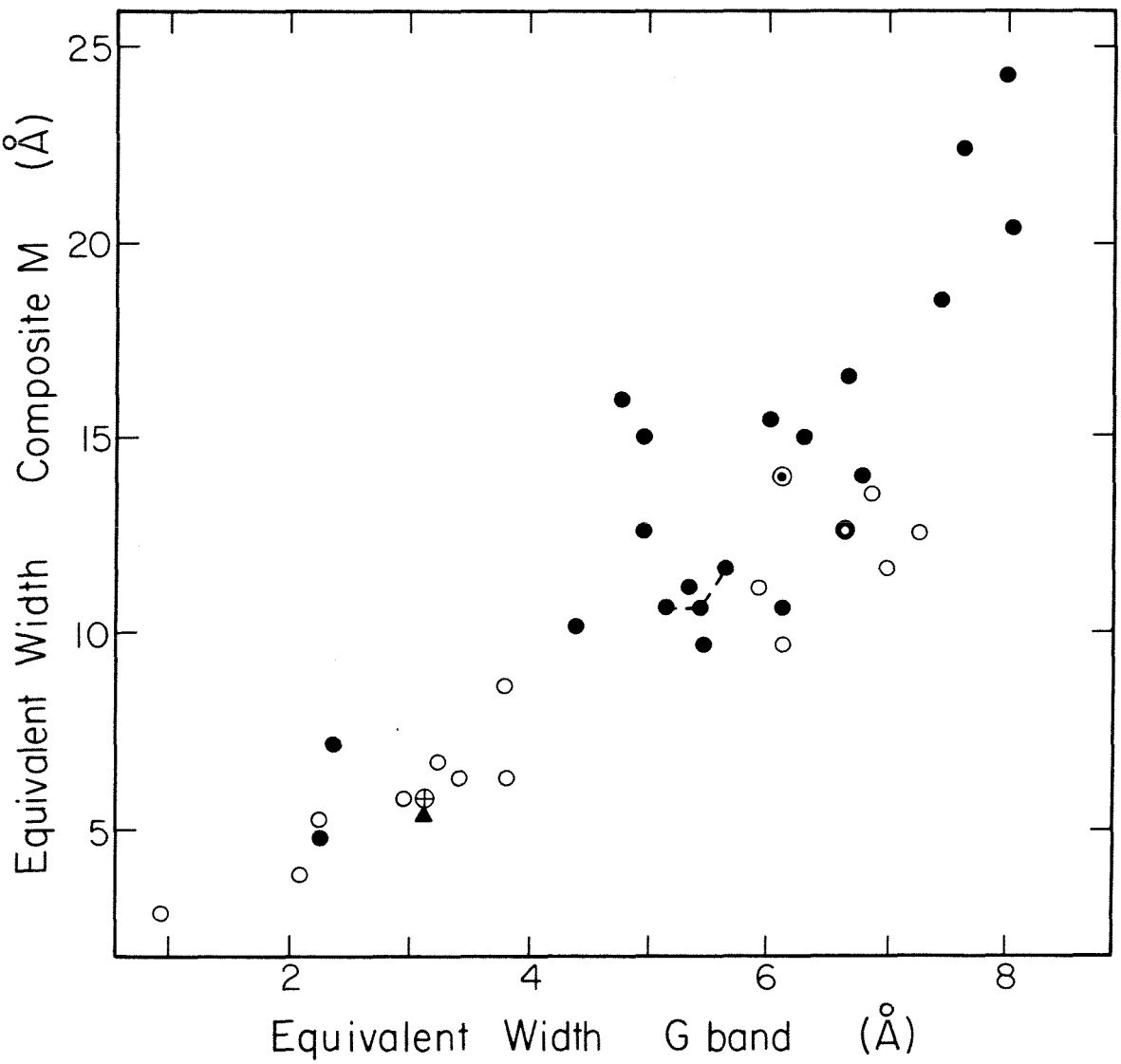
Equivalent Width Composite M (Å)
25
20
15
10
5
2
4
6
8
Equivalent Width G band (Å)

Figure 5b

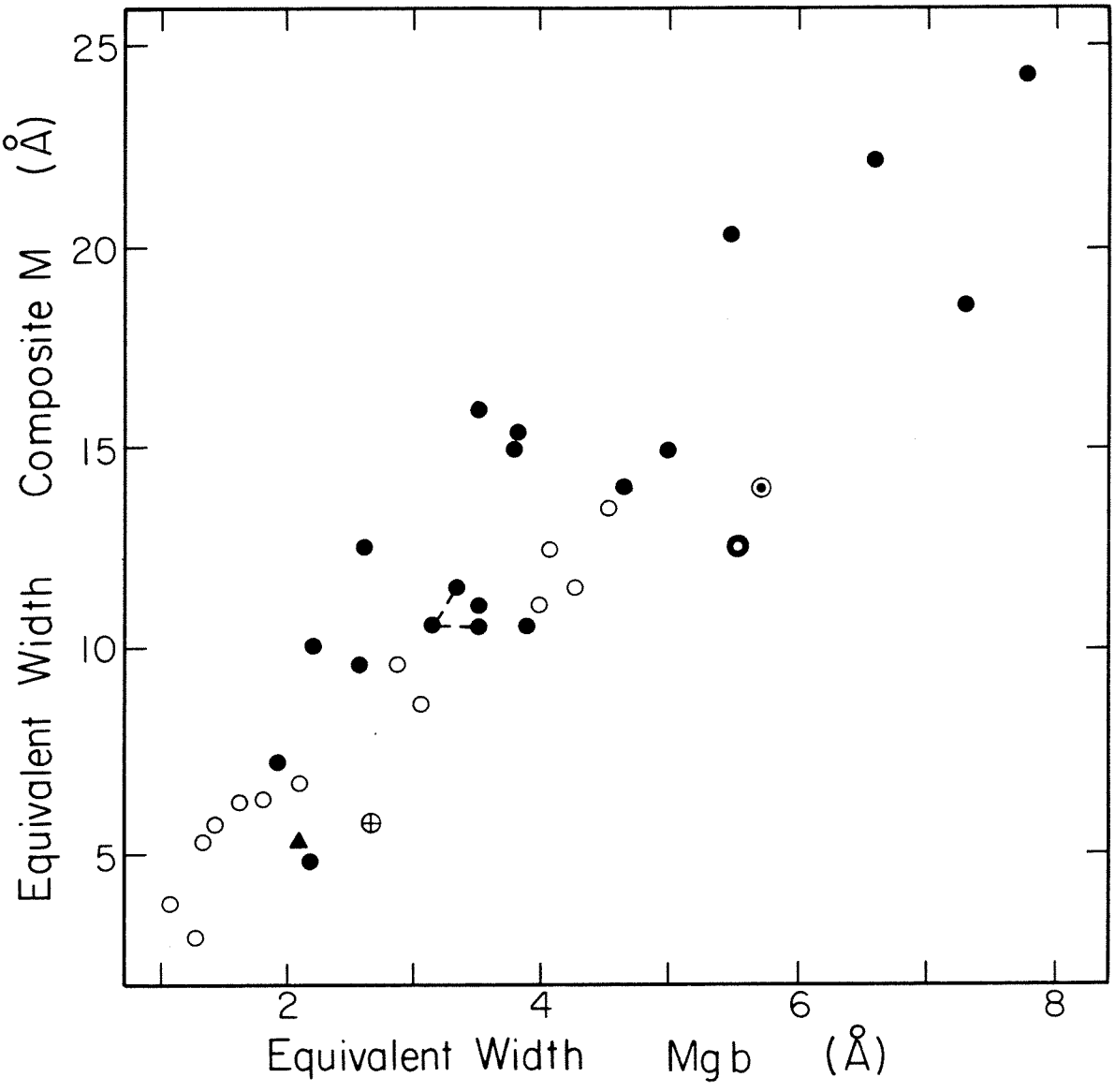
Equivalent Width Composite M (Å)
25
20
15
10
5
2
4
6
8
Equivalent Width Mg b (Å)

Figure 5c

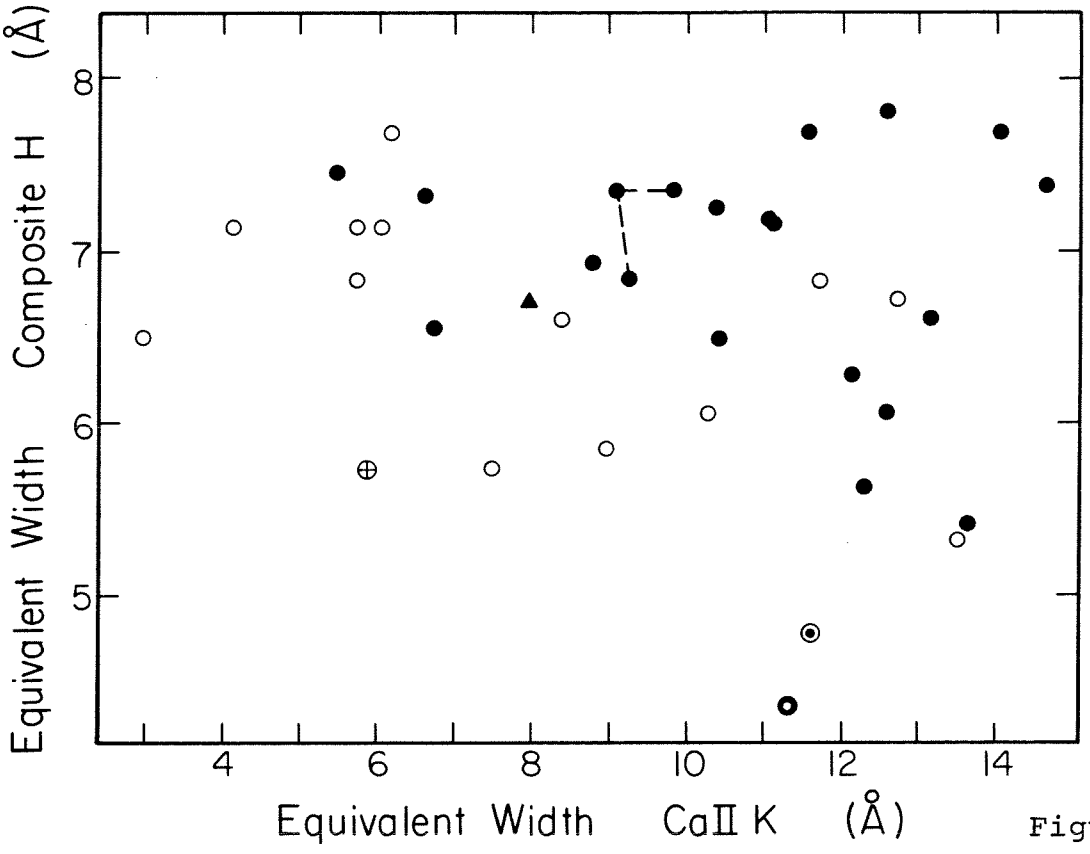

Figure 6a

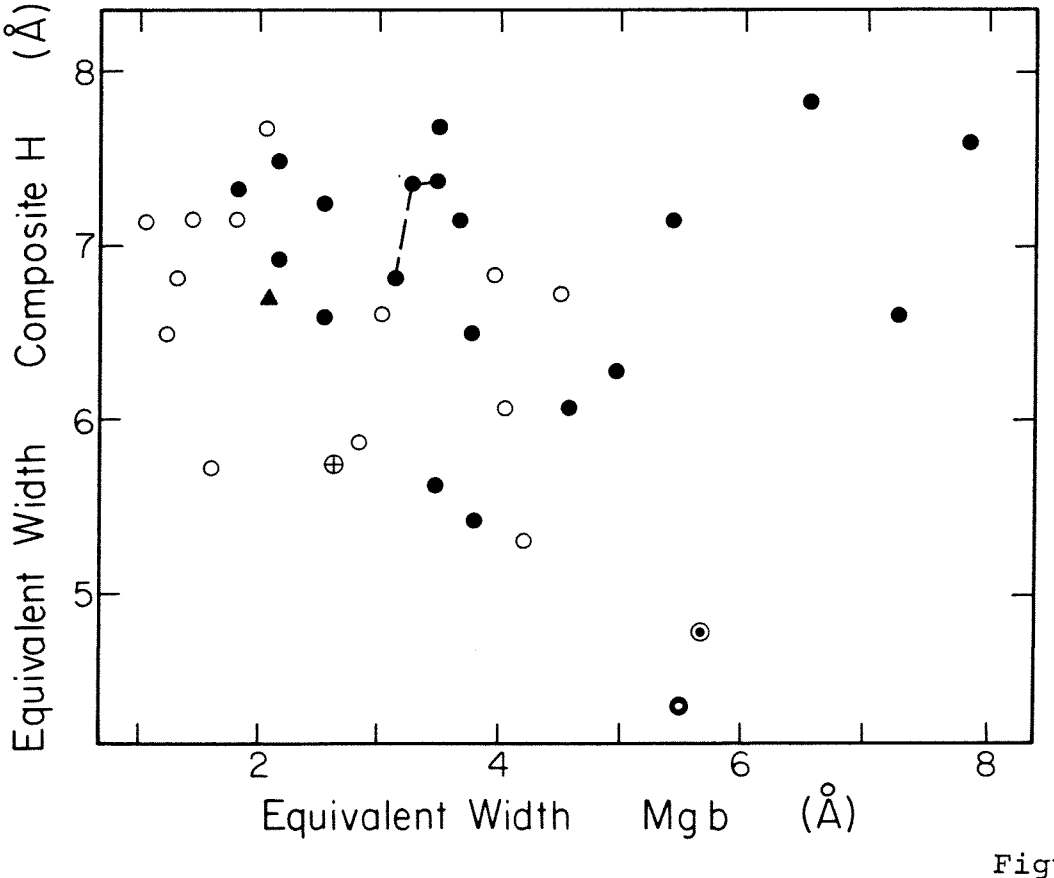

Figure 6b

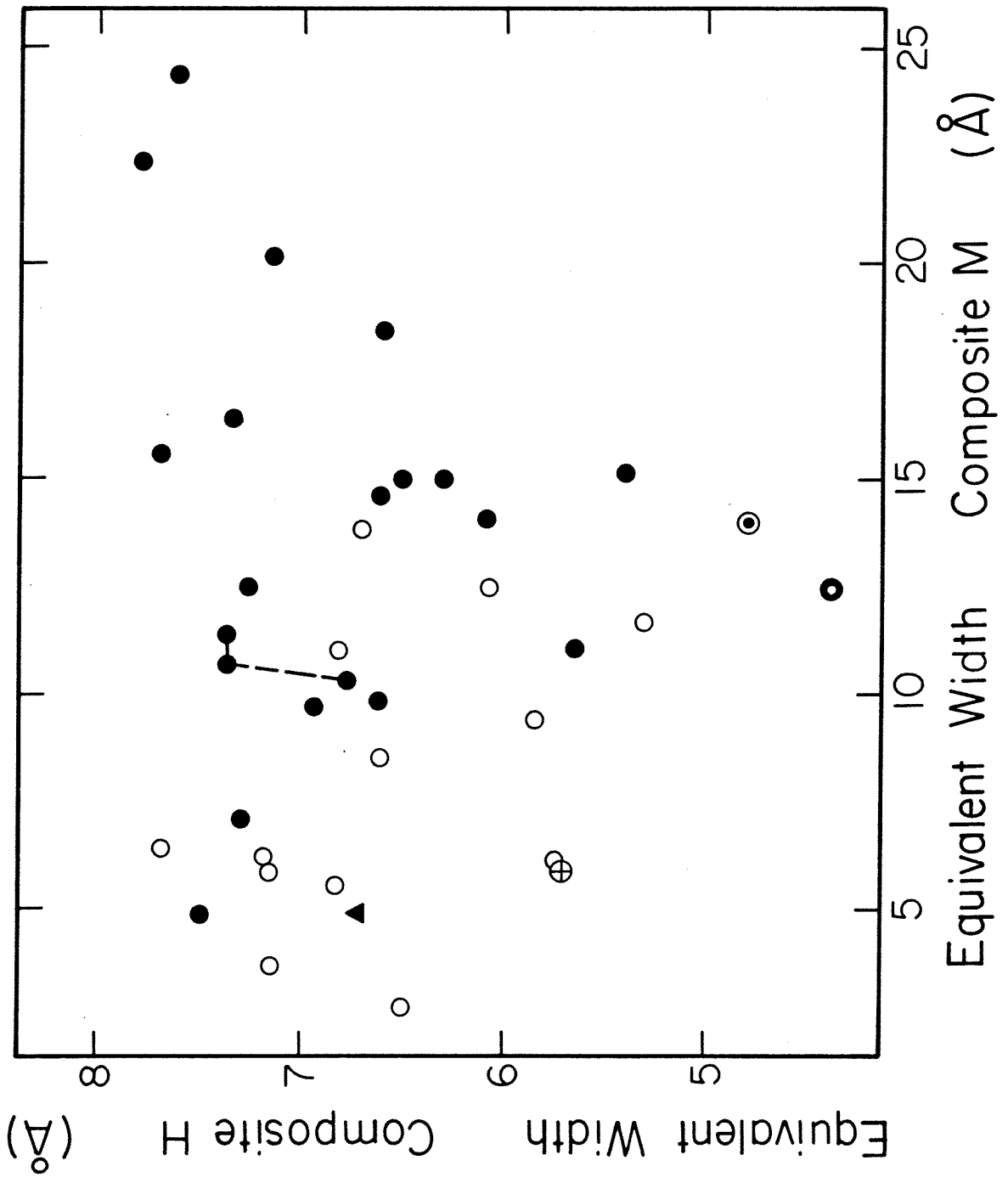
Equivalent Width Composite H (Å)
Equivalent Width Composite M (Å)
8
7
9
5
5
10
15
20
25

Figure 6c

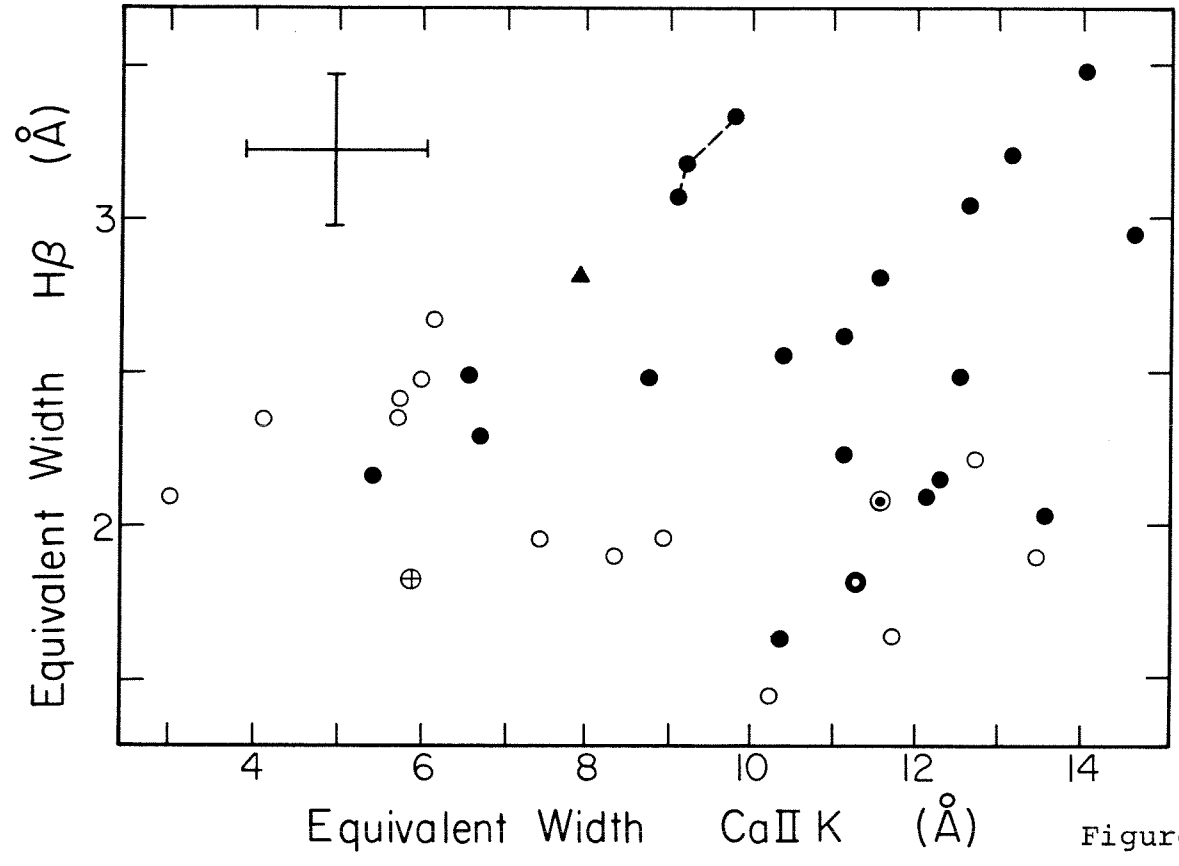

Figure 7a

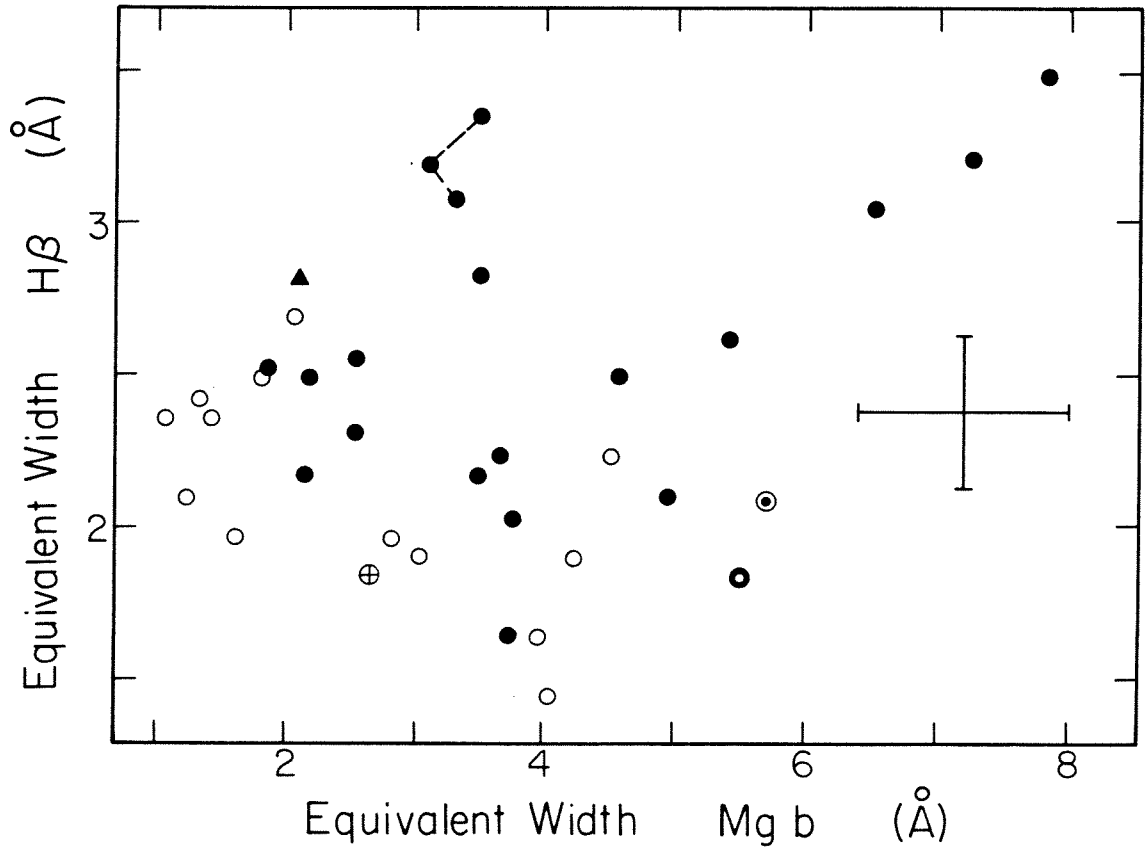

Figure 7b

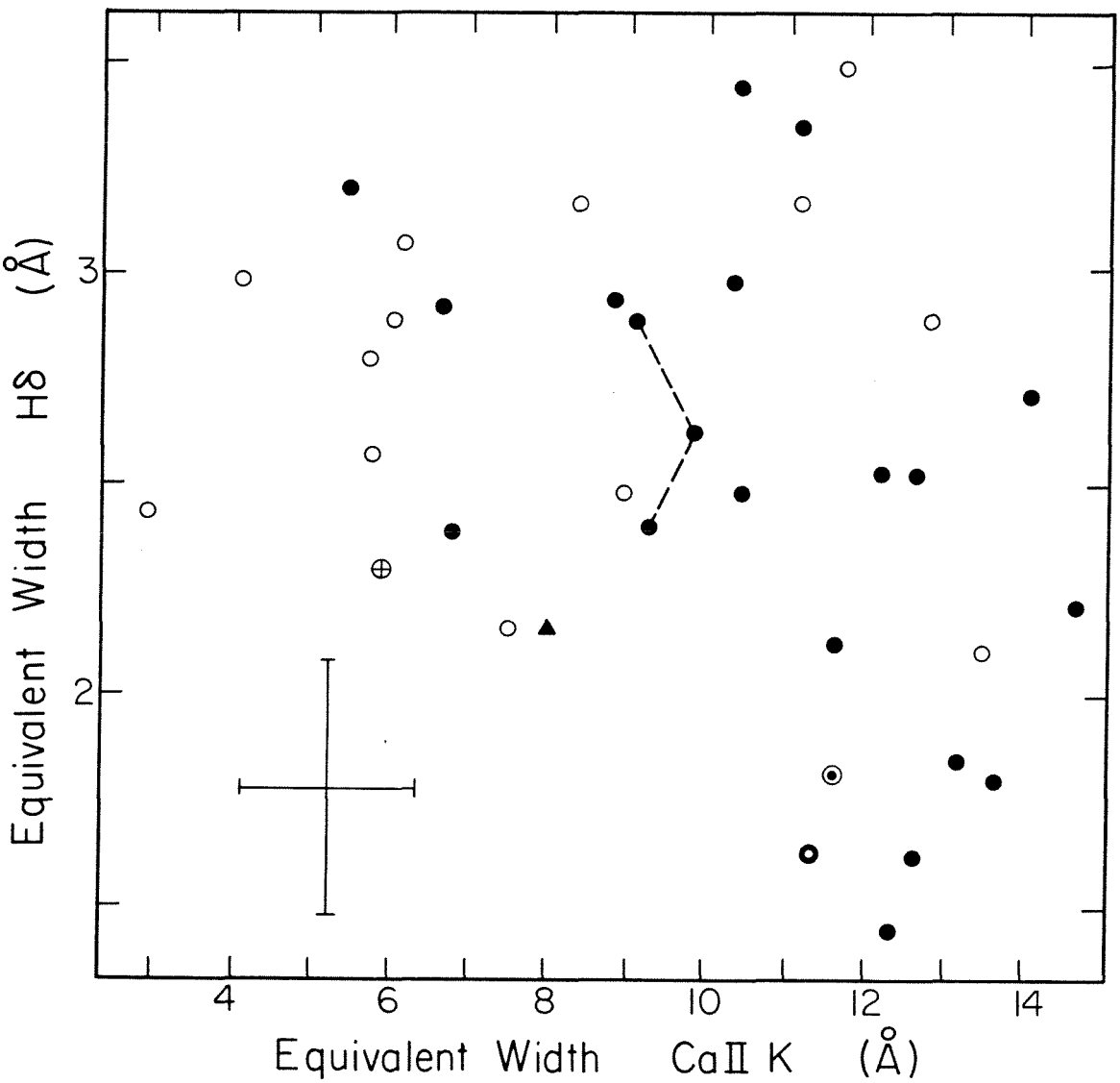
Equivalent Width Hδ (Å)
3
2
4
6
8
10
12
14
Equivalent Width CaII K (Å)

Figure 7c

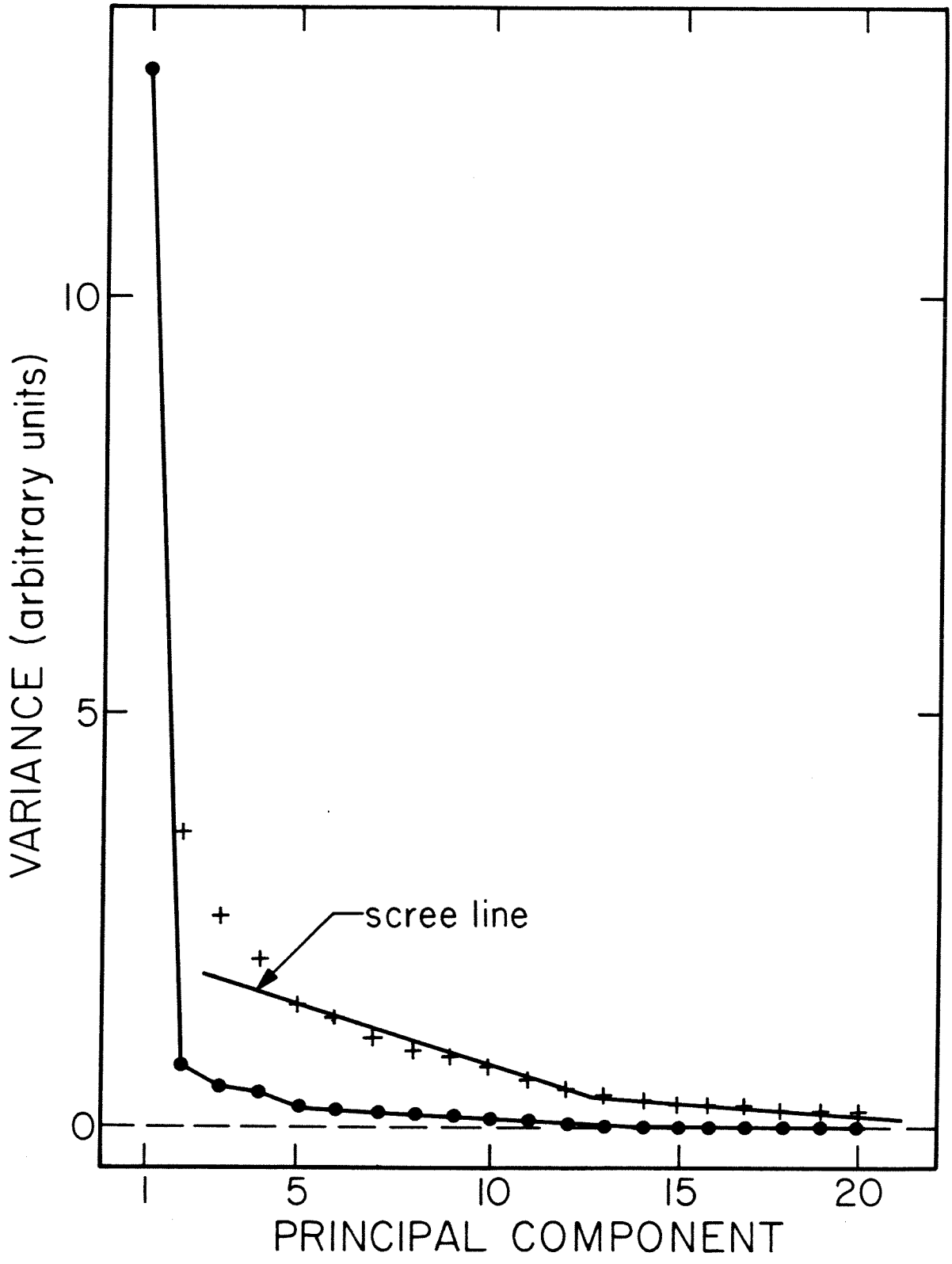
VARIANCE (arbitrary units)
10
5
0
scree line
1
5
10
15
20
PRINCIPAL COMPONENT

Figure 8

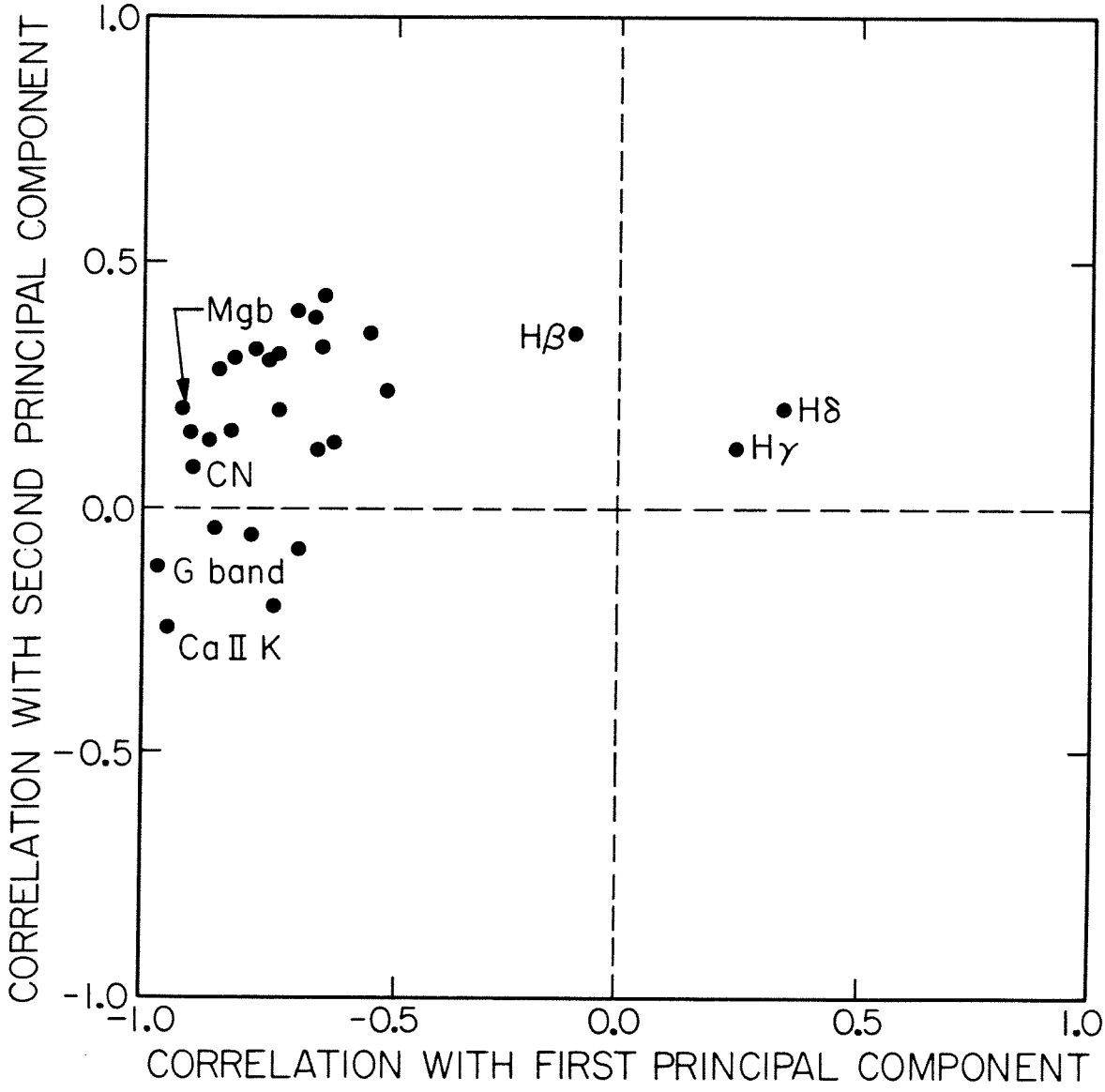
1.0
0.5
0.0
-0.5
-1.0
-1.0
-0.5
0.0
0.5
1.0
CORRELATION WITH SECOND PRINCIPAL COMPONENT
CORRELATION WITH FIRST PRINCIPAL COMPONENT
Mgb
Hβ
Hδ
Hγ
CN
G band
CaII K

Figure 9

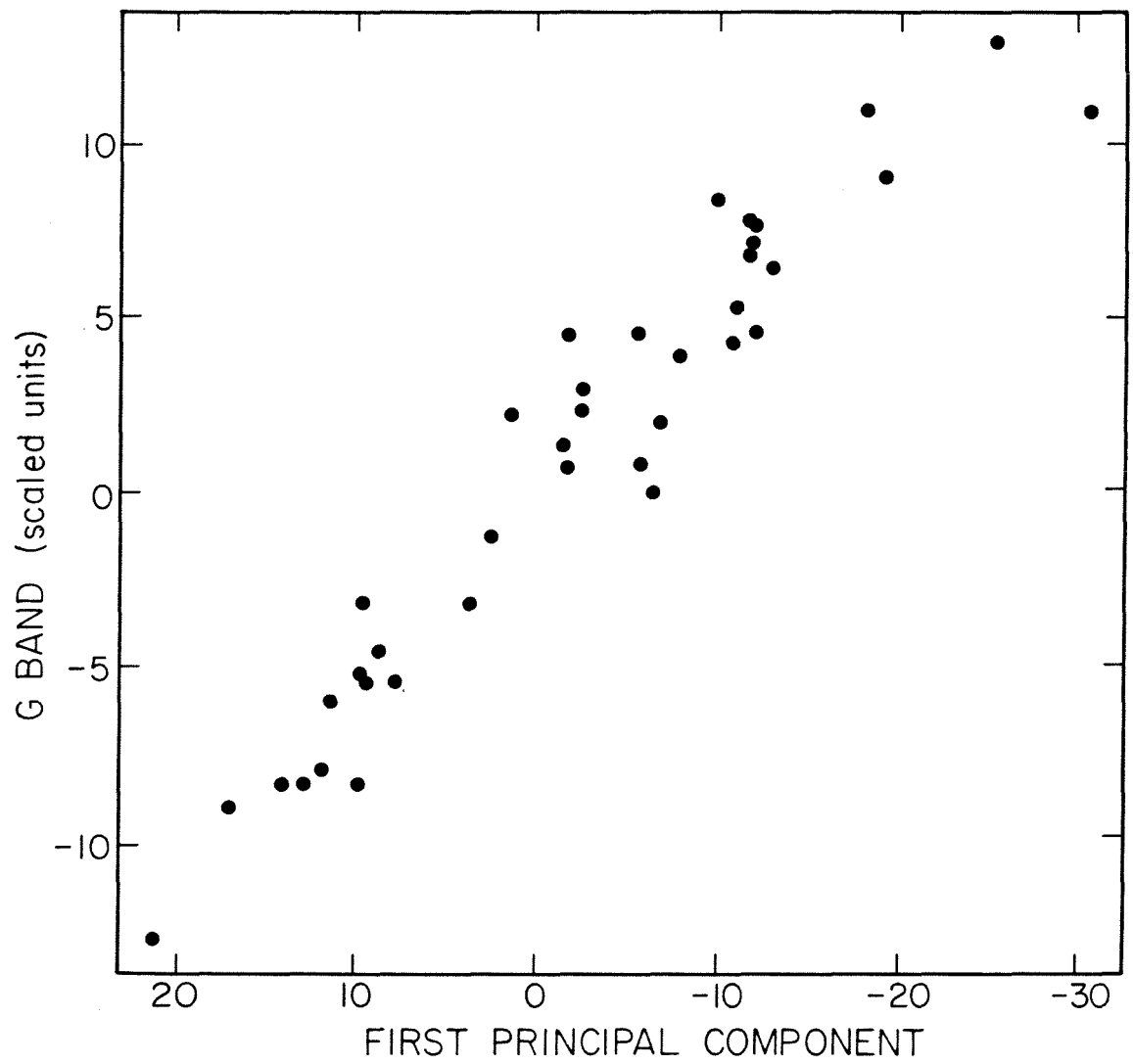
10
5
0
-5
-10
G BAND (scaled units)
20
10
0
-10
-20
-30
FIRST PRINCIPAL COMPONENT

Figure 10

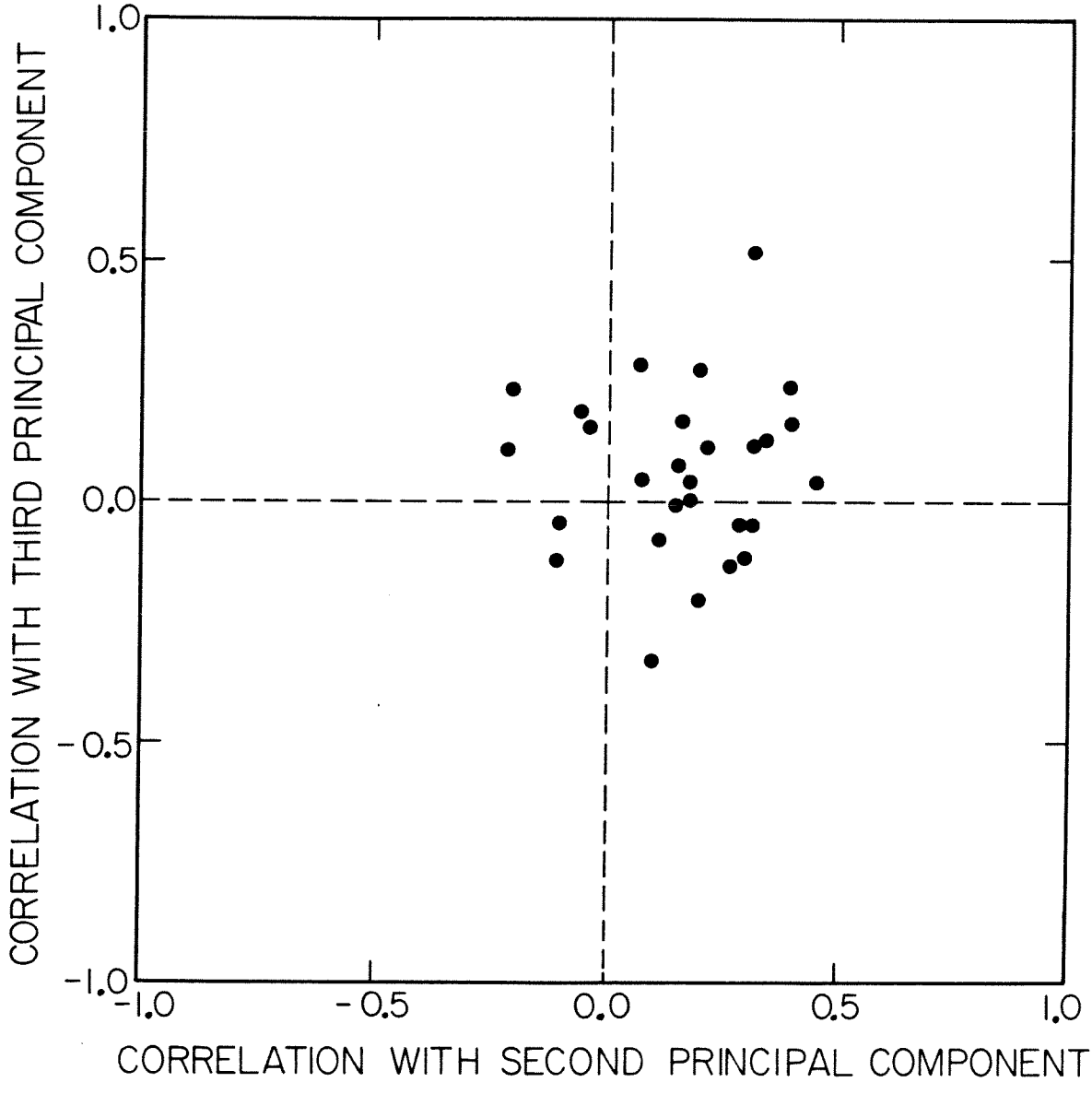
1.0
0.5
0.0
-0.5
-1.0
-1.0
-0.5
0.0
0.5
1.0
CORRELATION WITH THIRD PRINCIPAL COMPONENT
CORRELATION WITH SECOND PRINCIPAL COMPONENT

Figure 11

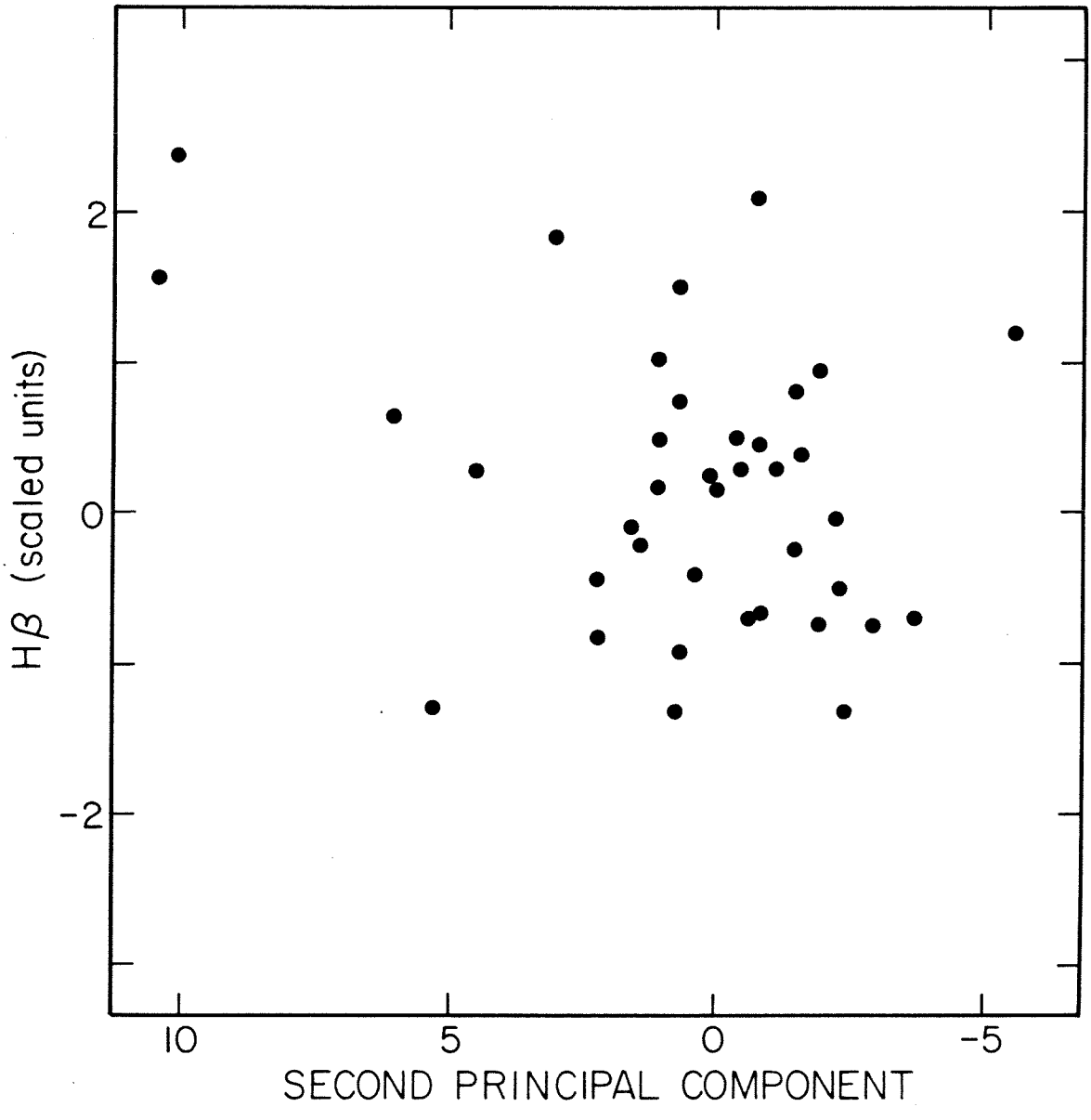

Figure 12

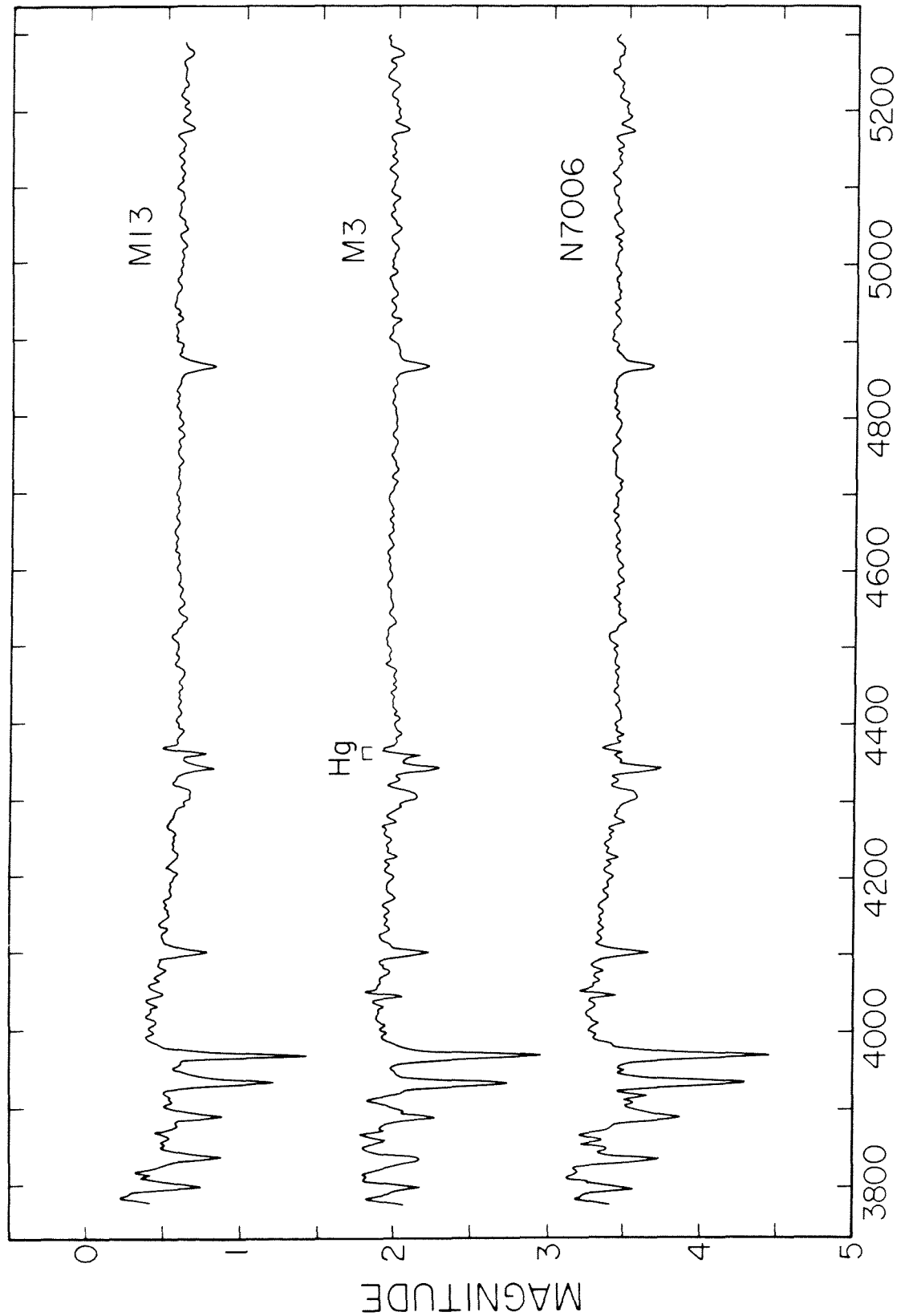
M13
M3
N7006
Hδ
MAGNITUDE
WAVELENGTH (Å)
0
1
2
3
4
5
3800
4000
4200
4400
4600
4800
5000
5200

Figure 13

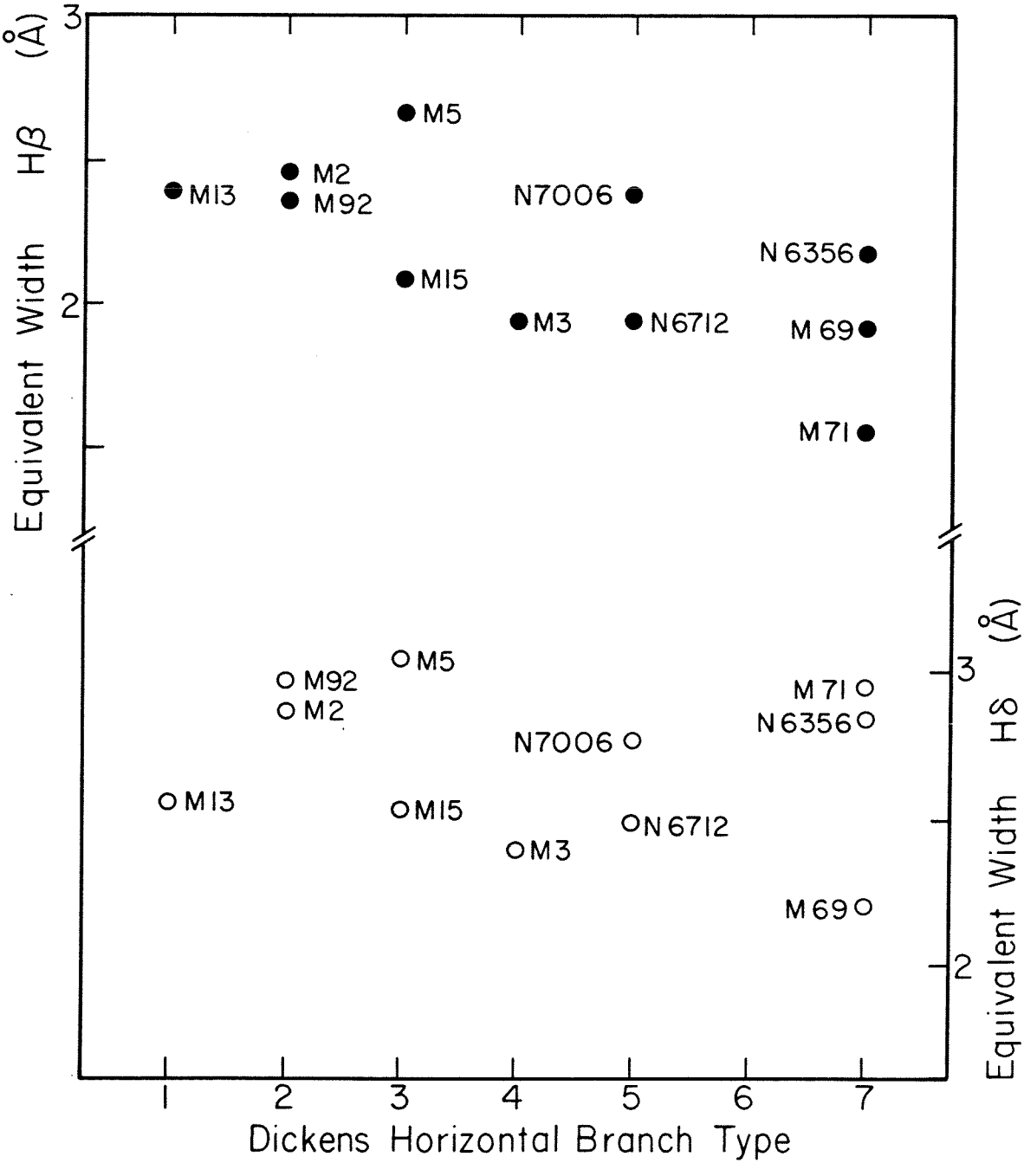
Equivalent Width Hβ (Å)
3
2
M5
M2
M92
M13
N7006
N6356
M15
M3
N6712
M69
M71
M5
M92
M2
M71
N6356
N7006
M13
M15
N6712
M3
M69
3
2
Equivalent Width Hδ (Å)
1
2
3
4
5
6
7
Dickens Horizontal Branch Type

Figure 14

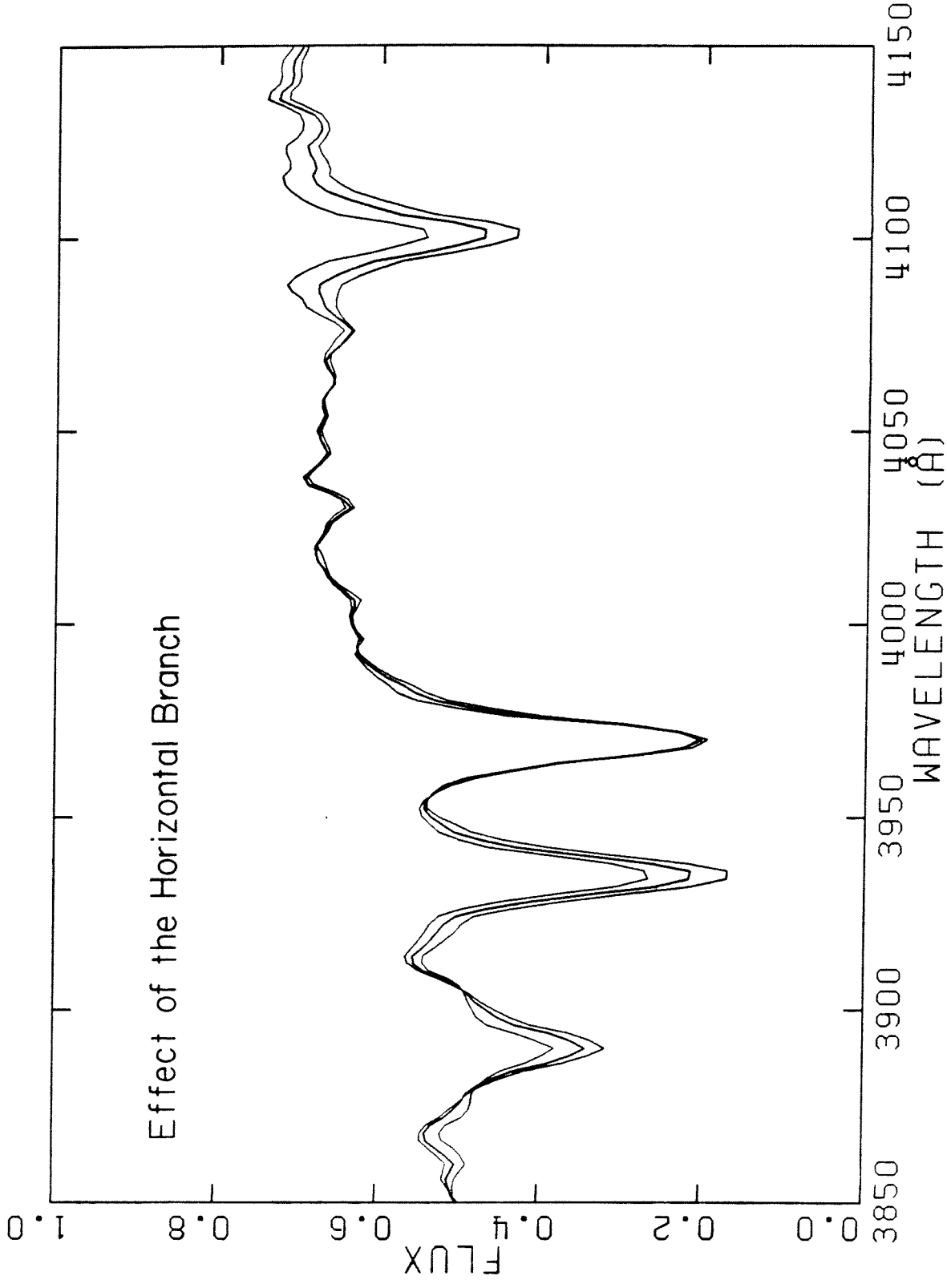
Effect of the Horizontal Branch
FLUX
0.0
0.2
0.4
0.6
0.8
1.0
3850
3900
3950
4000
4050
4100
4150
WAVELENGTH (Å)

Figure 15

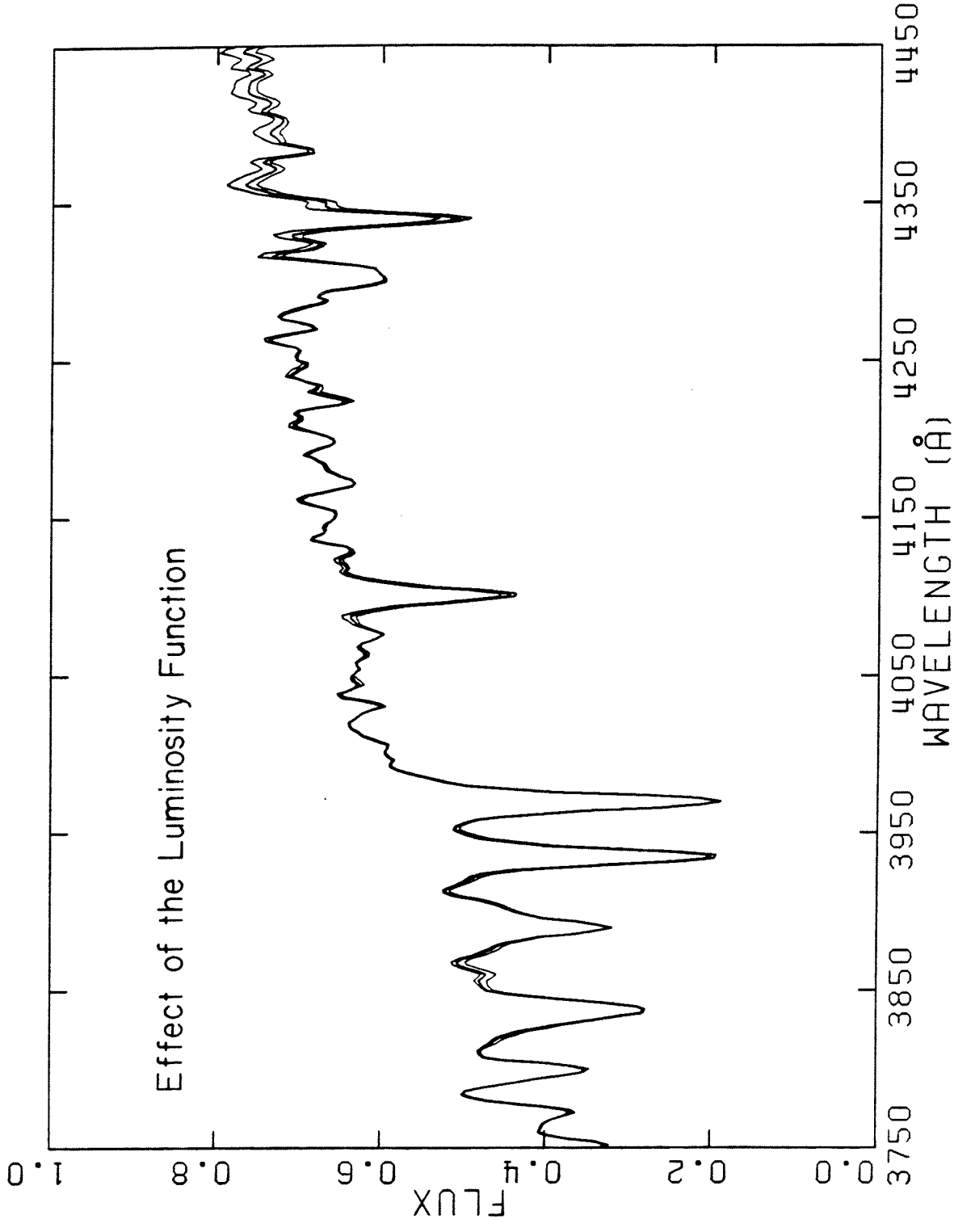
Effect of the Luminosity Function
FLUX
0.0
0.2
0.4
0.6
0.8
1.0
WAVELENGTH (Å)
3750
3850
3950
4050
4150
4250
4350
4450

Figure 16

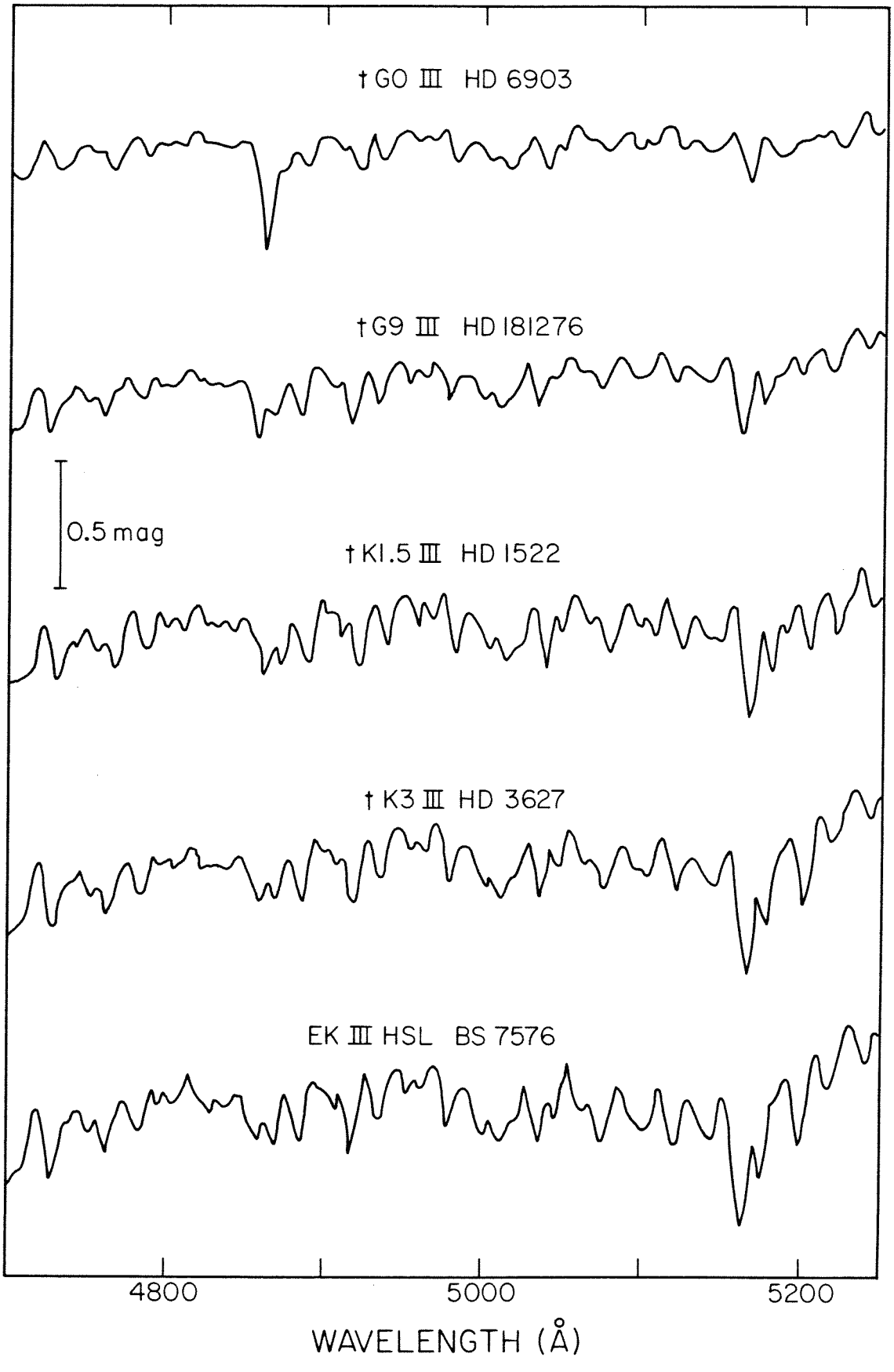
† G0 III HD 6903
† G9 III HD 181276
0.5 mag
† K1.5 III HD 1522
† K3 III HD 3627
EK III HSL BS 7576
4800
5000
5200
WAVELENGTH (Å)

Figure 17

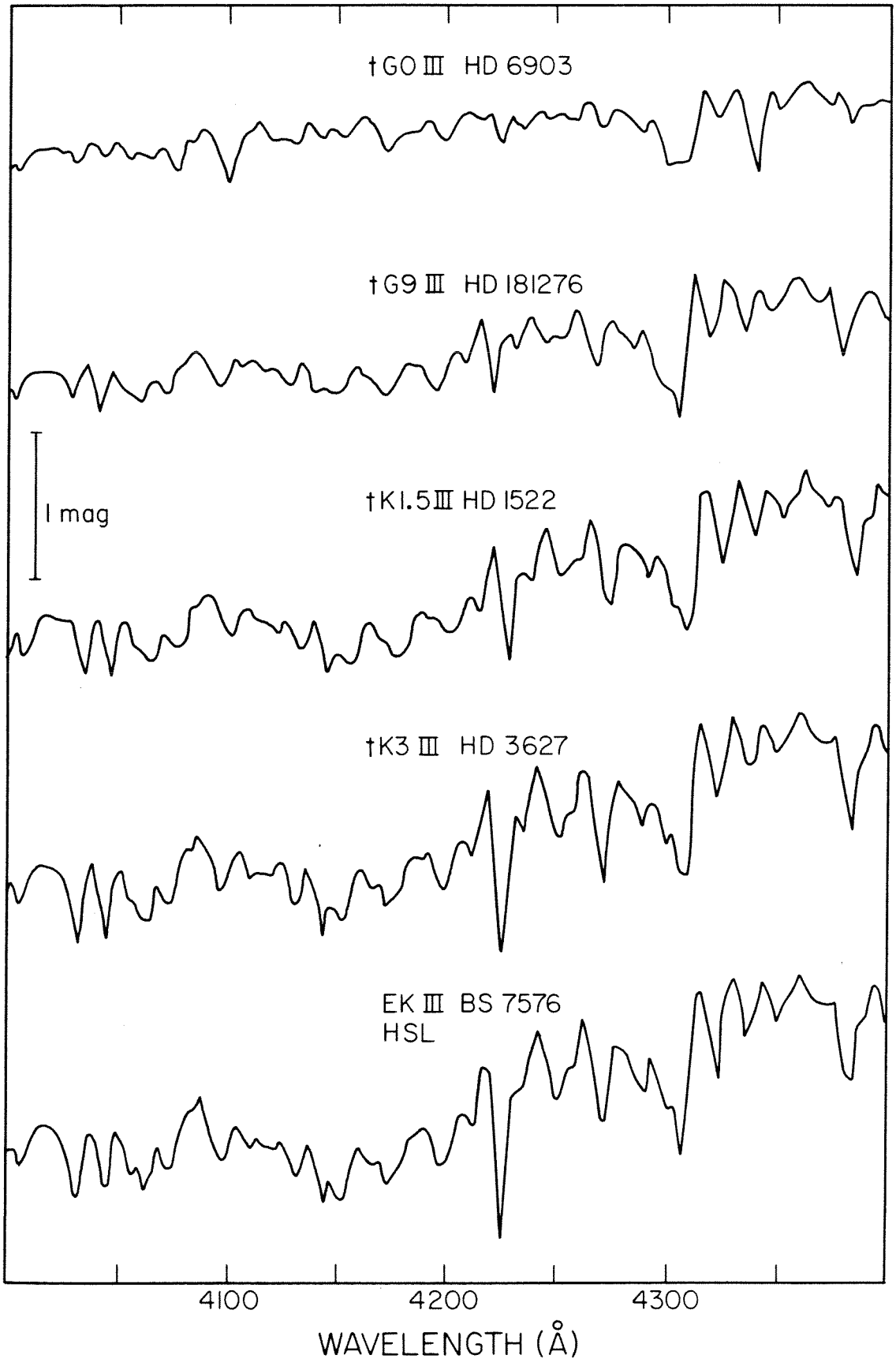
†G0 III HD 6903
†G9 III HD 181276
1 mag
†K1.5III HD 1522
†K3 III HD 3627
EK III BS 7576
HSL
4100
4200
4300
WAVELENGTH (Å)

Figure 18

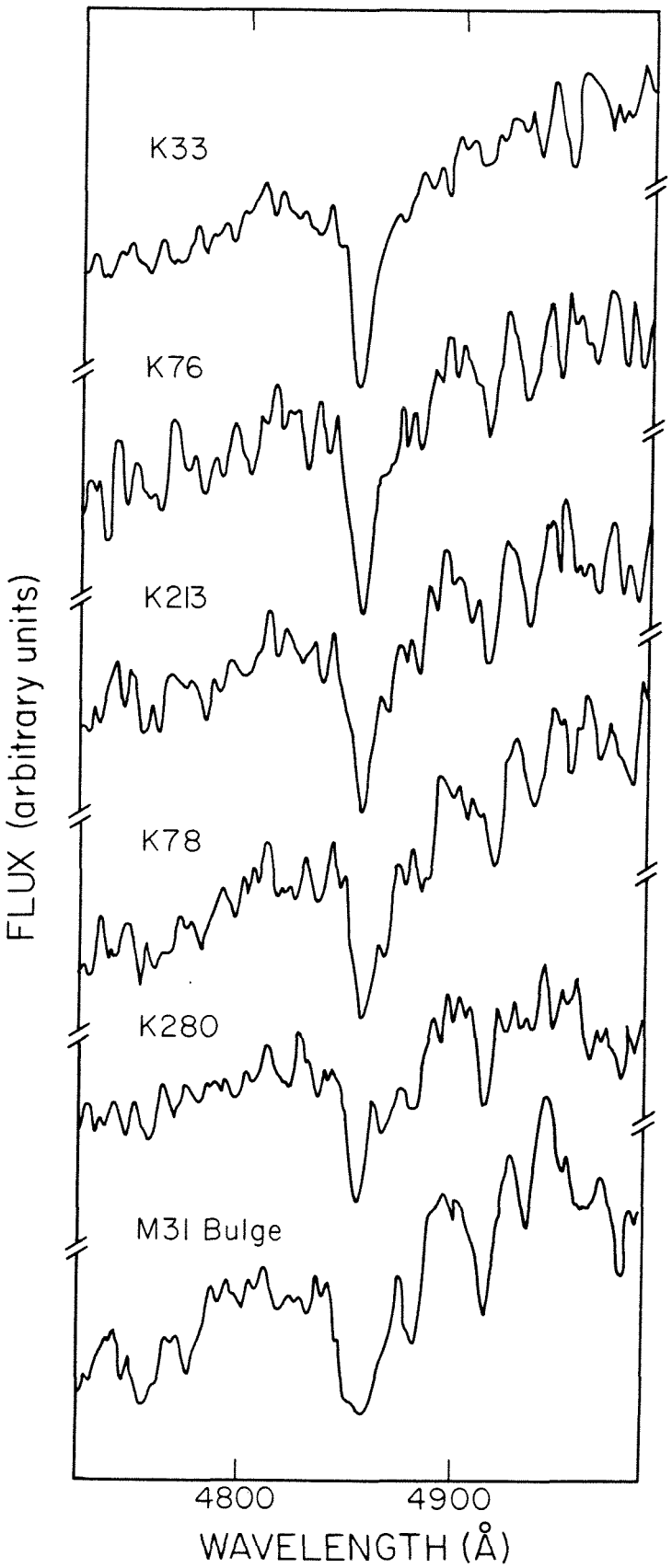
K33
K76
K213
K78
K280
M31 Bulge
FLUX (arbitrary units)
4800
4900
WAVELENGTH (Å)

Figure 19

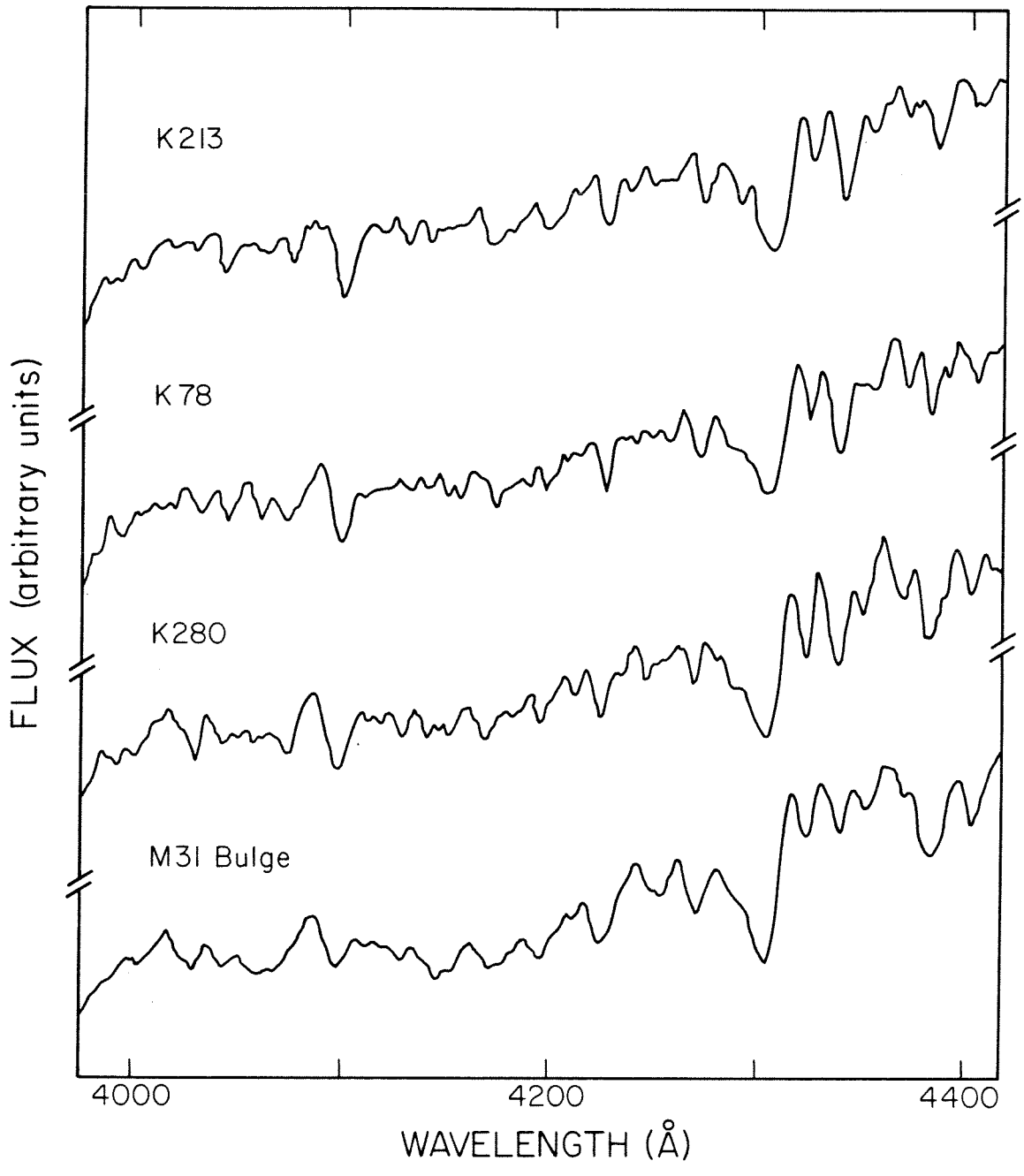
K213
K78
K280
M31 Bulge
FLUX (arbitrary units)
4000
4200
4400
WAVELENGTH (Å)

Figure 20

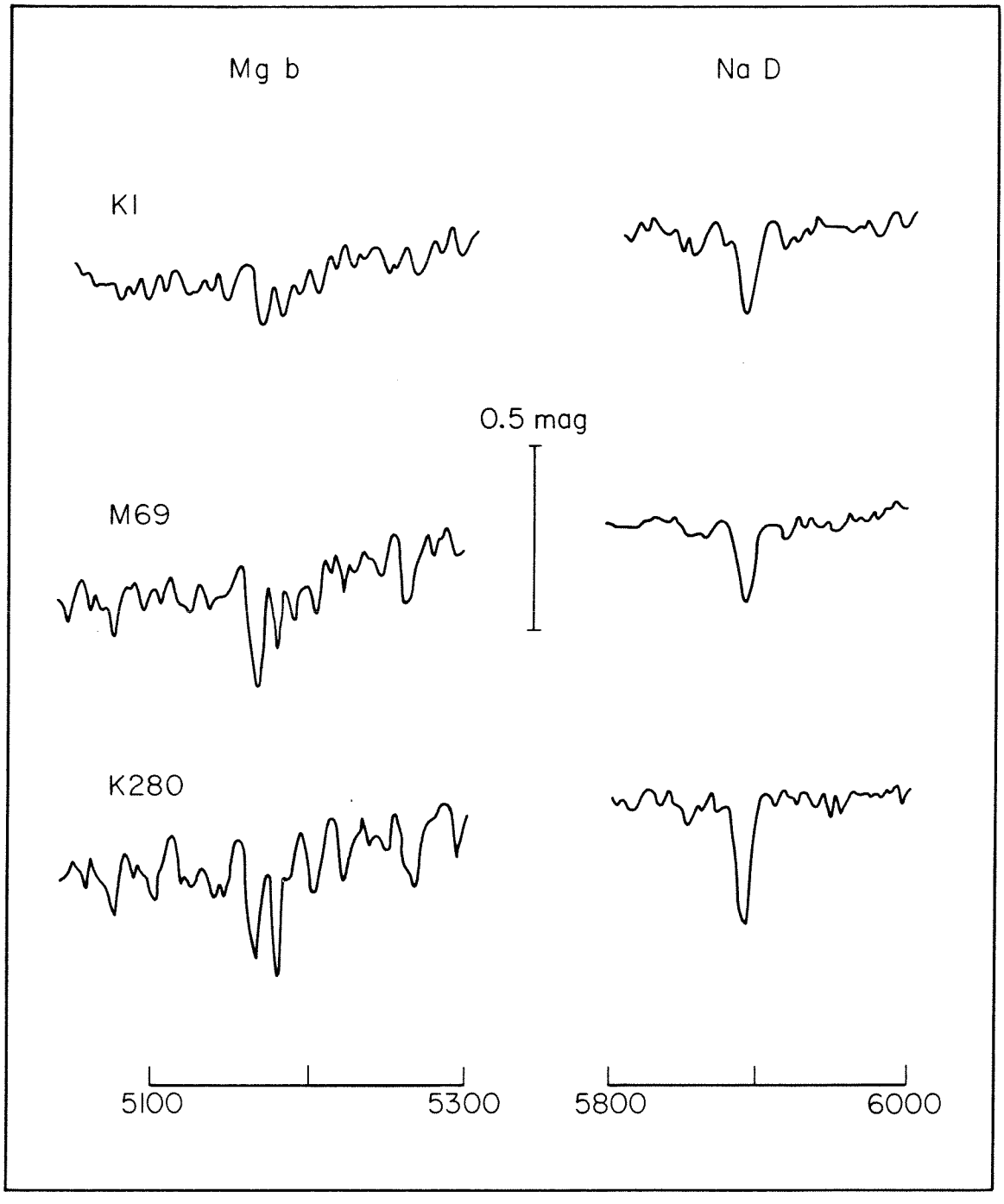

Figure 21

Chapter 2

ANALYSIS OF INTEGRATED SPECTRA OF RED STAR CLUSTERS IN THE MAGELLANIC CLOUDS

I. INTRODUCTION

a) Overview of Previous Work on Populous Clusters in the Magellanic Clouds

The development of our knowledge of star clusters in M 31 has been fairly straightforward, with a handful of important landmarks along the route. In contrast, the investigation of the "globular" clusters in the Magellanic Clouds has been colorful, with continually shifting observational and theoretical perspectives. Some of this may be ascribed to the accident that the Clouds are ten times closer to us, allowing a greater variety of observational techniques to be applied with small telescopes and simple equipment. However, much of the complexity (and interest) is intrinsic to the family of clusters. Whereas M 31 has long been viewed as a galaxy much like our own, leading to the expectation that its star clusters would share this similarity (as they in fact do – Chapter 1), it has been clear from the start that the star clusters in the Clouds could play an important role in unraveling a history of star formation very different from our own. We may now be at the threshold of being able to fulfill this promise, as a result of recent progress in the quantitative assessment of age and abundance for a few clusters.

For the purposes of review, we may divide the modern work on clusters in the Magellanic Clouds into three phases. At the beginning of the first phase, Shapley (1930) listed ten objects as true globular clusters and noted that none of them coincided with objects so designated in the NGC. These ten are now classified as red populous clusters. Interestingly, the honor of recognizing the blue populous clusters belongs not to later photometric investigators but to the redoubtable Annie Cannon: she classified the integrated spectra of eight clusters as early A-type. Thus, the separation of the compact, spheroidal clusters into a red group and a blue group was established by 1930. Considerably later, Shapley and Nail (1951) investigated one of the red clusters, N 1866, in more detail. They found many classical Cepheids, but no

RR Lyrae stars. They concluded that N 1866 was unlike globular clusters in the Galaxy, and also unlike open clusters, in which Cepheids are rare. Comparing the frequency of of variable and non-variable stars in the cluster with their frequency in the surrounding field, Shapley and Nail also made the important observation that the cluster could be taken almost to be a concentrated representation of the general stellar population in its vicinity. Many subsequent workers have noticed this tendency in color–magnitude diagrams (*e.g.*, Arp 1958; Arp and Thackeray 1967; Hardy, Melnick and Reheault 1980); it strengthens the belief that an understanding of the clusters can lead to a broader understanding of the history of the Clouds.

Although color–magnitude diagrams (CMDs) and photoelectric photometry of integrated light were the main avenues of advancement in the remainder of the first period, variable stars were again important in setting the stage. In 1953, Thackeray and Wesselink reported the existence of RR Lyrae stars in some of the clusters in each Cloud, thus establishing a link to Population II in the Galaxy. Tifft (1963) showed that the CMD of one of these clusters, N 121, was indeed similar to the CMD of a classical halo globular cluster, except that the horizontal branch was distinctly redder. Other color–magnitude work by Arp, Eggen and Sandage, Gascoigne, and Hodge led to a wide-ranging discussion of 17 red clusters by Gascoigne (1966), the culmination of the first period of investigation. Gascoigne argued that most of the clusters fell into one of three groups. Members of the first group (such as N 121, N 1466) were similar to metal poor galactic globulars. The SMC group (Lindsay 1, Kron 3, N 339 and N 419) was typified by a horizontal branch either red or absent and an integrated color much bluer that the stars on the giant branch. Gascoigne tentatively identified the SMC group with "intermediate age" clusters in the Galaxy, such as N 2158, thought to be about 10^9 y old (Arp 1962). The members of the third group, all in the LMC (N 2209, N 2231, Hodge 11), were distinguished by an ill-defined giant branch and the presence of blue stars just above the plate limit. These clusters appeared to have no

galactic counterparts. Gascoigne (1964) had earlier noted an important lack of correspondence in the opposite sense: there appeared to be no cluster in the Clouds like the metal rich galactic globular cluster N 6356.

Another summary point was reached with the *UBV* photometry of 52 clusters by van den Bergh and Hagen (1968), which superseded the earlier work of Gascoigne and Kron (1952). A division by color was strongly confirmed: all the clusters could be assigned unambiguously to a red group or to a blue group, with N 1987 the only exception. However, the members of the red group did not follow the well-defined relation between $B-V$ and the reddening-insensitive parameter $Q \equiv B-V-0.72\,(U-B)$ which van den Bergh (1967) had earlier established for galactic globular clusters. Moreover, van den Bergh stressed the presence in many of the red clusters of extremely red stars ($B-V \approx 2.0$) at the tip of the giant branch, a phenomenon rare or absent in galactic globulars.

At this point, the first long phase of research concluded with battle lines drawn: (1) clusters in the blue group were young, but their metal abundance was unknown; (2) the red group was clearly heterogeneous, containing some clusters which were old and at least moderately metal poor, some clusters which were younger, perhaps as young as 10^9 y, with metallicities unknown, and some clusters which defied classification.

The second phase has been one of consolidation and refinement. Walker (1970) initiated a series of studies which employ an electronographic camera to extend the CMD to $V \approx 21.5$, two magnitudes fainter than Gascoigne's (1966) limit; this program is still active (Walker 1979a,b). The new CMDs have many puzzling or ambiguous features, as expected. At least in the case of N 2209, however, a clear verdict could be delivered on a member of Gascoigne's LMC group: the blue stars are the upper end of an evolved main sequence, and the cluster is young, perhaps about the age of the

Hyades (but see §IIIc below).

Photometric activity turned to intermediate-band systems in the expectation that they would respond more sensitively to line blanketing and to ultraviolet light from hot stars. The conclusions from UBV photometry of the red group of populous clusters had been mainly negative in character, in that the clusters do not behave as galactic globular clusters do; now the principal aim was to impose some order upon the red group. Danziger (1973) used an 11-color system which included several narrow filters designed to monitor Hδ and specific metallic features. On the assumption that metallicity was the dominant parameter affecting the integrated spectra, Danziger classified his sample of 20 clusters into six groups. It now seems clear that Danziger underestimated the importance of relative youth in producing a spectrum like that of N1987, classified as "weaker-lined than M15, M92." However, his work was an important stimulus for further investigation. Searle, Wilkinson and Bagnuolo (1980; subsequently SWB), using a four color system, produced the first convincing classification of the red clusters – one which, moreover, embraced the blue and the red groups in a single sequence. SWB also demonstrated that Danziger's data were reasonably ordered by the new scheme.

In comparison with other approaches, the analysis of integrated spectra has so far been disappointing. Ford (1970) classified image tube spectra of 13 Cloud clusters according to the precepts designed by Morgan (1956) for the classification of galactic globular clusters. However, perhaps the most important result came from a direct comparison with the integrated spectrum of one galactic globular: none of the Cloud spectra had metallic lines as strong as those in 47 Tucanae, confirming spectroscopically the earlier remark of Gascoigne (1964) based on CMDs. In a study of 13 red clusters, Andrews and Lloyd Evans (1971) found little difficulty in assigning spectral types in much the same way that Kinman (1959) had done for galactic globulars. Kron 3 and Hodge 11 were singled out as peculiar, but only on the basis of the Balmer

lines H9 and H10; the exposures were long and weak. N419 was described as having "a typical halo-type spectrum." The compositeness of the spectra was judged indistinguishable from that of galactic globulars. The only systematic peculiarity noted was the lack of correlation between spectral type and the photometric parameter Q, in accord with van den Bergh and Hagen's (1968) result for Q and $B-V$. A companion study of blue clusters by Andrews and Lloyd Evans (1972) was oriented toward radial velocities and shed little light on the systematic properties of the absorption spectrum.

A more general development in Magellanic Cloud studies occurred during the second period which inevitably affected the perspective of cluster research. Evidence began to point to a general deficiency of metals in the Small Cloud, roughly -0.7 dex with respect to the sun, and a smaller but definite deficiency in the large cloud, perhaps -0.3 dex (reviews by Peimbert 1975 and van den Bergh 1975). It would be natural, by analogy to the Galaxy, and consistent with available evidence, to hypothesize that these general metallicities bound from above the metallicities of clusters within each Cloud.

It is clear that what have called the second phase of research is an ongoing enterprise. The third phase represents the new possibilities created by large telescopes in the southern hemisphere and by recent advances in instrumentation and in the theory of stellar evolution. The new emphasis will be on the quantitative assessment of age and abundances.

N2209 furnishes an example of several of these tendencies. Gascoigne *et al.* (1976) measured a new CMD from plates taken with the 4 meter Anglo-Australian telescope while it was still in the engineering phase. The evolved main sequence could be traced down to a definite turnoff. Combining DDO photometry of two stars in the cluster with the color of the subgiant branch, Gascoigne *et al.* estimated a logarithmic metal

deficiency relative to the sun of [Fe/H] = −1.2. They then used evolutionary tracks for an appropriate composition to estimate a turnoff age of 8×10^8 y. Analyzing the same data, Gustafsson, Bell and Hejlesen (1977) used, in addition to evolutionary models, another recent addition to the theoretical arsenal: extensive grids of model stellar atmospheres (Gustafsson *et al.* 1975). They concluded that a better estimate of the metallicity was [Fe/H] = −0.5, closer to the (by now) generally received estimate for the LMC interstellar medium.

As a final example of the new approaches to cluster research, we mention infrared photometry on the giant branch, particularly of the very red stars which had been the object of puzzlement since the days of the first CMDs. A quarter century after Arp's original suggestion (Arp 1958), Feast and Lloyd Evans (1973) finally proved spectroscopically that at least one of these is a carbon star. Using both spectroscopy and IR photometry, Mould and Aaronson (1979,1980) have greatly extended the sample of carbon (and ordinary M) stars. The infrared photometry may be a key to exploiting two areas of recent theoretical progress. First, infrared colors can provide a metallicity-insensitive estimate of the effective temperature along the giant branch, a most useful datum in restricting choice among a set of theoretical isochrones. Second, accurate bolometric luminosities are necessary for comparison with the theory of stellar evolution beyond the helium flash (Gingold 1975; Iben and Truran 1978).[1] Since the luminosity of a star on the asymptotic giant branch (AGB) depends on its core mass, the age of a cluster clearly influences the morphology of the upper giant branch. As the theory develops, fairly stringent restrictions may be placed on the ages of clusters with stars on the AGB above the first giant tip (Mould and Aaronson 1980).

---

1. Frogel, Cohen and Persson (1980) have found that the bolometric luminosities reported in Mould and Aaronson (1979) are systematically in error by almost two magnitudes.

b) Role of this Investigation

Despite its early importance in distinguishing red clusters from blue, spectroscopy of integrated light has contributed relatively little to the understanding of populous clusters in the Magellanic Clouds. Some fault for this lies with the observations themselves: many clusters have low surface brightness and require long exposures, even with a large telescope. Still, there are sound reasons for continuing to study integrated spectra. First, the turnoff region remains difficult to reach photographically (with the usual calibration problems at faint magnitudes) and nearly inaccessible to photoelectric photometry; but the turnoff contributes importantly to the integrated spectrum, particularly for the many clusters which have a weak giant branch and a red horizontal branch or giant clump. Second, with photometric data, the issue of metallic line strength must always be approached indirectly and with some trepidation, even for single stars; the integrated spectrum allows individual metallic features to be compared among themselves and with hydrogen lines. Finally, if the few determinations of age by direct observation of the turnoff can be used to calibrate features in the integrated spectrum, future spectroscopic observations may be able to probe the history of star formation in nearby galaxies for ages between those typified by young associations and by galactic globular clusters.

Further impetus for this investigation was provided by the availability of an integrating vidicon system at Cerro Tololo. This digital system promised several advantages: (1) straightforward summation of the signal from the area of the cluster with approximate subtraction of the (sometimes considerable) field contribution; (2) co-addition of exposures; (3) the superior accuracy in the measurement of equivalent widths and central depths afforded by an intrinsically linear detector.

II. OBSERVATIONS

a) Program and Instrumentation

The availability of a modern color–magnitude diagram was the principal criterion in the selection of clusters for the program. Thus, N 2209, with good determinations of age and abundance (Gascoigne *et al.* 1976; Gustafsson, Bell and Hejlesen 1977), and Kron 3, with a problematic CMD (Walker 1970; Gascoigne 1980), were included despite the long exposures required. N 1987, although lacking a CMD, was considered important because it is the only cluster in van den Bergh and Hagen's (1968) UBV study which cannot be assigned unequivocally either to the red or the blue group. For the rest of the sample, red clusters were chosen exclusively. Because of the rapid evolution of the main sequence turnoff for clusters $\lesssim 5 \times 10^8$ y old, the integrated color of a blue cluster is already a good indicator of its age; as to metallicity, the A-type integrated spectrum offers little hold for an analysis at low dispersion.

Integrated spectra of 17 red clusters in the Magellanic Clouds and 7 galactic globular clusters were obtained with the SIT vidicon (Atwood *et al.* 1979) attached to the 1.5 m telescope at Cerro Tololo. Table 1 summarizes the parameters of the spectrograph-detector combination. 170 pixels (8.5') were exposed along the slit, but only the central 128 pixels (6.4') were included in the reduction procedure. The spectral resolution was limited mainly by the spectrograph camera.

The clusters are listed in Table 2 together with *UBV* photometry, intermediate band photometry from SWB, and references to color–magnitude work. During a cluster observation, the telescope was scanned in declination over a range chosen at the telescope, considering both the surface brightness of the cluster and the density of the background field; this range is noted in Table 2. All observations were made with the telescope in focus. There was no moonlight.

b) Reduction Procedure

Initially, the data were fully reduced with the CTIO software package, but the results were unsatisfactory: the continuum energy distributions derived for the same object on different nights did not always agree to within the anticipated photometric errors, and, in the case of galactic globulars, the distribution sometimes differed systematically from previous determinations (van den Bergh and Henry 1962; Aller and Faulkner 1964).[2] Although spectrophotometry was not the aim of these observations, experience with SIT vidicons has shown that unexpected behavior in the continuum distribution may reflect instrumental problems, such as variations in gain or zero point, which can also affect the determination of equivalent widths. Therefore, all the data were reduced *ab initio* with the system developed for the SIT spectrographs at Palomar (the same system applied to the observations in Chapter 1). The chief advantage of the new system proved to be its large format, high resolution scan converter. The visual display was used to choose the limits of integration along the slit for object and for sky; to verify the adequacy of the compensation for S-distortion of the spectrum; and to monitor over the whole frame small changes in dark level or alignment – changes which are difficult to detect (and were not detected) in a selection of cuts across the target but which, uncompensated, materially degrade the quality of the final result.

Another substantial change concerned the CTIO standard stars, which consisted of Oke scanner standards (Oke 1964; Hayes 1970) and secondarily calibrated standards in the Clouds. As given in the CTIO reduction package, the standard magnitudes produced inconsistent corrections for instrumental response and, worse, left local features in the rectified spectra. A new set of standard magnitudes was prepared with reference to the original scanner magnitudes; fortunately, a calibration of the

---

2. These data were reduced with an early version of the CTIO "long slit" software; no remark, here or in what follows, should be taken to apply to the current CTIO software.

wavelength response of the neutral density filter required for observations of these bright stars had also been obtained as a precaution. The standard extinction coefficients did not agree well with the mean coefficients for Cerro Tololo given by Hayes and Latham (1975) and were replaced.

No claim of accuracy, in absolute terms, is made for the new set of magnitudes. They do produce final energy distributions which are smooth, reproducible, and in satisfactory agreement with independent data. An observation which yields a well behaved distribution is unlikely to be afflicted with the most common SIT problems; but, if poor standard magnitudes and extinction coefficients distort the distribution in any case, this important consistency check is not possible.

No flat field calibration was applied. Exposures were taken of the inside of the dome illuminated by an incandescent source, but twilight contaminated some of the frames, and the uniformity of the illumination was judged questionable. However, the uncorrected target response was locally smooth at the 3–4% level, in agreement with the specification given by Atwood *et al.* (1979). Both the local and the global uniformity of the target were considerably superior to those of the Palomar vidicons, for which flat field corrections had already proved to be of mainly cosmetic value (Chapter 1). In any case, the best attempts to flatten the data resulted in very small changes in the final magnitudes and no reduction of the noise level. Neither could flattening remove a blemish near the center of the target. The smaller clusters were placed so as to avoid the blemish, but in some cases the affected lines were included in order to maximize signal. The blemish appears (when it does) as a spurious bump in the spectrum near 4500 Å. This was ignored in fitting the pseudocontinuum described below, and there are no measured absorption features near the affected wavelengths.

After integration along the slit, the net signal (sky- and dark-subtracted) from a

single cluster observation was typically ~ 2500 photons in each wavelength bin near 4500 Å. Weak exposures are noted in Table 2.

The observations of two clusters, N 1783 and N 2209, were affected by a transient instrumental problem. The symptoms were: (1) a slight defocussing, manifested by a softer appearance on the scan converter; (2) a slight ($\lesssim 5°$) tilt and skewness to the field (the row on the target in which intensity reached maximum tilted more than the spectral lines, which remained well aligned with the columns). In partial response to this problem, the *S*-distortion was recalibrated separately for each of the two afflicted frames. Then, unusually tight limits were chosen for the object and sky bands in order to minimize the total number of rows involved. The final spectra are naturally of lesser quality, particularly blueward of 3850 Å and redward of 5100 Å. Fortunately, in view of its importance, N 2209 was less affected than N 1783. Since the exposure for N 2209 was also fairly strong ($\gtrsim 4000$ net photons in each wavelength bin near 4500 Å), the measurements of Hδ, Hγ and Hβ should be nearly as accurate as for other clusters. It is important to note that the SIT problem, whatever its origin, was truly transient: the frames immediately preceding and following the affected frames showed *no* peculiarities.

c) Measurement of Equivalent Widths

The following features were measured: Ca II K, Ca II H + Hε, G band, Hδ, Hγ, Hβ, and two other local spectrum parameters to be described below. It was disappointing to discover that Ca I λ4227 and Fe I λ4383 are, on average, too weak to permit useful comparisons over the full sample of clusters, although often the lines could be measured in individual cases. Inclusion of the Mg b triplet near 5175 Å was a constraint in choosing the spectral range for these observations; but the feature could not be reliably measured in the reduced spectra. The noise level increases noticeably to the red of Hβ as a result of declining grating efficiency (the peak of the blaze is below 3500 Å)

and probably of vignetting in the camera optics.

For the M 31 clusters considered in Chapter 1, the irregularity of the stronger-lined spectra frustrated attempts to define a pseudocontinuum which spanned more than one feature. As a group, the Cloud clusters have weaker metallic lines. This, coupled with lower spectral resolution, makes it possible to define a more conventional pseudocontinuum which extends over $\gtrsim$ 200 Å. Guidance from a more global continuum is also very desirable with blended features (such as Hγ and the G band) and with the extended Balmer line wings found in some clusters.

Four steps in the measurement process may be followed with reference to Figure 1.

1. The reduced spectrum was displayed as a plot of f_ν *versus* λ on a graphics terminal. It was found that the shape of the spectrum in the range $\lambda\lambda$4000-4800 could be well represented by two linear segments intersecting just to the blue of the G band (the extent of this G band break is measured in step 4). Although definite absorption features were ignored, an attempt was made to compensate for the general noise level so that the continuum segments did not rest on noise peaks, thereby inflating all equivalent widths.

2. The vicinity of each feature to be measured was displayed on a larger scale with the appropriate continuum segment redrawn. The line profile was outlined graphically, typically with about 10 segments, and then integrated numerically to derive an equivalent width (EW). Occasionally, a small vertical adjustment of the continuum segment (with unchanged slope) was allowed the better to fit the profile; but this was avoided in the interest of consistency.

As shown in the inset to Figure 1, the blue wing of Hγ was completed by symmetry; since there was no way similarly to "complete" the G band, its area was considered bounded by the profile of Hγ. A confluence of weak lines sometimes depressed the blue wing of Hδ, in which case the profile was again symmetrized by reference to the

red wing – a minor adjustment. No adjustments were needed for Hβ.

3. Because of the K break, the equivalent width of the K line could not be referred to either of the continuum segments defined above. The K break and EW(K) were measured in a consistent fashion as follows: the $\lambda\lambda$4000-4250 continuum segment was extended blueward and dropped parallel to itself until it rested on the local peak separating CaK from H8 and the CN bands. The required translation in magnitudes measures the K break and is denoted ΔK; this definition is essentially the one introduced by van den Bergh and Henry (1962). The lowered segment also functioned fairly well as a pseudocontinuum for the range $\lambda\lambda$3780-3980; in particular, it served to bound Ca H+Hε.

4. The break in continuum slope shortward of the G band, caused by the G band itself, by the blue CN band (degrading blueward from a bandhead at 4215 Å), and probably by increasing iron absorption, was measured in a reddening-insensitive manner. Define the *local* continuum slopes on each side of the break by

$$S_+ = \left.\frac{dm_\nu}{d(1/\lambda)}\right|_{\lambda=4400+}, \qquad S_- = \left.\frac{dm_\nu}{d(1/\lambda)}\right|_{\lambda=4400-}. \tag{1}$$

Ordinarily, the difference $S_+ - S_-$ would be insensitive to reddening of the Whitford type, $\Delta m = E(B-V)[a\lambda^{-1} + c]$ (Whitford 1958); as it happens, the break in Whitford's two-segment representation of the reddening law occurs at about 4370 Å, with one slope, a_+ applying redward and a different slope, a_-, applying blueward. However, it is easily verified that

$$\Delta S = S_+ - \frac{a_+}{a_-} S_- \tag{2}$$

is a reddening-free combination which measures curvature intrinsic to the spectrum (Searle and Zinn 1978 describe another approach to this problem based on transformation of the wavelength scale; the effect would be the same). The values $a_+ = 2.20$,

$a_- = 1.57$, have been freshly determined by least squares fits to the scanner data of Schild (1977).

Although the two pseudocontinuum segments were chosen in the $f_\nu - \lambda$ plane, it must be emphasized that equations (1) were used to obtain the numerical values of S_+ and S_-. Over the small wavelength ranges considered, linear segments in the $f_\nu - \lambda$ plane map satisfactorily onto different linear segments in the $m_\nu - \lambda^{-1}$ plane.

III. RESULTS AND DISCUSSION

a) Spectra

In Figure 2*a*, the spectra of clusters in the Magellanic Clouds are arranged approximately in order of Balmer line strength, as are the galactic globular clusters in Figure 2*b*.[3] The Cloud clusters show a striking range of hydrogen line strengths. The EW of Hδ in N 419 is more than twice as great as it is in M 15, whereas the H lines in N 121 are among the weakest in the whole sample. The great Balmer lines in clusters such as N 1987 or N 2209 are not caused by stars on the horizontal branch: synthetic spectra of model clusters (discussed below) reveal that the effect of the horizontal branch cannot be so large; and, in the case of N 2209, the CMD simply has no horizontal branch. Neither can extreme metal deficiency alone explain the Balmer lines: with the possible exception of Hodge 11 (Freeman and Gascoigne 1976; Walker 1979a), no cluster thusfar studied has a giant branch bluer than that of M 15; most are redder by an amount several times the mean reddening, $E(B-V) \approx 0.06$, suggested by van den Bergh and Hagen (1968) for old and intermediate age clusters. We are thus led to postulate age as the most significant factor. Some of the red clusters in the Clouds must be younger than any galactic globular cluster. Only for N 2209 has this relative youth been established in detail from the CMD (Gascoigne *et al.* 1976). The sections to follow will construct a preliminary framework in which characteristics of the

3. In what follows, "globular cluster" or "globular" will be used exclusively as shorthand for "globular cluster in the Galaxy."

integrated spectrum may be combined with data derived exclusively from the brighter individual stars to constrain the age of a cluster, sometimes within surprisingly tight limits.

b) Equivalent Widths

Equivalent widths and break parameters for all the clusters are given in Table 3.

Figure 3 shows that the equivalent widths of Ca K and the G band are tightly correlated. The relation is sensibly linear except for the three strongest-lined clusters, which appear to indicate a "saturation" of EW(K) with respect to EW(G band).

In Figure 3, clusters from the Galaxy and from both Clouds intermingle over the full range of line strength. Although the sample from the SMC is too small to support a definite conclusion, it is clear that the LMC clusters and the globular clusters define the same sequence. Of all the clusters, only N411 and N1846 might be considered outliers. Notice that M15 and N1987 are adjacent in the G−K diagram. As will become clear below, dilution of metallic features by turnoff stars ensures the weak-lined appearance of N1987, regardless of its metallicity, whereas the metal poor giants and horizontal branch stars in M15 would produce a similar spectrum even were its turnoff much redder (older). A comparison of metallic features within the narrow spectral range of these observation cannot discriminate between the effects of age and composition. Similarly, despite the broader wavelength coverage of his 11-color system, Danziger (1973) took his classification of N1987 as "weaker-lined than M15, M92" to imply a metal deficiency more extreme than any in the Galaxy.

The tightness of the relation in Figure 3 also constrains the mean size of random errors in the measured equivalent widths. These errors are difficult to estimate for a given spectrum; they compound the effect of signal-to-noise in the line itself with the effect of continuum placement, itself related to the overall quality of the spectrum and to the intrinsic line strength of the object. For the globulars, two spectra of

similar quality are usually available for comparison. Invariably, the estimate of error derived from one spectrum by varying the continuum and the line profile within "reasonable" limits is too pessimistic in light of the agreement between the two spectra, usually about ± 5%. The subjective element in the measurement process is counterbalanced by its consistency in application and can even be turned to advantage by allowing for varying degrees of signal-to-noise. Since only one good spectrum is available for most of the Cloud clusters, Figure 3 is taken as the best indication of the level of random error. This assertion is consistent with the two independent observations of N 121 shown in the figure.

In Figure 4, the median of the EWs of Hδ, Hγ and Hβ is plotted against EW(K). The median has the advantage of being resistant to outlying values, but it is a reasonable statistic only if the EWs of the three Balmer lines are comparable. This condition is fulfilled: the mean values are 4.58, 4.47, and 4.63 for Hδ, Hγ and Hβ; the median coincides with Hδ 9 times, with Hγ 8 times, and with Hβ 6 times. The group assignment according to the classification scheme of SWB has been appended to those clusters for which it is available.

Clearly, the Balmer lines introduce a degree of freedom not present in Figure 3. In fact, the bare distribution of points is confusing enough that some orientation is desirable even in a preliminary discussion. The straight line at the bottom of Figure 4 is a least squares fit to the points representing all the globulars (with the exception of M 30, discussed separately below). The departures from this line are small indeed. Within the scope of the present observations, the globulars define a one-parameter sequence. The crosses, labelled by age in units of 10^9 y, represent a sequence of model star clusters of solar abundance. These models, described in detail in Chapter 3, combine SIT spectra of MK standard stars according to the isochrones of Ciardullo and Demarque (1977) to produce a synthetic spectrum which is then measured exactly as if it were an observed cluster. [The synthetic spectrum does not extend to

Hβ, and EW(Hγ) is confused by the G band for metal rich clusters, so EW(Hδ) is plotted as the cleanest representative of Balmer line strength.]

The essential message of Figure 4 is that the gross physical properties of the red clusters in the Magellanic Clouds are bounded by two sequences: a sequence of globular clusters, all about 10^{10} y old but varying widely in metallicity, and an age sequence of solar abundance clusters. The natural inferences are that all the red clusters are metal poor to some degree and that most are younger than globular clusters by an amount significantly greater than the dispersion in age among the globulars themselves. Neither of these inferences is novel; but Figure 4, while it falls short of proof, strongly and compactly suggests both at once. The structure of this diagram will now be explored in detail.

c) "Young" Red Clusters

Figure 4 shows that the strength of the hydrogen lines in the integrated spectrum is a sensitive indicator of age for ages less than a few times 10^9 y. As an example of this discriminative power, a single spectrum of N419 (an easy object with high surface brightness) would seem to select decisively from among the options considered by Walker in his (1972) color–magnitude study: N419 is young, older than N2209 but closer to it than to a globular cluster with a red-stub horizontal branch.

If N2209 and N1987 were of solar abundance, Figure 4 would fix their ages at 10^9 y with an accuracy of perhaps $\pm$ 10%. Indeed, Gascoigne *et al.* (1976) assign an age $\sim 8 \times 10^8$ y to N2209 from a CMD extending to the turnoff. However, an estimate of the age of a star cluster is always linked to an estimate of its metallicity, no less so in the use of hydrogen line strength. This is made plain in Figure 5, which displays contours of constant EW(Hδ) in the plane of age and composition. Since it was not possible to assemble distinct and complete libraries of stars over a range of metallicity, the calculations were instead based on the theoretical hydrogen profiles of Kurucz (1979),

supplemented for temperatures below 6000 K by observed profiles from high dispersion spectra of globular cluster and open cluster giants. For clusters of solar abundance, the EW determined in this manner agrees with the EW determined from the full synthetic spectrum to better than 10% for EW(Hδ) > 8 Å.

Gascoigne *et al.* (1976) adopt [Fe/H] ≈ -1.2 for N2209 on the basis of two methods which gave [Fe/H] $= -1.4$ and [Fe/H] $= -1.0$. These estimates are used as limits, together with an allowance of $\pm$ 10% in the value of EW(Hδ) to determine the shaded box in Figure 5. The corresponding age is $2.4 \pm 0.6 \times 10^9$ y. Commenting on the same data used by Gascoigne *et al.*, Gustafsson, Bell and Hejlesen (1977) argue that [Fe/H] ≈ -0.5 is a better estimate. This value, with an assumed uncertainty of $\pm$ 0.2 in [Fe/H], is also shown in Figure 5 and leads to an age $1.4 \pm 0.5 \times 10^9$ y.

Although the main purpose of this discussion has been to stress the interplay of age and abundance in determining the strength of Balmer lines in the integrated spectrum, the age of N2209 is of interest in its own right. According to the integrated UBV colors given by Freeman and Gascoigne (1977), N2209 joins N1987 in the disputed territory between the red and blue groups; these two clusters are at least "the bluest of the red" and probably define the lower age limit of the red clusters.

In Figure 6, isochrones for several ages and compositions are superposed on the CMD for N2209 from Gascoigne *et al.* (1976). [Chapter 3 will describe the modifications to the Ciardullo and Demarque (1977) isochrones and the freshly-assembled temperature-color relations which were used to create these isochrones in the observational plane.] The isochrone for 2×10^9 y with (Y, Z) = (0.3, 10^{-3}) closely matches the observed maximum luminosity at the blue edge of the Hertzsprung gap, $V_{hg} \approx 19.8$, and passes through the giant clump at $(B-V)_{cl} \approx 0.8$. The model turnoff may be slightly too blue, but the observed turnoff at $(B-V)_{to} \approx 0.15$ is certainly bracketed by the isochrones for 2×10^9 y and 4×10^9 y. Allowing for uncertainties in pho-

tometry, distance modulus and reddening, we may choose an age $2.5 \pm 0.5 \times 10^9$ y as consistent with the main features of the CMD: turnoff color,[4] maximum luminosity in the shell narrowing phase, and position of the giant branch. This is precisely the age estimated previously from the strength of the hydrogen lines.

In conjunction with the isochrones, the color of the giant clump and the position of the giant branch for $V > 18$ support a metallicity closer to [Fe/H] = −1 than to the value [Fe/H] = −0.5 advocated by Gustafsson, Bell and Hejlesen (1977). However, interpretation of the giant branch is complicated by its sparseness, by the probable presence of at least two carbon stars near the luminosity of the first giant tip (Mould and Aaronson 1980), by the uncertain evolutionary status of the clump giants, and by the approximate treatment of convection in the giant models. If [Fe/H] = −0.3 is specified, the turnoff color indicates an age $1.3 \pm 0.3 \times 10^9$ y, again in agreement with the age inferred from hydrogen line strength.

A further indirect argument may be made from integrated colors. The colors given for N 2209 in Table 2 are slightly redder than those calculated for the Hyades by Gray (1965): $B-V = 0.49$, $U-B = 0.17$. Since, at given age, the HR locus of a cluster shifts to higher effective temperatures as metallicity decreases, and since the metal poor stars are bluer at given T_e, it follows that the more metal poor of a pair of clusters with the same integrated colors should be older. If the Hyades is $\sim 8 \times 10^8$ y old (Hirshfeld, McClure and Twarog 1978), then N 2209 should be older than the $\sim 8 \times 10^8$ y estimated by Gascoigne *et al.* This argument would be stronger were it not for the possibility of a substantial difference in luminosity function between the two clusters and for the statistical uncertainty in calculating an integrated color for the Hyades.

---

4. It is worth noting that the caveat regarding convection which traditionally accompanies the fitting of isochrones to the color of the turnoff does not here apply. $(B-V)_{to} \approx 0.15$ corresponds to an effective temperature $\log T_e \approx 3.91$, and, as Iben (1963) and others have pointed out, the convective envelope in models hotter than $\log T_e \approx 3.88$ is too shallow to influence the stellar radius (or thereby T_e).

d) "Old" Red Clusters

i) The Question of Age

In Figure 4, the group of "old" red clusters will be arbitrarily defined to comprise those clusters that lie below the line that passes through N 1841 and is parallel to the line defined by galactic globular clusters. Only N 121 lies below the line of globulars (subsequently denoted the "reference line"); but several clusters lie well above it. How might such objects differ from globulars?

The difference cannot simply be one of overall metallicity, for the reference line already reflects, more than it does any other factor, a sequence in metallicity with range sufficient to encompass the K line strengths of *all* the cloud clusters. Neither, according to the results of Chapter 1, can a variation in the power law index of the pre-horizontal-branch luminosity function between limits of 0 and 3.5 (where the Salpeter index is 2.35) produce so much as a 10% change in the equivalent width of Hδ for a cluster 10^{10} y old with $Z = 10^{-3}$.

A systematic difference in the distribution of stars along the horizontal branch (HB) is certainly capable of elevating a cluster above the reference line: in Figure 4, the trajectory emanating from 47 Tuc shows the effect, according to synthesis models, of substituting an M3- or M92-type distribution for the 47 Tuc HB. Thus, for example, N 2121 is suitably placed with respect to M 75 to lie on an HB trajectory. For N 2121 and for N 1978, however, this possibility may be rejected outright: neither cluster has more than a giant clump or stub HB, whereas M 75 has a well developed HB with stars on both sides of the RR Lyrae region. Instead of providing an explanation, the HB trajectory heightens the need for one. This follows because the red HB of 47 Tuc changes EW(Hδ) little from what it would have been in the absence of a horizontal branch (and even decreases it slightly, since the turnoff is bluer than the HB); but the blue HB of M 3 does enhance EW(Hδ). In consequence, a metallicity sequence

of globulars shorn of their horizontal branches would define a line passing near 47 Tuc but with a slope necessarily more shallow than that of the reference line. This implies that the agent which elevates N2121 above the reference line is stronger than might at first appear, since the hydrogen lines in the globulars are already bolstered by their horizontal branches. Unfortunately, the quantitative version of this argument is not yet reliable. There is some evidence that the synthesis models overestimate the enhancement of the Balmer lines caused by a blue HB, even when R_{hbgb}, the ratio of the number of stars on the HB to the number of stars on the giant branch above the HB, is set at $R_{hbgb} = 0.9$ (Iben *et al.* 1969) instead of $R_{hbgb} \approx 1.6$ as suggested by recent work (Renzini 1977). Again on the qualitative level, it must be remembered that a HB trajectory terminating at M15 is shorter and flatter that one beginning at 47 Tuc, because the HB light adds to light from a main sequence and giant branch already shifted to higher temperatures by low metallicity.

Having rejected overall metallicity, luminosity function and the horizontal branch as explanations for the elevated clusters, we are led naturally to age: *it is probable that most of the "old" red clusters are younger than any galactic globular cluster.* In the present sample, perhaps only N1466 and N121 fully qualify, by color–magnitude morphology and by position in Figure 4, as globular clusters in the traditional sense (Kron 3, which lies on the reference line, will be discussed separately below). Even N121 would be distinguished by its unusually red HB for a globular of its K line strength, although the extent of the anomaly would be within the bounds of observed freedom in HB structure – the "second parameter" in globulars. [In Figure 4, N121 is not significantly below the reference line, but its depressed position is both consistent with its HB and supported independently by the value of its narrow band Hδ index, lowest among the Cloud clusters measured by Danziger (1973)].

If N2121, N1978 and N416 are younger than globulars of comparable metallicity, then how much younger? In Figure 4, suppose for these clusters that EW(Hδ) is

enhanced by 30–50% over what it would be for corresponding clusters on a "modified" reference line of globulars without horizontal branches. Then Figure 5, read at $Z = 10^{-3}$ and an upper age of $\sim 12 \times 10^9$ y, suggests an age differential of $2-3 \times 10^9$ y. This can be only a rough first indication, because the hydrogen profiles used to construct Figure 5 do not include the effect of blending with metallic lines, important even at $Z = 10^{-3}$ for ages $\gtrsim 10^{10}$ y [Chapter 1 discusses this problem in another context]. However, such a differential is consistent with the expected effect of age on the structure of the horizontal branch. As pointed out by Rood (1973) and displayed clearly in Figure 7.1 of Renzini (1977), an age decrement of $\gtrsim 2 \times 10^9$ y at $Z = 10^{-3}$ suffices to transform an M 3-type HB into a red stub similar to that seen in N 1978. For larger decrements, the horizontal branch criterion loses sensitivity because the redward migration of the post-helium-flash stars is halted by the Hayashi line. Were the age differential too large, however, the hydrogen lines in the Cloud clusters would become too strong. Unfortunately, the lower bound is not very strong; Figure 5 indicates that a metal poor cluster, $Z \lesssim 10^{-3}$, must be older than $5-7 \times 10^9$ y if $EW(H\delta) \lesssim 4.5$ Å, the upper limit of the old group. More realistic hydrogen profiles, including metallic blending, should allow this limit to be sharpened.

Thus, observations and theoretical models together suggest that some old red clusters are $\gtrsim 3 \times 10^9$ y younger than globulars of similar metallicity. A more *direct* estimate based on Figure 4 would be possible with the use of synthetic spectra that allow a range of metal abundance; the capacity to produce purely theoretical spectra of this sort already exists (Gustafsson and Bell 1979). Still, the difficulty of obtaining a more *precise* estimate may perhaps be judged by the difficulty of determining the age spread of globulars. In that case, far more and better data than are available for the Cloud clusters have so far failed to decide whether the spread is very small, $\sim 10^8$ y (Eggen, Lynden-Bell and Sandage 1962), or quite sizeable, $\gtrsim 3-4 \times 10^9$ y (Sandage 1970; Rood 1973; Demarque and McClure 1977; Carney 1980).

ii) Kron 3, N1841 and M30

Kron 3 presents a puzzle. In Figure 4, it lies precisely on the reference line defined by galactic globular clusters. As mentioned by Gascoigne (1980), it also lies on Racine's intrinsic color-color relation for globulars. Since Kron 3 has at most a stub horizontal branch, these facts would be interpreted, according to the discussion in the last section, to indicate that the metallicity of Kron 3 is comparable to M 2 or M 79 but that the SMC cluster is a few times 10^9 y younger. Indeed, Gascoigne (1980) estimates [Fe/H] ≈ -1.5 from broad band photometry, close to the values -1.53 and -1.58 given for M 2 and M 79 in the compilation of Harris and Racine (1979). Furthermore, the integrated colors of Kron 3, $B-V = 0.70$ and $U-B = 0.10$ (averaging the colors given by van den Bergh and Hagen 1968 and by Alcaino 1978), agree closely with the colors predicted by a synthesis model characterized by (Y, Z, Age) = $(0.3, 10^{-3}, 7\times10^9)$: $B-V = 0.66$, $U-B = 0.08$. The predicted color of the giant branch at the level of the horizontal branch, $(B-V)_{0,g} = 0.85$, also agrees with the CMD shown by Gascoigne (1980). Thus, the difference between the integrated color of the cluster and the color of stars on its giant branch, a feature Gascoigne (1966) strongly emphasized in characterizing the "SMC group", can be explained by a cluster only modestly younger than globulars.

The problem with all this is the faint blue stars in Gascoigne's (1980) color–magnitude diagram. He takes these stars at the plate limit to be an evolved main sequence and estimates the age to be about 3×10^9 y. Even if [Fe/H] is closer to -1.0 than to -1.5, Figure 5 indicates that a cluster that young should show strong hydrogen lines in the integrated spectrum, EW(Hδ) $\gtrsim$ 8 Å. The purported turnoff stars in Kron 3 after all extend to $B-V \approx 0.15$, just as blue as the turnoff of N 2209 (for which EW(Hδ) $\approx$ 11 Å. Although Kron 3 is a difficult observation, the spectrum shown in Figure 2 certainly excludes such large equivalent widths. Moreover, the value of Danziger's Hδ index for Kron 3 is 0.257, quite close to the values for its neighbors in

Figure 4: 0.254 for N 1898, 0.267 for N1978. This contrasts sharply with the values for clusters whose SIT spectra show strong Balmer lines: for example, 0.344 for N1846, 0.391 for N419.

The present data therefore favor for Kron 3 an age closer to 7×10^9 y than to 3×10^9 y. A final hint may be drawn from the CMD. The giant branch of Kron 3 is well defined, with a clear subgiant branch, unlike N419, and a tight extension above the level of the horizontal branch, quite unlike N2209. Kron 3 also appears to have a genuine stub HB, slightly separated from the giant branch, not an amorphous giant clump (for consistency, one may draw the CMDs for all three cluster from Walker 1970, 1971, 1972). We await a CMD extending to $V \approx 22$ for the solution to the Kron 3 puzzle.

N1841 is unusual in that it is the only "old" Cloud cluster which lies above the reference line in Figure 4 and yet has a well developed horizontal branch (regardless of color). Danziger's Hδ index supports the elevation of N1841: 0.334 for N1841, compared, for example, to 0.255 for N1466 (near the reference line) or 0.321 for N2121 (already somewhat elevated). N1841 also keeps interesting company in Figure 4: M30, the only galactic globular cluster that lies above the reference line. A comparison of the CMDs for N1841 (Gascoigne 1966) and for M30 (Dickens 1972) reveals that they both possess M92-like HBs and agree as to the colors of the giant and subgiant branches. It is tempting to explore the possibility that the same agent strengthens the hydrogen lines in the integrated spectra of N1841 and M30.

Dickens (1972) notes that M30 has a relatively sparse giant branch and estimates $R_{hbgb} \approx 1.8$. Whether this is really a large value compared to other globulars remains an open question (Renzini 1977). However, one can address the question of what change in R_{hbgb} would be necessary to account for the elevation of M30 above the reference line. As discussed in Chapter 1 (Table 7) for a model with

(Y, Z, Age) = (0.3, 10^{-3}, 13×10^9 Gy) and a blue HB, decreasing R_{hbgb} from 1.6 to 0.9 decreases EW(Hδ) by about 12% and increases EW(Ca K) by about the same fraction. Such a vector traced back from the position of M 30 (or of N 1841) in Figure 4 falls well short of reaching the reference line (also, the vector appropriate to $Z = 10^{-4}$ would be shorter). But even this inadequate change in R_{hbgb} corresponds to a difference in helium abundance of $\Delta Y \approx 0.10$, regardless of the treatment of semiconvection (Renzini 1977, Table 5.1). The specter of this large or a larger spread in helium abundance is enough to motivate pursuit of another explanation. In the case of N 1841, moreover, the giant branch seems to be at least as well populated relative to the horizontal branch as it is in N 121 (although some HB stars may fall below the plate limit – see Gascoigne 1966).

Can age be the explanation? – two objections spring to mind. First, how can N 1841 retain a blue HB if, as argued above, clusters such as N 1978 have lost theirs to the age decrement? Second, why suspect M 30 alone among the metal poor halo clusters of such a decrement? Both of these apparently serious objections can be countered.

As shown by Renzini (1977, Figure 7.5), age affects the *shape* of the HB distribution much less at $Z = 10^{-4}$ than it does at $Z = 10^{-3}$. And, although, the peak of the distribution shifts in $\log T_e$ with age, the resulting shifts in color are much smaller than they would be at lower temperatures: $B-V$ increases by about 0.10 mag as the age decreases from 14 to 12×10^9 y. Thus, the blue horizontal branch of N 1841 is perfectly consistent with an age decrement of several times 10^9 y, particularly since a slight drop in metallicity could nullify any redward shift.

As for M 30, its peculiarity goes beyond the possibility of a large value of R_{hbgb}. In their study of the radial color distributions within 24 globular clusters, Chun and Freeman (1979) found eight clusters in which $B-V$ and $U-B$ increase toward the center; they state that the colors of the other clusters are radially uniform "within a

few hundredths of a magnitude." But their Figure 3*w* shows clearly that, in M 30, $B-V$ decreases toward the center by about 0.10 mag from its integrated color, $B-V = 0.59$, already the bluest globular, save M 15, in the list of Harris and Racine (1979). Williams and Bahcall (1979) detect a $B-V$ gradient in the same sense. Chun and Freeman may have questioned the significance of the measurement because $U-B$ does not change. However, Zinn (1980) also found a color gradient in M 30 using Gunn's intermediate band system (Thuan and Gunn 1976), and again the change in the violet color is small: $\Delta(u-v) = 0.017$ compared to $\Delta(v-g) = 0.067$ and $\Delta(g-r) = 0.077$, where the difference in color is in the sense (2' aperture) *minus* (1'.2 aperture). Quoted errors are typically 0.01 mag or less. Furthermore, the measurements of Chun and Freeman show that the change in $B-V$ occurs smoothly over the inner 40" of radius, compared to a core radius of 7" (Peterson and King 1975), whereas, in the clusters with colors decreasing outward, the gradient occurs entirely *within* the core radius.

It is here suggested that the inner region of M 30 is in the mean younger than the outer region. This does not imply "recent" or continuing star formation. The synthesis models of Chapter 3 indicate that, at $Z = 10^{-4}$, a decrement from 13×10^9 y to 9×10^9 y suffices to decrease $B-V$ by 0.10 mag. Also, importantly, $U-B$ is *constant* within about 0.01 mag for models with ages between 4×10^9 y and 13×10^9 y (this is not true for higher metallicities).

In summary, it is proposed that the "halo" cluster N 1841 and M 30 are, in whole or in part, several times 10^9 y younger than normal galactic globular clusters of similar metallicity. In the case of N 1841, this hypothesis meshes well with the previous discussion of other old Cloud clusters but is rather more provocative in the case of M 30. The two cases should be decided separately. Clearly, for both clusters it will be important to try to reach the main sequence.

e) The Clusters in the Middle

This group comprises N411, N2173, N1783, and N2243 and N339. Judged quickly from Figure 4, the last two objects could as well have been included among the old clusters, but reasons to think them younger will be given below. The clusters in the intermediate group are of SWB type V or V-VI, except for N339 (VII) and N2243 (unclassified).

It is unfortunate that there are so few intermediate clusters – split, moreover, between SMC and LMC – in the present sample, because this terramedia is potentially of great importance in delineating the age-abundance relations which may exist in the two Clouds. The lower age limit of the red clusters is anchored at about $1-2\times10^9$ by the relatively bright turnoffs of clusters such as N2209. However, as illustrated by Gascoigne (1980), turnoff dating with a CMD extending to $V=22$ reaches only to about 4×10^9 y. At the other end of the scale, theoretical uncertainties substantially complicate the age-abundance problem for clusters $\gtrsim 10^{10}$ y old. The "funnel" formed in Figure 4 by the evolutionary track for solar composition and the line of globulars, to first approximation an isochrone, shows that there will be observational as well as theoretical obstacles to the separation of age and abundance in old clusters. In contrast, clusters in the range (very roughly) $2-7\times10^9$ y occupy a large area in Figure 4 which has good extension along both the metallic axis and the hydrogen axis. Integrated spectra of clusters in the intermediate group may be one of the best hopes for actually tracing an age-abundance relation.

The present sample is too small even to begin the task. However, there are interesting indications that substantial differences in composition exist within the intermediate group. Consider first N411 and N2173, both SWB type V-VI. The SIT spectrum of N2173 is not among the best, but CaK and the G band are clearly stronger relative to hydrogen in N2173 than they are in N411. There is a large

separation in Figure 4. Although the reddening-free colors given by SWB agree closely ($\Delta Q_{ugr} = 0.02$, $\Delta Q_{vgr} = 0.04$, in the sense N2173 *minus* N411), the simple colors differ: $\Delta(u-g) = \Delta(v-g) = 0.11$, $\Delta(g-r) = 0.09$, with N2173 the redder, as would be expected from Figure 4. These differences are suggestive, although they are small enough to be caused by reddening. Hesser, Hartwick and Ugarte (1976) comment that N2173 has "no horizontal branch, otherwise looks like N1841," but their own instrumental CMD fails to support this remark. N2173 lacks the well defined, upward curving giant branch of N1841 and instead appears to have a giant clump, possibly with a gap below it. No CMD is available for N411.

It is tentatively suggested that N2173 is about 3×10^9 y old and more metal rich than N411. Without tracks for nonsolar composition in Figure 4, the age of N411 is uncertain. However, synthetic spectra for $Z = 10^{-4}$ (which, it will be recalled, lack a full library of metal poor stars and thus only bound EW(Ca K) from above) show that the isochrones for intermediate age must be steeper than the reference line for globular clusters. N411 may therefore be somewhat older than N2173. If the difference in composition between N2173 and N411 could be established by a photometric study of their bright stars, Figure 5 (or a more sophisticated variant of it) could be used to fix the ages.

N339 and N1466 have the same reddening-free colors, according to SWB, but again the raw colors are redder (by about 0.08 mag) for the cluster with stronger metallic lines, N339. Might it be that N339 is closer in age to N1846 than to N1466, but relatively metal rich? Gascoigne's (1966) CMD does not go faint enough to decide. Mould and Aaronson (1980) find a carbon star near N339 but regard its membership as open to question. Clearly, the clusters of the intermediate group require (and deserve) much more observational work.

There is a final datum which yields an independent clue to the nature of clusters

which lie near N339 and N2243 in Figure 4. The triangle in that figure represents the integrated spectrum of the "intermediate age" open cluster N2158 (Arp and Cuffey 1962). The measured spectra were obtained on two nights with the 1.5 m telescope and SIT spectrograph (Kent 1979) at Palomar. N2158 is considerably reddened, and this complicates an estimate of its age. However, comparison with the CMD of the nearly unreddened cluster N2420 (McClure, Forrester and Gibson 1974) shows that the diagrams are morphologically a very close match; both have a giant clump 0.60 ± 0.04 mag redward and just over 2 mag brighter than the turnoff. A reddening of about 0.34 mag applied to N2158 would bring it into coincidence with N2420. Arp and Cuffey estimate $E(B-V) = 0.43$, but a reddening this large is always subject to considerable uncertainty. McClure, Forrester and Gibson (1974) measure an ultraviolet excess $\delta(U-B) = 0.06$ for N2420; Arp estimates $\delta(U-B) = 0.06$ for N2158.

Altogether, it is reasonable to assume that N2158 is about as old as N2420 – 4×10^9 y according to Hirshfeld, McClure and Twarog (1978). This is also quite consistent with the position of N2158 in Figure 4 relative to the evolutionary line for clusters of solar composition.

f) The Break Parameters: ΔK and ΔS

Figure 7 shows that, surprisingly, the strength of the K break, ΔK, is little correlated with the equivalent width of the K line. It might be thought that a very strong K break, such as that seen in N1846 or N2121, would blanket the calcium line proper so as to reduce its equivalent width. The arrow in Figure 7 shows the effect of replacing EW(Ca K) as measured for N2121 with a value near the center of the regression of the G band on Ca K shown in Figure 3. The inferred value is larger, but the effect is too small to produce a neat relation from the scatter in Figure 7 (as a plot of ΔK against EW(G band) shows directly). Furthermore, 47 Tuc, which has the largest break in the sample, also has the strongest K line. By attaching values of ΔK to the points in Fig-

ure 4, it may be seen that even K line strength and hydrogen line strength together are a poor indicator of ΔK.

Does the K break represent another degree of freedom in the integrated spectra? In Figure 7, the sequence of models for clusters of solar composition behaves smoothly, with no twists or turns to create "natural" scatter. Although the galactic globular clusters are too few to *define* a curvilinear relation, a simple and satisfactory curve may easily be sketched for them; this would be impossible for the Cloud clusters. Also, the sequence of models and the sequence of globulars in no way bound the clusters, as they did in Figure 4.

Despite the reasonable errors suggested by the separation in Figure 7 of N121 as measured on different nights, it might be suggested that the K break is for some reason poorly determined, so that random error in ΔK creates most of the scatter. In fact, however, ΔK is well correlated with another spectrum parameter: the slope break, ΔS (Fig. 8). The *errors* in the measurement of ΔK and ΔS are in principle partially correlated, since the continuum slope S_- is used in the definition of ΔK. In Figure 8, the two observations of N121 and the arrow attached to N416, giving the change in ΔK induced by an imposed change in S_-, show that a correlation exists in practice. But the error vectors are much too short to *create* a large scale relation between ΔK and ΔS – they just degrade the existing correlation less than would independent errors.

Whatever its physical cause, the ΔK–ΔS correlation indicates a new degree of freedom which could complicate the determination of age and [Fe/H] for a cluster such as N1846 (Figs. 4 and 7). The slope break is largely the result of CH absorption, which, in metal poor stars, may form extensive wings on either side of the "ordinary" G band (Carbon *et al.* 1980). An enhancement of this absorption would increase ΔS but would *not* necessarily increase EW(G band) as here defined, since the pseudocon-

tinuum would also drop. It is therefore tempting to speculate that an enhanced K break (defined by elevation in Figure 7) is also caused, at least in part, by enhanced molecular absorption. At present, not even a good candidate may be put forward. The (0,0) band of the 3800 Å CH system degrades to the red from a *Q* head at 3889 Å and an *R* head at 3872 Å. In arc spectra (Pease and Gaydon 1965) the bands persist strongly to about 3970 Å; but there is no evidence for this system in stars. Indeed, Suntzeff (1980) finds that his scanner index of Ca II strength, which, by comparing the residual flux under H and K with the flux in a red sideband, essentially incorporates ΔK, correlates so closely with $B-V$ for individual giant stars in M 3, M 13, M 15 and M 92 that the scatter may be attributed to observational errors alone. Since the strength of the 4300 Å CH system varies widely among stars with the same $B-V$ in M 92 and in M 15 (Kraft 1979), the lack of corresponding variation in the K index argues against CH bands as an important contributor to the K break [I am indebted to R. Kraft for this remark]. Still, there is evidence for unexplained continuous absorption in the 4000 Å region of giant and subgiant CH stars (Bond and Neff 1969; Bond 1974). Very red carbon stars are now known to frequent many Cloud clusters (Mould and Aaronson 1980), so it would not be surprising if mild CH characteristics were found lower on the giant branch; however, known carbon stars only contribute about 2% of the visual integrated light of clusters in which they occur (Aaronson and Mould 1980).

In short, the significance of the apparent freedom in ΔK and of the correlation between ΔK and ΔS remains for now a cipher.

IV. SUMMARY AND FUTURE PROSPECTS

The main aim of this work has been to demonstrate that integrated spectra can play an important role in the *quantitative* analysis of the ages and abundances of star clusters in the Magellanic Clouds. In particular, Figure 4 shows that, by comparing the strength of the Balmer lines with the strength of a metallic feature, and

guided by a sequence of model star clusters and the empirical sequence of galactic globular clusters, one may infer age differences between fairly old clusters, for each of which a color–magnitude study to extremely faint magnitudes would be necessary even to approach the main sequence. Most Cloud clusters are younger than galactic globulars and lack a developed horizontal branch; these related properties enhance the contribution of the turnoff to the integrated spectrum.

Gascoigne (1980) has remarked that, "while abundance determination now seems under control, in that there are several practicable methods available, the same cannot be said for age determination." It is precisely our expanding knowledge of cluster abundances which the integrated spectrum approach can exploit in creating a practicable method for the determination of cluster ages (for example, Figure 5).

The next step in interpreting Figure 4 would be to derive from synthetic spectra an evolutionary track for a metal poor cluster. With the sequence of globulars as a check on the terminus of such a track, a first approximation to a (Z, Age) grid could be drawn in the (EW(CaK), < EW(H)>) plane. There are now enough stars with abundance determinations from high dispersion analysis (Morel *et al.* 1976) that a full library, say at [Fe/H] ≈ −1.5, could be assembled for use with the Ciardullo and Demarque (1977) isochrones. Real, not theoretical, stellar spectra are better for anchoring the framework of a (Z, Age) grid, but theoretical spectra could be used differentially to fill in lines of constant [Fe/H] and to explore the effects of abundance anomalies.

Figure 4 indicates that there are substantial variations in abundance among the older red clusters in the Clouds (SWB groups VI and VII). This is perfectly consistent with the results of SWB, since the sequence of galactic globular clusters, principally a metallicity sequence, passes through the centers of regions VI and VII in the Q–Q plane (SWB, Figs. 2 and 3). As discussed in §III*e*, it will be difficult to establish an

age–abundance relation in these regions. There are also hints of a range of abundance among the younger clusters, but the sample is small. Because of their great importance in testing the hypothesis of an age–abundance correlation, more clusters should be studied in SWB groups IV and V.

The degree of freedom in the K break and its correlate slope break raises the possibility that, even as regards the integrated spectrum, [Fe/H] tells less than the whole story of some Cloud clusters. First priority should be given to checking this result with careful photometric observations; a scanner with 15 Å pass bands would be quite sufficient for measuring ΔK and ΔS. Confirmation of the present findings would justify a full spectral synthesis of the K line region – not with the aim of matching high resolution spectra in detail, but with a view to exposing the magnitude of the effects to be expected from selective enhancement of various atomic and molecular species.

Broad and intermediate band photometric surveys have yielded valuable insights into the clusters in the Magellanic Clouds, but it is likely that this approach has done its work. Color–magnitude studies will always be of central importance and will always be difficult and slow, not a survey tool. Perhaps, then, a spectroscopic survey in integrated light, of size comparable to previous photometric surveys, is the next logical step in elucidating the group properties of the Cloud clusters. The rapid development of photometry and spectroscopy of individual stars will ensure that at its completion such a survey will be not only larger but subject to more detailed quantitative interpretation than the present pilot study.

TABLE 1

CHARACTERISTICS OF SPECTROGRAPH AND DETECTOR

Grating	600 line mm^{-1}, first order
Slit	5" for objects 10" for standard stars
SIT pixel size	35 μm square 3.3 Å along dispersion 3" on sky
Format	512 pixels along dispersion 128 pixels (384") along slit
Usable spectral range	λλ 3750 - 5170
Spectral resolution	8.5 Å

TABLE 2

SPECTROSCOPIC OBSERVATIONS AND OTHER DATA

Cluster	Spectroscopic Observations: Exposure (s)	n	Dec Scan (")	Note	CMD: Ref	Photometry: U-B	B-V	u-g	v-g	g-r	Q_{ugr}	Q_{vgr}	Class
SMC													
NGC 121	2400	2	30		1	0.14	0.79	0.54	0.37	0.37	0.14	0.12	VII
339	3900	1	60		2	.10	.70	.52	.31	.35	.14	.07	VII
411	2700	1	40		-	.24[a]	.62	.59	.29	.30	.27	.09	V-VI
416	1500	1	30		-	.21	.81	.54	.44	.34	.17	.21	VI
419	1800	4	40		3,4,2	.23	.68	.67	.28	.29	.36	.08	V
Kron 3	5400	2	30		5,6	.15	.71	-	-	-	-	-	[V-VI]
LMC													
NGC 1466	3600	1	30		2	0.13	0.68	0.43	0.24	0.27	0.14	0.06	VII
1783	3600	1	30	1	7,8	.20	.63	.61	.27	.21	.38	.13	V
1841	3300	1	25		2	-	-	.46	.27	.38	.05	.01	VII
1846	3600	1	40		9,10	.31	.74	.83	.36	.36	.44	.12	V
1898	3600	1	34		-	-.03	.75	-	-	-	-	-	
1978	2100	1	30		11,10	.23	.78	.66	.40	.35	.28	.16	VI
1987	4200	1	30	2	-	.18	.51	.58	.13	.15	.42	.03	IV
2121	7200	1	30		10	.25[b]	.84	.67	.47	.44	.19	.17	VI
2173	4800	1	25		10	.29[b]	.83	.71	.40	.39	.29	.13	V-VI
2209	7200	1	20	1	12,2	.20[c]	.55	.59	.15	.23	.34	-.01	III-IV
2243	4500	1	90		-	-	-	-	-	-	-	-	
Galaxy													
NGC 104	180	3	240			0.34	0.85	0.81	0.60	0.44	0.33	0.30	
362	360	2	216			.11	.72	.55	.38	.36	.16	.14	
1904	2400	1	36			.02	.63	.40	.24	.26	.12	.06	
6864	480	2	60			.14	.70	.72	.45	.51	.17	.10	
7078	240	2	120			-.04	.56	.43	.22	.31	.10	.01	
7089	300	2	120			.03	.61	.46	.24	.27	.17	.06	
7099	600	1	100			.01	.57	.37	.14	.22	.13	-.01	

TABLE 2 - Continued

Notes to spectroscopic observations

1. distorted SIT image (see text, §IIb)
2. emission lines in foreground or background field

References for CMDs

1. Tifft 1963
2. Gascoigne 1966
3. Walker 1972
4. Arp 1958
5. Gascoigne 1980
6. Walker 1970
7. Gascoigne 1962
8. Sandage and Eggen 1960
9. Hodge 1960a
10. Hesser, Hartwick and Ugarte 1976
11. Hodge 1960b
12. Gascoigne et al. 1976

References for colors

All uvgr colors (Clouds and Galaxy), uncorrected for reddening, are from Searle, Wilkinson and Bagnuolo (1980).

UBV colors for galactic globular clusters, corrected for reddening, are from Harris and Racine (1979).

Unless noted, UBV colors for Cloud clusters, uncorrected for reddening, are from van den Bergh and Hagen (1968)

[a] Alcaino 1978
[b] Bernard 1975
[c] Freeman and Gascoigne 1977

TABLE 3

EQUIVALENT WIDTHS AND BREAK PARAMETERS

Cluster	Equivalent Widths (Å)						Break Parameters			
	Hδ	Hγ	Hβ	Ca K	G band	Ca H + Hε	ΔK (mag)	S_+	S_-	ΔS
SMC										
NGC 121	2.5	2.0	2.9	7.2	3.9	5.9	0.14	2.20	1.41	0.22
339	3.9	3.9	4.4	8.9	5.0	7.6	.09	1.48	1.36	-0.42
411	7.2	8.8	5.8	4.7	5.2	9.0	.19	1.59	1.00	0.20
416	2.8	3.3	3.6	7.5	4.4	6.3	.17	1.81	1.15	0.20
419	9.5	9.4	6.4	6.1	4.6	8.7	.22	1.28	1.07	-0.22
Kron 3	1.9	3.1	3.3	6.4	3.9	4.6	.16	1.74	0.69	0.78
LMC										
NGC 1466	3.7	3.2	3.6	5.0	3.2	5.1	0.19	1.39	0.94	0.08
1783	6.0	5.0	5.5	4.3	2.7	5.7	.23:	1.57	1.23	-0.15
1841	4.5	4.5	3.6	4.7	4.4	8.6	.10	1.07	1.05	-0.40
1846	5.1	6.2	5.8	4.7	4.5	6.2	.31	1.86	0.89	0.61
1898	3.0	3.0	2.8	6.3	4.2	6.3	.15	2.11	1.18	0.46
1978	3.2	3.5	4.0	6.8	3.7	6.3	.20	1.83	0.96	0.48
1987	11.9	10.0	11.8	3.9	2.4	11.4	.14	0.74	0.60	-0.11
2121	1.8	4.0	4.1	6.1	4.6	4.6	.33	1.97	0.82	0.82
2173	7.4	6.0	6.3	8.7	6.7	10.5	.13	1.88	1.35	-0.02
2209	11.8	9.6	10.8	3.3	2.2	6.6	.33:	1.19	0.99	-0.20
2243	4.0	2.6	5.2	9.0	7.7	7.8	.16	1.51	0.87	0.29
Galaxy										
NGC 104	0.9	2.0	2.2	10.2	9.3	5.6	0.36	2.45	0.94	1.14
362	1.9	2.6	2.6	8.4	5.0	5.9	.21	1.78	1.17	0.14
1904	3.3	4.0	2.6	6.0	4.3	5.7	.11	1.57	1.06	0.08
6864	2.8	2.6	3.4	7.5	4.6	6.4	.22	1.99	1.15	0.38
7078	3.7	3.7	2.7	4.0	2.4	5.0	.12	1.56	1.35	-0.33
7089	3.4	3.1	2.9	6.2	3.5	6.4	.14	1.71	1.23	-0.01
7099	4.6	4.4	4.6	3.8	1.8	6.1	.09	1.01	0.87	-0.20

REFERENCES

Aaronson, M., and Mould, J. 1980, preprint.

Alcaino, G. 1978, *Astr. Ap. Suppl.*, **34**, 431.

Aller, L. H., and Faulkner, D. J. 1964, in *The Galaxy and the Magellanic Clouds*, ed. F. J. Kerr and A. W. Rodgers (Canberra: Austr. Acad. Sci.), p. 358.

Andrews, P. J., and Lloyd Evans, T. 1971, in *The Magellanic Clouds*, ed. A. B. Muller (Dordrecht: Reidel), p. 88.

-----. 1972, *M. N. R. A. S.*, **159**, 445.

Arp, H. C. 1958, *A. J.*, **63**, 273.

Arp, H., and Cuffey, J. 1962, *Ap. J.*, **136**, 51.

Arp, H. C., and Thackeray, A. D. 1967, *Ap. J.*, **149**, 73.

Atwood, B., Ingerson, T., Lasker, B. M., and Osmer, P. S. 1979, *Pub. A. S. P.*, **91**, 120.

Bernard, A. 1975, *Astr. Ap.*, **40**, 199.

Bond, H. E. 1974, *Ap. J.*, **194**, 95.

Bond, H. E., and Neff, J. S. 1969, *Ap. J.*, **158**, 1235.

Carbon, D. F., Langer, G. E., Butler, D., Kraft, R. P., Trefager, Ch. F., Suntzeff, N., Kemper, E., and Nocar, J. 1980, in preparation.

Carney, B. W. 1980, *Ap. J. Suppl.*, **42**, 481.

Chun, M. S., and Freeman, K. C. 1979, *Ap. J.*, **227**, 93.

Ciardullo, R. B., and Demarque, P. 1977, *Trans. Yale Univ. Obs.*, **33**, **34**, **35**.

Danziger, I. J. 1973, *Ap. J.*, **181**, 641.

Demarque. 1977, in *The Evolution of Galaxies and Stellar Populations*, ed. B. M. Tinsley and R. B. Larson (New Haven: Yale Univ. Obs.), p. 199.

Dickens, R. J. 1972, *M. N. R. A. S.*, **157**, 299.

Eggen, O. J., Lynden-Bell, D., and Sandage, A. R. 1962, *Ap. J.*, **136**, 748.

Feast, M. W., and Lloyd Evans, T. 1973, *M. N. R. A. S.*, **164**, 15P.

Ford, H. C. 1970, Ph.D. thesis, University of Wisconsin.

Freeman, K. C., and Gascoigne, S. C. B. 1977, *Proc. A. S. A.*, **3**, 126.

Frogel, J. A., Persson, S. E., and Cohen, J. G. 1980, *Ap. J.*, **239**, in press.

Gascoigne, S. C. B. 1962, *M. N. R. A. S.*, **124**, 201.

-----. 1964, in *The Galaxy and the Magellanic Clouds*, ed. F. J. Kerr and A. W. Rodgers (Canberra: Austr. Acad. Sci.), p. 354.

-----. 1966, *M. N. R. A. S.*, **134**, 59.

-----. 1980, in *Star Clusters*, ed. J. E. Hesser (Dordrecht: Reidel), p. 305.

Gascoigne, S. C. B., and Kron, G. E. 1952, *Pub. A. S. P.*, **64**, 196.

Gascoigne, S. C. B., Norris, J., Bessell, M. S., Hyland, A. R., and Visvanathan, N. 1976, *Ap. J. (Letters)*, **209**, L25.

Gingold, R. A. 1975, *Ap. J.*, **198**, 415.

Gray, D. F. 1965, *A. J.*, **70**, 362.

Gustafsson, B., and Bell, R. A. 1979, *Astr. Ap.*, **74**, 313.

Gustafsson, B., Bell, R. A., Eriksson, K., and Nordlund, Å. 1975, *Astr. Ap.*, **42**, 407.

Gustafsson, B., Bell, R., and Hejlesen, P. M. 1977, *Ap. J. (Letters)*, **216**, L7.

Hardy, E., Melnick, J., and Reheault, C. 1980, in *Star Clusters*, ed. J. E. Hesser (Dordrecht: Reidel), p. 343.

Harris, W. E., and Racine, R. 1979, *Ann. Rev. Astr. Ap.*, **17**, 241.

Hayes, D. S. 1970, *Ap. J.*, **159**, 165.

Hayes, D. S., and Latham, D. W. 1975, *Ap. J.*, **197**, 593.

Hesser, J. E., Hartwick, F. D. A., and Ugarte, P. 1976, *Ap. J. Suppl.*, **32**, 203.

Hirshfeld, A., McClure, R. D., and Twarog, B. A. 1978, in *The HR Diagram*, ed. A. G. D. Philip and D. S. Hayes (Dordrecht: Reidel), p. 163.

Hodge, P. W. 1960a, *Ap. J.*, **131**, 351.

----- 1960b, *Astr. Ap.*, **132**, 341.

Iben, I., Jr. 1963, *Ap. J.*, **138**, 452.

Iben, I., Jr., Rood, R. T., Strom, K. M., and Strom, S. E. 1969, *Nature*, **224**, 1006.

Iben, I., Jr., and Truran, J. W. 1978, *Ap. J.*, **220**, 980.

Kent, S. M. 1979, *Pub. A. S. P.*, **91**, 394.

Kinman, T. D. 1959, *M. N. R. A. S.*, **119**, 538.

Kraft, R. P. 1979, *Ann. Rev. Astr. Ap.*, **17**, 309.

Kurucz, R. L. 1979, *Ap. J. Suppl.*, **40**, 1.

McClure, R. D., Forrester, W. T., and Gibson, J. 1974, *Ap. J.*, **189**, 409. Morel, M., Bentolila, C., Cayrel, G., and Hauck, B. 1976, in *Abundance Effects in Classification*, ed. B. Hauck and P. C. Keenan (Dordrecht: Reidel), p. 223.

Morgan, W. W. 1956, *Pub. A. S. P.*, **68**, 509.

Mould, J., and Aaronson, M. 1979, *Ap. J.*, **232**, 421.

----- 1980, *Ap. J.*, **240**, in press.

Oke, J. B. 1964, *Ap. J.*, **140**, 689.

Pease, R. W. B., and Gaydon, A. G. 1965, *The Indentification of Molecular Spectra*, third edition (London: Chapman Hall).

Peimbert, M. 1975, *Ann. Rev. Astr. Ap.*, **13**, 113.

Peterson, C. J., and King, I. R. 1975, *A. J.*, **80**, 427.

Racine, R. 1973, *A. J.*, **78**, 180.

Renzini, A. 1977, in *Advanced Stages of Stellar Evolution*, ed. P. Bouvier (Geneva: Geneva Obs.), p. 149.

Rood, R. T. 1973, *Ap. J.*, **184**, 815.

Sandage, A. R. 1970, *Ap. J.*, **162**, 841.

Sandage, A. R., and Eggen, O. J. 1960, *M. N. R. A. S.*, **121**, 232.

Schild, R. E. 1977, *A. J.*, **82**, 337.

Searle, L., Wilkinson, A., and Bagnuolo, W. 1980, *Ap. J.*, **239**, in press.

Searle, L., and Zinn, R. 1978, *Ap. J.*, **225**, 357.

Shapley, H. 1930, *Star Clusters* (New York: McGraw Hill), pp. 187–188.

Shapley, H., and Nail, V. M. 1951, *A. J.*, **55**, 249.

Suntzeff, N. B. 1980, *A. J.*, **85**, 408.

Thackeray, A. D., and Wesselink, A. J. 1953, *Nature*, **171**, 693.

Thuan, T. X., and Gunn, J. E. 1976, *Pub. A. S. P.*, **88**, 543.

Tifft, W. G. 1963, *M. N. R. A. S.*, **125**, 199.

van den Bergh, S. 1967, *A. J.*, **72**, 70.

----- 1975, *Ann. Rev. Astr. Ap.*, **13**, 217.

van den Bergh, S., and Hagen, G. L. 1968, *A. J.*, **73**, 569.

van den Bergh, S., and Henry, R. C. 1962, *Pub. David Dunlap Obs.*, **2**, 281.

Walker, M. F. 1970, *Ap. J.*, **161**, 835.

----- 1971, *Ap. J.*, **167**, 1.

----- 1972, *M. N. R. A. S.*, **159**, 379.

----- 1979a, *M. N. R. A. S.*, **186**, 767.

----- 1979b, *M. N. R. A. S.*, **188**, 735.

Whitford, A. E. 1958, *A. J.*, **63**, 201.

Williams, T. B., and Bahcall, N. 1979, *Ap. J.*, **232**, 754.

Zinn, R. 1980, *Ap. J. Suppl.*, **42**, 19.

FIGURE CAPTIONS

Figure 1. N1846 is used to illustrate the procedure for measuring equivalent widths (EWs), the K break ΔK and the slope break ΔS. EW(Hβ), EW(Hγ) and EW(G band) are reckoned from the red pseudocontinuum segment, EW(Hδ) from the blue segment. The "lowered" blue segment bounds CaK and CaH+Hε; at its red end, it defines ΔK. As explained in the text, ΔS is measured near 4300 Å in a manner insensitive to reddening. The inset shows in more detail the measurement of Hγ and the G band.

Figure 2. SIT spectra. (*a*) and (*b*) show clusters in the Magellanic Clouds; (*c*) shows galactic globular clusters. Tick marks on the vertical axes are at 0.5 mag intervals. The deleted wavelengths correspond to the location of a flaw on the silicon target. The spectra have been hanned (1–2–1 smoothed) from a raw resolution of 2.7 pixels FWHM. N1783 and, to a lesser degree, N2209, were affected by a transient instrumental problem which caused a slight compression of the wavelength scale and additional smoothing.

Figure 3. In the correlation between the equivalent widths of CaK and the G band, there is no separation between clusters in the LMC, SMC and the Galaxy. The scatter in the common relation sets an upper limit to the combined errors in the two equivalent widths. Here and in subsequent figures, *dashed segments* connect two independent observations of N121.

Figure 4. The equivalent width of CaK is plotted against the median of the equivalent widths of Hδ, Hγ and Hβ. The distribution of clusters in the Clouds is bounded by two loci: at bottom, a *straight line* fitted to six galactic globular clusters (*triangles*), to first approximation a metallicity sequence at constant age; *line segments and crosses*, an age sequence of model star clusters of solar abundance, labelled in units of 10^9 y. Roman numerals give the color class assigned by Searle,

Wilkinson and Bagnuolo (1980). The Cloud clusters are, with few exceptions, younger than galactic globular clusters and of lower metallicity than the Sun.

Figure 5. From the integrated spectra of model star clusters, isopleths of EW(Hδ) in the plane of age and composition. The two *shaded areas* illustrate the limits which may be placed on the age of N 2209 according to two estimates of its metallicity (§ IIIc). *Dashed curves* show the effect of adding an M 3-type horizontal branch to the metal poor clusters. Since the theoretical hydrogen profiles do not include contamination by metallic lines, the isopleths are less precisely determined for equivalent widths EW $\lesssim$ 4 Å.

Figure 6. Isochrones for various ages and compositions superposed on the color-magnitude diagram of N 2209 (from Gascoigne *et al.* 1976). An age $2-3\times10^9$, with $Z = 10^{-3}$, fits the main features of the CMD.

Figure 7. In Cloud clusters, the equivalent width of Ca K (reckoned from the "lowered" pseudocontinuum segment illustrated in Fig. 1) is unrelated to the strength of the K break; in galactic globulars, the two quantities increase together. *Line segments and crosses*, models for clusters of solar composition, labelled by age in Gy. The *arrow* is explained in the text.

Figure 8. In Cloud clusters and in globulars, the K break ΔK correlates closely with ΔS, a reddening-insensitive measure of the change in spectral slope that occurs in the region of the G band. The *arrow* is explained in the text.

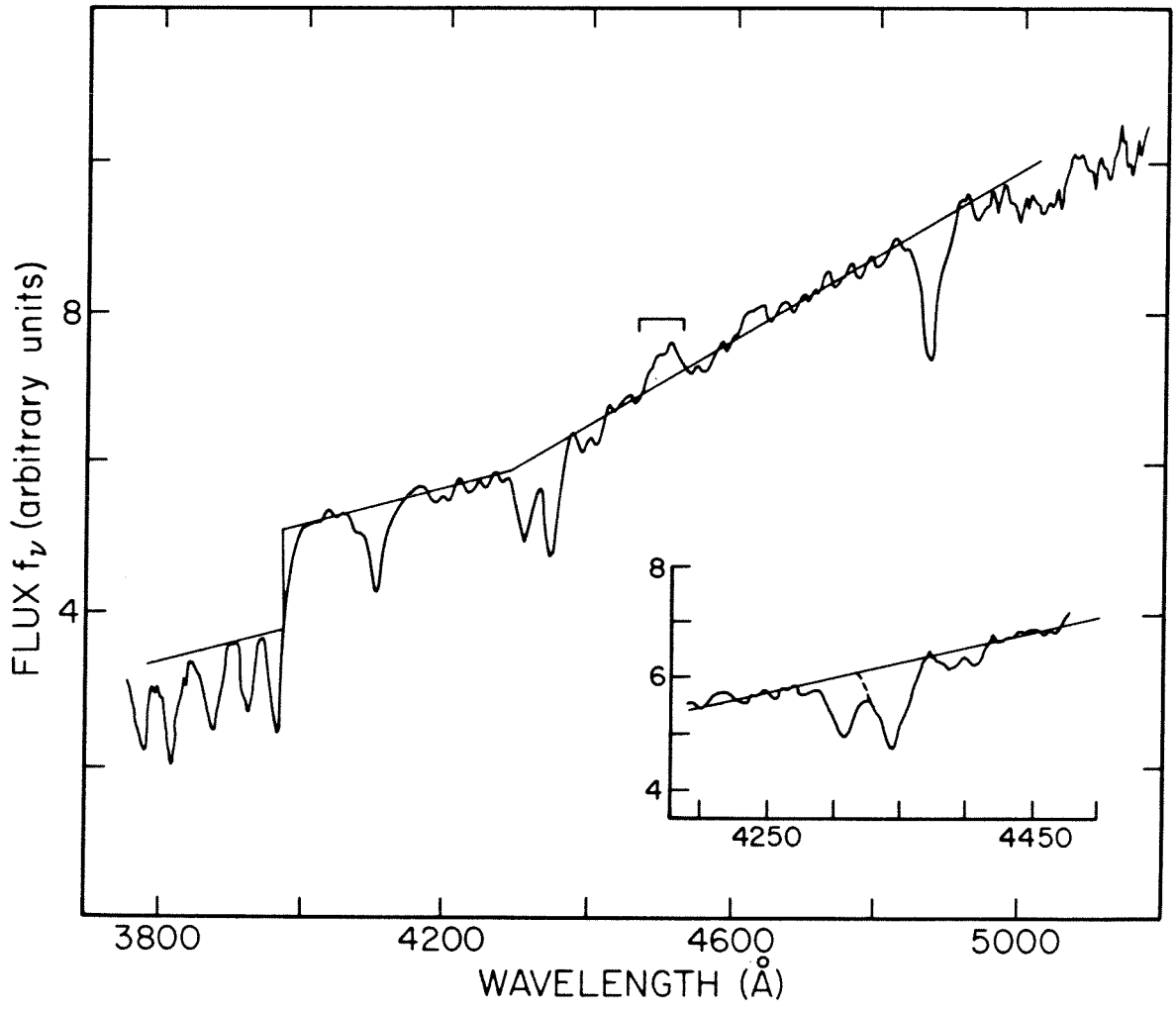
FLUX f_ν (arbitrary units)
8
4
3800
4200
4600
5000
WAVELENGTH (Å)
8
6
4
4250
4450

Figure 1

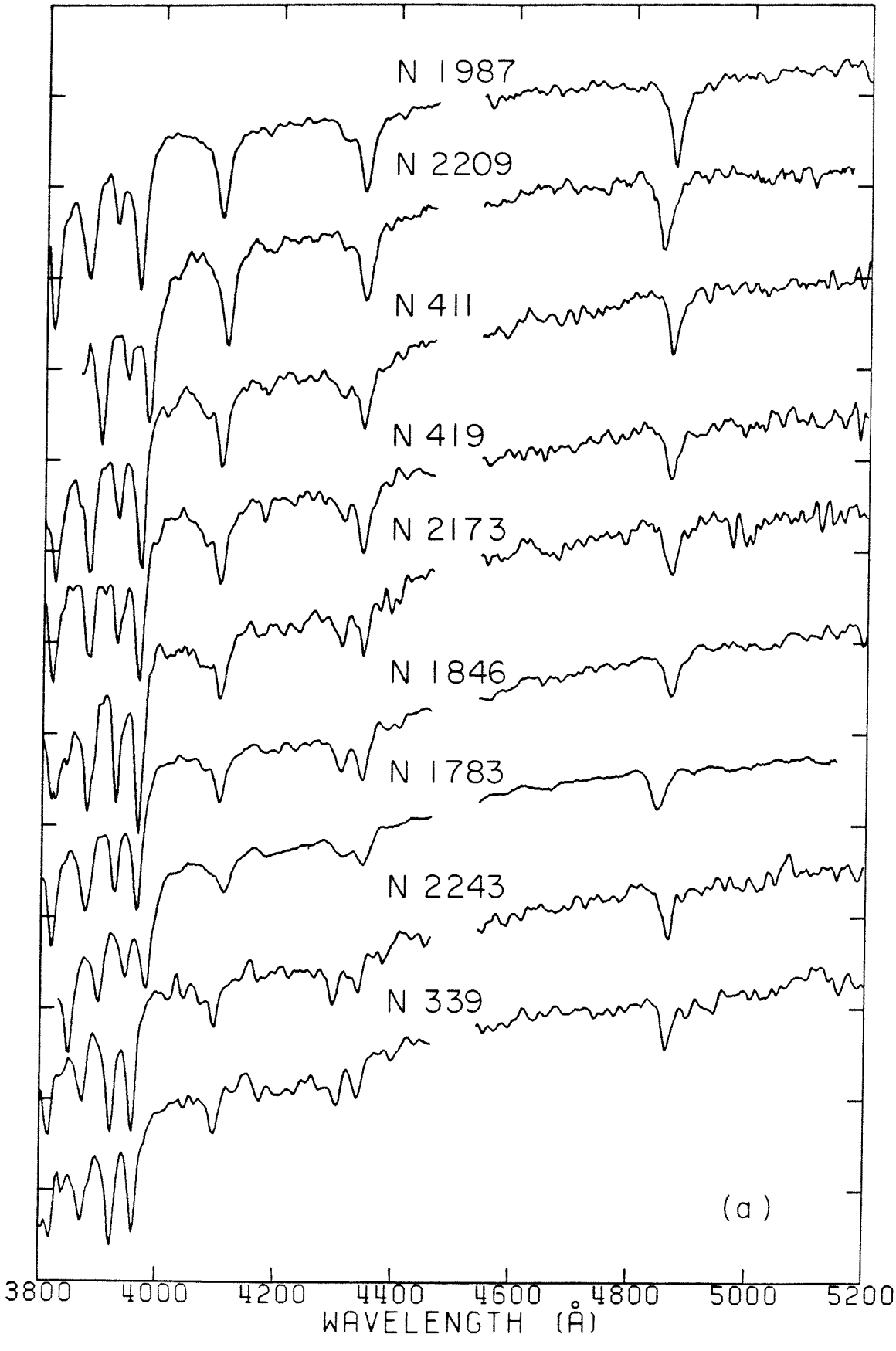
N 1987
N 2209
N 411
N 419
N 2173
N 1846
N 1783
N 2243
N 339
(a)
3800
4000
4200
4400
4600
4800
5000
5200
WAVELENGTH (Å)

Figure 2a

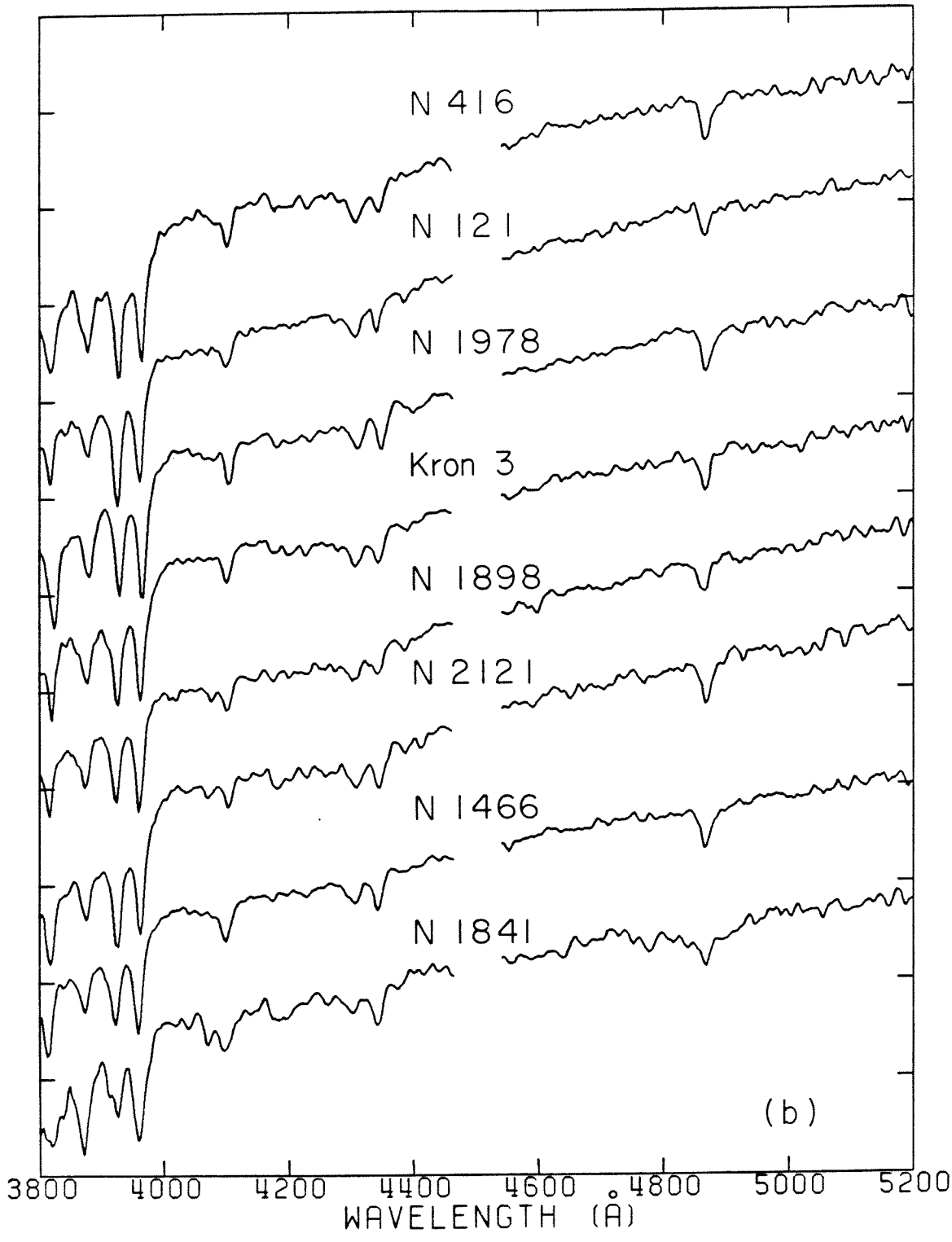
N 416
N 121
N 1978
Kron 3
N 1898
N 2121
N 1466
N 1841
(b)
3800
4000
4200
4400
4600
4800
5000
5200
WAVELENGTH (Å)

Figure 2b

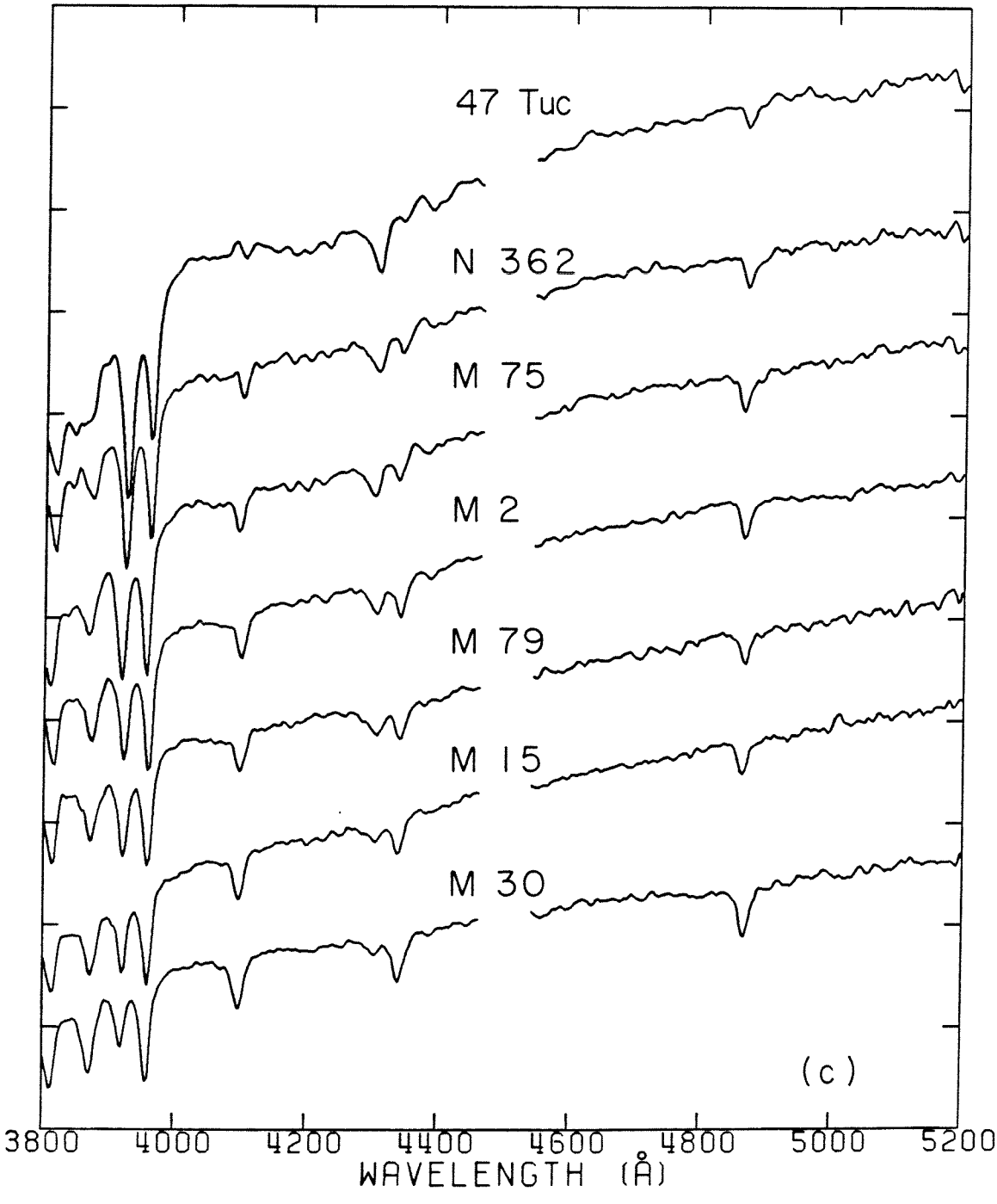
47 Tuc
N 362
M 75
M 2
M 79
M 15
M 30
(c)
3800
4000
4200
4400
4600
4800
5000
5200
WAVELENGTH (Å)

Figure 2c

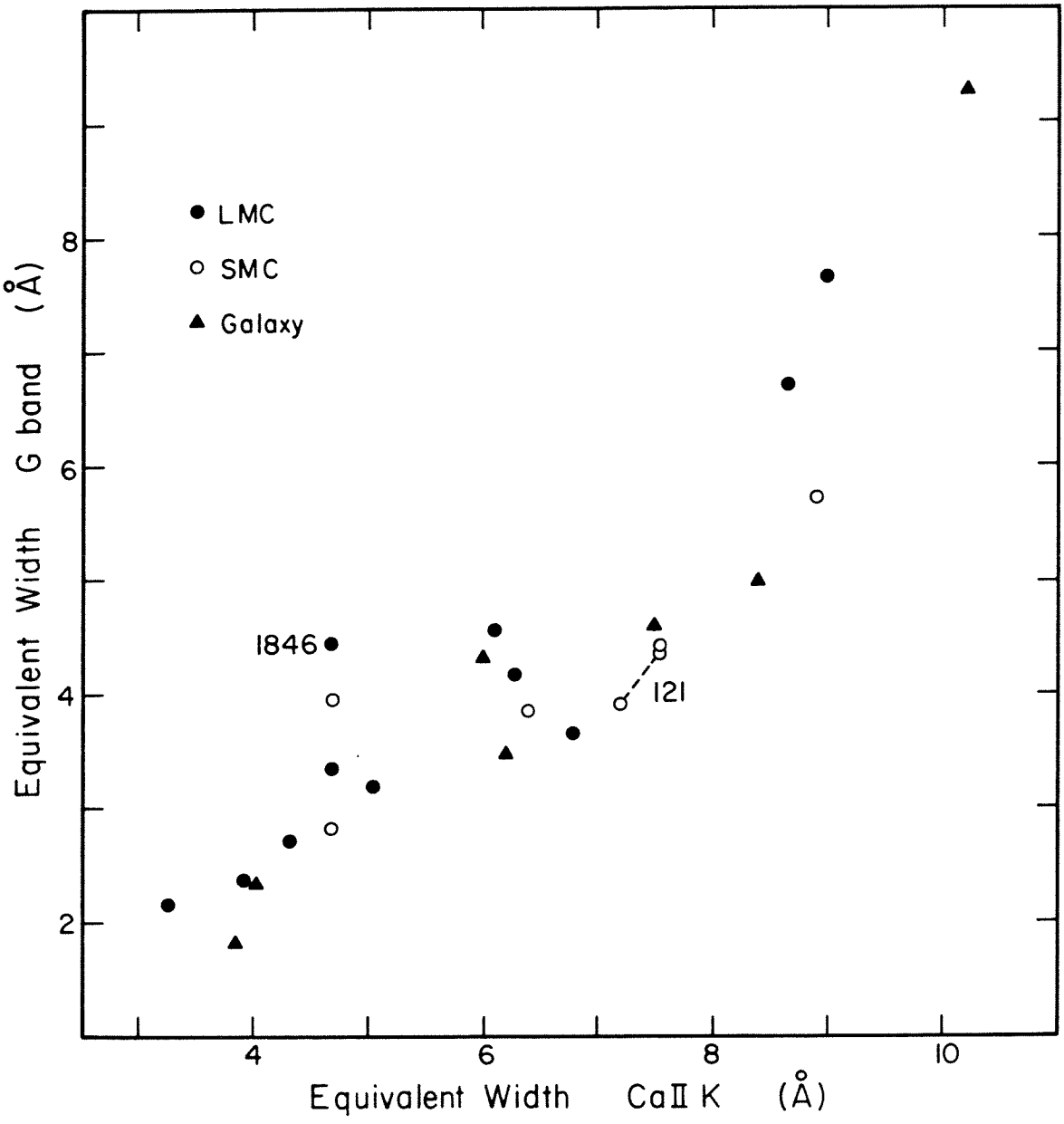
LMC
SMC
Galaxy
1846
121
Equivalent Width G band (Å)
Equivalent Width CaII K (Å)
2
4
6
8
4
6
8
10

Figure 3

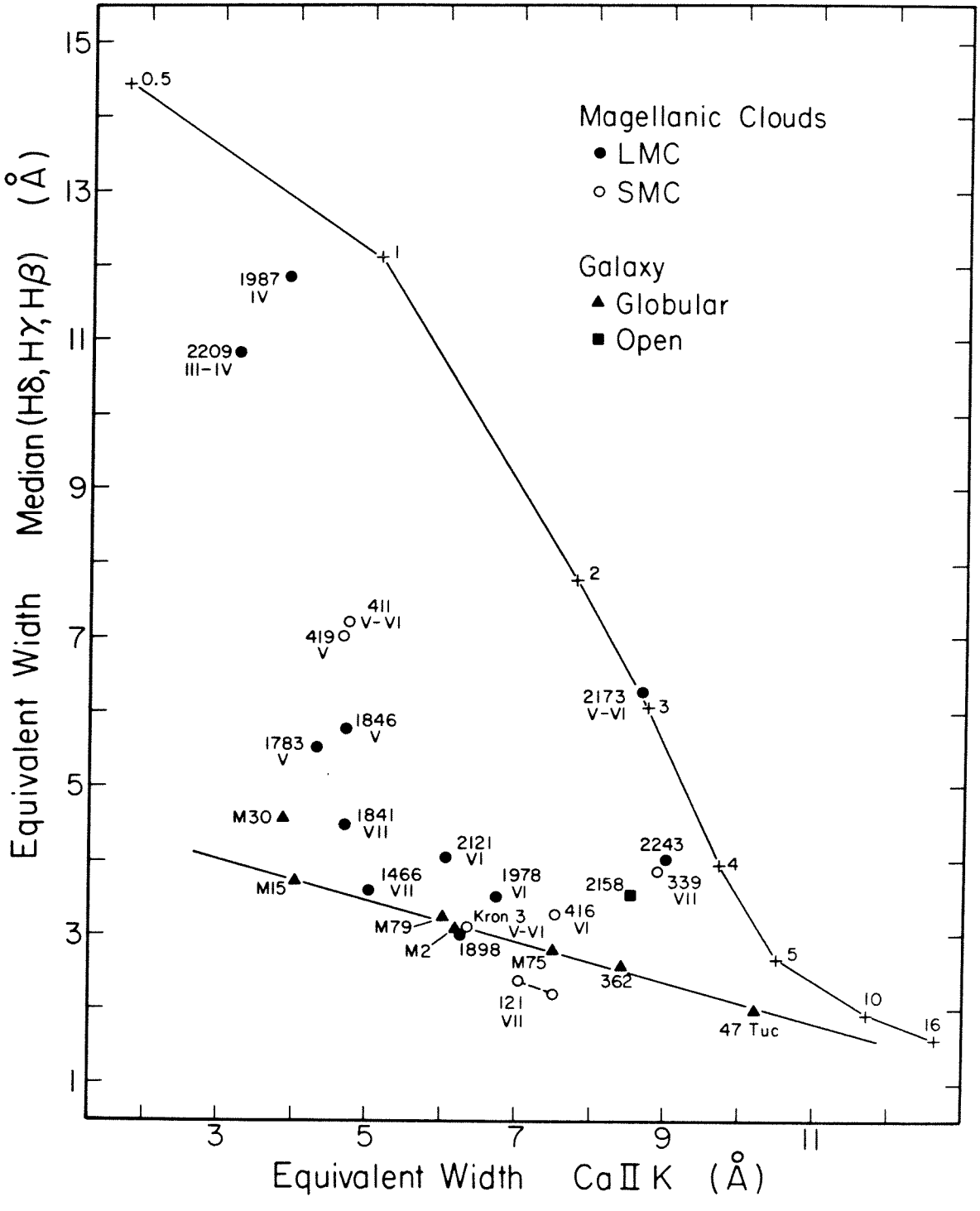
Magellanic Clouds
● LMC
○ SMC
Galaxy
▲ Globular
■ Open
0.5
1
2
3
4
5
10
16
1987 IV
2209 III-IV
411 V-VI
419 V
1846 V
1783 V
2173 V-VI
M30
1841 VII
2121 VI
1466 VII
M15
1978 VI
2158
2243
339 VII
416 VI
Kron 3 V-VI
M79
M2
1898
M75
362
121 VII
47 Tuc
Equivalent Width Median (Hδ, Hγ, Hβ) (Å)
Equivalent Width CaII K (Å)

Figure 4

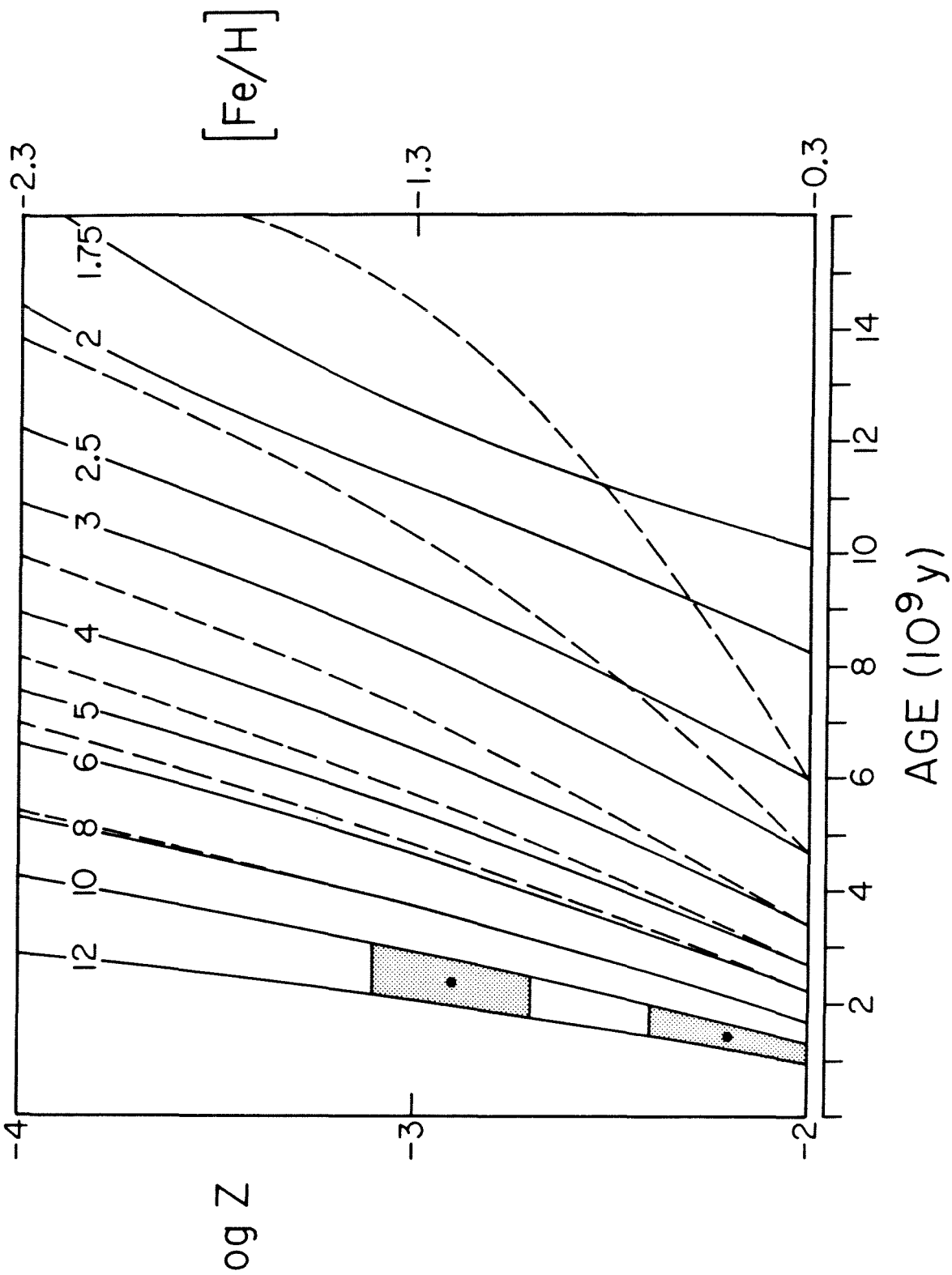

Figure 5

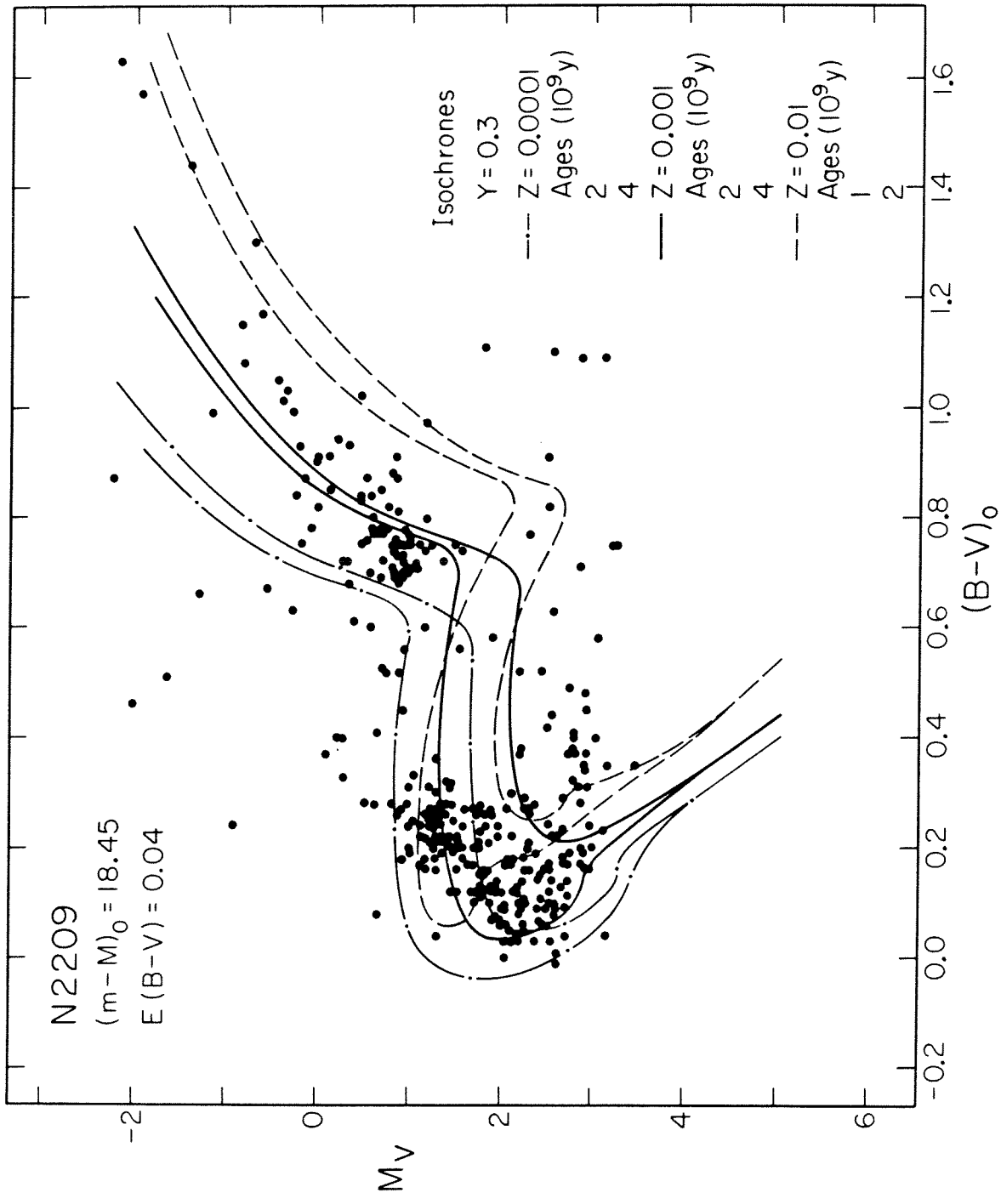
N2209
$(m-M)_0 = 18.45$
$E(B-V) = 0.04$
Isochrones
Y = 0.3
Z = 0.0001
Ages (10^9y)
2
4
Z = 0.001
Ages (10^9y)
2
4
Z = 0.01
Ages (10^9y)
1
2
M_V
$(B-V)_0$
-2
0
2
4
6
-0.2
0.0
0.2
0.4
0.6
0.8
1.0
1.2
1.4
1.6

Figure 6

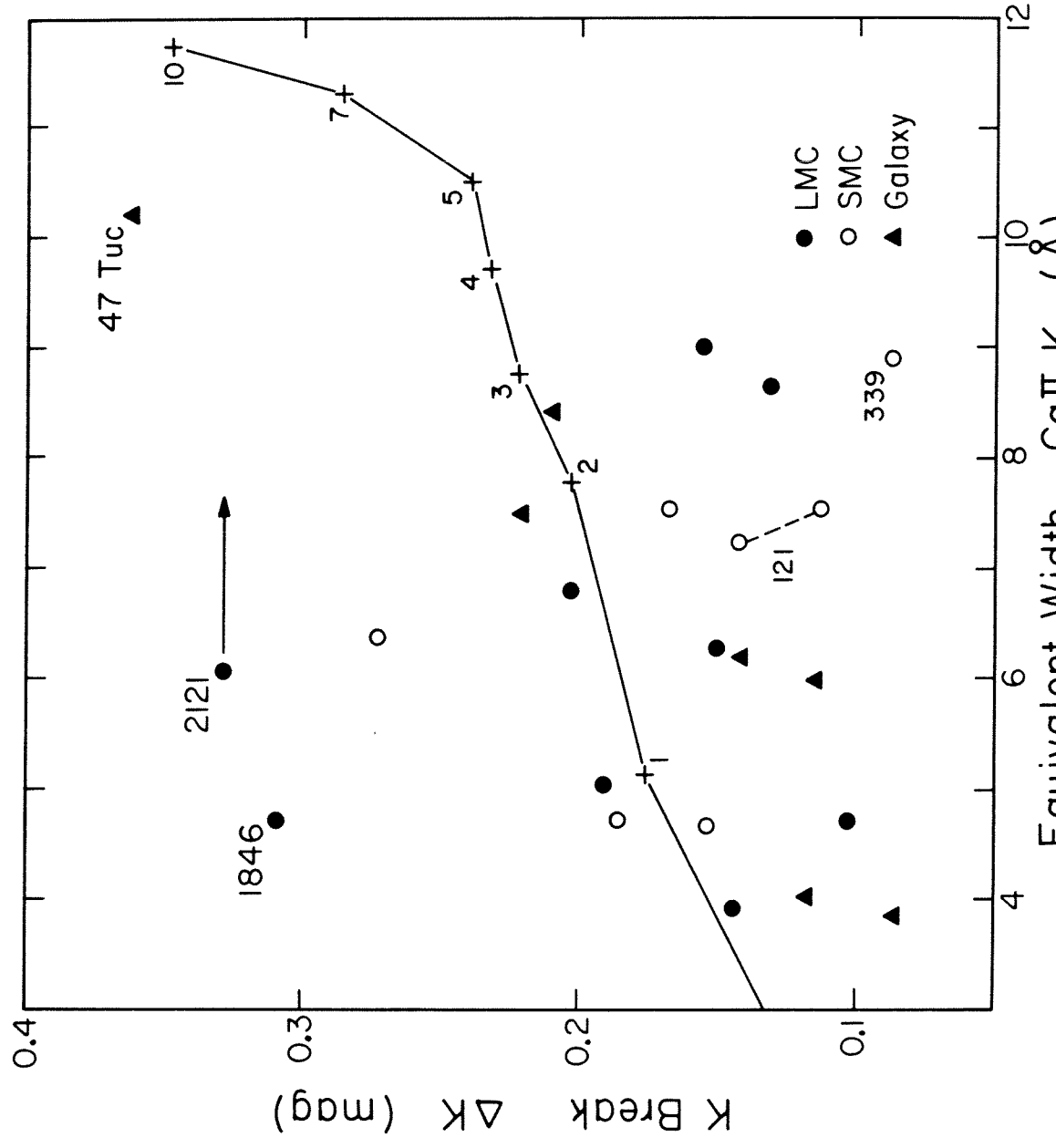
K Break ΔK (mag)
0.4
0.3
0.2
0.1
Equivalent Width CaII K (Å)
4
6
8
10
12
LMC
SMC
Galaxy
47 Tuc
2121
1846
339
121
1
2
3
4
5
7
10

Figure 7

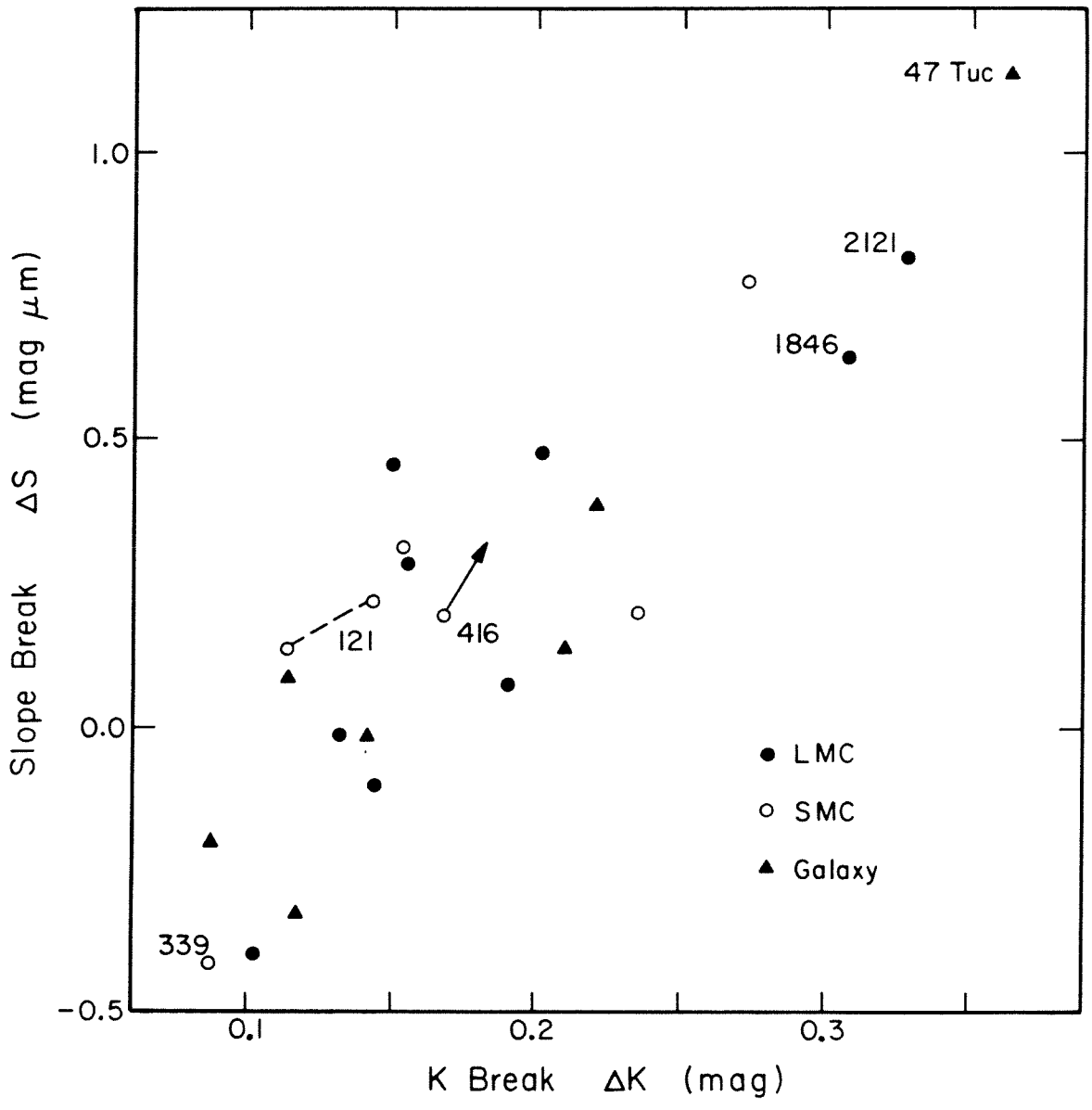
47 Tuc
2121
1846
121
416
339
LMC
SMC
Galaxy
1.0
0.5
0.0
-0.5
0.1
0.2
0.3
Slope Break ΔS (mag μm)
K Break ΔK (mag)

Figure 8

Chapter 3

SYNTHESIS MODELS OF STAR CLUSTERS: INTEGRATED SPECTRA, INTEGRATED COLORS AND THEORETICAL COLOR–MAGNITUDE DIAGRAMS

I. INTRODUCTION

In attempting to synthesize colors and spectral indices of composite stellar systems, previous investigators have taken one of two approaches. In the optimizing synthesis approach, light from single stars is mixed by trial and error (Spinrad and Taylor 1971) or by an automatic technique (e.g., Lasker 1970; Faber 1972; O'Connell 1976) to match the integrated light. The evolutionary model approach instead employs theoretical isochrones, usually adjusted with reference to observations (Tinsley 1968; Dixon, Ford and Robertson 1972; Searle, Sargent and Bagnuolo 1973; Barbaro and Bertelli 1977; Tinsley 1978; Mould 1978; Aaronson *et al.* 1978).

A potential strength of the optimizing approach, its ability to populate the HR diagram in ways unforeseen by models, is vitiated by the instability of unconstrained models to small observational errors (Williams 1976) and the consequent necessity to impose "astrophysical" constraints which (of course) allow only the foreseen and which may even compromise the derived values of those parameters left unconstrained (Peck 1980). On the other hand, the second approach is only as good as its models. If observations are used in an essential way, not just to modify theoretical isochrones but to replace portions of them (as in Tinsley 1978), some of the freedom to vary theoretical parameters is lost. Only recently have evolutionary models attempted to incorporate the effects of varying metallicity, a long-perceived weakness in both approaches to synthesis. The technique has ranged from schematic corrections to both colors and isochrones (Tinsley 1978), to detailed empirical corrections to colors (Aaronson *et al.* 1978), to full theoretical synthesis of a spectral feature (Mould 1978).

The present work explores a theoretical approach made possible by the availability for the first time of both a uniform set of model isochrones covering a wide range of composition (Ciardullo and Demarque 1977), and photometric colors from grids of

model stellar atmospheres covering a wide range of temperature, gravity and composition (Bell and Gustafsson 1978; Kurucz 1979). Using theoretical colors, one may hope to assess the *differential* effects of varying metallicity more finely than is possible using empirical corrections to colors for stars of solar composition.[1] For example, the ultraviolet colors of giant stars are sensitive both to temperature and to gravity. At T_e = 4000 K, the change in gravity on the giant branch corresponding to a change in metallicity from Z = 10^{-1} to Z = 10^{-2}, $\Delta \log g$ = 0.8 (Ciardullo and Demarque 1979), induces at constant metallicity (Z = 10^{-2}) a change in $U-B$ which is actually slightly larger than the change resulting from the difference in composition at constant gravity (Bell and Gustafsson 1978).[2] In the calculation of Balmer line profiles for composite light, the steep gravity dependence of hydrogen line strength in A stars also calls for careful tracking of $\log g$ near the turnoff and along the horizontal branch.

Naturally, the compositional freedom of the theoretical colors has its corresponding disadvantage: uncertainty as to how well the colors represent real stars. The present work responds to this problem in two ways. First, reference is made to studies that compare the model colors to observations and recommend corrections (Relyea and Kurucz 1978; Buser and Kurucz 1978; Gustafsson and Bell 1979). Second, because the effects of incompleteness in the line list and deficiencies if the treatment of strong lines are increasingly serious as the metallicity rises, the synthesis models for solar composition instead use empirical colors. Since the colors for field giants and dwarfs refer to what is for practical purposes a single locus in the temperature–gravity plane, there is no danger of a mismatch in gravity for given T_e.

---

1. In what follows, "solar" will often be used to stand briefly (if inaccurately) for "of solar composition".
2. The composition and gravity effects are of opposite sign. Contrary to the discussion in Cohen, Frogel and Persson (1978), this cancellation appears to be significant even for Z< 10^{-3} in producing (within observational error) a single sequence of globular cluster giants in the $(U-V, V-K)$ diagram, despite the considerable range in Z among metal poor globulars.

The sections to follow aim principally to set out clearly and completely the sources of the isochrones, colors and Balmer line profiles, together with modifications and additions (including an effective temperature scale for cool stars), so that as theoretical advances are made, the synthesis models may be improved incrementally and the effects of each change assessed. *UBVK* colors will be emphasized, for all the usual reasons – extensive observations of stars, star cluster and galaxies, and intensive investigations of the photometric system itself, particularly with regard to its tenuously defined response function (Golay 1974; Buser and Kurucz 1978) – but colors in the Gunn *uvgr* system (Thuan and Gunn 1976) will also be calculated for preliminary comparison with Zinn's (1980) observations of globular clusters and the study of clusters in the Magellanic Clouds by Searle, Wilkinson and Bagnuolo (1980).

As a secondary aim, spectroscopic observations of MK standard stars were obtained in order to generate from isochrones for solar composition full synthetic spectra of moderate resolution (about 7 Å) over the wavelength range λλ3700–4500. Equivalent widths determined from the synthetic spectra were applied extensively in Chapter 2.

Although some comparison with observations will be made in order to demonstrate the utility and the possible limitations of the present models, the discussion will barely scratch the surface of possible applications (some are found in Chapters 1 and 2). The models are primarily a resource for future work.

II. ISOCHRONES AND BOLOMETRIC LUMINOSITY FUNCTIONS

The basic data are the isochrones and bolometric luminosity functions of Ciardullo and Demarque (1977, subsequently CD), which are in turn based on the evolutionary sequences for red giant stars by Sweigart and Gross (1978) and for earlier stages by Mengel *et al.* (1979). The isochrones cover the ranges $0.1 \leqq Y \leqq 0.4$ and $0.00001 \leqq Z \leqq 0.1$ for ages between 0.2×10^9 and 25×10^9 y, but full loci extending

through the red giant region are not given for all combinations of parameters. Although this uniform set of isochrones has already proved its value in a number of investigations, a few technical problems and necessary modifications will be discussed in the next three sections.

a) Technical Problems

The most luminous 0.05 mag interval of the bolometric luminosity functions (BLFs) often contains 5 or 10 times as many stars as do nearby 0.05 mag intervals. It may be verified from the tracks in Sweigart and Gross (1978) that this is an artifact and not a pause in evolution just before the helium flash. Closer investigation reveals that the second-brightest "box" (in magnitude and temperature) is also sometimes afflicted. Therefore, a test for the two brightest boxes is referred to the more populous of the third and fourth boxes: if the ratio of stars in the brighter to the fainter box exceeds two, the population of the fainter replaces that of the brighter (since the isochrone can graze the corner of a box, it is unsafe to use any single box as referent for a ratio test).

BLFs are given for three power-law luminosity functions, $n(m) = A(s)m^{-s}$, where $n(m)$ is the number of stars in the mass interval $(m, m+dm)$ and s takes the values 0, 2.35 (Salpeter value) and 4. However, in the course of extending the main sequence to lower masses, it was found that *all* the values given by CD for $s = 0$ are incorrect – they actually apply to the case $s = -1$. Since such a rising mass function is more extreme than has even been suggested for stellar systems, the correct values for $s = 0$ were inserted. At the same time, the case $s = 4$ was replaced by $s = 3.5$. For M3, Gunn and Griffin (1979) suggest $s \approx 3$ based on fits of dynamical models to star counts and radial velocities. From star counts in three globular clusters, Da Costa (1977) finds values ranging from $s \approx 1.7$ for N6397 to $s \approx 3.6$ for 47 Tucanae (these values refer to the present mass function averaged over the whole cluster, but for

these objects, as Da Costa shows, the present mass function is probably little different from the initial mass function). Thus, $s = 3.5$ reasonably represents steep mass functions in observed clusters; but its behavior is less extreme than that of $s = 4$ [see Frogel, Persson and Cohen (1980) for an example].

b) Additions to the Isochrones

i) Lower Main Sequence

A lower main sequence is joined to the lower terminus of each CD isochrone, usually between 0.4 and 0.6 $M_\odot$. Twenty mass intervals are constructed between the terminus and the lower mass cutoff, here taken to be 0.2 $M_\odot$. Da Costa (1977) finds that the power-law rise of the luminosity function in 47 Tuc and N6752 should be cut at about 0.2 $M_\odot$; a value between 0.2 and 0.3 $M_\odot$ is a better fit to the data for N6397. Gunn and Griffin (1979) suggest that the M3 mass function peaks at about 0.3 $M_\odot$. The luminosity function for the solar neighborhood given by Wielen (1973), combined with the infrared data of Veeder (1974), indicates that locally the mass function turns over at about 0.15 $M_\odot$.

The slope of the mass-luminosity relation, $d \log L / d \log m = 2.2$, is taken from Veeder (1974), and the slope of the temperature-luminosity relation, $d \log L / d \log T_e = 12.0$, is essentially Veeder's value (≈ 9.2) adjusted to conform to the temperature scale discussed below.

ii) Horizontal Branch

Since the theory of mass loss along the giant branch is too poorly developed to suggest more than an *ad hoc* prescription for distribution of stars along the zero age horizontal branch (ZAHB), and since questions about the influence of the horizontal branch tend in practice to be framed in terms of globular cluster prototypes, it was decided to include three "standard" distributions of stars along the HB, each based on a real cluster: 47 Tucanae, M3 or M92. Based on color–magnitude diagrams

(CMDs), a histogram in $B-V$ was constructed for the horizontal branch of each cluster; RR Lyrae variables were included in number approximately normalized to the same area as the CMD. The histogram in $B-V$ is then converted to a histogram in $\log T_e$ using the color-temperature relations of §III*e* for an appropriate composition. Table 1 gives the results. Provision is also made for specifying a clump HB: all the stars are placed on the giant branch at the predicted intersection with the horizontal branch.

The placement of the horizontal branch locus in the $(M_b, \log T_e)$ plane, as a function of composition, is based the theoretical sequences of Sweigart and Gross (1976). A very rough attempt was made to include the early stages of evolution off the ZAHB.

Observationally, the ratio R_{hbgb} of the number of stars on the HB to the number of stars on the first giant branch (RGB) above the level of the horizontal branch is not yet securely determined. Iben *et al.* (1969) found $R_{hbgb} \approx 0.9$ for a sample of metal-poor globulars, but Renzini (1977) advocates $R_{hbgb} \approx 1.6$ based on plate material extending to fainter magnitudes. In the case of 47 Tuc, where there is no question of blue HB stars falling below the plate limit, Lee (1977) find $R_{hbgb} \approx 1.75$.

$R_{hbgb} = 1.6$ has been chosen as the default value for all three horizontal branches in the present models. More discussion of this problem, and some results of varying R_{hbgb}, will be found in Chapter 1. It is worth pointing out, though, that increasing R_{hbgb} by adding very blue HB stars has less effect on *UBV* colors than might be supposed, for several reasons: the droop of the HB locus in the $(M_b, \log T_e)$ plane, the large bolometric corrections, and the fact that the colors, particularly $B-V$, decrease only slowly for $T_e > 10,000$ K.

iii) Asymptotic Giant Branch

Following Aaronson *et al.* (1978), an asymptotic giant branch (AGB) is added schematically by multiplying the luminosity function along the RGB by a fixed factor

and by shifting the temperature of the giant branch to a number-weighted mean of the RGB and AGB loci. The enhancement factor is chosen to be 1.2 (Simoda and Tanikawa 1970; Lee 1977). The temperature shift was determined from the CMDs of Sandage (1970) and Lee (1977), again with the aid of the temperature-color relations given below. The AGB is terminated 0.6 mag above the horizontal branch. Since almost nothing is known of the properties of the second giant branch in clusters younger than globulars, provision is made for the AGB to be deleted. This has almost no effect on the integrated colors; the AGB is included mainly for comparison with the detailed CMDs of galactic globulars.

c) Convective Mixing Length

The treatment of convection in the surface layers is perhaps the most serious physical uncertainty affecting models of stellar interiors in the mass range of the CD isochrones. Although luminosity is little affected, the radii, and thereby the effective temperatures, of models in the range $3.6 < \log T_e < 3.9$ are sensitive to the choice of mixing length. [This discussion is framed in terms of local mixing length theory (Böhm-Vitense 1958) since, except for a pilot study in which Deupree and Varner (1980) attempted a simplified two-dimensional treatment, all interiors models have used this formalism.] Still, a serious attempt should be made to choose the parameters of the theory, despite its inadequacies, so as to achieve consistency with basic observations. This point has been made concretely in a valuable and clarifying study of local convection theories by Gough and Weiss (1976). They show that, if the parameters of various formulations are chosen so that in each case a 1 $M_\odot$ model evolves to match the present Sun, the physical structure of the final model is almost unique, even though the numerical values of corresponding parameters, such as mixing length, may be quite different. In other words, the details of the formulation are not so important as its overall *calibration*. Although this statement is less true of red giants, in which the structure of the convective zone is more complex, it at least

encourages one to choose the best mixing length for a given set of values, without undue concern over its numerical value.

i) Giant Branch

The CD isochrones are based on evolutionary tracks which employ throughout their length a mixing length ratio $\alpha = 1.0$ ($\alpha \equiv l/H_p$, where l is the mixing length and H_p is the pressure scale height). Since, for plausible ages and compositions, the CD giant branches are clearly cooler than those in globular clusters, Ciardullo and Demarque (1979) present formulae which may be used to adjust the giant branch to different effective values of α:

$$\delta \log T_e = [0.020 \log (L/L_\odot) + 0.143] \log \alpha \qquad (1)$$

$$\delta \log g = 4\, \delta \log T_e \, .$$

The formula for $\delta \log T_e$ is based on evolutionary tracks computed by Sweigart (1978) for different values of α (the interiors code was of course the same as that used to generate the tracks for the CD isochrones).

Demarque and McClure (1977a) recommended $\alpha = 1.6$, based on fits to *UBV* color–magnitude diagrams. Aaronson *et al.* (1978) instead use $V-K$ data from Cohen, Frogel and Persson (1978, subsequently CFP) to fix the location of giant branch more accurately in the (M_b, $\log T_e$) plane (since the infrared color is a sensitive and nearly composition-free indicator of T_e) and thus to tabulate shifts to the CD isochrones for clusters of "known" metallicity. Incorporating observations from CFP and from Frogel, Persson and Cohen (1980), Figure 1*ab* shows that the present models, adjusted to $\alpha = 1.5$ by formula (1), reproduce well the giant branches in the (M_K, $V-K$) plane of both the extremely metal poor globular M92 and the open cluster M67, two orders of magnitude more metal rich. Flags at various values of $V-K$ show the considerable sensitivity of this color to a temperature change of 50 K. M92 is

compared to an insochrone with (Y, Z, Age) = (0.3, 10^{-4}, 13 Gy); to good approximation, Z alone fixes the position of this theoretical giant branch. For M 67, (Y, Z, Age) = (0.3, 10^{-2}, 5 Gy) is chosen on the basis of high resolution abundance studies by Griffin (1975, 1979) and by Cohen (1980), both of whom find a deficiency of −0.3 or −0.4 dex relative to the Sun. [The $(V-K)-T_e$ calibration which has been applied to the shifted isochrones is discussed in §IIIa below].

Because of the good agreement in Figure 1*ab*, which carries over to the usual color–magnitude diagram, $\alpha = 1.5$ has been chosen as the default value for all models. Frogel, Persson and Cohen (1980) have argued that a suggested revision of the metallicity of 47 Tucanae to [Fe/H] ≈ −1.3 (see §VIa) implies that the magnitude of the temperature correction must vary with metallicity or with mass. Indeed, vectors attached to the (Z, Age) = (10^{-3}, 16 Gy) isochrone in Figure 1*c* show that an adjustment to $\alpha \approx 1.2$ is necessary in order to bring it into rough agreement with the middle portion of the observed 47 Tuc giant branch. [It is best to avoid the tip region, where the effect of convection in the low density atmospheres is most uncertain, where the fit is sensitive to small errors in the distance modulus (because the locus is more horizontal) – and where the isochrones generally have the wrong slope anyway]. It is beyond the scope of this discussion to inquire whether such an adjustment signals a real change in l/H, or a variation with metallicity of the *effect* of a given l/H (see below), or merely the inadequacy of the mixing length treatment. It is worth making plain, however, that adjusting a $Z = 10^{-3}$ isochrone to $\alpha = 1.2$ produces a poor fit to the M 67 giant branch in Figure 1*b*, and a still worse fit results if M 67 is closer to solar metallicity. Clearly, the theoretical basis for the temperature correction must be expanded, if only by exploring with existing models the effect of varying the mixing length for several compositions.

ii) Turnoff and Main Sequence

Ciardullo and Demarque (1979) recommend that a smooth transition be constructed between the shift given by formula (1) on the giant branch and a shift 1/5 as large on the main sequence (MS). This must be rejected as a general prescription, both because it fails to reproduce the position of the present Sun in the HR diagram and because it ignores changing conditions in the stellar interior which cause the response to convective transport to vary with temperature.

An interpolated CD isochrone for (Y, Z, Age) = (0.23, 0.02, 4.5 Gy) requires a positive shift $\delta \log T_e \approx 0.02$ at $1\,L_\odot$ to match the solar temperature. Formula (1) with $\alpha = 1.5$ and fivefold reduction would lead to $\delta \log T_e = 0.005$. However, the models on which the CD isochrones are based, as well as earlier ZAMS models that employed the Bohm-Vitense formulation of mixing length theory, indicate for $\alpha = 1.5$ a much larger shift. In fact, from Sweigart (1978), from Demarque and Larson (1964) and from Iben (1963), we may read off at $L = L_\odot$ a shift $\delta \log T_e \approx 0.02$ in each case between the loci for $\alpha = 1$ and $\alpha = 2$, just the amount needed for agreement with the Sun. The procedure here adopted, therefore, is to derive shifts from models with various values of α (naturally, comparing α's only *within* a homogeneous set of models), to assume the shift to be proportional to $\log \alpha$, and to normalize the shifts so that an isochrone with (Y, Z, Age) = (0.23, 0.02, 4.5 Gy) passes through the position of the Sun in the HR diagram.

Shifts for solar composition are taken as a function of temperature from Figure 3 of Copeland, Jenssen and Jørgensen (1970, subsequently CJJ), which agrees well with Figure 3 of Iben (1963). Above $\log T_e \approx 3.9$, the models are radiative – the shift is zero. For low temperatures, $\log T_e \lesssim 3.6$, the temperature gradient in the convective region (or the whole star) becomes nearly adiabatic and there is no sensitivity to mixing length (Limber 1958). CJJ also compute mixing length shifts for several compositions and find that $d \log T_e / d \log \alpha$ is smaller for metal poor compositions than for metal

rich; their table 4 has been used to calibrate the effect.

For an isochrone of given composition, the turnoff shift is first determined according to its temperature. A smooth transition is effected from the shift given by (1) along the giant branch to the turnoff value. The rest of the main sequence is treated according to the previous discussion. It is clear that this somewhat elaborate procedure will have little effect on the integrated colors of the models. The shifts are important, however, if a fit to the region of the turnoff (including its color) is to be used as one criterion for the absolute determination of age or to compare the ages of clusters that differ in metallicity.

We recall that, for given α, the shift here applied to the giant branch has no dependence on composition. It is also possible that α itself varies with composition, or with other parameters. Thus, on the giant branch particularly, the mixing length ratio is best regarded as a convenient parameter with which to shift the isochrones into better agreement with clusters of known composition. When this composition is itself in doubt, one may for simplicity explore the hypothesis that α is nearly constant, or that it at least varies monotonically with composition. It is interesting in this regard to note that, if the *sense* of the CJJ result for the main sequence also holds for the giant branch, then changing α to 1.2 (the value necessary to match a Z = 0.001 isochrone to 47 Tuc – Fig. 1*c*) would shift the isochrones for Z = 0.01 and Z = 0.02 in Figure 1*b* even *farther* than indicated by the arrows, since formula (1) is tied to Z = 0.001. Thus, the already poor fit to M 67 for $\alpha = 1.2$ is probably worse than it appears. If this speculation is borne out by calculation, and if the temperature of the 47 Tuc giant branch is to be reconciled with $[Fe/H] \approx -1.3$, it would seem necessary either to invoke a minimum in the mixing length ratio conveniently at or near the metallicity of 47 Tuc or to postulate abundance anomalies that can seriously affect the boundary temperature of stars all along the giant branch.

d) Interpolated Isochrones

The isochrones are parametrized by Z (10^{-4}, 10^{-3}, 10^{-2}, 4×10^{-2}), while the compositions of the model atmospheres are referred to the Sun (0, −1, −2 dex). The mismatch cannot be ignored. For metal poor compositions, the colors were interpolated, as will be described below. However, because of its importance as a reference, and because it can be used with *empirical* colors, an isochrone for solar composition was interpolated between Z = 0.01 and Z = 0.04. Plots of $\log T_e$ against various functions of composition were prepared over the full range of Z for the turnoff and for selected points on the main sequence and red giant branches. Based on the approximate linearity of the plots, interpolation in $(5+\log Z)^{1.8}$ was adopted for $\log T_e$ at fixed luminosity on the MS or RGB. The turnoff region was more difficult to handle. Interpolation in $\log T_e$ is impossible on the nearly flat part of the subgiant branch, and for young clusters the isochrones have small hooks and dips which change with Z at constant age. For the turnoff region, therefore, priority was given to locating the turnoff point itself correctly, through interpolation in temperature and luminosity. The shape of the surrounding region was then borrowed from the nearer of the interpolating isochrones, joined smoothly to the MS and RGB of the interpolant. Similarly, because experience has shown that the position of an isochrone is more important than the precise luminosity function in determining integrated colors, the three luminosity functions for the interpolated isochrone were adopted *in toto* from the nearer neighbor.

III. COLORS THEORETICAL AND EMPIRICAL

a) Temperature Scale

The K and M stars have long been the key problem in constructing a scale of effective temperature for the full range of spectral types. Recently, Wing and Ridgway (1979) and Ridgway, Joyce, White and Wing (1980, subsequently RJWW) have proposed a

new scale for late-type giants, based on angular diameters from lunar occultation, in which M stars are considerably hotter than has been generally supposed. For example, the new calibration diverges from the widely-used Johnson calibration (Johnson 1966, subsequently J66) at K3, becoming hotter by 200 K at M0 and by over 400 K at M4.

This new scale is largely adopted here, but it calls into question and demands a rediscussion of the scale for dwarfs and, indirectly, of the role of $V-K$ as a pure indicator of effective temperature. Figure 2 shows that the $(V-K)$–$\log T_e$ relations for giants by RJWW and for dwarfs by Veeder (1974) diverge rapidly below 4000 K. However, if RJWW *color* temperatures T_c are substituted for T_e, the relation agrees very well with Veeder's. It is then no surprise to discover that Veeder's effective temperatures were in fact derived from black body fits to the flux distribution - *i.e.*, color temperatures. Thus a satisfactory solution would seem to be to extend the RJWW $T_e - T_c$ relation to dwarfs, bringing Veeder's scale into agreement. Then one would be left with only the task of explaining, for dwarfs as for giants, how T_c and T_e can differ so strongly at lower temperatures (see discussion in RJWW). Unfortunately, the best available dwarf calibrators – all two of them – do not support this solution. Veeder finds T_e = 3750 K for the equal components of the eclipsing binary YY Gem, in good agreement with T_e = 3720 K computed from the diameter of the mean component (J66) or with the mean of the individual temperatures determined by Leung and Schneider (1978), $T_e = 3775 \pm 200$ K. Entered at $V-K$ = 3.85 (Veeder 1974), the RJWW calibration predicts T_e = 3870 K.

The disagreement is much more serious for CM Draconis, a dM4e eclipsing binary studied by Lacy (1977). [I am indebted to T. B. Ake for calling this system to my attention.] He finds $T_e = 3150 \pm 100$ K for the equal components. From Lacy's value $V-K$ = 5.06, the Veeder relation predicts T_e = 3200 K; the RJWW calibration gives T_e = 3570 K, a discrepancy of over 400 K.

If the eclipsing binaries are taken to support the Veeder scale for dwarfs, and yet the RJWW scale is to be maintained, both on the basis of the angular diameters and because of strong secondary evidence (Tsuji 1978), then $V-K$ must be abandoned as a "pure" temperature indicator – albeit still an excellent one. Indeed, it would be surprising if $V-K$ were completely immune to gravity, since TiO bands alone contribute about 1 mag of absorption in V at M4 (Smak and Wing 1979) and since the 7100 Å absorption at mid-M is stronger in giants than in dwarfs of the same effective temperature (Wing, Dean and MacConnell 1976), implying a still larger difference at given T_e under the assumption of separate temperature scales. However, Wing (1973) has presented evidence that the red TiO bands are relatively insensitive to changes in abundance, and this may carry over to the blanketing in V.[3] $V-K$ is here taken to be independent of composition.

The present work adopts a compromise temperature scale. A fiducial line, $\log T_e = -0.04\,(V-K)+3.74$, is chosen about midway between the Veeder and the RJWW relations (Fig. 2). At given T_e, $V-K$ is adjusted a fraction β of the way from the appropriate locus, giant or dwarf, to the fiducial. The default value in all synthesis models is $\beta = 1/2$, and the two resulting default scales are used to construct the UBV color-temperature relations for solar composition. However, the models permit β to be varied in order to explore the effects of different temperature scales on integrated $V-K$ colors; the UBV colors are not varied since they are much less sensitive.

As to higher temperatures, the J66 scale is followed between 4500 K and 10,000 K. Above 10,000 K, a transition is made to Hayes's (1978) scale, which is in turn based on the empirical calibration derived by Code *et al.* (1976) from interferometric angular diameters and far ultraviolet photometry.

---

3. None of this discussion contradicts the conclusions of CFP regarding the insensitivity of $V-K$ to variations in gravity and metallicity for $T_e \gtrsim 4000$ K, where molecular absorption is unimportant.

b) Empirical Colors for Solar Composition

For temperatures below 4500 K, the $(V-K)$–$\log T_e$ relations discussed in the last section are regarded as fundamental in the sense that *UBV* colors for a given temperature are assigned by first reading off $V-K$, then referring to observations to match $U-B$ and $B-V$ to $V-K$. *UBVK* colors for cool giants are taken from Lee (1970); for cool dwarfs from J66. Between 4500 K and 10, 000 K, the temperature and the *UBVK* colors are adopted as a unit for each spectral type in J66. Above 10, 000 K, T_e and *UBV* for the spectral types in Hayes (1978) are combined with $V-K$ for the same type in J66. Finally, from graphs of each color against $\log T_e$, *UBVK* colors for dwarfs and for giants are read off at regular temperature intervals. The resulting empirical colors are given in Table 2.

Bolometric corrections for stars cooler than 4000 K are derived from J66 through the $(V-K)$–$\log T_e$ calibrations; above 4000 K, *BC*s from the model atmospheres are used. The zero point adjustments necessary to reconcile the different scales will be discussed in tne next section.

c) Theoretical UBV Colors and Bolometric Corrections

Bell and Gustafsson (1978, subsequently BG) computed *UBVR* colors in the ranges $4000 \leqq T_e \leqq 6000$, $0.75 \leqq \log g \leqq 3.0$ and $-3.0 \leqq [A/H] \leqq 0.0$ from the grid of atmospheres given by Gustafsson *et al.* (1975). The Kurucz (1979) ATLAS models cover the ranges $5500 \leqq T_e \leqq 50,000$, $0.0 \leqq \log g \leqq 4.5$, and $-2.0 \leqq [A/H] \leqq 0.0$; *UBV* colors are given with the models. For $B-V$, the agreement between the two grids is excellent in the region of overlap: 0.03 mag for $[A/H] = 0$, 0.02 mag for $[A/H] = -1$ (mean absolute deviation). For $U-B$, it is essential to apply the zero point shift of −0.2 mag recommended for their colors by Gustafsson and Bell (1979). Then the agreement is again good: 0.04 mag for $[A/H] = 0$, 0.03 mag for $[A/H] = -1$. [It should be noted that the zero point shift is based on a comparison with the Sun, field stars and globu-

lar cluster giants, not on a comparison with other models.]

A small correction has been applied to $U-B$ in the Kurucz models, about +0.1 mag at T_e = 7000 K and tapering on both sides to zero at 8500 K and 5500 K. The correction, based on a comparison with a standard main sequence of solar abundance (Buser and Kurucz 1978, Fig. 2), has been arbitrarily extended to nonsolar compositions (so that color differences are preserved). The ATLAS $U-B$ colors given by Carney and Aaronson (1979) are used, but only as differences, to guide the extension of dwarf UV excesses to 4500 K.

The bolometric corrections calculated in the Kurucz and the BG models agree very well with observations. As discussed by the authors, the discrepancies reach 0.1 mag only for the coolest BG models and in the region $13,000 \lesssim T_e \lesssim 20,000$ K for the Kurucz models (in the latter case, the models may in fact be better than the observations). Thus, the only obstacle to combining the grids and joining them to the empirical BCs for cool temperatures is the problem of normalization (even BG err in directly comparing their scale to J66). Johnson sets $BC_\odot = 0.0$. BG adopt $BC = -0.07$ for their solar model. Making a small empirical adjustment to his solar model, Kurucz estimates $BC_\odot = -0.194$ on his scale. In the present work, all BCs are adjusted to the Kurucz scale.[4]

d) UBV Colors for Cool, Metal Poor Stars

There is only fragmentary evidence to guide the extension of the theoretical grids for metal poor stars to lower temperatures, but, fortunately, neither the integrated colors nor the color–magnitude diagrams of the synthesis models are very sensitive to this step. The giant branches of clusters as metal poor as M92 do not extend into the uncertain region; even in 47 Tuc, only the giant tip is affected. The cool lower main sequence contributes negligibly to the integrated UBV light and lies below the

4. The bolometric corrections in BG are actually adjusted by −0.20 mag, since this secures a better match to Kurucz in the region of overlap.

magnitude limit of CMDs.

Roughly speaking, stars of moderate metal deficiency, $[A/H] \gtrsim -1$, begin to assume nearly "normal" *UBV* colors (*i.e.*, those appropriate to solar composition) for temperatures $T_e \lesssim 3750$ K. This tendency has long been recognized qualitatively. It is illustrated in the $(U-B\,,\,B-V)$ plane by the gradual convergence of the "maximum abundance effect" (Eggen 1969; Sandage 1969) with the Hyades main sequence for $B-V \gtrsim 0.8$. Also, early attempts to classify high velocity stars revealed that M giants and dwarfs, unlike G and K stars, showed no consistent peculiarities relative to the standard types (Keenan and Keller 1953 – by now, of course, the refined MK system is able to accommodate some of the small differences, as in Morgan and Keenan 1973).

With infrared observations it is possible to explore more quantitatively whether the apparent reversion to normal *UBV* colors is absolute – tied only to temperature – or mainly relative, in that the blanketing vectors tend to fall along the normal temperature sequence and become confused with it. Figure 3 of Mould and Hyland (1976) shows that halo dwarfs have in the mean the same $B-V$ as do old disk stars at $V-K \approx 4$ ($T_e \approx 3700$ K on the present scale); for cooler temperatures, the halo stars are (uncertainly) perhaps 0.1 mag *redder* in $B-V$ than the disk stars. A similar plot of $U-B$ against $V-K$ shows no separation between halo and disk beyond $V-K \approx 4$. Since the long baseline of $V-K$ ensures that it is a much more composition-insensitive temperature indicator than $U-B$ or $B-V$, this confluence of *UBV* is largely absolute; it must in any case be regarded so for the purposes of the present models, since a single $(V-K)-T_e$ relation is adopted for all compositions.

For giant stars in globular clusters, the same reversion to normal colors may be seen in plots of $U-B$ or $B-V$ against $V-K$ with data from CFP and Frogel, Persson and Cohen (1980).

It is beyond the scope of this work to discuss the reasons for the approximate

reversion effect in both giant and dwarf stars. Rayleigh scattering (Böhm-Vitense and Szkody 1974) and atmospheric convection (Bessell and Wickramasinghe 1979) both affect the continuum colors more as the metallicity drops; some molecular features decrease in strength while others initially increase (Cottrell 1978); in any case, to simulate the interplay of all these factors is beyond the capabilities of current model atmosphere programs. In practice, the procedure has simply been to connect smoothly the theoretical colors for all compositions to the empirical colors for solar composition at temperatures below 4000 K.

e) Tables of UBV Colors

Table 3 presents colors over the ranges $3000 \leq T_e \leq 35,000$, $0.0 \leq \log g \leq 4.5$, $-2 \leq [A/H] \leq 0$ (note that for $T_e \geq 4000$ K, the case $[A/H] = 0$ is distinct from the fully empirical colors in Table 2). Some sections of the table represent extensions of the theoretical colors into regions of the $(M_b, \log T_e)$ plane not occupied by the usual Hertzsprung-Russell sequences, but they have been included for completeness and to avoid unexpected behavior in interpolation. In the synthesis models, the colors for a given $(\log T_e, \log g)$ point on the theoretical isochrone are obtained by bicubic polynomial interpolation in Table 3. When empirical colors are used for solar composition, the turnoff separates giants from dwarfs (along the horizontal branch, stars with $\log T_e > 3.85$ are considered to be dwarfs).

f) Empirical uvgr Colors

The intermediate band Gunn *uvgr* system has been described by Thuan and Gunn (1976). One of its notable advantages relative to the *UBVR* system is the *u* passband: fully filter-defined, entirely shortward of the Balmer jump, and sufficiently narrow that second order extinction coefficients are unnecessary (the response curve of Gunn *u* is in fact quite similar to that of Strömgren *u*). However, *uvgr* is at a distinct disadvantage with regard to the number and weight of stellar observations which can

be used to calibrate a synthesis procedure, and theoretical colors have not been calculated. The final synthetic colors must be interpreted with an awareness of this limitation.

Zinn (1980) fully describes the early version of the Gunn system common to his work and the studies of Bagnuolo (1976) and Searle, Wilkinson and Bagnuolo (1980; subsequently SWB). The present work draws from Bagnuolo the empirical colors as a function of spectral type for stars of solar composition; but, his temperature scale has been completely replaced with the calibration discussed above. Too few late K and M stars were observed to delineate their colors accurately, particularly with regard to the steep rise in $u-g$ for giants which covers nearly 2 magnitudes between 5000 K and a peak near 3750 K (a more gentle analogue is seen in $U-B$). The accuracy of the dwarf-giant separation is questionable throughout the range of spectral types.

Bagnuolo observed no metal poor stars. To make possible a preliminary calibration, L. Searle graciously provided a selection of spectrophotometric scans of globular cluster giants (Searle and Zinn 1978) together with a prescription for calculating *uvgr* colors from them. About 15 stars, from M92, M13 and M71, were in common with the infrared program of CFP and could be assigned accurate temperatures from $V-K$. These stars were used, with a rough allowance for the known difference in metallicity between the three clusters, to construct color-temperature relations for giants with $[Fe/H] \approx -2$. For dwarfs, the reference points were three extreme subdwarfs in Zinn's (1979) list of standards: HD 19445, HD 84937 and BD+17 4708, all with $[Fe/H] \approx -2$ (Carney 1979). Although the resulting calibration is crude, it has at least the virtue of being best determined where the need is greatest: along the giant branch and around the turnoff of a typical globular cluster (but somewhat cooler than the turnoff, thus nearer to the maximum of the abundance effect).

Table 4 gathers the *uvgr* colors for normal and extremely metal poor compositions. Previously discussed bolometric corrections were applied to the Gunn magnitudes through the relation

$$g - V = 0.377\,(g - r) + 0.055\ ,$$

which is derived from 18 of Zinn's (1979) standards with $-0.9 < g - r < 1.3$; the standard deviation from the fit is 0.02 mag.

IV. BALMER LINE PROFILES

For $T_e > 5500$ K, theoretical profiles for Hδ and Hβ are drawn from Kurucz (1979). As may be seen from Kurucz's comparison of model profiles with observations of Vega, the theory of Balmer line formation is highly developed for the hotter stars. However, the profiles tabulated for 4000 K and 4500 K by Carbon and Gingerich (1969) bear no resemblance to real Balmer lines in cool giants (this problem reflects known deficiencies of the model atmospheres more than inadequacies in the line formation theory). Therefore, for $T_e < 5500$ K, empirical profiles have been joined onto the theoretical grid. J. Cohen kindly provided tracings of echelle spectra of globular cluster giants, some of which could be assigned temperatures from the infrared photometry of CFP. The Arcturus atlas (Griffin 1968), Hiltner and Williams's (1946) atlas of high resolution scans, and Krishna Swamy's (1966) profiles for K dwarfs all provided useful points of reference. It is not claimed that the resulting profiles are fit to be applied diagnostically to single stars. However, since giants above the level of the horizontal branch contribute 25% or more of the composite light at Hβ in a cluster such as M 3, it is at least worth avoiding systematic errors in the gross properties of the profiles – full width and equivalent width.

For $T_e \geq 5500$ K, separate sets of profiles are maintained for [A/H] = 0 and −1. The very small differences between profiles at given T_e for [A/H] = −1 and −2 are

overwhelmed by the influence of the temperature distribution, so profiles for [A/H] = −1 are used for all metal poor compositions.

A composite profile is prepared as follows. Since individual profiles are insensitive to gravity for $T_e \lesssim 7500$ K, such points on the isochrone are assigned to a single temperature sequence of profiles. At higher temperatures, a full temperature-gravity grid of profiles is entered at the value of $\log g$ closest to the actual gravity at the isochrone point. Then, after bracketing the actual temperature with two tabulated temperatures, interpolation in flux is carried out at each of 22 wavelength points along the profile, out to 50 Å from line center. Before addition to the composite profile, the interpolated profile is weighted by the total luminosity of the isochrone point at Hδ or Hβ (for a particular luminosity function). This luminosity is determined from the absolute magnitudes at B and V together with an approximate relation between $B-V$ and continuum slope in the region λλ4000–5000. For comparison with observation, the final composite profile is given both at full resolution and as convolved with two approximate (Gaussian) instrumental profiles with default widths of 5.0 Å and 9.75 Å.

A composite width parameter has proved to be a useful adjunct to the calculation of full synthetic profiles. For each of the profiles in the temperature-gravity grid, the full width at 10% percent depth has been read off and separately tabulated. For each luminosity function, a composite full width is then calculated as a simple luminosity-weighted mean of the individual widths along the isochrone. Less expensive to compute than the synthetic profile, the composite width serves as a good indicator of the differential effect to be expected from changes in horizontal branch distribution, turnoff temperature, *etc.*. In fact, the simple weighted mean usually agrees with the the width of the synthetic profile to better than 5% over the whole range of hydrogen equivalent widths.

V. SYNTHETIC SPECTRA

In order to explore the behavior of metallic features in composite spectra, and to supplement the synthetic Balmer line profiles – particularly at small equivalent widths where the theoretical profiles are less accurate and where contamination by metallic lines may be important – empirically based synthetic spectra have been calculated for the wavelength region λλ3750–4450. The Cassegrain SIT spectrograph (Kent 1979) on the Palomar 1.5 m telescope was used to obtain spectra of about fifty MK "dagger" standards (Morgan and Keenan 1973). The spectra cover the region λλ3650–5250 with about 7 Å (FWHM) resolution. Each final spectrum is the sum of three or more widened spectra (about 20 pixels across the dispersion), so that the net signal is typically $\gtrsim 1.5 \times 10^4$ photons at CaK and greater at longer wavelengths (examples of these spectra are given in Chapter 1). All spectra were reduced to fluxes f_λ. Although an effort was made to observe all stars, particularly extreme spectral types, at airmasses less than 1.5, and in some cases to scan the slit across the image of the star, no blanket estimate of spectrophotometric accuracy can be given. However, because line strengths are the main interest, the effect of the continuum slope in fixing the relative luminosity-weight of lines at various wavelengths in the composite spectrum is secondary to the temperature and luminosity sensitivity of the lines themselves.

Table 5 lists the library of stars of solar composition. A temperature was assigned to each spectral type in accordance with the calibration of §IIIα. Not listed are about 15 metal poor stars chosen on the basis of high resolution abundance analyses to have [Fe/H] ≈ −2. The temperature coverage for cool giants and particularly for cool dwarfs was inadequate to constitute a true metal poor library (even allowing that hot stars can be borrowed from the normal library). A trial synthesis of the spectrum of M92 based on this library confirmed that the metallic features were greatly but still insufficiently weakened relative to a normal synthesis with the same isochrone.

Ordinarily, the synthetic spectrum would be assembled by associating with each isochrone point the spectrum of the nearest spectral type, dwarf or giant. The coverage of types in Table 5 is sufficiently coarse and irregular that a more refined procedure is desirable. A separate spectrum is therefore constructed for each point along the isochrone by linear interpolation between the empirical spectra which bracket it in temperature. After luminosity- and number-weighting, this interpolated spectrum joins the composite.

Equivalent widths determined from these synthetic spectra were central to the interpretation given in Chapter 2 to the integrated spectra of clusters in the Magellanic Clouds, and examples of the spectra themselves are given in Chapter 1 (Figs. 15 and 16). The spectra and theoretical profiles will not be further discussed here.

VI. COMPARISON OF SYNTHETIC COLORS WITH OBSERVATIONS

Before any comparison can be made, the colors and the isochrone must be matched with respect to metallicity. For the purpose of computing integrated colors, it would probably be more accurate to use an interpolated isochrone rather than interpolated colors; and this was done for the case of solar composition. However, it is also vital to compare the theoretical color–magnitude diagrams with observational diagrams for star clusters in the Galaxy and in the Magellanic Clouds. For that purpose, and particularly for analyzing young clusters, the original isochrones are superior to the less smooth interpolations. Finally, in the case of *uvgr* colors, there is as yet no alternative to interpolation between the empirical colors for the Population I and extreme Population II samples.

a) The UBV Color Plane

The choice of evils – interpolated isochrones or interpolated colors – should soon largely disappear with the publication of colors for compositions 3, 1/3, 1/30 and 1/300 times solar (see Kurucz 1979; Bell and Gustafsson 1978 already include the

1/3-solar case). For now, the following procedure has been adopted after comparing the behavior of the tabulated compositions in the color-temperature plane. Approximate colors for Z = 0.01 are obtained by averaging the colors for solar and 1/10-solar compositions, separately for each value of the gravity. Where comparison can be made, this apparently crude formula is remarkably consistent. The mean difference between the interpolated $B-V$ colors, intended to represent [A/H] = −0.3, and the colors *calculated* by BG for [A/H] = −0.5 is $\Delta(B-V) = 0.01$, with a dispersion σ_Δ of only 0.003 mag (the colors for [A/H] = −0.3 are the redder, as should be). For $U-B$, the corresponding values are $\Delta(U-B) = 0.02$, $\sigma_\Delta = 0.01$. This comparison embraces all the temperatures and gravities in the BG grid. Although no similar check is available for the Kurucz grid, the total magnitude of the composition effect is any case declining with temperature, becoming negligible for $T_e \gtrsim 10,000$ K.

Colors for Z = 0.001 ([A/H] ≈ −1.3) are approximated by averaging the colors for 1/10- and 1/100-solar compositions. For Z = 0.0001, the 1/100-solar colors are used as is; in the BG grid, the differences in either $U-B$ or $B-V$ between 1/100- and 1/1000-solar are generally 0.06 mag or less (and have zero mean as well in the case of $B-V$).

Figure 3 shows age sequences of models in the $(U-B, B-V)$ plane for the four compositions: Z = 0.02, 0.01, 0.001, and 0.0001, all with Y = 0.3. Also shown are a selection of galactic globular clusters from the compilation of Harris and Racine (1979) and a small group of elliptical galaxies from Visvanathan and Sandage's (1977) list of Virgo "calibrators".[5] Short vectors show the effect of adding to the models for an age of 13 Gy one of the horizontal branches described in §IIb: an M92 type for Z = 0.0001, and M3 type for Z = 0.001, a 47 Tuc type for Z = 0.01, none for Z = 0.02. The dotted line which connects the termination points of these vectors therefore

5. Colors for the galaxies are effective aperture colors from the Second Reference Catalogue of Bright Galaxies (de Vaucouleurs, de Vaucouleurs and Corwin 1976), corrected for an assumed reddening $E(B-V) = 0.02$.

constitutes, according to the models, a locus of star clusters with age 13 Gy and "mean" horizontal branch properties.

The mean isochrone well represents the run of the observations, from the most metal poor globulars to typical elliptical galaxies; the influence of the horizontal branch is essential in securing this agreement for the globular clusters. To what extent, though, does agreement imply uniqueness? Several features of the models help us to evaluate the question. First, it is interesting to note the behavior of the horizontal branch vectors. For Z = 0.01, the vector is short and nearly parallel to the evolutionary track. For Z = 0.0001, the vector is longer but, perhaps surprisingly, causes no change in $U-B$; this happens because so many stars on the M92 horizontal branch are in the "crook" of the $(U-B)-T_e$ curve, and also because the turnoff for Z = 0.0001 is much bluer than that for Z = 0.01 and so accords less weight proportionally to the horizontal branch. Were an M92 vector to be attached to the point (Z, Age) = (0.0001, 10 Gy), its terminus would be bluer in $B-V$ than any observed cluster. The models therefore favor ages $\gtrsim$ 13 Gy for the most metal poor globulars. The vector for Z = 0.001 limits the ages differently: vectors beginning from 10 Gy or 13 Gy are both clearly acceptable, but a vector from 16 Gy falls significantly short of the observed region. However, the standard horizontal branch places no useful limits by the time Z reaches 0.01, a characteristic which meshes with the second general feature of the model loci: their confluence in the region of red colors. The points (0.01, 16) and (0.02, 7) lie within typical observational errors of each other, despite the great disparity in age.

Thus, a partial answer to the question of uniqueness – partial because only the $(U-B\,,\,B-V)$ diagram has so far been considered – is that the models significantly restrict the ages of metal poor clusters but become less predictive with increasing metallicity. Of course, if the composition of a metal rich cluster is known independently, the point along the appropriate track which best fits the observed colors

yields the age – in principle. But it is precisely in the realm of the metal rich clusters that the present work conflicts with some recent abundance analyses. The metallicity of 47 Tuc or of M71 (observationally very similar to 47 Tuc) has long been thought to be in the range $-0.6 \lesssim [A/H] \lesssim -0.3$. However, Pilachowski, Canterna and Wallerstein (1980, for 47 Tuc) and Cohen (1980, for M71) have argued from high dispersion spectra that the metallicity of both clusters should be revised to $[A/H] \approx -1.2$ to -1.3 (these authors also review the earlier estimates). In Figure 3, the vector that shows the effect of adding a 47 Tuc horizontal branch to the model cluster for (Z, Age) = (0.01, 13*Gy*) points, fittingly, to 47 Tuc itself. While it is clear from the discussion above that this happenstance cannot be taken to fix the age and abundance of 47 Tuc with precision, it is just as clear that no point on the track for Z = 0.001 is within striking range of the observed colors of 47 Tuc. This situation will be explored further when color–magnitude diagrams are considered in § VII.

The elliptical galaxies in Figure 3 cluster around the segment for clusters of solar composition between 10 and 13 Gy old.[6] If the redder Virgo ellipticals are more metal rich than the Sun, these ages are upper limits. Of course, the single burst models do not fully describe galaxies. Still, if most of the star formation occurred during the initial collapse of these ellipticals, the models suggest that the event took place about 13 Gy ago.

The models in Figure 3 are repeated in Figure 4, but now clusters in the Magellanic Clouds and three open clusters in the Galaxy are shown for comparison. As orientation, the dashed line extends the track for solar composition to smaller ages using the models of Barbaro and Bertelli (1977), and the dotted line is Racine's (1973)

---

6. It is interesting to compare the adopted models, which use empirical colors, with colors which differ only in that they use theoretical colors for solar composition (excepting the coolest giants; see § III*c*). Such models lie almost precisely on the locus in Figure 3, but the age calibration differs slightly: the point for 13 Gy with theoretical colors corresponds to an age of about 11 Gy on the adopted scale. At 1 Gy the two models coincide. This "sliding" effect is no accident, as the Appendix shows.

intrinsic mean line for globular clusters (which nearly coincides with the 13 Gy isochrone in Fig. 3). Colors for the Cloud clusters were taken from van den Bergh and Hagen (1968), except for N 2209 and Hodge 11, not in that list, which were measured by Freeman and Gascoigne (1977). Individual reddenings for some of the younger clusters were adopted from Barbaro and Bertelli (1977), but otherwise a correction for $E(B-V) = 0.07$ (van den Bergh and Hagen 1968; de Vaucouleurs 1978) has been uniformly applied in order to reduce the *systematic* displacement of the colors.

The model loci in Figure 4 successfully bound the observed colors of clusters in the Magellanic Clouds, except for Hodge 11. In that case, models suggest the cluster to be extremely metal poor (Freeman and Gascoigne 1977) but far older, not younger (Walker 1979), than N 2209.[7] The three open clusters are also reasonably placed in Figure 4 [colors for the Hyades are from Gray (1965), those for M 67 and N 188 from Goodenough and Hartwick (1970)]. The Hyades lies on the track for solar composition, age about 1 Gy. M 67 and N 188 are both indicated to be somewhat metal poor, with M 67 about 3 Gy and N 188 roughly 5 Gy old, although the funneling of tracks makes the latter estimate difficult. Ages will be further discussed in §VII.

b) The BVK Color Plane

Figure 5 shows that the models also account well for the array of globular clusters in the $(B-V, V-K)$ plane; $V-K$ colors have been taken from Aaronson *et al.* (1978). As in Figure 3, a 13 Gy isochrone satisfactorily accounts for the run of colors over the full range of metallicity. M 71 again falls near the Z = 0.01 evolutionary track for an age of 10–13 Gy. The given position of M 13 is somewhat surprising in view of its metallicity, $[A/H] \approx -1.5$ (Cohen 1978; Griffin 1979; Pilachowski, Wallerstein and Leep 1980), but its separation in $V-K$ from the isochrone and from the track for Z = 0.001

---

7. The locus of models with the composition (Y, Z) = (0.2, 0.0001) runs closely along the locus for (0.3, 0.0001), with slightly different ages. Walker (1979) has suggested that H 11 may be enriched in helium, but this result indicates that even a substantial increase, say to 0.4, would do little or nothing to approach the observed colors for H 11.

is about 0.15 mag, the nominal error estimated by Aaronson *et al.*.

The reversal in $V-K$ for ages greater than 13 Gy in the Z = 0.02 and Z = 0.01 tracks may be traced to the giant branch, even though its temperature at given luminosity becomes uniformly cooler with increasing age. The strength of the decrease or reversal in the rate of evolution up the giant branch which occurs when the hydrogen-burning shell passes outward through the discontinuity in hydrogen abundance left by the convective envelope (Thomas 1967) depends on both stellar mass and composition (Sweigart and Gross 1978). The effect is larger for metal rich compositions generally. For Z = 0.01, the resulting peak in the giant branch luminosity function is both stronger and more luminous for 0.9 $M_{\odot}$ than for 0.7 $M_{\odot}$ (Sweigart, private communication). Compared to the 13 Gy isochrone, the luminosity function of the less massive stars on the 20 Gy isochrone is weighted to lower luminosities and bluer $V-K$ colors – hence the reversal.

c) The UVK Color Plane: What Colors are Possible?

The loci of models in the $(U-V, V-K)$ plane present a remarkable appearance (Fig. 6): the tracks overlap and intertwine to such an extent that, over much of the diagram, the ability to separate the effects of age and abundance is almost wholly lost. True, the observations obediently confine themselves within the narrow swath traced out by the models, but this might seem the only positive aspect of the situation. However, perhaps the very feature that appears to compromise most the diagnostic value of these colors – the near degeneracy of the model loci – may instead be turned to advantage in another context.

Consider the fact that the models for (Z, Age) = (0.02, 10 Gy) and (0.01, 4 Gy) have almost the same *UVK* colors; an arbitrary superposition of the two models must therefore have these colors still. It seems reasonable to hope that a group of model galaxies made up of various combinations of the model clusters would occupy a con-

siderably smaller fraction of the available area in the $(U-V, V-K)$ plane than it would in a color plane for which the clusters themselves spread out more normally. The Appendix shows that this problem of determining which parts of color space are permitted to model galaxies can be solved generally. The result for the *UVK* plane is shown as the dashed region in Figure 6. This "realm of galaxies" incorporates not only all of the individual models for $s = 2.35$ shown in the figure (with the exception of the Z = 0.01, 0.5 Gy point, which is of lesser realiability), but all of the models for $s = 0$ and $s = 3.5$ as well. *No model galaxy composed of these model clusters, in whatever combination, with whatever relative strengths, may lie outside the dashed region.* Since age, composition, luminosity function and strength may be varied independently, this statement admits an essentially arbitrary history of star formation.

In contrapositive form, the statement bears directly on observation: *a real galaxy which lies outside the permitted region must include at least one stellar subpopulation which is outside the scope of the models.* Of the galaxies observed by Frogel, Persson and Cohen (1980), some are redder in $V-K$ than the reddest model cluster in this work and, therefore, trivially require an additional stellar component (suggested by those authors to be red stars more luminous than the theoretical tip of the first giant branch); it is not appropriate to discuss such systems here. However, some galaxies are bluer than the reddest cluster and yet appear to be "outsiders" in Figure 6. Within the context of the present models, but otherwise free of assumptions, it may be stated flatly that the apparent UV excess of such galaxies could not be the result of recent star formation.[8]

d) The uvgr Colors

The synthetic *uvgr* colors will be discussed in less detail than were the *UBVK* colors. The agreement with observations is less good, but the calibrating stellar

8. It need hardly be emphasized that this is an illustration of the potential value of constructing permitted color regions, not an analysis of the galaxy observations. The Appendix suggests other applications.

photometric data are less extensive. The latter deficiency will have to be remedied before an analysis *via* models can fully exploit the advantages of this intermediate band system.

In analogy to Figure 3 for the *UBV* plane, Figure 7 shows shows evolutionary tracks in the *ugr* plane together with observations of populous clusters in the Magellanic Clouds (SWB) and globular clusters in the Galaxy (Zinn 1980). A correction for a mean reddening $E(B-V) = 0.07$ has again been applied to the Cloud clusters. The most metal poor globulars and some of the Cloud clusters group near the 13 Gy isochrone at $Z \approx 10^{-4}$, as might be expected. However, many clusters lie below the track for solar composition and therefore show a $u-g$ or a $g-r$ deficiency with respect to it. Since the corresponding phenomenon in the *UBV* diagram is not seen, the possibility of a color-dependent distortion in the *uvgr* stellar photometry (which constitutes the synthesis library) relative to the cluster photometry should at least be considered. From the discussion in Chapter 2 (see Fig. 4), it is unlikely that N 1846 should be associated with the solar isochrone at an age of about 7 Gy. Also, the distribution of clusters in $g-r$ relative to the metal poor globulars agrees tolerably well with the relative distribution in $B-V$. Thus, a systematic error in $g-r$ is probably not the cause of the "low" clusters. A relative distortion in $u-g$ for large values of the index seems a more likely explanation. Still, *uvgr* is not *UBV*. Consistency between the models and the observations in one system does not guarantee that a disagreement in the other system is an artifact. N 1846 does lie slightly below the solar line in Figure 3, whereas the discussion in Chapter 2 would suggest that the cluster is significantly metal poor. Perhaps the strictly defined ultraviolet color in the Gunn system merely exposes this problem more clearly. If so, the *uvgr* colors may eventually help to track down deficiencies in the synthesis models as applied to the Magellanic Clouds.

Figure 8 encourages the notion that the observed colors of the Cloud clusters are telling us something about our neighbor galaxies, not just casting doubt on the photometric library. In this diagram, which compares the two reddening-insenstive indices $Q(ugr)$ and $Q(vgr)$ (see Zinn 1980), galactic globular clusters follow fairly well the 13 Gy isochrone over the full range of metallicity. Agreement is not perfect: the isochrone turns over too sharply at the metal poor end; most of the clusters lie below the line in the range $0.10 < Q(vgr) < 0.25$ (where, however, there are also no tie points to define the isochrone accurately); and some clusters (including 47 Tuc) extend past the point for Z = 0.01, as does not happen in Figure 3. However, considering that the track for Z = 0.0001 is based on colors computed from a rather small set of spectrophotometric scans, and that colors for intermediate metallicities had to be approximated with less external guidance than was available for the *UBV* system, the overall agreement is satisfying and suggests that some of the Cloud clusters have a genuine ultraviolet deficiency relative to models based on stars in the Galaxy.[9] From Figure 9, again the $(Q(ugr), Q(vgr))$ plane, it is apparent that the candidates are intermediate age clusters, members of groups IV and V in the SWB classification scheme. Clusters in these groups tend to contain very luminous M giants and carbon stars (Mould and Aaronson 1980). Carbon stars alone, however, contribute only about 2% of the visible light of clusters in which they are found (Aaronson and Mould 1980) and so do not directly influence the $Q-Q$ diagram (except perhaps to a minor degree through $g-r$).

There are other suggestive features in Figure 9, but in view of possible photometric offsets, they must be interpreted cautiously, in outline rather than detail. First, no point on the solar evolutionary track with an age $\gtrsim 4$ Gy falls within the classification regions; this is so even if the ultraviolet colors are systematically in error. The

9. It may be noted in passing that the horizontal branch vectors for the metal poor compositions differ from the vector illustrated by SWB in that they could, by their orientation, contribute significantly to the observational scatter in colors. However, it is not clear that such an explanation is viable (see discussion in Chapter 1 and in Zinn 1979).

implication is that *all* clusters that formed in either Cloud more then 4–5 Gy ago are to some degree metal poor. Second, the evolutionary tracks for metal poor compositions bridge the gap between regions VII and III. This is necessary if clusters such as N 2209 (III–IV) are to be both young ($\sim 2 \times 10^9$ y) and metal poor ([Fe/H] ≈ -1; see discussion in Chapter 2). It also suggests how difficult it might be to establish by *direct* estimates the existence (proposed by SWB and others) of age–abundance relations in the Clouds. For, if Cloud clusters which lie near the middle of group VII have a metallicity typical of globulars in that vicinity, such as M 5 with [Fe/H] about −1.5 or −1.6 (Zinn 1979; Pilachowski, Wallerstein and Leep 1980), the net change in metallicity around the full curve from N 2209 to mid-VII would be only about −0.6 dex. Given the difficulties and uncertainties in securing individual determinations of age and abundance, this is an uncomfortably small range in which to establish a correlation. If the metallicity of N 2209 were closer to [A/H] = −0.5 (Gustafsson, Bell and Hejlesen 1977), the available range is more promising. But perhaps the salient point is simply that Figure 9 may reflect *some* age–abundance relation without reflecting the *simplest* such relation we can imagine.

VII. COLOR–MAGNITUDE DIAGRAMS

Figures 10–13 show color–magnitude diagrams and a selection of theoretical isochrones for the globular clusters M 92 and 47 Tuc and for the open clusters M 67 and N 188. Since this discussion aims to explore the characteristics of the models rather than to apply them in detail, only the sources of the data and a list of the major conclusions will be presented.

The stellar observations for M 92 (Fig. 10) are taken from Sandage (1970) and Sandage and Walker (1964). The diagram for 47 Tuc (Fig. 11) consists of the stars observed photoelectrically by Hartwick and Hesser (1974), tabulated in Hesser and Hartwick (1977). For M 92, a distance modulus $m - M = 14.13$ is obtained by assuming

that the absolute visual magnitude of its RR Lyrae stars is $M_V = +0.6$ (McDonald 1977); for 47 Tuc, the assumption is $M_V = +0.8$ at the position of the RR Lyrae gap. Figure 12 shows color–magnitude observations for M 67 from Eggen and Sandage (1964). The distance modulus is adopted from Racine (1971), adjusted to a Hyades modulus of 3.2 [Hanson (1980) reviews the Hyades distance problem]; Racine's value is very close to that of Eggen and Sandage when the Hyades moduli are made to correspond. For N 188 (Fig. 13), the photographic observations are from McClure and Twarog (1977) while the distance modulus is that of Eggen and Sandage (1969), again adjusted to a new Hyades distance. For reddenings, reference was made to Twarog's (1978) summary of work on M 67 and N 188.

Examination of the CMDs prompts the following observations:

1. The isochrones for Y = 0.2 fit better than those for Y = 0.3. Demarque and McClure (1977b) noted this for the main sequence of four halo clusters. The subgiant branch is also steeper and in better accord with observed shapes (the upper giant branch is insensitive to Y). The quality of the fit cannot, of course, be taken as a *determination* of the helium abundance.

2. From Figures 10 and 11, and from other CMDs not shown, it is consistent to assign an age of 16 (+2,-3) Gy to the globular clusters. Taken at face value, Figure 11 implies for 47 Tuc a metallicity somewhere between −1.2 (Pilachowski, Canterna and Wallerstein 1980) and the "conventional" value of −0.5, perhaps $[Fe/H] \approx -0.9$ with a corresponding age of 16 Gy. Dickens, Bell and Gustafsson (1979) also estimate $[Fe/H] \approx -0.8$, based primarily on a comparison of Stromgren photometry of individual stars with theoretical colors.

It is worth noting that the isochrone for Z = 0.01, although clearly too red, implies an age of about 13 Gy from the *luminosity* of the turnoff [the stars near $M_V = 4$, $B-V = 0.52$ are part of the turnoff, as shown by the extensive photographic data in

Hesser and Hartwick (1977)]. Thus, the temperature adjustment procedure described above, which ensures that the isochrones reproduce the position of the Sun in the HR diagram, removes most or all of the variation in cluster ages found by Carney (1980), even without a major revision of the metallicity of 47 Tuc.

3. The model age of M67 is 4–5 Gy. The Z = 0.01 isochrone fits the giant branch, consistent with the fit in $V-K$ (§IIc), but the corresponding main sequence is too blue; the Z = 0.02 isochrone fits the main sequence, but the giant branch is too red. It is not surprising that Z = 0.02 fits the main sequence since, in Figure 12, the Sun is embedded in the locus of M67 stars [the Sun also lies between the isochrones for Y = 0.2 and Y = 0.3, closer to Y = 0.2, as it should for a primeval solar helium abundance of $Y \approx 0.23$ (Bahcall *et al.* 1968)]. Similar remarks apply to N188, which has a model age of 7–10 Gy. The ages for M67 and N188 are 2–3 billion years older than those given by McClure and Twarog (1978), also based on the Yale isochrones. The difference is a consequence of temperature adjustment along the main sequence.

4. It may be seen from Figure 10 that the present models strongly exclude ages less than 13 Gy for M92. Even if the ratio of carbon or nitrogen to iron were to be enhanced tenfold, the resulting change in the position of the turnoff would be too small to reduce the fitted age to less than 13 Gy (sample tracks are given in Demarque 1980). Aaronson *et al.* (1980) have proposed a value $H_0 = 95\ \mathrm{km\,s^{-1}\,Mpc^{-1}}$ for the global value of the Hubble ratio. According to standard Friedman models with $H_0 = 100$, the time τ_0 since the big bang has been 9.1 Gy for $\Omega = 0.06$ (Gott *et al.* 1974), or 7.6 Gy for $\Omega = 0.4$ (Davis *et al.* 1980).

The latter value is so strongly excluded by the models that, if the corresponding values of H_0 and Ω are supported, it would be necessary to seek basic deficiencies in the red giant models, not just uncertainties in the construction of the isochrones.[10] For $H_0 = 55$ (Sandage and Tammann 1975), the age is 16.5 Gy for $\Omega = 0.06$ or 13.8 Gy for $\Omega = 0.4$.

---

10. For example, Noerdlinger and Arigo (1980) have shown that the settling of helium during the evolution of globular cluster stars reduces their luminosity at turnoff compared to models without diffusion. This can reduce the inferred age by up to 20%, if turnoff luminosity is the sole criterion. However, the effect on the *temperature* of the turnoff is negligible; in the context of the present models, in which the whole morphology of the turnoff is considered (including color), an age of (say) 10 Gy for M92 would still be untenable.

APPENDIX

ON THE COLORS OF COMPOSITE SYSTEMS

Consider two photometric colors, $A-B$ and $B-C$, together with a set **S** of objects for which such colors have been measured or calculated. We ask: what limits may be placed on the colors of a composite object **C** constructed from members of **S**? More precisely, let **C** be composed of an arbitrary subset of **S**, each member of which has been scaled arbitrarily in luminosity – that is, **C** is the most general possible composite.

The problem may be solved by considering ratios of luminosities rather than differences of magnitudes. Let $x \equiv c/b$, $y \equiv a/b$, where a, b and c are luminosities though the three filters: $A-B = -2.5\log(a/b)$. Consider first the combination of two objects, subscripted 1 and 2, into a joint object subscripted c. Parametrize the relative luminosities of the objects by

$$\zeta \equiv \frac{b_2}{b_1+b_2} \; ; \qquad 0 \leq \zeta \leq 1 \, . \tag{1}$$

Then

$$x_c = \frac{a_1+a_2}{b_1+b_2} = (1-\zeta)x_1 + \zeta x_2 \, , \tag{2}$$

and similarly for y. Or, considering x and y to be the components of a vector $\mathbf{z}$, we have

$$\mathbf{z}_c = (1-\zeta)\mathbf{z}_1 + \zeta \mathbf{z}_2 \; ; \qquad 0 \leq \zeta \leq 1 \, . \tag{3}$$

Thus, in the space of ratios, the composite object must lie on the line connecting the constituent objects and, furthermore, the trajectory from one to the other is linear in the strength parameter ζ.

The form (3) is familiar from the definition of a convex set and permits an immediate generalization to the full problem of n objects. We seek that set which includes all

the line segments joining the constituent objects, and all the segments joining the points so generated, and no others: this is the *convex hull* (or convex closure) of S, the "smallest" convex set contained in S (*e.g.*, Royden 1968).

In practice, the convex hull may be drawn by inspection. Figure 14 shows the ratio plane that corresponds to the $(U-V, V-K)$ color plane together with points representing model star clusters of various ages and compositions (described in §VIc). The dashed segments outline the convex hull of these points; all "galaxies" composed of these model clusters must lie in the hull. Translated back to the $(U-V, V-K)$ plane, the hull appears as the dashed boundary in Figure 6. It may be noted that, if physical considerations allow one to exclude certain models – for example, the models with (Z, Age) = (10^{-4}, 2 Gy) at the upper left in Figure 14 are unlikely to contribute significantly to a generally much older and more metal rich elliptical galaxy – the hull may be modified trivially. Also, the effect of adding to a given object a certain percentage of young stars or metal-poor stars may be evaluated quickly using the linearity of (3) in ζ.

The hull method may be used in a more fundamental way by using as constituents not model clusters but the full library of individual stars from which the clusters are made. Although the color limits so obtained are weaker, they involve no assumptions about stellar evolution and define the realm of possibility for any model. This fact can be used prior to any computation as a zero-order check of the ability of a given stellar library to reproduce the colors of the observed composite system that is to be modeled. For example, Figure 15 shows the ratio plane corresponding to the $(u-g, g-r)$ plane of Gunn colors, together with sequences of colors for dwarf and giant stars. It may first be noted that the stellar sequence is largely concave upward. Thus, on the side of low ratios (red in $u-g$, blue in $g-r$), the addition of the hull has little enlarging effect; composite models are essentially bounded in this direction by the stellar sequence itself (this is also seen for the sequence of models in Figure 6).

In the direction of large ratios, it is the chord connecting the hottest and the coolest stars which defines the boundary. Given a desired composite color, it is easy to explore the necessary extensions to high and low temperatures by varying the slope of a line through the target color and observing its intersections with the stellar sequence. Such a procedure is particularly attractive if the composite object is simple, such as a binary star, and the more so if limits may be placed on the colors of one member.

It is worth emphasizing that the constituent colors or sequences of colors need not be stellar. They could, for example, be black bodies or synchrotron sources. Also, most of this development may be extended to higher dimensionalities.

TABLE 1

THREE HORIZONTAL-BRANCH DISTRIBUTIONS (NORMALIZED TO 1000 STARS)

Type	log T_e											
	3.675	3.700	3.725	3.750	3.775	3.80	3.85	3.90	3.95	4.10	4.25	4.40
47 Tuc	11	430	503	56	...	...	...	...	...	...	...	
M 3	...	9	60	132	146	204	209	150	60	19	11	
M 92	...	...	...	...	...	75	193	365	285	70	12	

NOTE.--Each column heading is the lower temperature limit of an interval; the next column heading is the upper limit.

TABLE 2

EMPIRICAL UBVK COLORS FOR SOLAR COMPOSITION

T_e (K)	U - B		B - V		V - K	
	giant	dwarf	giant	dwarf	giant	dwarf
2500	0.70	1.50	1.53	2.16	8.90	7.72
2750	0.93	1.47	1.54	1.98	7.96	6.82
3000	1.23	1.37	1.56	1.80	7.08	6.00
3250	1.57	1.18	1.59	1.62	6.20	5.24
3500	1.84	1.16	1.61	1.54	5.04	4.54
3750	1.92	1.24	1.59	1.46	4.09	3.89
4000	1.70	1.23	1.45	1.31	3.51	3.23
4250	1.40	1.04	1.29	1.17	2.95	2.78
4500	1.12	0.88	1.15	1.05	2.58	2.45
4750	0.84	0.73	1.01	0.96	2.28	2.15
5000	0.63	0.58	0.91	0.88	2.05	1.95
5250	0.48	0.44	0.83	0.82	1.82	1.78
5500	0.31	0.29	0.71	0.71	1.60	1.60
6000	0.05		0.54		1.24	
6500	0.00		0.40		1.00	
7000	0.05		0.32		0.77	
7500	0.09		0.24		0.60	
8000	0.11		0.17		0.40	
8500	0.10		0.11		0.27	
9000	0.07		0.07		0.15	
9500	0.03		0.02		0.03	
10000	-0.03		-0.01		-0.08	
11000	-0.21		-0.08		-0.21	
12000	-0.33		-0.10		-0.28	
14000	-0.49		-0.14		-0.41	
16000	-0.60		-0.18		-0.50	
20000	-0.76		-0.22		-0.65	
25000	-0.91		-0.25		-0.79	
30000	-1.02		-0.28		-0.92	

NOTE.—Colors for $T_e < 3500$ K are less reliable and should be used with caution.

TABLE 3

THEORETICAL UBV COLORS AND BOLOMETRIC CORRECTIONS

U - B [A/H] = 0

T_e (K)	log g (cgs)								
	0.0	0.75	1.5	2.0	2.5	3.0	3.5	4.0	4.5
3000	1.22	1.22	1.22	...	...	...	1.37	1.37	1.37
3500	1.84	1.84	1.84	1.84	...	...	1.17	1.17	1.17
3750	1.92	1.90	1.88	1.88	...	1.30	1.24	1.24	1.24
4000	1.90	1.90	1.53	1.32	1.17	1.08	1.15	1.19	1.23
4500	1.30	1.29	0.99	0.86	0.76	0.69	0.80	0.84	0.88
5000	0.70	0.70	0.61	0.51	0.44	0.37	0.47	0.51	0.55
5500	...	0.51	0.41	0.32	0.24	0.17	0.24	0.26	0.28
6000	...	...	0.35	0.26	0.17	0.09	0.08	0.06	0.05
6500	...	...	...	0.21	0.15	0.10	0.04	-0.01	-0.05
7000	...	...	...	0.25	0.21	0.16	0.10	0.04	-0.02
7500	...	...	...	0.29	0.26	0.22	0.17	0.11	0.05
8000	..	...	...	0.17	0.20	0.18	0.14	0.08	0.02
8500	...	...	...	0.00	0.05	0.08	0.09	0.08	0.04
9000	...	...	...	-0.09	-0.04	0.01	0.03	0.04	0.03
10000	...	...	...	-0.27	-0.20	-0.15	-0.11	-0.08	-0.06
12000	...	...	...	-0.52	-0.44	-0.39	-0.35	-0.32	-0.29
15000	...	...	...	-0.76	-0.66	-0.61	-0.60	-0.55	-0.53
20000	...	...	...	...	-0.94	-0.85	-0.80	-0.61	-0.76
25000	...	...	...	...	...	-1.02	-0.96	-0.93	-0.91
35000	...	...	...	...	...	...	-1.12	-1.10	-1.09

TABLE 3 - Continued

U - B [A/H] = -1

T_e (K)	log g (cgs)								
	0.0	0.75	1.5	2.0	2.5	3.0	3.5	4.0	4.5
3000	1.22	1.22	1.22	...	...	...	1.37	1.37	1.37
3500	1.84	1.84	1.84	1.84	...	...	1.17	1.17	1.17
3750	1.92	1.90	1.88	1.88	...	1.30	1.14	1.14	1.14
4000	1.85	1.59	1.20	1.04	0.92	0.84	0.95	1.00	1.03
4500	1.20	0.95	0.69	0.56	0.47	0.41	0.45	0.49	0.52
5000	0.58	0.48	0.35	0.25	0.17	0.11	0.15	0.20	0.22
5500	...	0.28	0.21	0.11	0.03	-0.04	-0.02	0.00	0.02
6000	...	...	0.18	0.09	-0.01	-0.05	-0.08	-0.10	-0.13
6500	...	...	...	0.12	0.06	0.00	-0.07	-0.13	-0.17
7000	...	...	...	0.19	0.15	0.09	0.03	-0.04	-0.11
7500	...	...	...	0.25	0.22	0.18	0.13	0.06	-0.01
8000	...	...	...	0.16	0.18	0.16	0.11	0.05	-0.02
8500	...	...	...	0.02	0.07	0.10	0.11	0.09	0.05
9000	...	...	...	-0.09	-0.03	0.02	0.06	0.07	0.05
10000	...	...	...	-0.26	-0.19	-0.14	-0.10	-0.07	-0.04

NOTE.--Colors for $T_e > 10{,}000$ K may be taken from the tabulation for [A/H] = 0.

TABLE 3 - Continued

U - B [A/H] = -2

T_e (K)	log g (cgs)								
	0.0	0.75	1.5	2.0	2.5	3.0	3.5	4.0	4.5
3000	1.22	1.22	1.22	...	...	...	1.37	1.37	1.37
3500	1.84	1.84	1.84	1.84	...	...	1.17	1.17	1.17
3750	1.92	1.90	1.88	1.88	...	1.00	1.04	1.04	1.04
4000	1.65	1.38	1.11	0.97	0.86	0.80	0.83	0.86	0.88
4500	1.02	0.76	0.54	0.43	0.35	0.30	0.34	0.36	0.38
5000	0.45	0.29	0.20	0.10	0.02	-0.03	0.00	0.05	0.08
5500	...	0.15	0.11	0.01	-0.08	-0.16	-0.13	-0.10	-0.08
6000	...	...	0.12	0.02	-0.04	-0.13	-0.19	-0.21	-0.23
6500	...	...	...	0.07	0.01	-0.06	-0.12	-0.19	-0.23
7000	...	...	...	0.17	0.12	0.06	-0.01	-0.09	-0.16
7500	...	...	...	0.24	0.21	0.16	0.10	0.03	-0.05
8000	...	...	...	0.16	0.17	0.15	0.10	0.04	-0.03
8500	...	...	...	0.02	0.07	0.10	0.11	0.09	0.05
9000	...	...	...	-0.08	-0.02	0.03	0.06	0.07	0.06
10000	...	...	...	-0.25	-0.18	-0.13	-0.08	-0.06	-0.03

NOTE.--Colors for T_e> 10,000 K may be taken from the tabulation for [A/H] = 0.

TABLE 3 - Continued

B - V [A/H] = 0

T_e (K)	log g (cgs)							
	0.0	0.75	1.5	2.0	2.5	3.0	3.5	4.5
3000	1.78	1.68	1.58	...	...	...	1.71	1.79
3500	1.74	1.66	1.61	1.56	...	1.50	1.52	1.54
4000	1.63	1.53	1.42	1.38	1.34	1.30	1.31	1.32
4500	1.36	1.25	1.17	1.13	1.11	1.08	1.02	1.02
5000	0.92	0.93	0.93	0.91	0.89	0.87	0.86	0.87
5500	...	0.71	0.73	0.71	0.71	0.70	0.69	0.66
6000	...	...	0.52	0.52	0.53	0.55	0.55	0.55
6500	...	...	...	0.39	0.40	0.41	0.42	0.44
7000	...	...	...	0.27	0.29	0.30	0.32	0.35
7500	...	...	...	0.12	0.18	0.21	0.24	0.28
8000	...	...	...	0.03	0.06	0.10	0.15	0.21
8500	...	...	...	-0.02	-0.01	0.02	0.05	0.12
9000	...	...	...	-0.04	-0.04	-0.02	0.00	0.07
10000	...	...	...	-0.06	-0.08	-0.07	-0.06	-0.01
12000	...	...	...	-0.10	-0.12	-0.12	-0.12	-0.09
15000	...	...	...	-0.14	-0.16	-0.17	-0.16	-0.14
20000	...	...	...	...	-0.20	-0.22	-0.22	-0.21
25000	...	...	...	...	...	-0.25	-0.26	-0.25
35000	...	...	...	...	...	...	-0.28	-0.30

TABLE 3 - Continued

B - V [A/H] = -1

T_e (K)	log g (cgs)							
	0.0	0.75	1.5	2.0	2.5	3.0	3.5	4.5
3000	1.82	1.73	1.62	...	...	...	1.76	1.85
3500	1.75	1.66	1.63	1.58	...	1.50	1.56	1.57
4000	1.62	1.50	1.38	1.31	1.26	1.23	1.25	1.26
4500	1.28	1.16	1.06	1.01	0.97	0.96	0.93	0.90
5000	0.96	0.90	0.81	0.79	0.77	0.76	0.76	0.76
5500	...	0.65	0.60	0.60	0.60	0.60	0.60	0.61
6000	...	...	0.44	0.44	0.45	0.46	0.47	0.49
6500	...	...	...	0.32	0.34	0.35	0.37	0.40
7000	...	...	...	0.22	0.25	0.27	0.28	0.32
7500	...	...	...	0.10	0.15	0.19	0.21	0.25
8000	...	...	...	0.01	0.04	0.09	0.14	0.20
8500	...	...	...	-0.03	-0.02	0.00	0.03	0.09
9000	...	...	...	-0.05	-0.05	-0.03	-0.01	0.05
10000	...	...	...	-0.06	-0.08	-0.07	-0.06	-0.01

NOTE.—Colors for $T_e > 10{,}000$ K may be taken from the tabulation for [A/H] = 0.

TABLE 3 - Continued

B - V [A/H] = -2

T_e (K)	log g (cgs)							
	0.0	0.75	1.5	2.0	2.5	3.0	3.5	4.5
3000	1.82	1.73	1.62	...	...	...	1.76	1.85
3500	1.77	1.68	1.65	1.60	...	1.59	1.58	1.59
4000	1.62	1.52	1.41	1.33	1.29	1.25	1.27	1.31
4500	1.25	1.15	1.05	1.00	0.96	0.94	0.93	0.90
5000	1.02	0.78	0.73	0.72	0.71	0.72	0.72	0.73
5500	...	0.58	0.54	0.53	0.53	0.54	0.55	0.57
6000	...	...	0.40	0.40	0.41	0.42	0.44	0.46
6500	...	...	...	0.30	0.32	0.33	0.35	0.38
7000	...	...	...	0.20	0.23	0.25	0.27	0.31
7500	...	...	...	0.09	0.15	0.18	0.20	0.25
8000	...	...	...	0.01	0.04	0.09	0.14	0.19
8500	...	...	...	-0.03	-0.02	0.00	0.02	0.08
9000	...	...	...	-0.05	-0.05	-0.03	-0.01	0.05
10000	...	...	...	-0.06	-0.07	-0.07	-0.06	-0.01

NOTE.—Colors for $T_e > 10{,}000$ K may be taken from the tabulation for [A/H] = 0.

TABLE 3 - Continued

-B.C. [A/H] = 0

T_e (K)	log g (cgs)			
	0.0	2.0	3.0	4.5
3000	4.25	4.00	...	3.40
3500	2.10	2.10	2.05	1.97
3750	1.50	1.50	1.50	1.50
4000	1.00	1.02	1.05	1.06
4500	0.60	0.62	0.64	0.65
5000	0.21	0.39	0.41	0.42
5500	0.16	0.24	0.26	0.26
6000	...	0.14	0.16	0.19
6500	...	0.06	0.10	0.14
7000	...	0.02	0.06	0.12
7500	...	0.02	0.04	0.11
8000	...	0.04	0.05	0.11
8500	...	0.11	0.11	0.14
9000	...	0.20	0.19	0.20
10000	...	0.40	0.38	0.38
12000	...	0.80	0.78	0.78
15000	...	1.33	1.33	1.33
20000	...	1.96	2.02	2.08
25000	...	...	2.52	2.63
35000	...	...	3.37	3.38

TABLE 3 - Continued

-B.C. [A/H] = -1 or -2

T_e (K)	log g (cgs)			
	0.0	2.0	3.0	4.5
3000	4.25	4.00	...	3.40
3500	2.10	2.10	2.05	1.97
3750	1.50	1.50	1.50	1.50
4000	1.02	1.00	1.01	1.01
4500	0.62	0.62	0.63	0.63
5000	0.25	0.39	0.42	0.42
5500	0.20	0.26	0.30	0.30
6000	...	0.17	0.22	0.24
6500	...	0.11	0.16	0.21
7000	...	0.06	0.11	0.19
7500	...	0.05	0.09	0.18
8000	...	0.09	0.10	0.17
8500	...	0.15	0.16	0.22
9000	...	0.24	0.23	0.26
10000	...	0.45	0.43	0.42

NOTE.--B.C.s for $T_e > 10{,}000$ K may be taken from the tabulation for [A/H] = 0.

TABLE 4

EMPIRICAL uvgr COLORS
SOLAR COMPOSITION

T_e (K)	u - g		v - g		g - r	
	giant	dwarf	giant	dwarf	giant	dwarf
2500	1.70	2.57	0.60	1.16	1.63	1.82
2750	1.88	2.46	0.75	1.30	1.59	1.67
3000	2.14	2.30	0.98	1.37	1.52	1.50
3250	2.54	2.11	1.54	1.38	1.45	1.30
3500	2.77	1.96	1.73	1.37	1.34	1.14
3750	2.83	1.82	1.75	1.32	1.18	0.97
4000	2.66	1.68	1.71	1.24	0.97	0.80
4250	2.05	1.39	1.49	0.96	0.71	0.59
4500	1.52	1.16	1.05	0.79	0.51	0.44
5000	0.83	0.87	0.49	0.59	0.26	0.24
5500	0.44	0.44	0.29	0.38	0.11	0.10
6000	0.13	0.13	0.14	0.20	0.00	0.00
6500	0.11	0.11	0.05	0.09	-0.10	
7000	0.17	0.17	-0.08	-0.04	-0.23	
7500	0.21	0.21	-0.17	-0.12	-0.30	
8000	0.26	0.25	-0.28	-0.22	-0.40	
8500	0.27	0.23	-0.34	-0.30	-0.49	
9000	0.23	0.09	-0.39	-0.35	-0.58	
9500	-0.04	-0.06	-0.43	-0.41	-0.64	
10000	-0.29	-0.18	-0.47	-0.47	-0.68	
11000	-0.47	-0.35	-0.52	-0.52	-0.72	
12000	-0.60	-0.48	-0.56	-0.56	-0.75	
14000	-0.82	-0.69	-0.61	-0.61	-0.78	
16000	-0.98	-0.86	-0.65	-0.65	-0.79	
20000	-1.12	-1.12	-0.72	-0.69	-0.81	
25000	-1.32		-0.74		-0.83	
30000	-1.43		-0.76		-0.84	
35000	-1.52		-0.78		-0.84	

TABLE 4 - Continued

EXTREMELY METAL POOR COMPOSITION

T_e (K)	u - g		v - g		g - r	
	giant	dwarf	giant	dwarf	giant	dwarf
2500	1.70	2.57	0.60	1.16	1.63	1.82
2750	1.88	2.46	0.75	1.30	1.59	1.67
3000	2.14	2.30	0.98	1.37	1.52	1.50
3250	2.54	2.11	1.54	1.38	1.45	1.30
3500	2.77	1.96	1.73	1.37	1.34	1.14
3750	2.79	1.77	1.74	1.28	1.20	0.97
4000	2.35	1.45	1.59	1.07	1.08	0.80
4250	1.76	0.98	1.04	0.73	0.83	0.57
4500	1.14	0.72	0.68	0.60	0.64	0.42
5000	0.48	0.30	0.28	0.31	0.31	0.22
5500	0.17	-0.02	0.10	0.10	0.13	0.08
6000	0.06	-0.06	0.00	-0.03	0.00	-0.02
6500	0.08	-0.01	-0.06	-0.09	-0.10	
7000	0.17	0.11	-0.12	-0.16	-0.23	
7500	0.21	0.18	-0.18	-0.21	-0.30	
8000	0.26	0.23	-0.28	-0.26	-0.40	

NOTE.--Colors for $T_e > 8000$ K may be taken from the tabulation for solar composition.

TABLE 5

SYNTHESIS STARS

Giant			Dwarf		
Sp	HD	T_e	Sp	HD	T_e
B2 III	35468	23100	B2 III	35468	23100
A0 V	103287	9410	A0 V	103287	9410
			A1 V	86986	9160
A7 III	28319	7900	A7 IV	76644	7900
F2 IV	40535	6700	F2 IV	40535	6700
F5 III	17918	6400	F5 V	27524	6400
F6 IV	11443	6270	F6 IV	11443	6270
G0 III	6903	5900	G1 V	27836	5835
G8.5 III	82635	4875			
G9 III	181276	4810			
K0 III	188947	4710	K0 V	75732	5200
K1.5 III	1522	4540			
K3 III	3627	4250			
K4 III	69267	4060	K5 V	201091	4290
K7 III	70272	3875	K7 V	201092	4020
M0 III	89758	3830			
M1 IIIab	218329	3770			
M2 III	219734	3680			
M3 II	40239	3540			

REFERENCES

Aaronson, M., Cohen, J. G., Mould, J., and Malkan, M. 1978, *Ap. J.*, 223, 824.

Aaronson, M., and Mould, J. 1980, preprint.

Aaronson, M., Mould, J., Huchra, J., Sullivan, W. T., Schommer, R. A., and Bothun, G. D. 1980, *Ap. J.*, **239**, in press.

Bagnuolo, W. G., Jr. 1976, Ph.D. thesis, California Institute of Technology.

Bahcall, J. N., Bahcall, N. A., and Shaviv, G. 1968, *Phys. Rev. Letters*, **20**, 1209.

Barbaro, G., and Bertelli, G. 1977, *Astr. Ap.*, **54**, 243.

Bell, R. A., and Gustafsson, B. 1978, *Astr. Ap. Suppl.*, **34**, 229.

Bessell, M. S., and Wickramasinghe, D. T. 1979, *Ap. J.*, **227**, 232.

Böhm-Vitense, E. 1958, *Zs. Ap.*, **46**, 108.

Böhm-Vitense, E., and Szkody, P. 1974, *Ap. J.*, **193**, 607.

Buser, R., and Kurucz, R. L. 1978, *Astr. Ap.*, **70**, 555.

Carbon, D. F., and Gingerich, O. 1969, in *Theory and Observations of Normal Stellar Atmospheres*, ed. O. Gingerich (Cambridge: MIT Press), p. 377.

Carney, B. W. 1979, *Ap. J.*, **233**, 211.

-----. 1980, *Ap. J. Suppl.*, **42**, 481.

Carney, B. W., and Aaronson, M. 1979, *A. J.*, **84**, 867.

Ciardullo, R. B., and Demarque, P. 1977, *Trans. Yale Univ. Obs.*, **33, 34, 35.**

-----. 1979, in *Problems of Calibration of Multicolor Photometric Systems*, ed. A. G. D. Philip (*Dudley Obs. Rept.*, No. 14), p. 317.

Code, A. D., Davis, J., Bless, R. C., and Hanbury Brown, R. 1976, *Ap. J.*, **203**, 417.

Cohen, J. G. 1978, *Ap. J.*, **223**, 487.

-----. 1980, *Ap. J.*, in press.

Cohen, J. G., Frogel, J. A., and Persson, S. E. 1978, *Ap. J.*, **222**, 165.

Copeland, H., Jensen, J. O., and Jørgensen, H. E. 1970, *Astr. Ap.*, **5**, 12.

Cottrell, P. L. 1978, *Ap. J.*, **223**, 544.

Da Costa, G. S. 1977, Ph.D. thesis, Australian National University.

Davis, M., Tonry, J., Huchra, J., and Latham, D. W. 1980, *Ap. J. (Letters)*, **238**, L113.

Demarque, P. 1980, in *Star Clusters*, ed. J. E. Hesser (Dordrecht: Reidel), p. 281.

Demarque, P., and Larson, R. B. 1964, *Ap. J.*, **140**, 544.

Demarque, P., and McClure, R. 1977a, *Ap. J.*, **213**, 716.

-----. 1977b, in *The Evolution of Galaxies and Stellar Populations*, ed. B. M. Tinsley and R. B. Larson (New Haven: Yale Univ. Obs.), p. 199.

Deupree, R. G., and Varner, T. M. 1980, *Ap. J.*, **237**, 558.

de Vaucouleurs, G. 1978, *Ap. J.*, **223**, 730.

de Vaucouleurs, G., de Vaucouleurs, A., and Corwin, H. G. 1976, *Second Reference Catalogue of Bright Galaxies* (Austin: Univ. Texas Press).

Dickens, R. J., Bell, R. A., and Gustafsson, B. 1979, *Ap. J.*, **232**, 428.

Dixon, M. E., Ford, V. L., and Robertson, J. W. 1972, *Ap. J.*, **174**, 17.

Eggen, O. J. 1969, *Ap. J. Suppl.*, **19**, 31.

Eggen, O. J., and Sandage, A. 1964, *Ap. J.*, **140**, 130.

-----. 1969, *Ap. J.*, **158**, 669.

Faber, S. 1972, *Astr. Ap.*, **20**, 361.

Freeman, K. C., and Gascoigne, S. C. B. 1977, *Proc. A. S. A.*, **3**, 136.

Frogel, J. A., Persson, S. E., and Cohen, J. G. 1980, preprint.

Golay, M. 1974, *Introduction to Astronomical Photometry* (Dordrecht: Reidel), p. 74 *et seq.*

Goodenough, D. G., and Hartwick, F. D. A. 1970, *Pub. A. S. P.*, **82**, 921.

Gott, J. R., Gunn, J. E., Schramm, D. N., and Tinsley, B. M. 1974, *Ap. J.*, **194**, 543.

Gough, D. O., and Weiss, N. O. 1976, *M. N. R. A. S.*, **176**, 589.

Gray, D. F. 1965, *A. J.*, **70**, 362.

Griffin, R. 1975, *M. N. R. A. S.*, **171**, 181.

-----. 1979, *M. N. R. A. S.*, **187**, 269.

-----. 1979, *M. N. R. A. S.*, **187**, 277.

Griffin, R. F. 1968, *A Photometric Atlas of the Spectrum of Arcturus* (Cambridge: Cambridge Philosophical Society).

Gunn, J. E., and Griffin, R. F. 1979, *A. J.*, **84**, 752.

Gustafsson, B., and Bell, R. A. 1979, *Astr. Ap.*, **74**, 313.

Gustafsson, B., Bell, R. A., Eriksson, K., and Nordlund, Å. 1975, *Astr. Ap.*, **42**, 407.

Gustafsson, B., Bell, R. A., and Hejlesen, P. M. 1977, *Ap. J. (Letters)*, **216**, L7.

Hanson, R. B. 1980, in *Star Clusters*, ed. J. E. Hesser (Dordrecht: Reidel), p. 71.

Hartwick, F. D. A., and Hesser, J. E. 1974, *Ap. J. (Letters)*, **194**, L129.

Hesser, J. E., and Hartwick, F. D. A. 1977, *Ap. J. Suppl.*, **33**, 361.

Harris, W. E., and Racine, R. 1979, *Ann. Rev. Astr. Ap.*, **17**, 241.

Hayes, D. S. 1978, in *The HR Diagram*, ed. A. G. D. Philip and D. S. Hayes (Dordrecht: Reidel), p. 65.

Hiltner, W. A., and Williams, R. C. 1946, *Photometric Atlas of Stellar Spectra* (Ann Arbor: Univ. Michigan Press).

Iben, I., Jr. 1963, *Ap. J.*, **138**, 452.

Iben, I., Jr., Rood, R. T., Strom, K. M., and Strom, S. E. 1969, *Nature*, **224**, 1006.

Johnson, H. L. 1966, *Ann. Rev. Astr. Ap.*, **4**, 193.

Keenan, P. C., and Keller, G. 1953, *Ap. J.*, **117**, 241.

Kent, S. M. 1979, *Pub. A. S. P.*, **91**, 394.

Krishna Swamy, K. S. 1966, *Ap. J.*, **145**, 174.

Kurucz, R. L. 1979, *Ap. J. Suppl.*, **40**, 1.

Lacy, C. H. 1977, *Ap. J.*, **218**, 444.

Lasker, B. M. 1970, *A. J.*, **75**, 21.

Lee, S.-W. 1977, *Astr. Ap. Suppl.*, **27**, 381.

Lee, T. A. 1970, *Ap. J.*, **162**, 217.

Leung, K.-C., and Schneider, D. P. 1978, *A. J.*, **83**, 618.

Limber, D. N. 1958, *Ap. J.*, **127**, 387.

McClure, R. D., and Twarog, B. A. 1977, *Ap. J.*, **214**, 111.

------. 1978, in *Chemical and Dynamical Evolution of Our Galaxy*, ed. E. Basinska-Grzesik and M. Mayor (Geneva: Geneva Obs.), p. 193.

McDonald, L. F. 1977, Ph.D. thesis, University of California at Santa Cruz.

Mengel, J. G., Sweigart, A. V., Demarque, P., and Gross, P. G. 1979, *Ap. J. Suppl.*, **40**, 733.

Morgan, W. W., and Keenan, P. C. 1973, *Ann. Rev. Astr. Ap.*, **11**, 29.

Mould, J., and Aaronson, M. 1980, *Ap. J.*, **240**, in press.

Mould, J., and Hyland, A. R. 1976, *Ap. J.*, **208**, 399.

Noerdlinger, P. D., and Arigo, R. J. 1980, *Ap. J. (Letters)*, **237**, L15.

O'Connell, R. W. 1976, *Ap. J.*, **206**, 370.

Peck, M. L. 1980, *Ap. J.*, **238**, 79.

Pilachowski, C. A., Canterna, R., and Wallerstein, G. 1980, *Ap. J. (Letters)*, **235**, L21.

Pilachowski, C. A., Wallerstein, G., and Leep, E. M. 1980, *Ap. J.*, **236**, 508.

Racine, R. 1971, *Ap. J.*, **168**, 393.

------. 1973, *A. J.*, **78**, 180.

Relyea, L. J., and Kurucz, R. L. 1978, *Ap. J. Suppl.*, **37**, 45.

Renzini, A. 1977, in *Advanced Stages in Stellar Evolution*, ed. P. Bouvier (Geneva: Geneva Obs.), p. 213.

Ridgway, S. T., Joyce, R. R., White, N. M., and Wing, R. F. 1980, *Ap. J.*, **235**, 126.

Royden, H. L. 1968, *Real Analysis*, second edition (New York: MacMillan), p. 207.

Sandage, A. 1970, *Ap. J.*, **162**, 841.

Sandage, A., and Tammann, G. A. 1975, *Ap. J.*, **197**, 265.

Sandage, A., and Walker, M. F. 1966, *Ap. J.*, **143**, 313.

Searle, L., Sargent, W. L. W., and Bagnuolo, W. G., Jr. 1973, *Ap. J.*, **179**, 427.

Searle, L., Wilkinson, A., and Bagnuolo, W. G., Jr. 1980, *Ap. J.*, **239**, in press.

Searle, L., and Zinn, R. 1978, *Ap. J.*, **225**, 357.

Simoda, M., and Tanikawa, K. 1970, *Pub. Astr. Soc. Japan*, **22**, 143.

Smak, J., and Wing, R. F. 1979, *Acta Astr.*, **29**, 187.

Spinrad, H., and Taylor, B. J. 1971, *Ap. J. Suppl.*, **22**, 445.

Sweigart, A. V. 1978, in *The HR Diagram*, ed. A. G. D. Philip and D. S. Hayes (Dordrecht: Reidel), p. 333.

Sweigart, A. V., and Gross, P. G. 1976, *Ap. J. Suppl.*, **32**, 367.

-----. 1978, *Ap. J. Suppl.*, **36**, 405.

Thomas, H.-C. 1967, *Zs. Ap.*, **67**, 420.

Thuan, T. X., and Gunn, J. E. 1976, *Pub. A. S. P.*, **88**, 543.

Tinsley, B. M. 1968, *Ap. J.*, **151**, 547.

-----. 1978, *Ap. J.*, **222**, 14.

Tsuji, T. 1978, *Astr. Ap.*, **62**, 29.

Twarog, B. A. 1978, *Ap. J.*, **220**, 890.

van den Bergh, S., and Hagen, G. L. 1968, *A. J.*, **73**, 569.

Veeder, G. J. 1974, *A. J.*, **79**, 1056.

Visvanathan, N., and Sandage, A. 1977, *Ap. J.*, **216**, 214.

Walker, M. F. 1979, *M. N. R. A. S.*, **186**, 767.

Wielen, R. 1973, in *Highlights of Astronomy* (Vol. 3), ed. G. Contopoulos (Dordrecht: Reidel), p. 395.

Williams, T. B. 1976, *Ap. J.*, **209**, 716.

Wing, R. F. 1973, in *Variable Stars in Globular Clusters and Related Systems*, ed. J. D. Fernie (Dordrecht: Reidel), p. 165.

Wing, R. F., Dean, C. A., and MacConnell, D. J. 1976, *Ap. J.*, **205**, 186.

Wing, R. F., and Ridgway, S. T. 1979, in *Problems of Calibration of Multicolor Photometric Systems*, ed. A. G. D. Philip (*Dudley Obs. Rept.*, No. 14), p. 253.

Zinn, R. 1980, *Ap. J. Suppl.*, **42**, 19.

FIGURE CAPTIONS

Figure 1. In the plane of $V-K$ and absolute K (2.2 micron) magnitude, theoretical isochrones adjusted to a mixing length ratio $\alpha \equiv l/H_p = 1.5$ (the distance moduli are discussed in §VII). (*a*) M92. The isochrone for $Z = 10^{-4}$, 13 Gy, includes a small blueward shift (about 25 K at $M_K \approx -3.3$) to account for AGB stars, which are not shown. Arrows show the effect of adjusting α to 1.2. (*b*) M67. Adjustment to $\alpha = 1.2$ (*arrows*) makes the giant branch too red. (*c*) 47 Tuc. The two isochrones correspond approximately to "conventional" and "new" estimates of the cluster's metallicity (see text).

Figure 2. The relationship between $V-K$ and effective temperature for cool giant stars, on the new scale proposed by Ridgway *et al.* (1980) (*solid curve, upper left*), is compared to Veeder's (1974) calibration for dwarfs (*solid line, lower left*). The *crosses* show *color* temperatures for giants from Ridgway *et al.*. Both scales are merged with Johnson's (1966) scale for hotter stars (*solid curve, right*).

Figure 3. *UBV* colors for globular clusters and elliptical galaxies. Four evolutionary tracks of the integrated color of the model star clusters (*solid lines*) are labelled by the age in units of 10^9 y. Tracks from *top to bottom*: $Z = 10^{-4}$, 10^{-3}, 10^{-2}, 2×10^{-2} (all with $Y = 0.3$ and power law luminosity functions, $s = 2.35$). Vectors leaving the points for 13 Gy, ending in *crosses*, show the effect of adding a "standard" horizontal branch (see text). The *dotted line* connecting the crosses is an approximate isochrone for clusters 13 Gy old.

Figure 4. The same evolutionary tracks as in Figure 3, now superposed on observed (reddening-compensated) colors for star clusters in the Magellanic Clouds and for three open clusters in the Galaxy. The *dashed line* (from Barbaro and Bertelli 1977) extends the solar evolutionary track to younger ages: 5.9, 3.2, 2.5, and 0.9×10^8 y. The *dotted line* is Racine's (1973) "intrinsic" mean line for globulars.

Figure 5. Globular clusters and theoretical evolutionary tracks in the *BVK* plane. Tracks from *left to right*: $Z = 10^{-4}$, 10^{-3}, 10^{-2}, 2×10^{-2}. The horizontal branch vectors define an approximate 13 Gy isochrone, as in Figure 3. $V-K$ data from Aaronson *et al.* (1978).

Figure 6. As in Figure 5, but now the *UVK* plane. Tracks from *left to right* (termination points): $Z = 10^{-4}$, 10^{-3}, 10^{-2}, 2×10^{-2}. The *dashed line* defines the region within which *all* composite systems made up of these models (and also models for $s = 0$ and $s = 3.5$, not shown) must lie; see text and Appendix.

Figure 7. Cluster evolutionary tracks in the Gunn *ugr* plane, superposed on reddening-compensated colors for globular clusters and clusters in the Magellanic Clouds. Tracks from *top to bottom*: $Z = 10^{-4}$, 10^{-3}, 2×10^{-2}, with ages in units of 10^9 y as before. Horizontal branch vectors leave the 13 Gy points and define an approximate isochrone (*crosses and dotted line*).

Figure 8. (After Zinn 1980) Evolutionary tracks and observed globular clusters in the plane of the reddening-insensitive colors $Q(ugr)$ and $Q(vgr)$. Tracks from *left to right*: $Z = 10^{-4}$, 10^{-3}, 10^{-2}, 2×10^{-2}.

Figure 9. (After Searle, Wilkinson and Bagnuolo 1980) Again the $Q-Q$ plane, with evolutionary tracks as in Figure 8 (*left to right*: $Z = 10^{-4}$, 10^{-3}, 2×10^{-2}), now superposed on observations of clusters in the Magellanic Clouds. The *dashed lines* delimit the classification regions of SWB (Roman numerals I–VII).

Figure 10. Theoretical isochrones superposed on the color-magnitude diagram of M92 from Sandage (1970). Sources for the reddenings and distance moduli used in this and the next three figures are given in the text (§ VII). An age of 13–16 Gy is indicated.

Figure 11. Theoretical isochrones superposed on the color-magnitude diagram of 47 Tuc (photoelectric data from Hesser and Hartwick 1977); stars near $M_V = 4$,

$(B-V)_0 = 0.52$ belong to the turnoff. The data are consistent with a metallicity of [Fe/H] ≈ -0.9.

Figure 12. Isochrones for Z = 0.01 and Z = 0.02 are superposed on Eggen and Sandage's (1964) photoelectric data for M 67. An age of 4–5 Gy is indicated, depending on metallicity. The Sun is shown as a circled dot, embedded in the M 67 main sequence.

Figure 13. Theoretical isochrones superposed on McClure and Twarog's (1977) photographic data for N 188. It is difficult to fit the main sequence with Z = 0.01, even if the distance modulus were considerably changed. On the other hand, to fit the color of the giant branch with Z = 0.02 would require adjustment to a mixing length ratio $\alpha \approx 1.9$ (compared to the default value of $\alpha = 1.5$).

Figure 14. The model clusters are plotted in a space linear in flux *ratios* instead of magnitudes: (L_U/L_V, L_K/L_V), where L_U, L_V and L_K are luminosities through the U, V, and K filters. Thus, objects red in $V-K$ are to the right and those blue in $U-V$ are toward the top. The *dashed line* outlines the convex hull of the plotted points. As shown in the Appendix, the hull exclusively defines the region of ratio space available to model galaxies composed of these clusters. Some of the models which brace the hull are labelled. *A*: (10^{-4}, 2, 2.35) [where the three numbers are Z, age in units of 10^9 y, and the value of the power-law index of the luminosity function, s]; *B*: (10^{-4}, 4, 0.0); *C*: (10^{-4}, 13, 0.0); *D*: (10^{-3}, 13, 0.0) with a 47 Tuc horizontal branch; *E*: (0.02, 20, 3.5); *F*: (0.02, 13, 0.0).

Figure 15. A flux ratio diagram, (L_u/L_g, L_r/L_g), for the stars which constitute the library of *uvgr* colors. Both Pop. I and Pop II stars, giants and dwarfs, are plotted. Two chords which pass through the "target" color illustrate how their intersections with the stellar sequence quickly bracket the extremes of temperature that are needed in order to produce a given composite object.

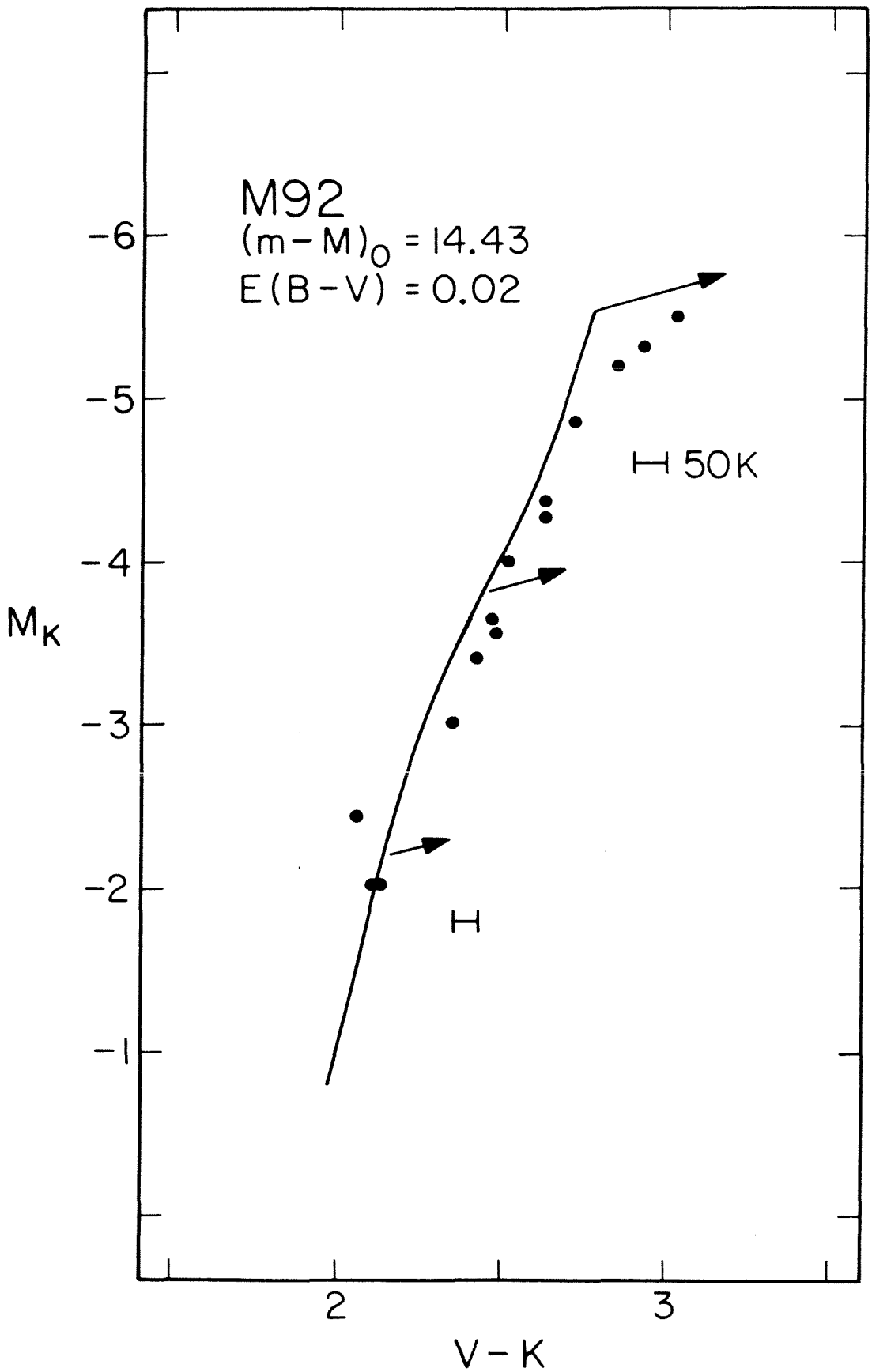

Figure 1a

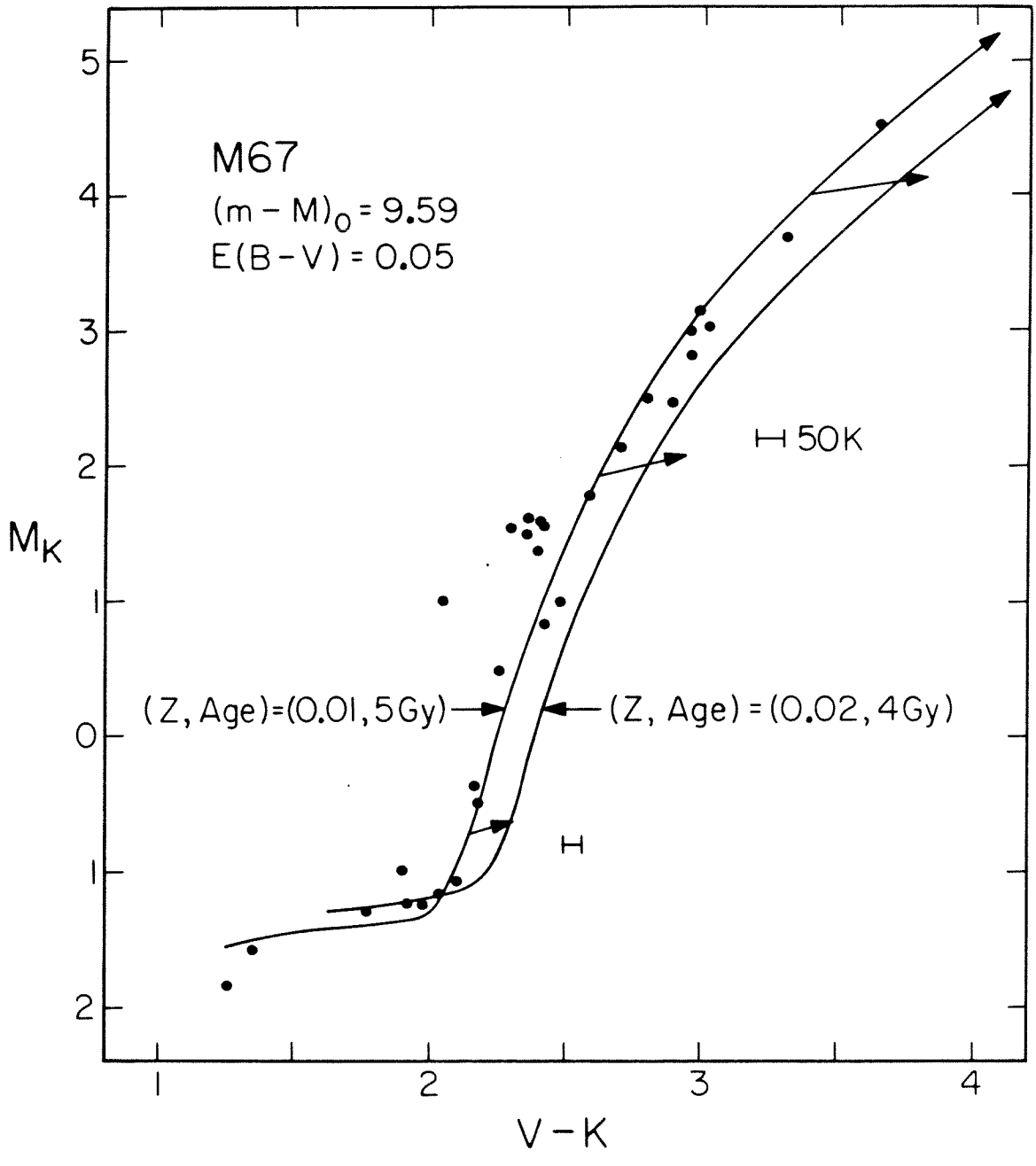
M67
(m - M)0 = 9.59
E(B-V) = 0.05
H 50K
(Z, Age)=(0.01, 5Gy)
(Z, Age) = (0.02, 4Gy)
H
MK
V-K
5
4
3
2
1
0
1
2
1
2
3
4

Figure 1b

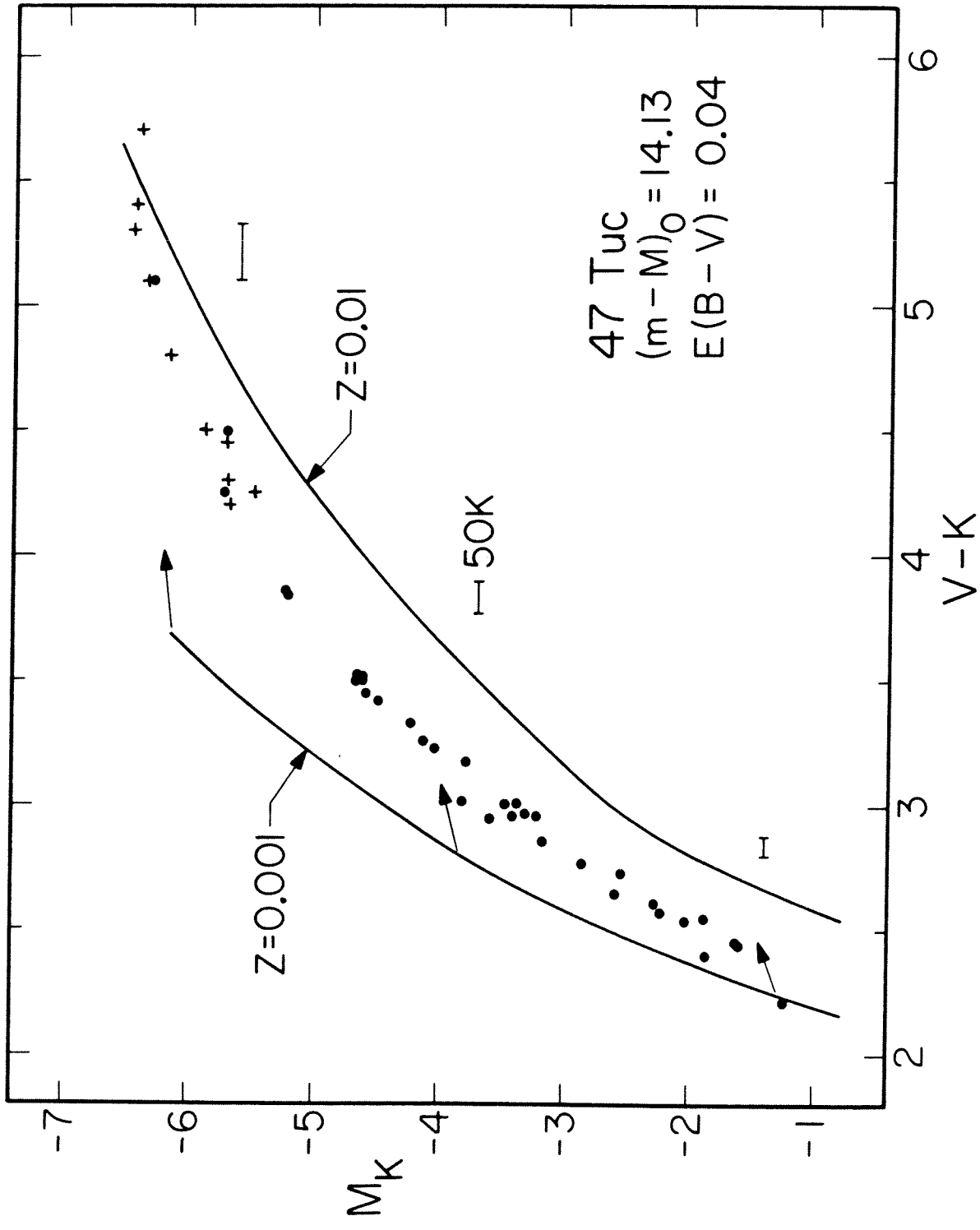

Figure 1c

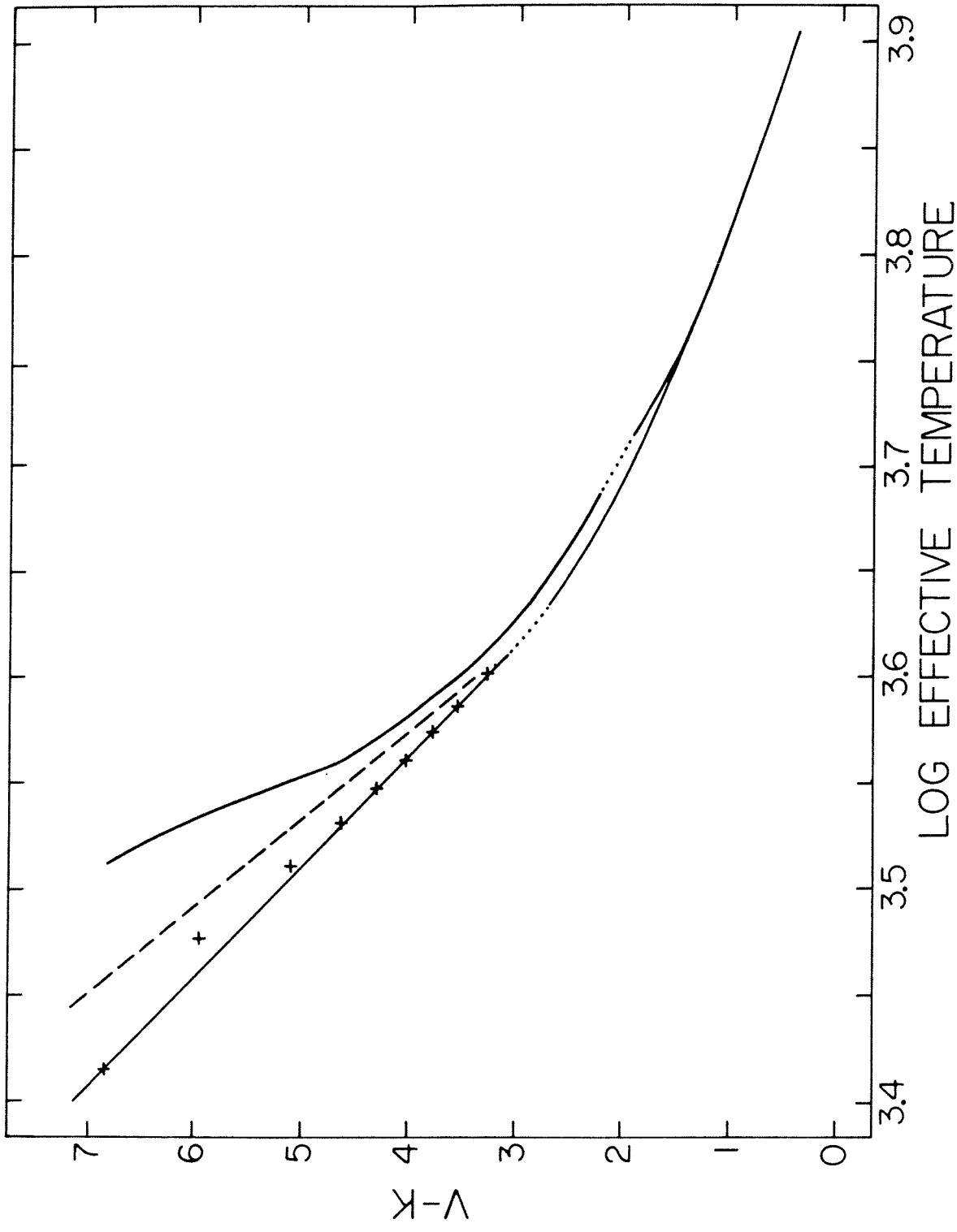

Figure 2

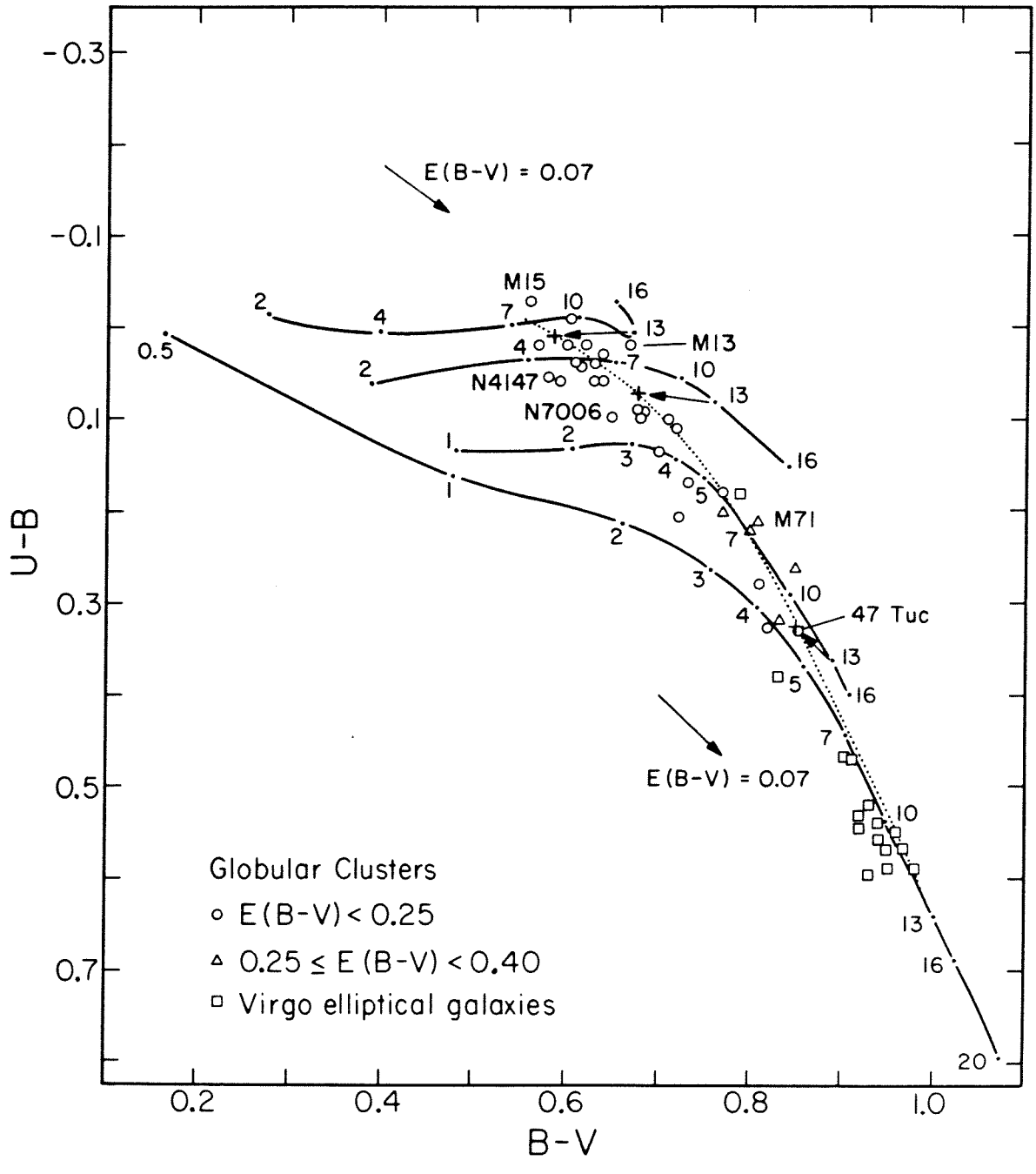
E(B-V) = 0.07
M15
M13
N4147
N7006
M71
47 Tuc
E(B-V) = 0.07
Globular Clusters
o E(B-V)< 0.25
Δ 0.25 ≤ E (B-V) < 0.40
□ Virgo elliptical galaxies
U-B
B-V
-0.3
-0.1
0.1
0.3
0.5
0.7
0.2
0.4
0.6
0.8
1.0

Figure 3

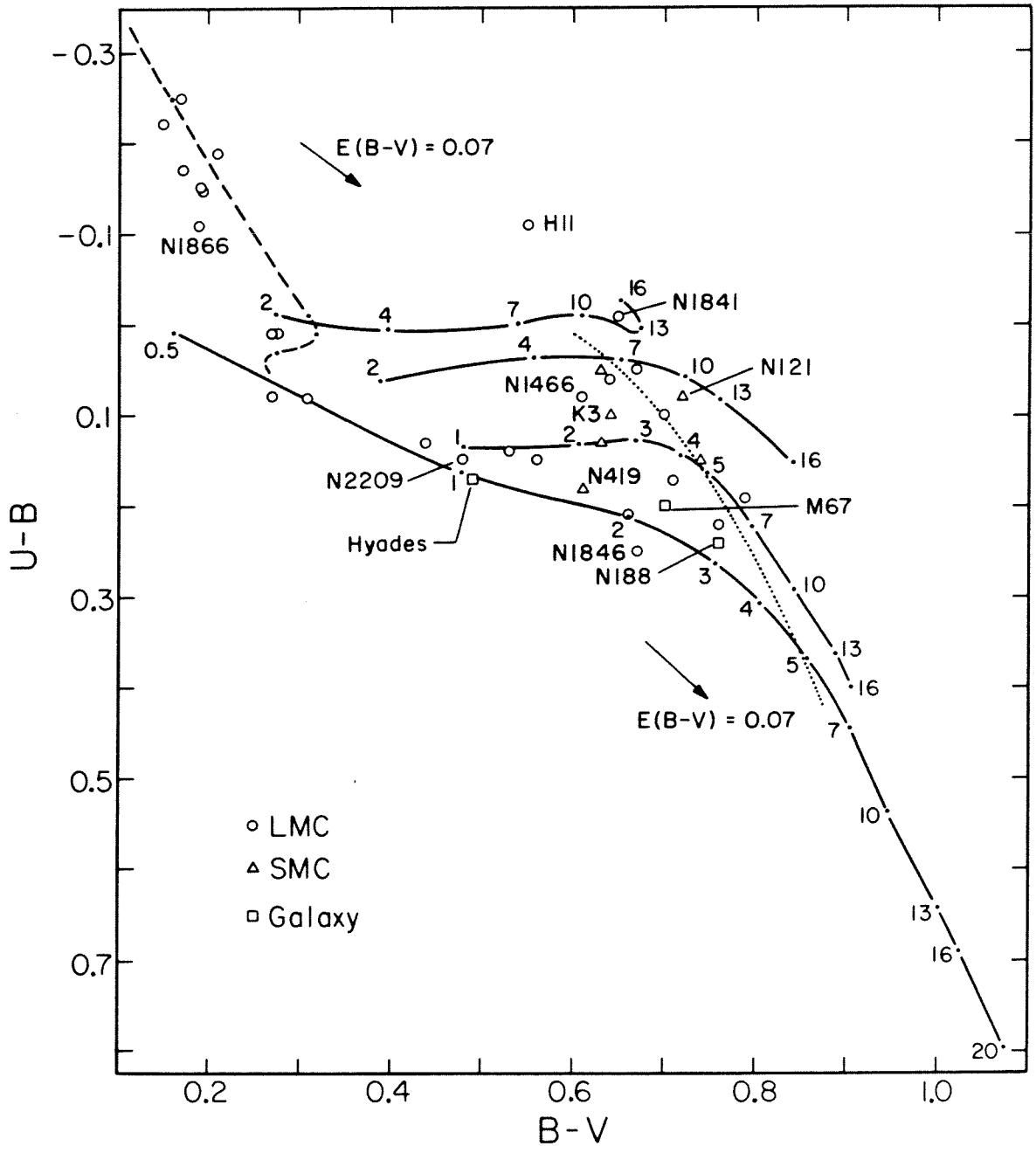
E(B-V) = 0.07
HII
N1866
N1841
N121
N1466
K3
N2209
N419
M67
Hyades
N1846
N188
E(B-V) = 0.07
LMC
SMC
Galaxy
U-B
B-V
-0.3
-0.1
0.1
0.3
0.5
0.7
0.2
0.4
0.6
0.8
1.0

Figure 4

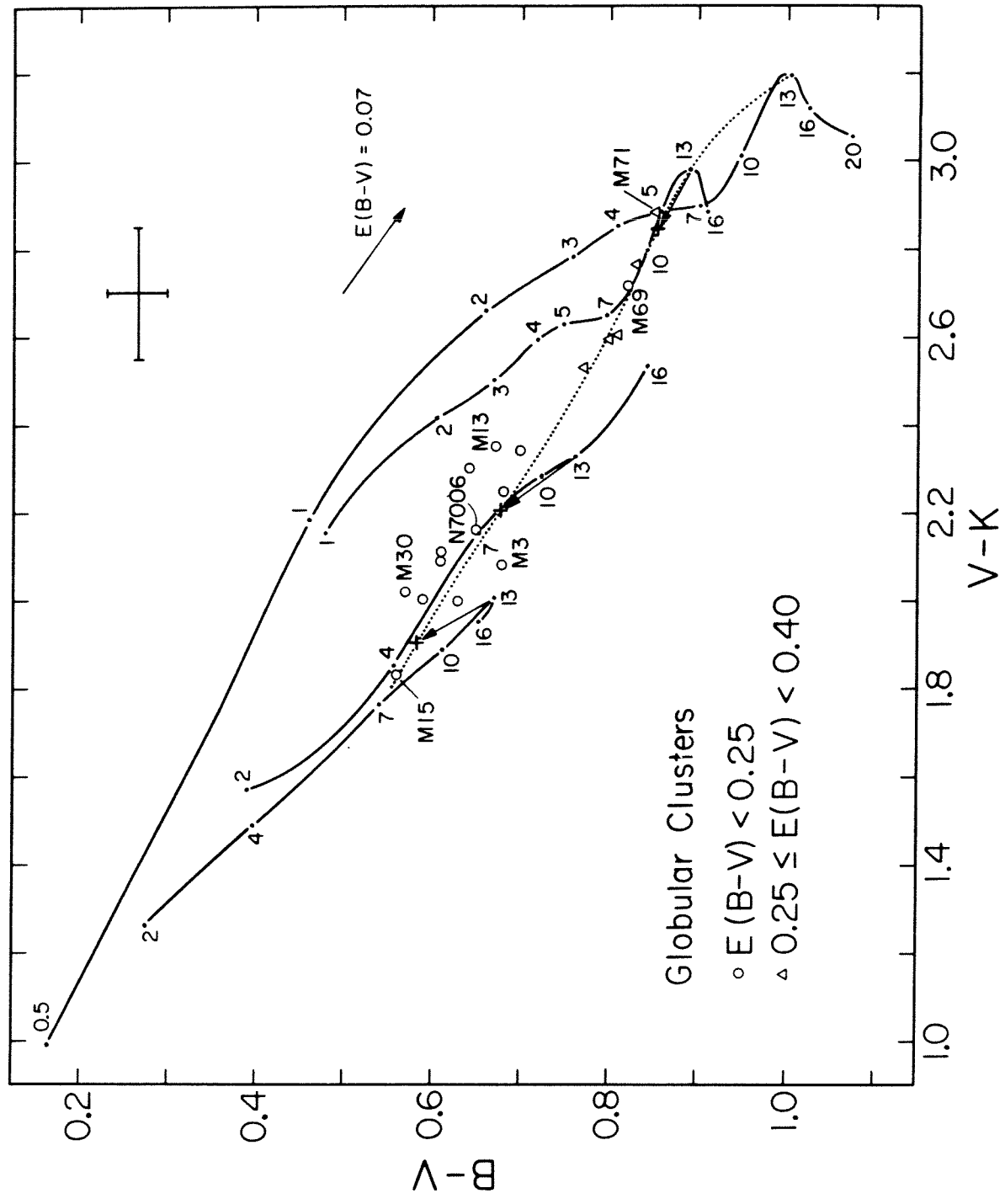
E(B-V) = 0.07
M71
M69
M13
N7006
M30
M3
M15
Globular Clusters
○ E(B-V) < 0.25
△ 0.25 ≤ E(B-V) < 0.40
B-V
V-K
0.2
0.4
0.6
0.8
1.0
1.0
1.4
1.8
2.2
2.6
3.0

Figure 5

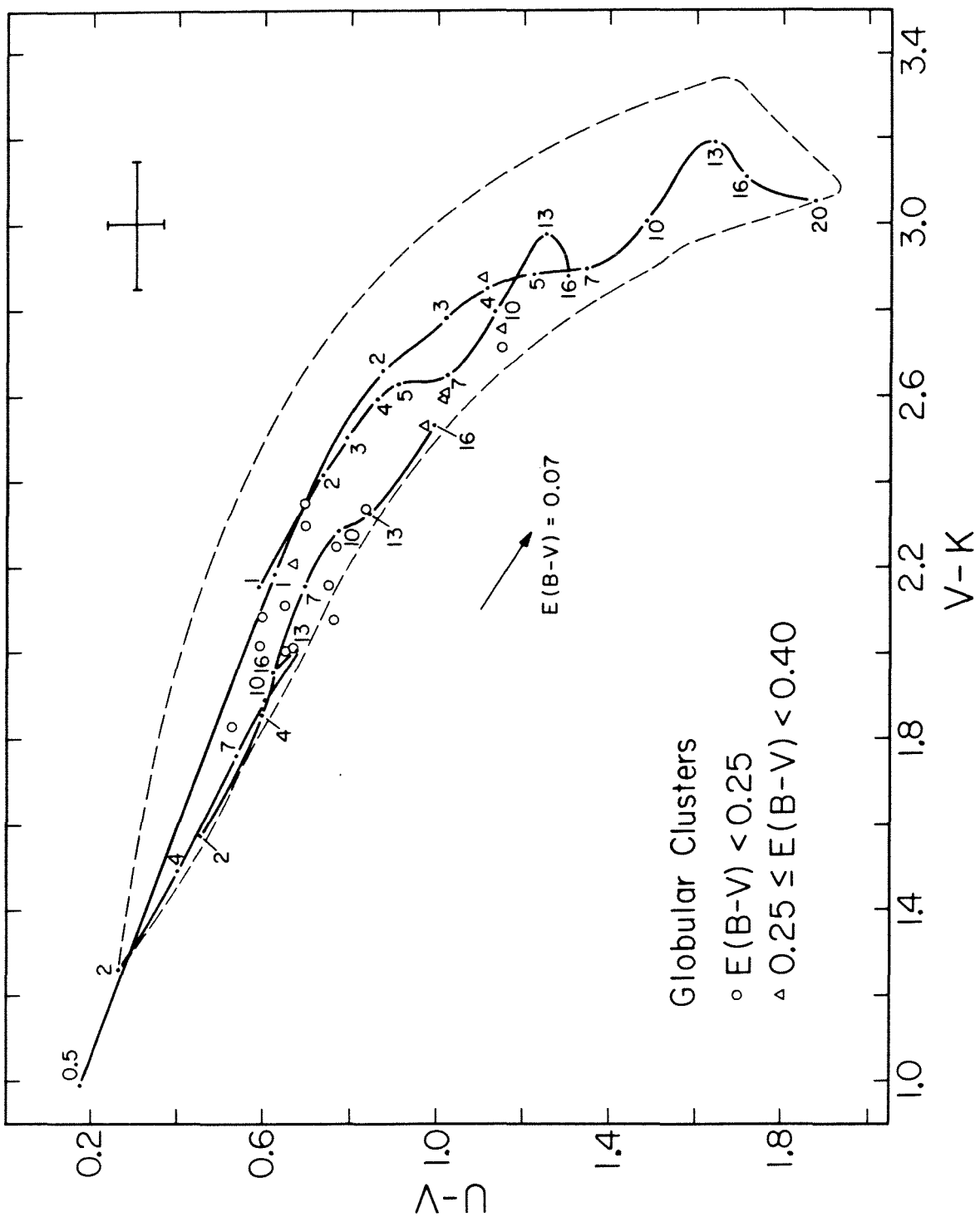
U-V
V-K
0.2
0.6
1.0
1.4
1.8
1.0
1.4
1.8
2.2
2.6
3.0
3.4
E(B-V) = 0.07
Globular Clusters
○ E(B-V) < 0.25
△ 0.25 ≤ E(B-V) < 0.40

Figure 6

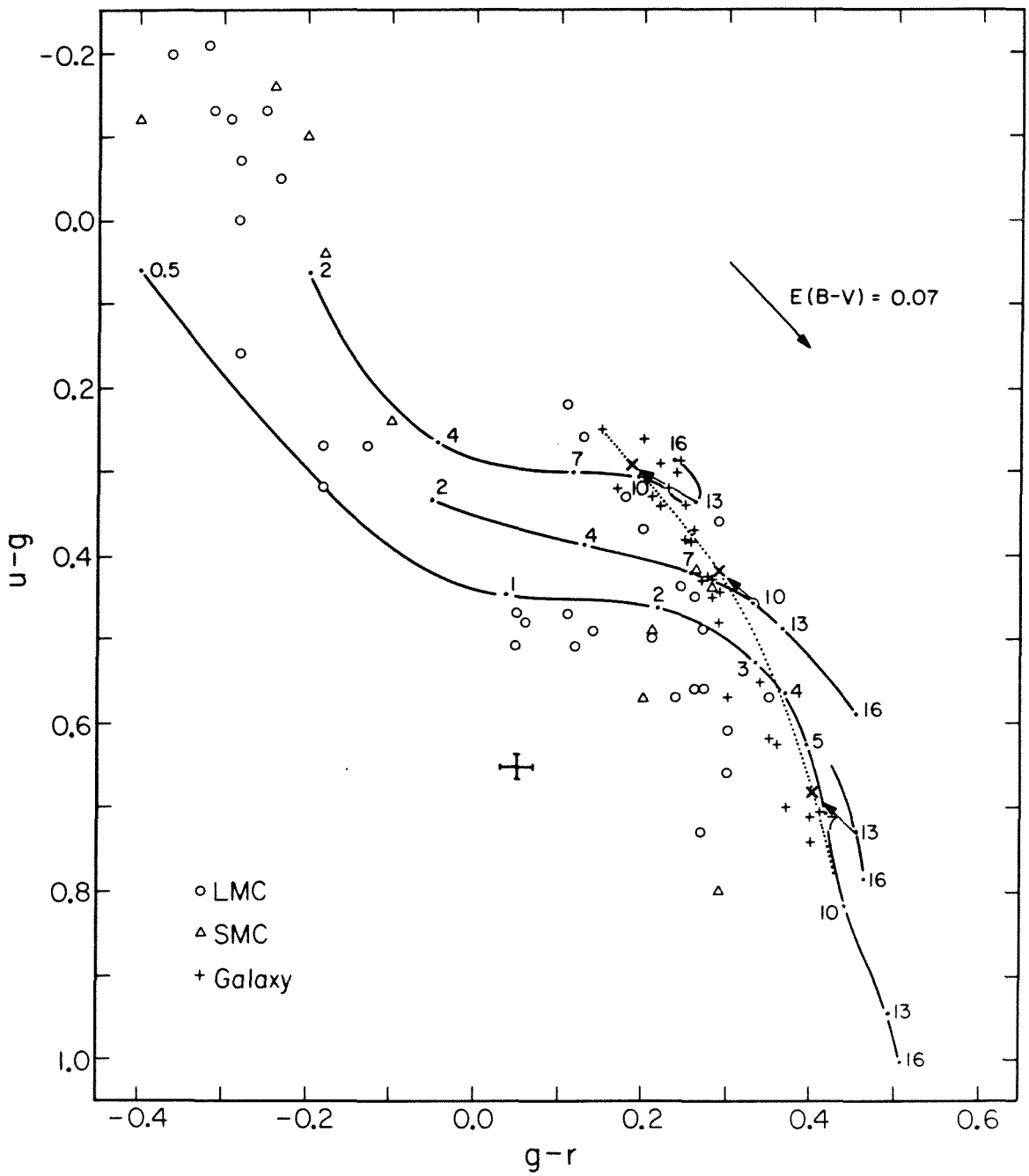

Figure 7

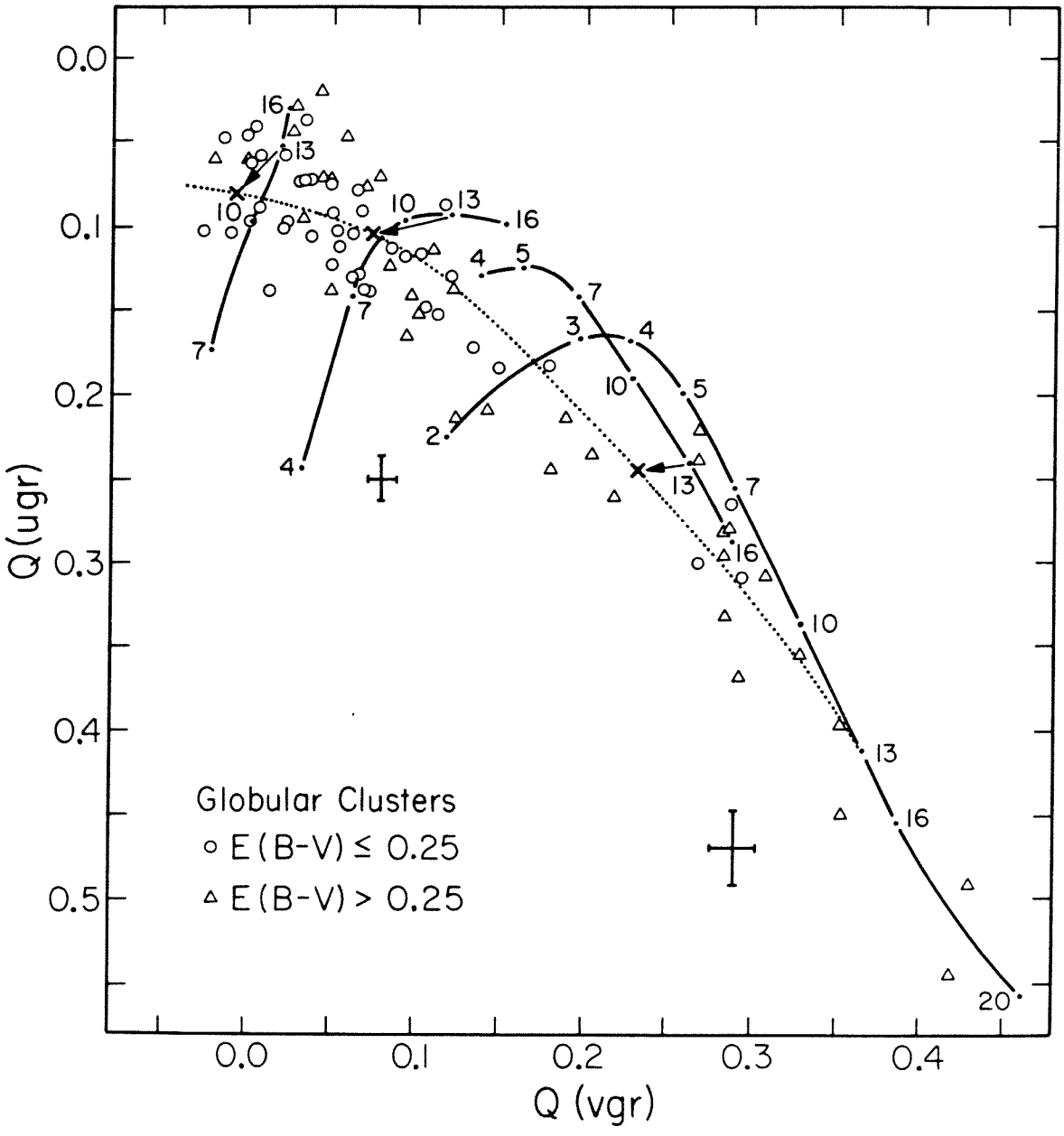

Figure 8

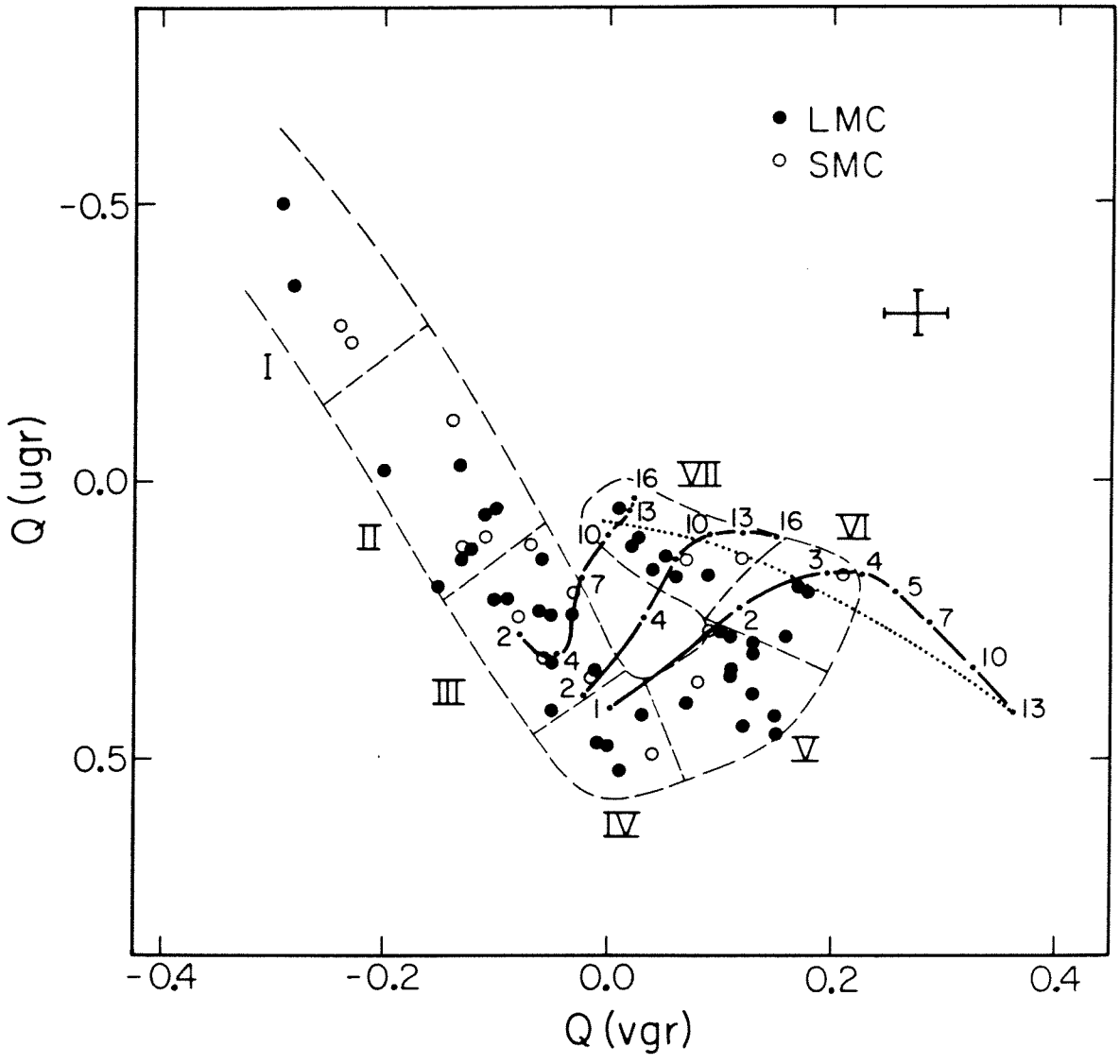

Figure 9

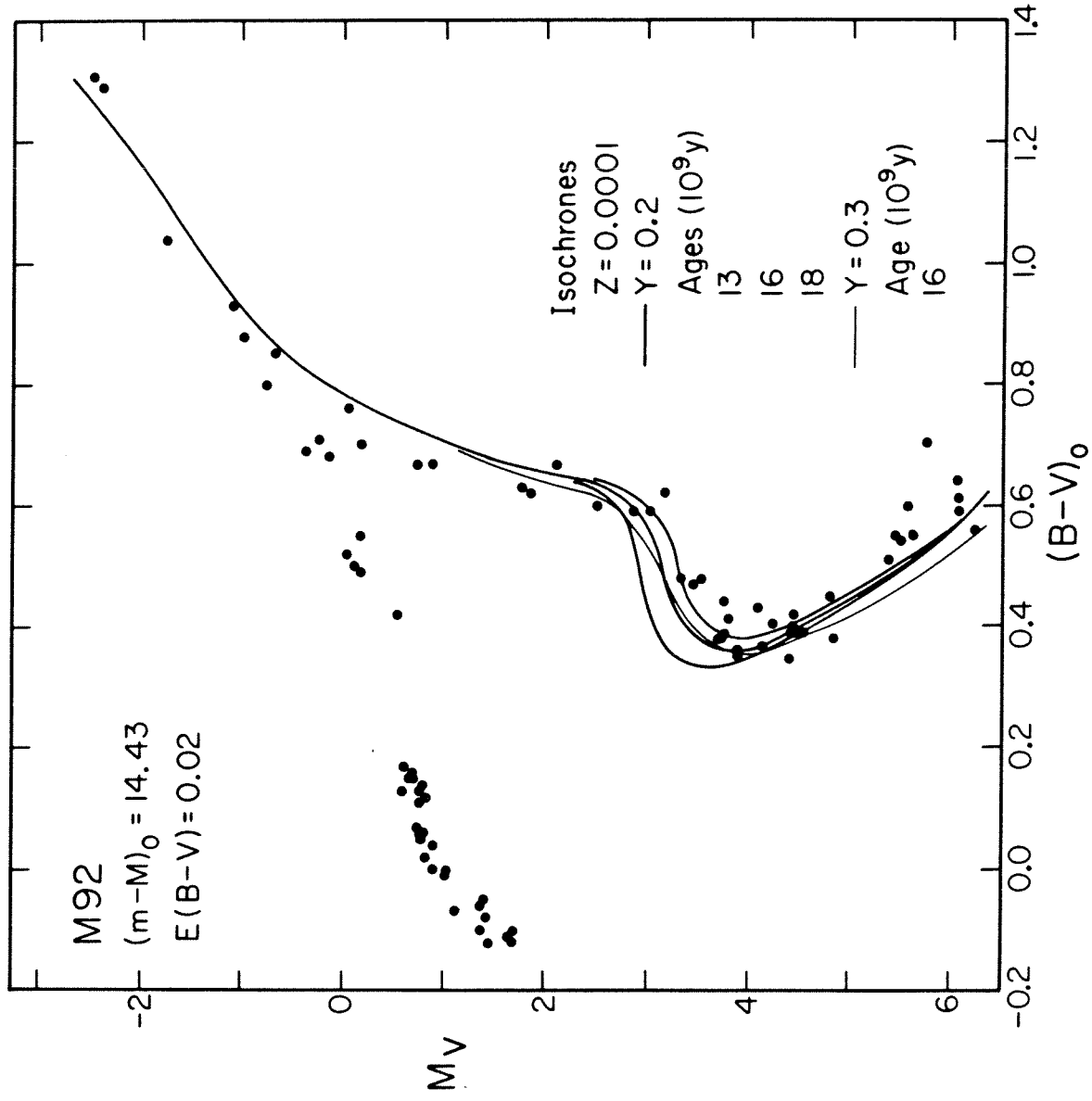
M92
$(m-M)_0$ = 14.43
E(B-V)= 0.02
Isochrones
Z= 0.0001
Y= 0.2
Ages (10^9y)
13
16
18
Y= 0.3
Age (10^9y)
16
M_V
$(B-V)_0$
-2
0
2
4
6
-0.2
0.0
0.2
0.4
0.6
0.8
1.0
1.2
1.4

Figure 10

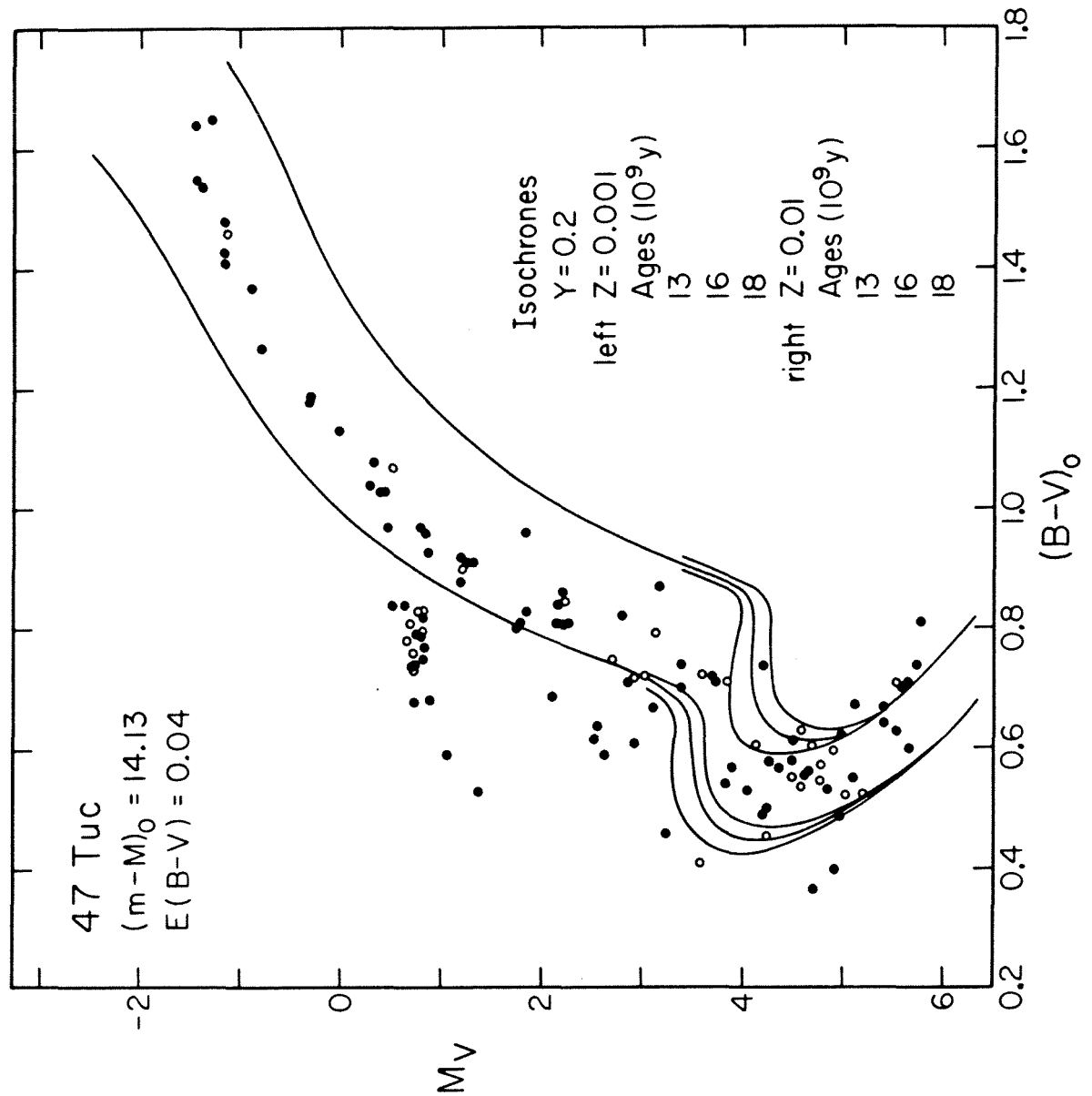
47 Tuc
(m-M)$_0$ = 14.13
E(B-V) = 0.04
Isochrones
Y = 0.2
left Z = 0.001
Ages (10^9y)
13
16
18
right Z = 0.01
Ages (10^9y)
13
16
18
M_V
$(B-V)_0$
-2
0
2
4
6
0.2
0.4
0.6
0.8
1.0
1.2
1.4
1.6
1.8

Figure 11

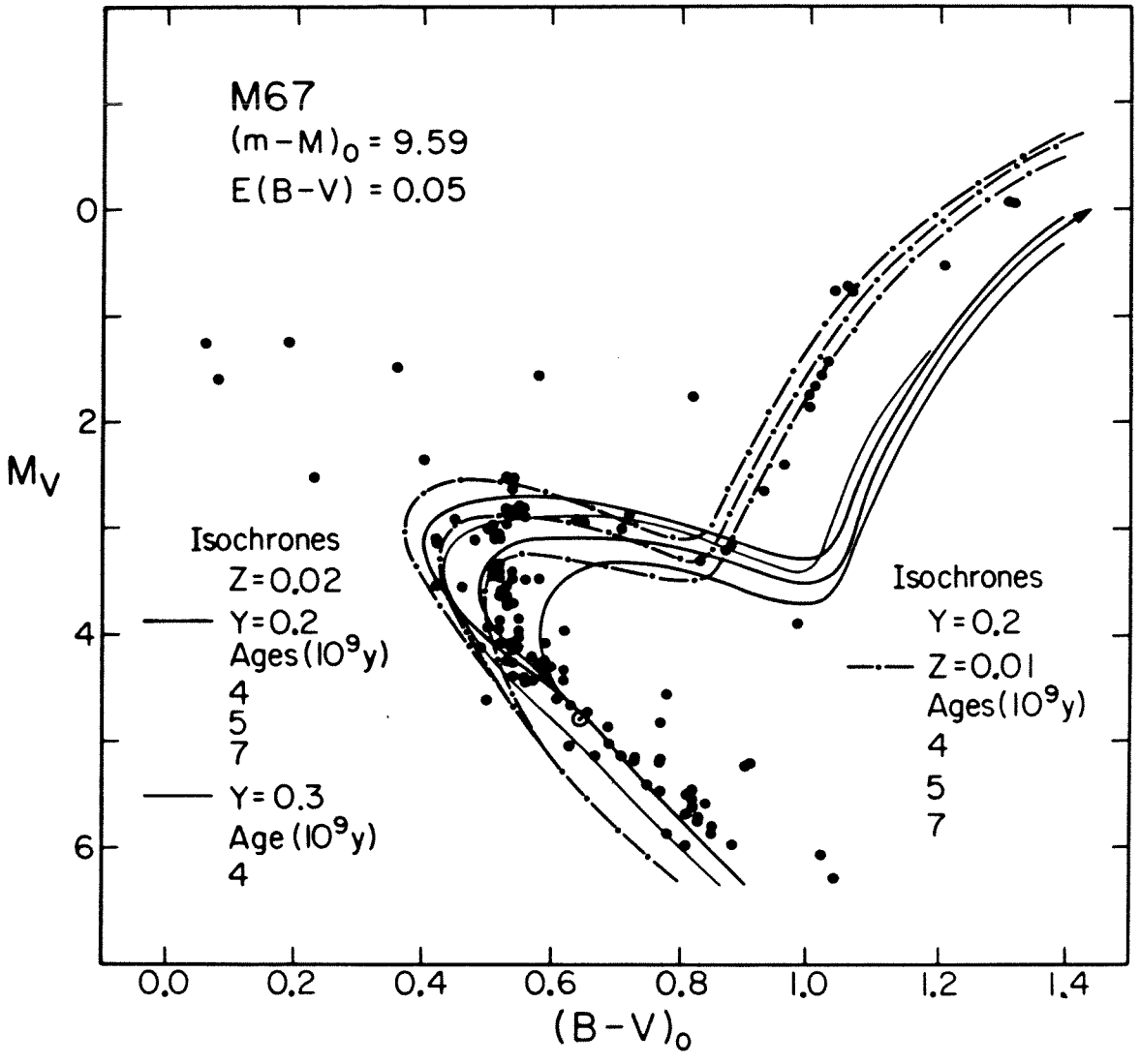
M67
(m-M)o = 9.59
E(B-V) = 0.05
Isochrones
Z=0.02
Y=0.2
Ages(10^9y)
4
5
7
Y=0.3
Age(10^9y)
4
Isochrones
Y=0.2
Z=0.01
Ages(10^9y)
4
5
7
MV
(B-V)o
0
2
4
6
0.0
0.2
0.4
0.6
0.8
1.0
1.2
1.4

Figure 12

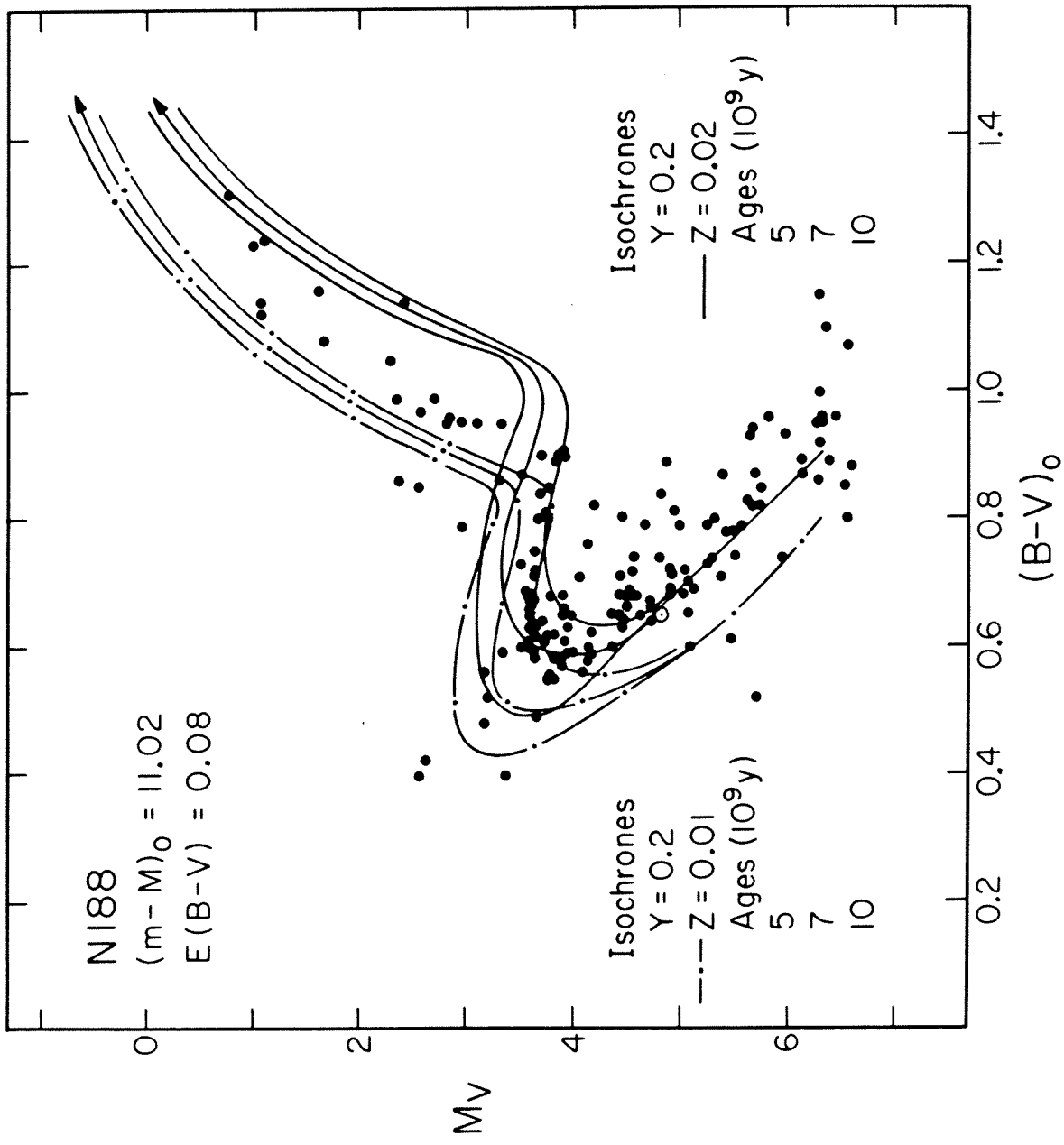
N188
(m-M)o = 11.02
E(B-V) = 0.08
Isochrones
Y = 0.2
Z = 0.02
Ages (10^9 y)
5
7
10
Isochrones
Y = 0.2
Z = 0.01
Ages (10^9 y)
5
7
10
MV
(B-V)o
0
2
4
6
0.2
0.4
0.6
0.8
1.0
1.2
1.4

Figure 13

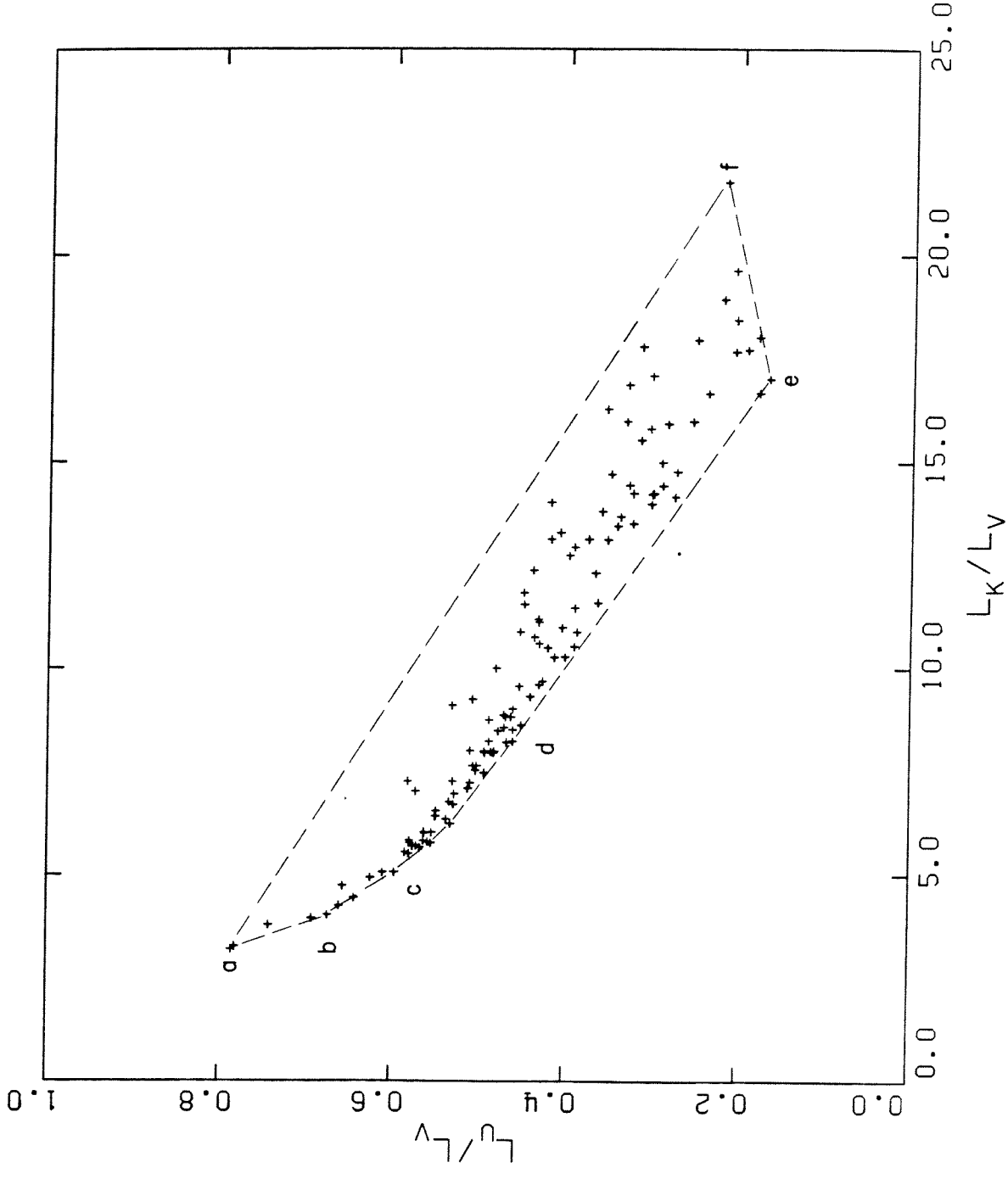

Figure 14

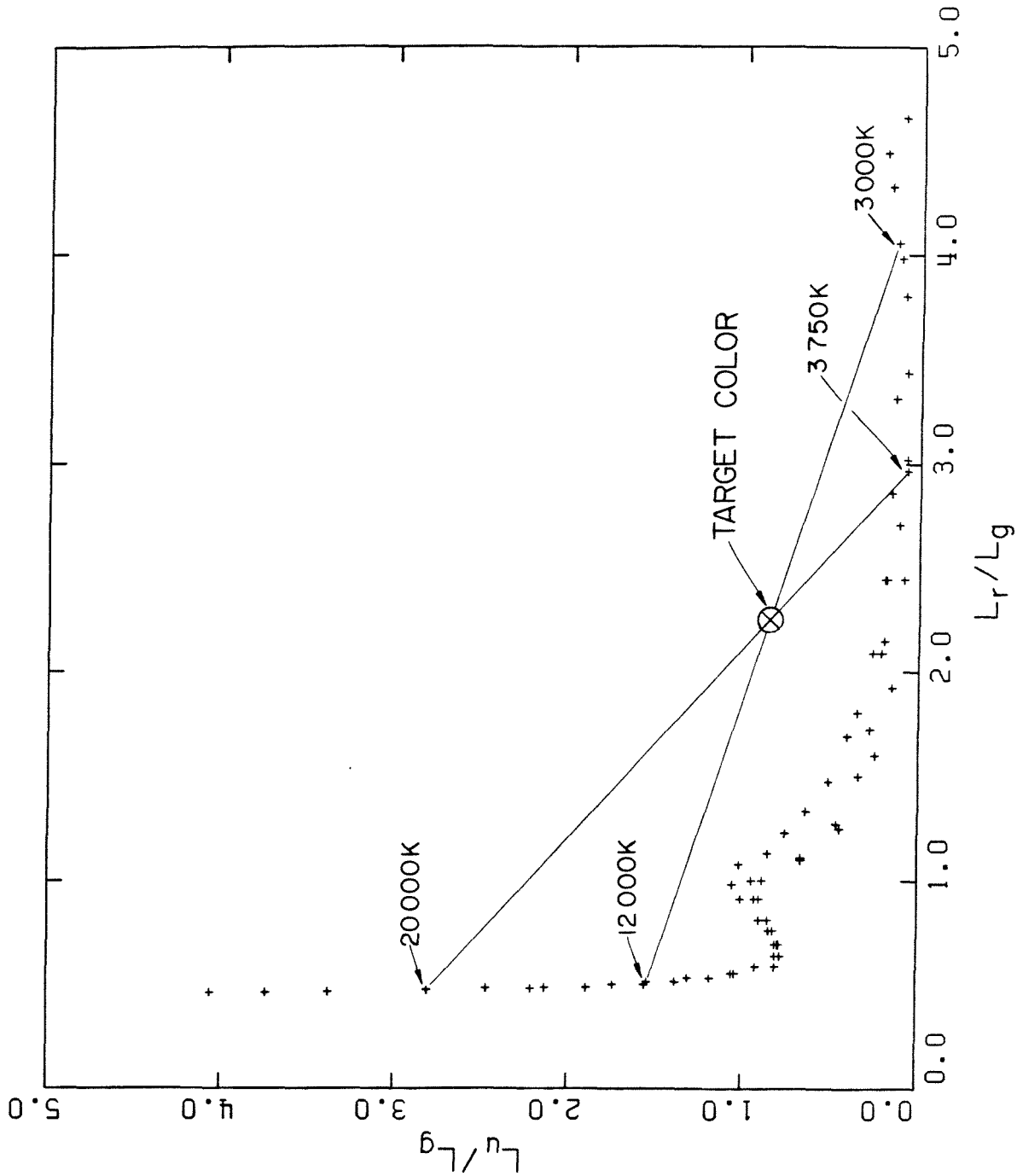
TARGET COLOR
3750K
3000K
20000K
12000K
L_r/L_g
L_u/L_g
0.0
1.0
2.0
3.0
4.0
5.0

Figure 15